SURFACE SCIENCE STUDIES OF COBALT AND RHODIUM SINGLE CRYSTAL SURFACES

BY

TROND RAMSVIK

Thesis submitted in partial fulfilment of the requirements for
the Norwegian academic degree *Doktor Ingeniør*

Department of physics
Norwegian University of Science and Technology (NTNU)
Trondheim, Norway

October 2001

Abstract

The main topic of this thesis is the investigation of small molecules adsorbed on the transition metals cobalt and rhodium surfaces by means of predominantly high-resolution core level photoemission and near edge x-ray absorption fine structure (NEXAFS). The thesis can be divided into three parts where the following phenomena are examined:

1) internal molecular vibrations in the core level photoemission spectra
2) hybridisation and thermal decomposition of adsorbates
3) growth and surface alloy formation of metal-on-metal systems

The influence on the C 1s spectra of photoemission induced internal vibrations after chemisorption is presented for two molecules, acetylene (C_2H_2) and carbonmonoxide (CO). In the former case the fine structure of the C-H vibrational stretch mode of acetylene on Co(0001) single crystal surface is resolved. The measured vibrational energy splitting is (389 ± 8) meV, which is ~6 % lower than what has been reported for gaseous acetylene. The corresponding S-factor of 0.17 ± 0.02 is considerably higher than those reported for other systems. For CO molecules adsorbed on metal surfaces the C-O stretch vibration has a vibrational energy which is about half that of the C-H stretch in hydrocarbons. The progression of this vibrational mode for the systems CO/Co(0001), CO/Rh(100) and CO/Rh(111) have been thoroughly investigated. CO adsorbs in on-top sites on Co(0001) resulting in a vibrational splitting of (210 ± 3) meV from the adiabatic C 1s peak. For CO on Rh(100) two adsorption sites, on-top and bridge, are populated. Similar analyses of the vibrational fine structure gives a vibrational splitting of (221 ± 4) meV for on-top site and (174 ± 11) meV for bridge site. Investigations of the C-O vibrational properties on Rh(111), where CO populates on-top and three-fold hollow sites, show the same trend as for CO on Rh(100), namely decreasing vibrational splitting with increasing co-ordination. A tendency of increasing S-factor with increasing co-ordination is also reported.

Acetylene hybridisation and thermal decomposition on two crystal orientation of cobalt, Co(0001) and Co($11\bar{2}0$), have been investigated using a variety of experimental techniques: NEXAFS shows that acetylene chemisorb strongly to both cobalt surfaces. For the system C_2H_2/Co(0001) a state of hybridisation close to sp^3 has been deduced, which is considerably stronger than what has been reported earlier. Photoemission spectroscopy measurements show

that acetylene starts to decompose at a temperature ~100 K lower for $Co(11\bar{2}0)$ compared to Co(0001). For the anisotropic $Co(11\bar{2}0)$ surface the acetylene decomposition lead to formation of an ordered carbon overlayer. By combining these results with STM and LEED measurements a hard sphere model has been proposed for this overlayer.

Rare earth metals induce solid state reactions when thin overlayers are deposited onto a variety of metals and followed by annealing. Using high-resolution photoemission spectroscopy, LEED and temperature programmed desorption (TPD) a true surface alloy is shown to form with new electronic states when La on Rh(100) is annealed to 1350 K. These states alter the hybridisation of CO significantly compared to clean Rh(100) and as-deposited La on Rh(100). TPD experiments show CO desorption peaks at significantly lower temperature than CO on the as-deposited La/Rh(100), but still higher than the desorption peaks found for CO on Rh(100).

The homoepitaxial growth of cobalt on $Co(11\bar{2}0)$ has been studied by STM. The diffusion of Co adatoms is found to be highly anisotropic with larger mobility of added Co atoms parallel than perpendicular to [0001], i.e. along the zigzag rows of the unreconstructed $Co(11\bar{2}0)$ surface.

Preface

This thesis is submitted by the author, Trond Ramsvik, in partial fulfilment of the requirements for the doctoral degree "Doktor Ingeniør" at the Norwegian University of Science and Technology (NTNU). The work presented has been carried out over 4 years, starting in August 1997. During the period, I have taken an equivalent of one academic year of courses. In addition, I have assisted in the teaching of undergraduate students, also adding up to one year. Most of the research was carried out at the Department of Physics at NTNU under the supervision of Professor Anne Borg. I also had the privilege of spending 1 year of this period at the Department of Synchrotron Radiation Research at Lund University in Sweden.

Most of the experimental work presented in this thesis has been performed at the national synchrotron radiation facility MAX-lab in Lund University (Sweden) and at our home STM laboratory in Trondheim. The result of the research is presented as seven scientific papers, all submitted to scientific journals. These papers form the second part of this thesis. In the first part an introduction in the field of surface science is presented, together with a review of the experimental techniques. It must be emphasised that the review does only include the techniques I have participated in myself. The contents have been written for non-expert readers with the intention to facilitate the understanding of the second part. The seven papers comprising the second part are:

I. *Hybridisation and vibrational excitation of C_2H_2 on Co(0001)*
T. Ramsvik, A. Borg, T. Worren and M. Kildemo
Submitted to Physical Review B

II. *Acetylene chemisorption and decomposition on cobalt single crystal surfaces*
T. Ramsvik, A. Borg, H. J. Venvik, F. Hansteen, M. Kildemo and T. Worren
Submitted to Surface Science

III. *Molecular vibrations in core-ionised CO adsorbed on Co(0001) and Rh(100)*
T. Ramsvik, A. Borg, M. Kildemo, S. Raaen, A. Y. Matsuura, A. J. Jaworowski, T. Worren and M. Leandersson
Surface Science 492 (2001) 152.

IV. *Vibrationally resolved C 1s photoemission from CO adsorbed on Rh(111): The investigation of a new chemically shifted C 1s component*
M. Smedh, A. Beutler, T. Ramsvik, R. Nyholm, M. Borg, J. N. Andersen, R. Duschek, M. Sock, F. P. Netzer and M. G. Ramsey
Surface Science 491 (2001) 99.

V. *Investigation of the La-Rh(100) surface alloy*
M. Kildemo, T. Ramsvik and S. Raaen
Surface Science 490 (2001) 1.

VI. *Study of CO adsorption on La-Rh(100) surface alloys*
M. Kildemo, T. Ramsvik and S. Raaen
Accepted for publication in Surface Science

VII. *Homoepitaxial growth of Co on Co(11$\bar{2}$0) studied by STM*
T. Worren, T. Ramsvik and A. Borg
Applied Surface Science 142 (1999) 48-51

In addition, I have contributed to the following scientific papers (not included in this thesis):

VIII. *CO adsorption on the Rh(100) surface studied by high resolution photoelectron spectroscopy*
F. Strisland, A. Ramstad, T. Ramsvik, A. Borg
Surface Science, 415 (1998) 1020.

IX. *CO adsorption on the Pt/Rh(100) surface studied by high-resolution photoemission*
A. Ramstad, F. Strisland, T. Ramsvik, A. Borg
Surface Science, 458 (2000) 135.

My position in the author list in the respective papers reflects the amount of work that has been my responsibility. In papers I-III I have the main responsibility, while a significant amount of research and preparations have been done in papers V-VII. Using synchrotron radiation to perform surface science experiments demand the participation of several people. In all the papers listed I have been involved in the experimental work.

Acknowledgements

During my doctoral studies I have been working must of the time in Trondheim for the Group of Surface Physics. However, I also had the pleasure of spending one year at the Department of Synchrotron Radiation Research at Lund University in Sweden. This thesis consists of experimental studies, which would not have been possible without the co-operation with a large number of people.

Trondheim

First of all, many thanks go to my supervisor Prof. Anne Borg for her support, encouragement, advice and sound criticism whenever needed. She gave me great confidence from my very first day as a graduate student, despite the little knowledge I had in surface physics. Regardless of her tight schedule she always found time for technical and scientific assistance. I especially acknowledge her active participation during my weeks at the beamlines. During all the moments of despair both in the STM-lab here in Trondheim and in Lund she helped keeping up the spirit.

Synchrotron radiation experiments require the contribution of a group of people. The co-operation with Dr. Turid Worren, Dr. Morten Kildemo, Fredrik Hansteen, Prof. Steinar Raaen, Dr. Frode Strisland and Dr. Audun Ramstad from my department in Trondheim has been essential for the results presented in this thesis. They all made the work at the beamlines stimulating and enjoyable. The help from the administrative and technical personnel is also highly appreciated. In particular Eli Monsøy, Tor Jacobsen and Arnulf Bjølstad deserve a special gratitude.

Lund

A big tribute goes to my second supervisor in Lund, Dr. Jesper Andersen who gave me invaluable help with experiments and technical details throughout the year at the Department of Synchrotron Radiation Research at Lund University. During the first 4 months of my stay in Lund I also had the pleasure of working in the departments STM-lab under the enthusiastic supervision of Dr. Struan Gray, who always had time for discussions, no matter its relevance.

Many thanks go to my former colleagues in Lund, Dr. Mats Leandersson, Dr. Anne Matsuura, Dr. Alex Jaworowski, Dr. Maria Smedh and Dr. Anders Sandell. With their positive and friendly attitude they made me feel welcome from the very first day. Mats, Anne and Alex also assisted me during 2 weeks of beamtime, and had to cope with my bad humour when things went wrong during the experiments. The assistance of the MAX-lab staff is also

gratefully acknowledged. A special gratitude goes to the coffee-machine at MAX-lab, which kept me going throughout the whole night at the beamlines.

The work presented in this thesis was supported financially by the Norwegian Research Council in the period 1997 - 2000. Additional financial support in 2000 and 2001 was received from Department of Physics at NTNU.

Finally I thank my parents and my girlfriend Giovanna for always being a support during my doctoral period. Giovanna has also been of great help in making some of the figures presented in the thesis.

Contents:

1. Introduction

A solid sample is always in contact with other media via its surface. Due to the break in symmetry the surface can reveal properties that differ significantly with the bulk. And it is through these properties that the interactions with the outside world take place. The study of surface phenomena is therefore of great importance in physics, both for a fundamental understanding about the nature that surrounds us and for developments in the variety of surface related technologies that exist today (heterogeneous catalysis, microelectronics, electrochemistry, corrosion and many others). The choice of materials made for this thesis, rhodium and cobalt, are both highly catalytic active. Hence concerning the technological aspect the field of heterogeneous catalysis is considered most relevant.

The aim of this work can accordingly be split up in two parts:

- to increase the general knowledge of fundamental processes on single crystal surfaces
- to make a surface science contribution to the ongoing research in the field of heterogeneous catalysis

The majority of the catalysts used in the chemical and petroleum technologies is heterogeneous, and thus plays a key role in the chemical industry. The reactants are introduced as gases or liquids onto a catalytic active material, and all chemical reactions take place on the surfaces.

1.1. The "Surface-Science approach" to Heterogeneous Catalysis

Before the appliance of surface science, catalysts were viewed as a "black box" that, in a "mysterious way", changed the incoming reactant molecules to the desired products. The appearance of UHV[1] techniques around forty years ago offered the opportunity to study the catalysts on an atomic scale using idealised systems. The assumption is that the small metal particles within a catalyst can be substituted by monocrystalline metal surfaces, which act as model systems of the active surface. Such investigations are commonly called the "surface science approach" and have led to the development of many experimental techniques and models (for short reviews, see [1,2]). The study of such well-defined surfaces at low-pressure conditions is today a generally accepted method to approach a deeper understanding of the elementary processes that take place on heterogeneous catalysis. An important conclusion from these investigations is that not only the type of material but also the arrangement of atoms can

[1] UHV = ultra-high vacuum, typically at pressures below 10^{-8} mbar.

change the catalytic properties significantly for certain reactions. For example in a study of T. P. Beebe et al. [3] the dissociative sticking of methane, CH_4, was shown to increase in the order Ni(111) < Ni(100) < Ni(110), i.e. with increasing exposure of sublayer atoms. In fact the initial reaction rates for the surfaces Ni(110) and Ni(100) are ~7 to 10 times higher than the initial rate for the Ni(111) surface at 450 K.. Another important example is the dissociation of CO on cobalt where the close-packed surface Co(0001) is reported [4] to be less active than the more open $Co(11\bar{2}0)$ and $Co(10\bar{1}2)$ surfaces [5,6]. Similar conclusions have been made for acetylene on cobalt singel crystal surfaces. Thermal decomposition of acetylene adsorbed on $Co(11\bar{2}0)$ is reported to take place around 100 K below the temperature found on Co(0001) (see paper II). In Figure 1.1 the different low index crystallographic planes are illustrated for face-centred cubic (fcc) and hexagonal closed packed (hcp) single crystals. These are the structures comprising rhodium (fcc) and cobalt (hcp) single crystals.

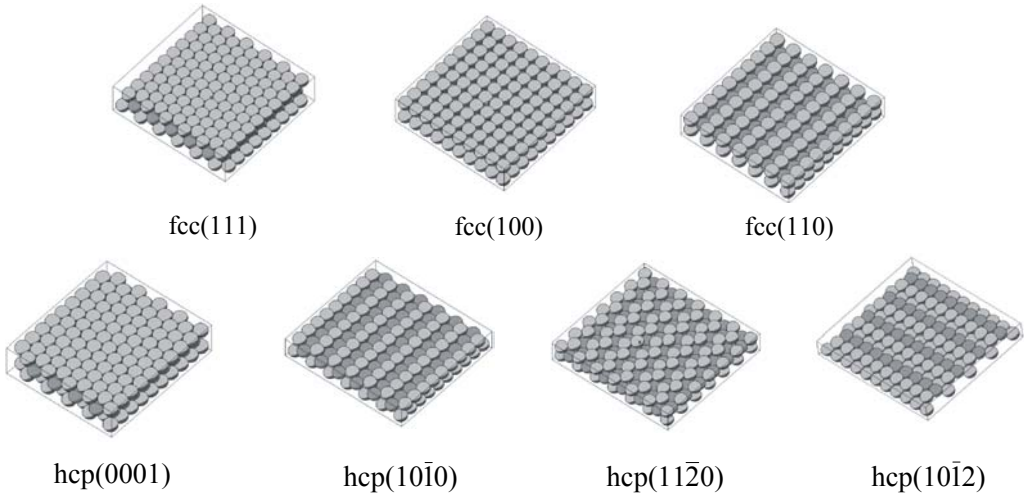

Figure 1.1: Schematic representation of low-index single crystal surfaces of face-centred cubic (fcc) and hexagonal close-packed (hcp) crystals.

There exist cases where the "surface science" approach has paid off in view of producing catalysis of technological interests. A famous example is the Au-Ni surface alloy catalyst for steam reforming [7]. In the investigations leading to the catalysis well-characterised single crystal surfaces were studied using a combination of scanning tunneling microscopy (STM), molecular beam scattering experiments, and density functional theory (DFT). Still, nearly all the commercially available catalysts in operation today were discovered and developed principally by empirical methods. An explanation for this lack of results of technological implementations is the immense gap that exists between the "surface science

approach" and real catalytic reactions. In the latter case the reactions are carried out under quite different conditions, typically at atmospheric (or higher) pressures and with far more complex surfaces. Therefore considerable efforts are made to bridge these so-called "pressure and material gaps" separating UHV and technical catalytic investigations [1,2,8-12].

1.2. Internal molecular vibrations in the core-ionised state

The frontiers of surface instrumentation are constantly being improved towards detection of finer detail such as atomic spatial resolution, higher energy resolution, and shorter time scales. One example that has evoked some attention is the ability to resolve the vibrational structure for molecules adsorbed on surfaces by use of high-resolution photoemission spectroscopy. For gaseous molecules excitations of internal molecular vibrations during a core-level photoemission process are today well established [13,14]. Molecules adsorbed on surfaces are more problematical since the natural line width is larger than in the gas phase. This broadening appears due to e.g. additional excitation of low-energy vibrational modes, frustrated translations of the molecule along the surface, and shorter life times of the created core holes. The latter is a consequence of the metallic screening of the core hole providing additional decay channels. Nevertheless, vibrational split lines were unambiguously observed in the core-level photoemission spectra in 1997 by Andersen et al. [15]. By comparing the C 1s vibrational fine structure of ethylene (C_2H_4) and ethylidyne (C_2H_3) with their deuterated counterparts (C_2D_4, C_2D_3) they demonstrated that the additional features on the high binding energy sides originated from the C-H stretch vibration. Soon afterwards Föhlisch et al. presented vibrational resolved core-level photoemission spectra of adsorbed CO on Ni(100) [16] showing vibrational energy splittings of the C-O stretch mode around half of the value found for C-H.

The ability to resolve the vibrational components in a photoemission spectrum has several advantages. For the vibrational fine-structure of adsorbed CO it has been demonstrated ([16], Paper III and IV) that the vibrational energy splitting is sensitive to the adsorption sites, with a trend identical to that found in electron energy loss spectroscopy. Furthermore it is known that the vibrational intensity distribution of the C-H stretch mode in the C 1s spectra can be used to identify what hydrocarbon group that is present in the gas-phase molecule. Andersen et al. [15] showed that the similarities between molecule in adsorbed and gas-phase are sufficient to use this fingerprinting method for adsorbed molecules on a surface as well. All the same, due to the bonding situation there exist some differences between the two phases (Paper I). Hence by careful comparisons to the corresponding molecule in gas-phase additional information about the molecular bonds to the surface can be made. Finally, the identification of

the vibrational components in the core-level photoemission spectra is important to extract reliable information and to avoid the misinterpretation of them as being due to chemical shifts.

1.3. Selected systems for this work

The selected materials in this thesis, rhodium (Rh) and cobalt (Co), are both used extensively as industrial catalysis. Rhodium, with additives like Pt, Pd or Ru, is an essential catalytic ingredient in e.g. automotive exhaust catalysts [17]. Cobalt, together with iron and ruthenium, are the most effective catalysts for the so-called Fischer-Tropsch process [17, 18], which refers to the conversion of synthesis gas to long straight chain paraffins,

$$nCO + (2n+1)H_2 \xrightarrow{Co,Ru,Fe} C_nH_{2n+2}\ nH_2O, \quad n > 1 \qquad (1.1)$$

Therefore in line with the "surface science approach" natural starting points for this process is the study of CO and unsaturated hydrocarbons on the surface. These have been the topics in Paper I, II and III. However, the main goals in Paper I and III have been the investigations of internal molecular vibrations, and thus represent a more fundamental study.

For rhodium the adsorption of CO has been studied as well, both on clean rhodium (Paper III and IV) and on a La-Rh surface alloy (Paper V and VI). Although reasoning can be given in connection with heterogeneous catalysis, the motivations have primarily been more fundamental properties of surfaces. For the systems CO on Rh(100) and Rh(111) the purpose was to present a thorough investigation of the internal vibrations for the C-O bond following the core-ionisation, and their relations with different adsorption-sites. The objective of the La-Rh surface alloy study was to investigate the changes in electronic properties at the surface of an alloy formed by annealing a thin overlayer with low work function on a transition metal surface.

2. Experiments

Numerous surface science techniques are today available to characterise a surface (see e.g. [1,19-22]). The experimental methods relevant for this work are photoemission spectroscopy (PES), Near-edge X-ray absorption Fine Structure (NEXAFS), Scanning Tunneling Microscopy (STM), Low Energy Electron Diffraction (LEED) and Thermal programmed desorption (TPD). In addition to the methods cited, Auger electron spectroscopy (AES) has been employed to characterise the surface (see figure 2.3). The most important experimental methods are photoemission spectroscopy (PES) and near-edge X-ray absorption fine structure (NEXAFS). Scanning tunnelling microscopy (STM) has also been a central technique during the doctoral work. In the following sections experimental aspects of these surface science techniques are presented, including sample preparation, ultra high vacuum environment and description of the light sources employed in this work.

2.1. Surface sensitivity

In macroscopic objects, typically less than 10^{-8} of the total amount of atoms are situated at the surface. Hence a criteria for surface analysis techniques is that they must have a high surface sensitivity. With the exception of STM and TPD all methods used in this thesis record emitted photoelectrons from the sample, either due to incoming photons (PES, NEXAFS and XPD) or scattered electrons (LEED). Empirically it has been found that the mean free path, or escape depth, of these emitted electrons as a function of the kinetic energy behaves in a similar way for all solids investigated [23,24]. This universal curve is shown in Figure 2.1.

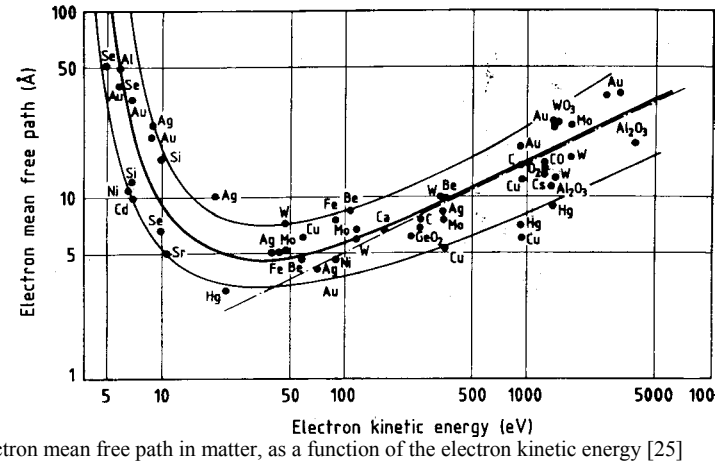

Figure 2.1: Electron mean free path in matter, as a function of the electron kinetic energy [25]

At kinetic energies of 50-100 eV, i.e. around the minimum of the universal curve, the emitted electrons have a mean free path of 5 to 10 Å in solid materials. This corresponds to the thickness of only a few atomic layers. The electrons emitted from the sample without any energy loss hence originate from a very shallow surface region. By carefully choosing the experimental parameters to obtain outcoming electrons with kinetic energies at or near the minimum, surface sensitivity is achieved.

2.2. Sample preparations

General

Even if the surface of a crystal may appear very smooth at the first glance experiments show that it is heterogeneous at a microscopic scale, i.e. when observed with e.g. an electron microscope. It exhibits steps of various heights which separate terraces of atomic planes in which point defects such as adatoms, vacancies and kinks can be observed (see illustration in figure 2.2).

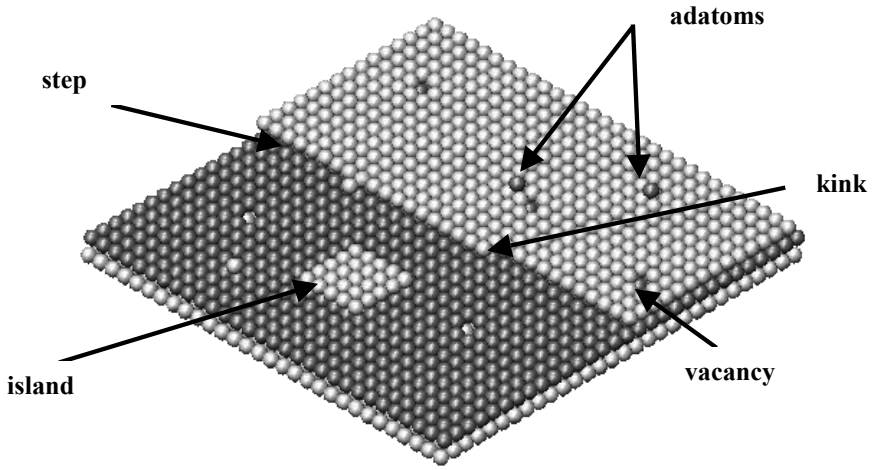

Figure 2.2: Schematic drawing of a stepped FCC(100) surface exhibiting point defects.

However, at the atomic scale the surface atoms are found to form ordered rows characterised by well defined interatomic distances. Depending on the preparation of the sample, the size of the well ordered terraces can extend from a few atomic rows to thousands. As mentioned in the introduction many of the fundamental properties in surface science can only be obtained by studying ideal systems, i.e. with low density of steps and point defects. In addition, contamination from the ambient atmosphere or segregation from the bulk further complicate fundamental studies of surfaces. Therefore, for virtually all surface experiments the first step is

the sample preparation. A single crystal must be cut with an orientation well within 1^{o} of the desired crystallographic orientation. And by a series of finer polishing steps, the surface can be brought to optical flatness. Atomic-scale flatness is achieved by annealing in UHV (sec. 2.3), often at temperatures near the melting point of the sample. The crystallographic ordering can be monitored by low energy electron diffraction (LEED) (see sec. 2.6) as emergence of a sharp pattern. For some materials annealing is sufficient also to obtain chemical purity through desorption into the vacuum. However, for metals nonvolatile impurities are often found to segregate from the bulk. To remove these unsolicited species chemical cleaning methods (e.g. oxidation cycles) and ion sputtering are employed, followed by an additional annealing cycle. As a typical example the final stage cleaning cycle of a Rh(100) single crystal preparation is given (see also experimental part of Paper III, V and VI). The rhodium surface is bombarded with 1-2 keV Ar^{+}-ions for a total of ~30 min. During the first 15 min. the sample is kept at room-temperature (~300 K) and then heated to 1100 K to assure high mobility of the Rh atoms. Possible segregation of carbon from the bulk is removed by keeping the sample at 1075 K in an oxygen atmosphere ($\sim 5 \cdot 10^{-8}$ mbar). At the surface the oxygen molecule will dissociate and react with the carbon atoms to create volatile molecules, mainly CO. A following anneal of the sample to 1300 K in UHV will remove these molecule and the atoms will rearrange to create a more smooth surface. By repeating this process an atomically clean surface can be achieved with large terraces.

Special case of cobalt

The preparation of cobalt single crystal surfaces differ from the more general procedure described above. The reason can mainly be attributed to the hcp $\rightarrow$ fcc phase transition that takes place at ~700 K [26, 27]. This temperature is found too low to dersorb the atomic oxygen used in an oxygen treatment. Achieving large terraces is also problematical due to the restricted anneal temperature. Therefore the traditional way of obtaining an atomic flat cobalt single crystal surface, with insignificant amount of contamination, has been repeating cycles involving ion bombardment with either Ar^{+} or Ne^{+}, followed by long annealing close the phase transition temperature. To avoid excessive disordering during the ion bombardment the ion energy is often kept low, typically around 0.5 keV. However, even for anneal temperatures below ~700 K carbon segregation is often a problem. In addition, ion bombardment has shown to remove carbon atoms inefficiently. Hence alternative cleaning procedures have been tried out.

R. L. Toomes and D. A. King [28] successfully employed hydrogen to react with the residual oxygen to form water molecules subsequent of an oxygen treatment. Anneal of the sample to 660 K then resulted in desorption into vacuum. In our experimental works, oxygen was found to react very efficiently with carbon, creating a "carbon-free" cobalt surface after 2-3 oxygen treatments. Using hydrogen to remove residual oxygen also gave the desired effect. Figure 2.3 shows the amount of oxygen on the Co(0001) surface during a cleaning cycle with hydrogen and oxygen, measured by Auger electron spectroscopy (AES).

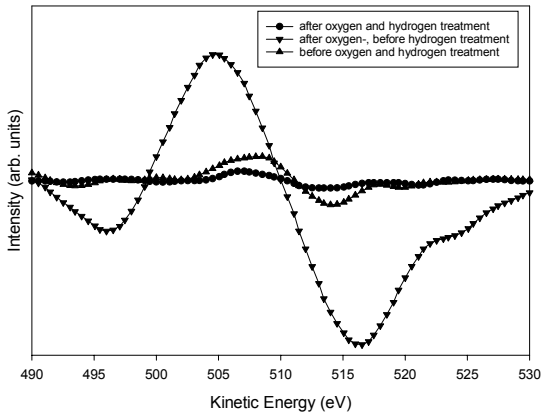

Figure 2.3: Derivative O KVV Auger electron spectra for different stages of oxygen and hydrogen treatment of Co(0001). Triangles down (▼) SHOWS the Auger spectrum after Ar^+ bombardment and before any chemical cleaning, triangles up (▲) shows the effect after annealing the sample at ~600 K in oxygen and circles (●) the results after a subsequent anneal in hydrogen.

From the spectra it is seen that hydrogen treatment reduces the amount of oxygen below the amount after Ar^+-bombardment. However, further decrease of the residual oxygen is found problematical using additional hydrogen treatment. Hence such a method was not suitable as a "final-stage" cleaning in our experiments. To obtain a cobalt surface with non-traceable quantity of contamination, a more efficient process was found to be cycles of cleaning including oxygen-treatment until no carbon is detected. The oxygen was then removed by additional cycles of Ar^+-bombardment and annealing.

2.3. Ultra high vacuum

All measurements reported in this thesis were performed in an ultrahigh vacuum (UHV) system, maintained at a pressure below ~$2\text{-}3\cdot10^{-10}$ mbar. Residual gases adsorbing on the surface of a crystal can cause a significant error in the measurement of experimental data, thus it is crucial to maintain a sufficiently low pressure in the experimental chamber. For example, if

the ambient pressure is 10^{-6} mbar and with a sticking coefficient of unity, the surface will be contaminated with one monolayer of the gas in approximately one second. If the pressure is lowered to 10^{-10} mbar, it will take at least 10^4 seconds (nearly 3 hours) to reach the same coverage of background gas. This is much longer that a typical experimental measurement time of 15 to 30 minutes. Common techniques to monitor the concentration of impurities on the surface are photoemission spectroscopy and Auger-Electron Spectroscopy. In this thesis the former technique has been the principal method. (see sec. 2.4).

2.4. Photoemission Spectroscopy

Photoemission spectroscopy can be divided into two fields, depending upon the energy of the incident photon. For energies less than ~100 eV the technique is here referred to as valence band photoemission spectroscopy (sec. 2.4.2) and for energies in the range from ~100 to ~1500 eV as core-level photoemission spectroscopy (sec. 2.4.3). The low and high energy ranges probe the valence band and the localised core-levels of the sample, respectively. All the photoemission spectroscopy measurements have been performed using photons from synchrotron radiation (see sec. 2.10).

2.4.1. Basic principles

In principle photoemission spectroscopy is a very simple process. A beam of photons with energy hν penetrate a surface, and are absorbed by an electron of a certain binding energy (E_B) below the Fermi level (photoelectric effect). The electrons emerge from the surface with a kinetic energy

$$E_k = h\nu - E_b = h\nu - (E_B + \Phi_S) \qquad (2.1)$$

where Φ_S is the work function of the sample and E_b is the binding energy relative to the vacuum level. Their kinetic energy distribution is analysed either in a given emission direction (angle resolved photoemission) or after an integration over all possible directions (integrated photoemission)[2]. The energy distribution of photoemitted electrons should simply be the energy distribution of electron states in the solid surface or adsorbates shifted up in energy by an amount hν relative to the vacuum level (see Fig. 2.4). In practise, the process is not as simple as this. For example the probabilities of absorption by a photon are not the same for all electron states. Nevertheless the relative simplicity of this one electron-process to probe the electronic

[2] In this thesis all photoemission spectra have been recorded in a normal emission mode and integrated over a small aperture.

state in such a direct fashion is undoubtedly an important explanation for the wide application of the technique today.

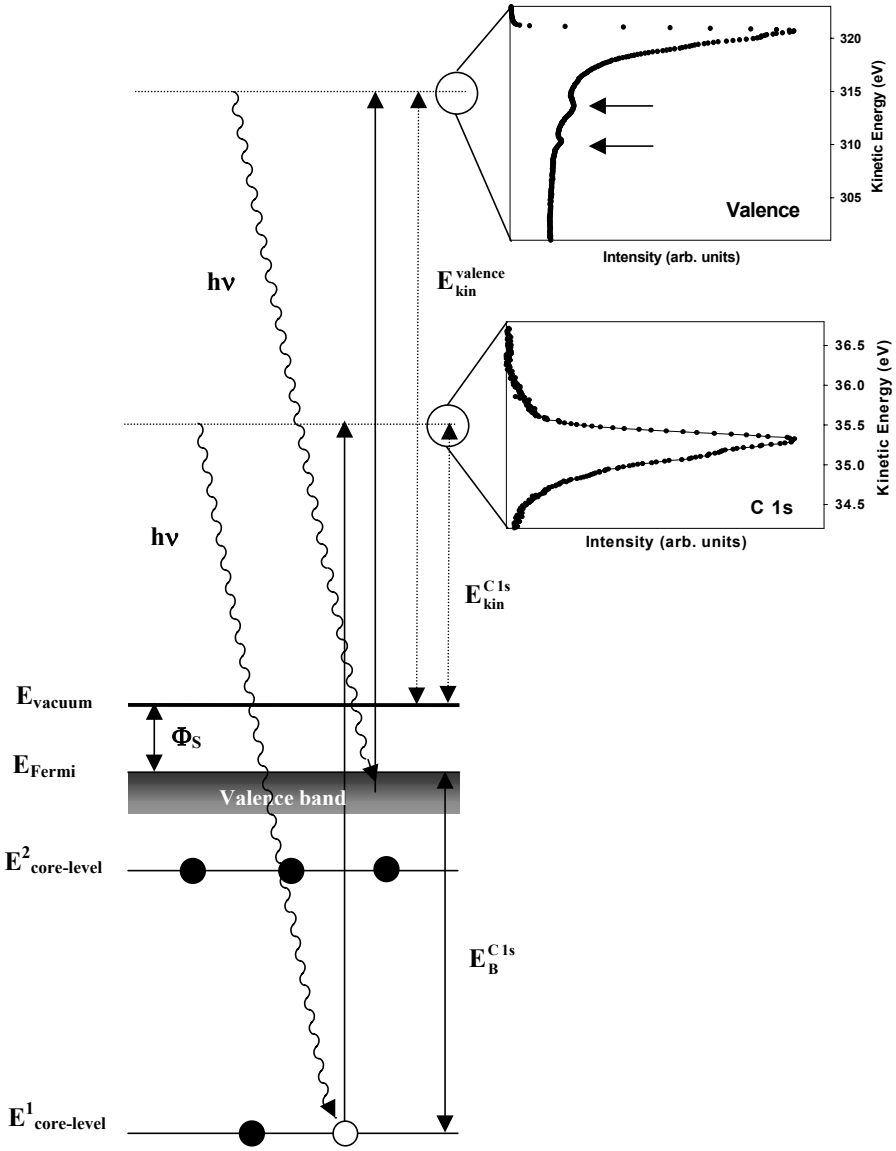

Figure 2.4: Graphical description of the photoemission process, with hν = 321 eV. The grey-shaded area represents the valence band of the sample. The inset figures give examples of recorded photoemission spectra where the lower and upper spectrum show the C 1s core level and valence band spectra of 1 L of CO on Co(0001) deposited at 110 K, respectively. The two arrows in the upper inset figure indicate CO related peaks (see sec. 2.4.2)

The photoemission spectrum uniquely identifies the elemental composition of the sample and to some extent also gives information on how the atoms are chemical bonded (see sec. 2.4.3).

A more comprehensive description of the binding energy is based on the total energy of the system: E_B is defined as the difference in total energy of a system before (N electrons) and after (N-1) ionisation, i.e.

$$E_B = E^{total}_{final\,state}(N-1) - E^{total}_{initial\,state}(N) \qquad (2.2)$$

where E_B is given with respect to some reference level. For single atoms or molecules this reference is usually the vacuum level, while for solids the Fermi level is often more practical.

In case of monoenergetic photons the binding energy can be determined experimentally by

$$E_B = h\nu - E^{analyser}_{kin} - \Phi_{analyser} \qquad (2.3)$$

$\Phi_{Analyser}$ is the workfunction of the electron analyser and is a known instrumental value. The process is illustrated schematically in Figure 2.5. When an electron is excited into vacuum it has an kinetic energy E_{kin}. To enter the analyser this photoelectron has to overcome the workfunction of the analyser, hence looses energy. The result is a detected energy of $E^{analyser}_{kin}$.

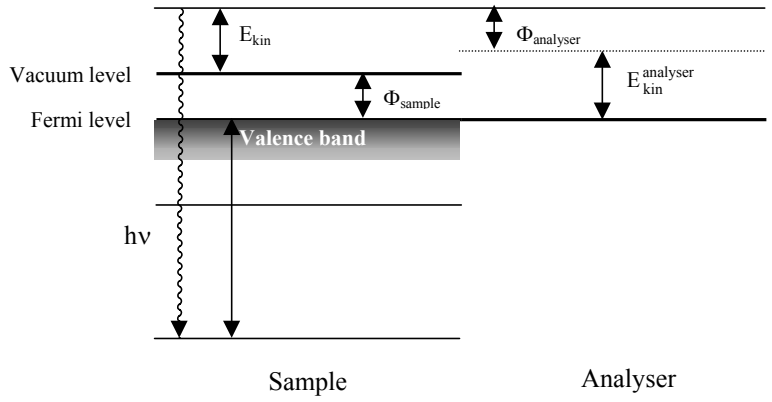

Figure 2.5: Energy-level diagram giving a graphical description of equation (2.3). Sample and analyser are both grounded.

2.4.2. Valence Band Photoemission Spectroscopy

The valence band refers to the levels occupied by electrons with low binding energies, i.e. near the Fermi edge (see figure 2.4). In this energy region the orbitals are quite delocalised, and the valence electrons interact strongly, forming bands. Since valence band spectroscopy

involves the outer shells of the atoms, the technique is generally very sensitive to the local chemical environment in the surface. As an example the valence band spectrum of CO adsorbed on Co(0001) is given in the upper inset spectrum of figure 2.4.

For clean Co(0001) the valence band is characterised by a narrow cobalt d band, extending to only 2 eV binding energy, and a flat featureless region above 2 eV where no metal levels appear [29]. Hence, the two features seen at ~7.4 eV and ~10.7 eV (marked with arrows) must be emission from electronic states of the adsorbed CO. Indeed previous work have shown that these can be assigned to the ($5\sigma + 1\pi$) and the 4σ orbitals of CO, respectively [30, 31].

The valence band measurements presented in this thesis (see Paper V and VI) are all recorded at normal emission.

2.4.3. High Resolution Core Level Photoemission Spectroscopy

In core level photoemission spectroscopy the more strongly bound electrons around the nuclei are probed. The atomic orbitals are more localised in this case, and hence reflect more the properties of the individual atoms. Even in solids these electron levels are normally assumed not to mix with the levels of neighbouring atoms. Therefore the properties of core level photoemission in general do not apply for valence band photoemission due to the intermixing levels in the valence band. Since all the measurements in this thesis were performed using high-brilliance light from synchrotron storage rings the technique is called high-resolution core-level photoemission spectroscopy to distinguish it from measurements using conventional Al-K_α ($h\nu = 1486$ eV) or Mg- K_α ($h\nu = 1254$ eV) X-ray sources.

Elemental analysis

Throughout most of the history of core level spectroscopy the main purpose has been to provide a compositional analysis of a surface. Observations of certain binding energy peaks in a spectrum can be taken as an indication of the presence of a particular elemental species [32]. A simple application is the detection of contaminants such as atomic carbon or atomic oxygen on a surface.

Core level shifts

Chemical shifts

Beside the element specific character, an important property of the core-level photoemission is the chemical shift. Changes of the local charge and potential of an atom lead

to a shift of the core level binding energy position [33]. Investigation of such shift can hence give information of how the atoms are chemically bound in a system. Since the first unambiguous observation was made in 1964 by Hagström and co-workers [34] these shifts have developed into a routine technique to identify and distinguish between different chemical species in a system.

In sec. 2.4.1 the core-level binding energy was defined based on the total energy of the system (eq. (2.2)). The chemical shift can be expressed in the same way between two systems A and B as [33]

$$\begin{aligned}\Delta E_B &= \left\{E^A_{final}(N-1) - E^B_{final}(N-1)\right\} - \left\{E^A_{ground}(N) - E^B_{ground}(N)\right\} \\ &= \Delta E^{B-A}_{final}(N-1) - \Delta E^{B-A}_{ground}(N) \end{aligned} \qquad (2.4)$$

Hence the shift is determined as the difference between the change in total energy of system A and B in the final (ionised) state and the corresponding change in the ground (unperturbed) state. Which term that dominates the chemical shift is highly system dependent. For two chemically dissimilar atoms on the same system, the ionisation energies will refer to the same initial state. The shift will thus be entirely due to the first term in eq. (2.4), i.e. the two final states. For example a large chemical shift between CO adsorbed in on-top (system A) and bridge-sites (system B) is found on Ni(100) where it is known that the two sites have quite similar total energies [35, 36]. Hence the chemical shift is in this case dominated by the final state term in eq. (2.4). However, in many other situations the shifts may be mainly determined by the initial state total energy terms. Figure 2.6 shows a similar chemical shift between CO adsorbed in on-top and bridge sites on Rh(100).

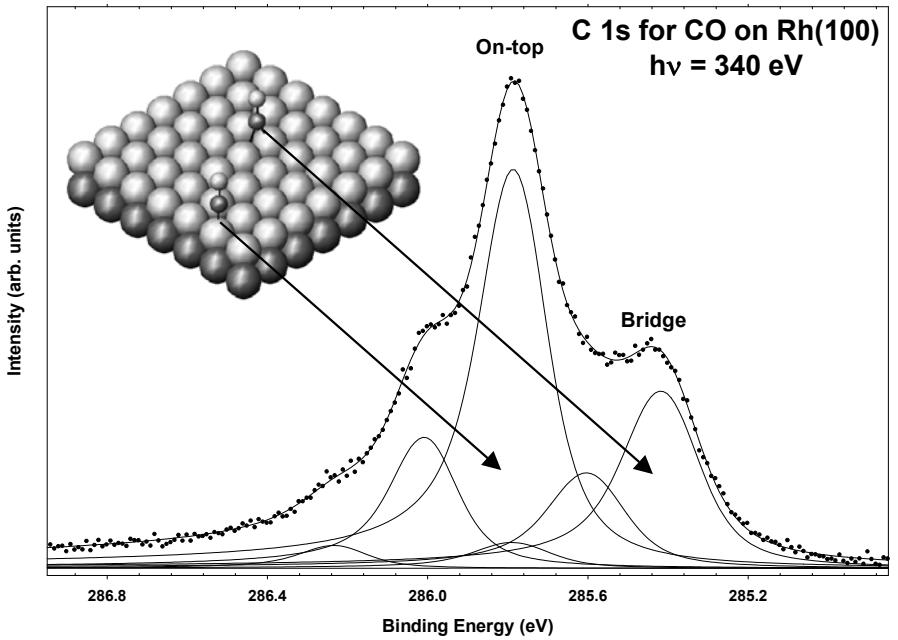

Figure 2.6: C 1s spectrum for CO adsorbed on a Rh(100) surface. The two main contributions at 285.78 eV and 285.41 eV originate from CO molecules adsorbed in on-top and bridge sites respectively, as illustrated in the inset figure. The experimental resolution was ≤ 70 meV.

The peaks at 285.78 eV and 285.41 eV are shown to originate from CO adsorbed in an upright position in on-top and bridge site, respectively [37, 38], giving a chemical shift of 0.37 eV. The additional lines on the high binding energy side of both peaks are due to vibrational losses (see later in this sec.)

Surface core-level shifts

The different amount of interaction with neighbouring atoms between the bulk and the surface creates a shift denoted surface core level shift (SCLS), and is found for most elements. For earlier elements of the transition metals (i.e. less than half filled d-bands) the SCLS tend to be to higher binding energies compared to the bulk contribution, and to lower binding energies for elements where the d-band is more than half filled. An example of the latter case is shown in Figure 2.7 for Rh(100), which has 8 electrons in the 4d band.

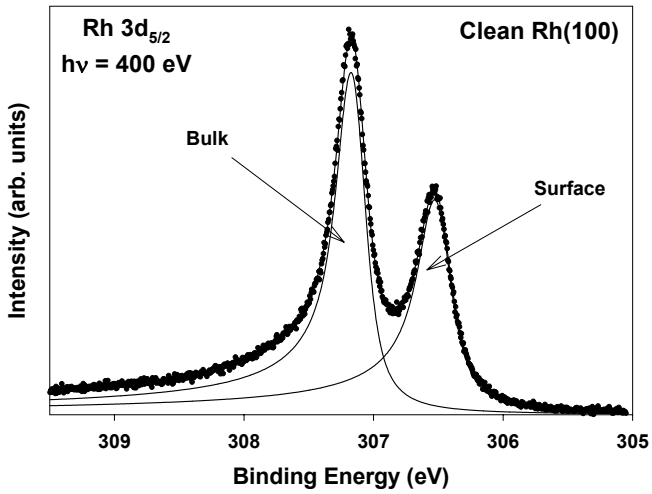

Figure 2.7: $3d_{5/2}$ core level photoemission spectrum of clean Rh(100) single crystal surface. The binding energies of the bulk and surface contribution are 307.18 eV and 306.53 eV, respectively. The experimental resolution was ~100 meV.

The separation (SCLS) is found to be 0.65 eV, which is in excellent agreement with the value reported in literature [39].

A simple, qualitative explanation of the SCLS for transition metals can be given based on the change in the d-band going from bulk to surface. Due to the lower coordination at the surface, and hence a lower number of hybridisation between the atoms, the d-band is expected to be narrowed. Since the occupancy is mostly unchanged for the surface atoms, the center of the d-band must shift up (down) in energy for d-band filling less than half (more than half) to assure alignment of the Fermi-levels. This shift is accompanied by shifts in the core-levels.

Equivalent core approximation

Based on thermodynamic arguments Johansson and Mårtensson [40] and Rosengren and Johansson [41] developed a method to calculate core level shifts. The main assumption of their model is a fully screened final (core-ionised) state, which actually occurs in metals. For the atomic valence electron orbitals, a core of the element of atomic number Z with one electron removed from a deep lying inner shell, can be replaced by a core of a Z+1 atom. This model is known as the *equivalent core approximation*. To connect the initial (unperturbed) state with the final state of the core ionisation process Johansson and Mårtensson introduced a Born Haber cycle as shown in Figure 2.8.

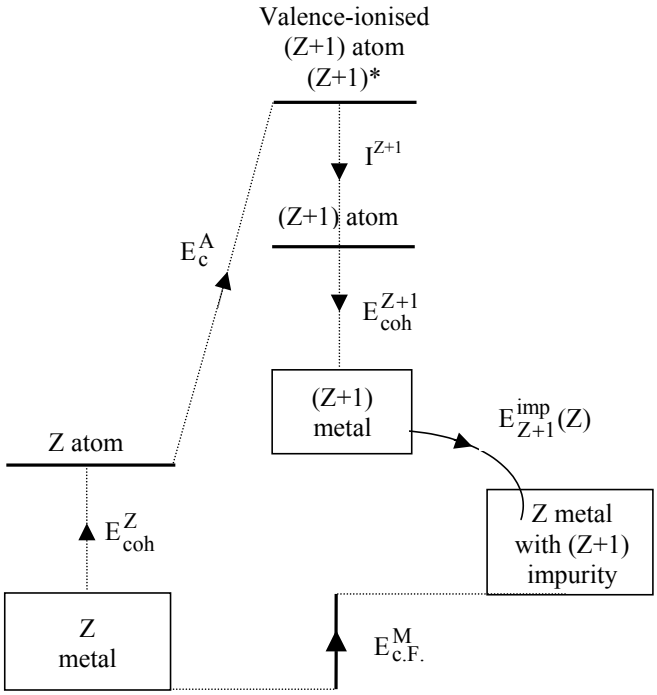

Figure 2.8: Born-Haber thermodynamical cycle for the calculation of the core level binding energy shifts [40]

From a metal of element Z one atom is removed (*cohesive energy,* $+E_{coh}^{Z}$ *per atom*) and then core-ionised (*binding energy of the free atom,* $+E_c^A$). Adding a valence electron releases the ionisation energy of a (Z+1)-atom ($-I^{Z+1}$). By bringing together a large number of such atoms a (Z+1)-metal is built (*cohesive energy,* $-E_{coh}^{Z+1}$ *per atom*). The last step is to dissolve the solid into a Z-metal ($+E_{imp}^{Z+1}(Z)$). The result of this process is the energy needed to bring a core-electron to the Fermi-level:

$$E_{c,F}^{M} = E_{coh}^{Z} + E_c^A - I^{Z+1} - E_{coh}^{Z+1} + E_{imp}^{Z+1}(Z) \qquad (2.5)$$

This expression can be used to calculate core-level shifts for molecules in different adsorption sites (see above), in alloys and intermetallic compounds and for surface atoms. The expression for the latter can be deduced by replacing the cohesive energies with surface cohesive energies ($E_{coh}^{Z,surf}$, $E_{coh}^{Z+1,surf}$), while the dissolution energy becomes a surface dissolution energy, $E_{imp}^{Z+1,surf}(Z)$. This gives the following expression for the surface core level shift:

$$\Delta E_{scls} = \left(E_{coh}^{Z+1} - E_{coh}^{Z+1,surf}\right) - \left(E_{coh}^{Z} - E_{coh}^{Z,surf}\right) - \left(E_{imp}^{Z+1}(Z) - E_{imp}^{Z+1,surf}(Z)\right) \qquad (2.6)$$

The variation in dissolution energy when going from the bulk to the surface is small, and is often discarded. Furthermore the first two terms give the variation of energy per surface atom, i.e. the surface energy. Eq. (2.6) can therefore be rewritten

$$\Delta E_{scls} = \gamma^{Z+1} - \gamma^{Z} \tag{2.7}$$

where γ^{Z+1} and γ^{Z} are the surface energies of the Z+1 and the Z metal, respectively.

In this thesis, the equivalent core approximation will only be used for qualitative arguments.

Line shapes and fitting procedures

The shape of a core-level photoemission peak depends on a range of physical parameters:

- Experimental resolution
- Finite lifetime of the core-hole
- Inelastic scattering of the photoelectrons
- Electronic shake-up and shake-off processes
- Vibrational excitations

The most important contributions are the broadening of the spectrum due to the experimental resolution and the natural lifetime width. To obtain information of how and to what extend each of these effects contribute to the measured peak, a proper decomposition is needed.

For the solid state the core-level photoemission line shape was calculated by S. Doniach and M. Šunjić [42] based on a theory developed by G. D. Mahan [43], P. Nozières and C. T. DeDominicis [44] for the corresponding problem of X-ray absorption. By combining this theory with the effect of a finite lifetime of the core hole, S. Doniach and M. Šunjić deduced the following expression for the line shape

$$f(E) = \frac{\Gamma(1-\alpha)}{\left(\varepsilon^2 + \gamma^2\right)^{(1-\alpha)/2}} \cos\left[\frac{\pi\alpha}{2} + (1-\alpha)\arctan\left(\frac{\varepsilon}{\gamma}\right)\right] \tag{2.8}$$

Eq. (2.8) is simply a convolution of $(1/\varepsilon^{1-\alpha})$, representing the electron-hole pair production over the Fermi edge, and a Lorentzian function describing the lifetime broadening. Γ is a gamma function and 2γ describes the full width at half-maximum (FWHM) of the Lorentzian. Furthermore, ε is the energy relative to the position of the maximum and α is an asymmetry parameter. The validity of eq. (2.8) is limited by assuming a free-electron idealisation with a constant density of states at E_f. Therefore the best results are obtained for simple sp metals such

as Na, Mg and Al. However, for the transition metals studied in this thesis, rhodium and cobalt, the Doniach-Šunjić expression is found applicable.

To obtain the final shape of the core-level photoemission spectrum other effects such as broadening induces by vibrations (molecules), phonons (solids), and limited experimental resolution must be taken into account. Both the phonons [45] and the experimental resolution can be described with Gaussian functions, while unresolved vibrational effects leads to an asymmetric broadening of the peaks. Hence, the overall line shape can be described by convoluting eq. (2.8) with a Gaussian function, with a slightly increased α, as exemplified in Fig. 2.6 and 2.7.

Vibrational Fine Structure in the core-level lines of adsorbates

General

A molecule is a system of bound nuclei, which can be stretched and compressed relative to each other. When an electronic transition takes place the nuclei undertake a redistribution of electronic charge that gives rise to a change in the Coulombic force. The bond strength is thus changed and the nuclei seek new equilibrium positions. This process induces vibrations and the absorption spectrum shows a structure characteristic of the vibrational energy levels of the molecule. Simultaneous electronic and vibrational transitions are known as *vibronic transitions.* Such transitions takes place in e.g. NEXAFS and XPS where electrons are excited to energy levels near threshold and into vacuum, respectively. In this thesis only vibrational fine structure of core-ionised molecules will be discussed.

The time scale of an electronic excitation caused by the electric field of a photon is about 10^{-17} to 10^{-18} sec. The typical lifetime of a core-hole in low-Z atoms before it is screened by nearby electrons (corresponding to the total lifetime of the electronic final state) is shown to be in the 10^{-15} – 10^{-14} sec. range. This again is fast compared to the vibrational motion of the nuclei, which typically occurs in approximately 10^{-13} sec.. The so-called *Born-Oppenheimer approximation* [46], which states that one can separate the nuclear and electronic degrees of freedom, is therefore well justified. Moreover, the *Franck-Condon principle* can be employed allowing the internuclear distance to be considered constant during the fast electronic excitation processes. Hence, the nuclear locations remain unchanged during the actual transition, but then readjust once the electrons have adopted their final distribution. An additional simplification is obtained when the displacement from the equilibrium position, $\Delta r = r\text{-}r_e$, are small. The potential energy can then be expressed as the first few terms of a Taylor series:

$$V(\Delta r) = V(0) + \left(\frac{dV}{d\Delta r}\right)_0 \Delta r + \frac{1}{2}\left(\frac{d^2V}{d\Delta r^2}\right)_0 \Delta r^2 + \frac{1}{3!}\left(\frac{d^3V}{d\Delta r^3}\right)_0 \Delta r^3 + \ldots \qquad (2.9)$$

Here the subscript 0 denotes that the derivates are evaluated at the equilibrium length, $\Delta r = 0$. At this point the potential energy curve is going through a minimum, and therefore the first derivative is identical to zero. If the displacement is small enough, the third order term can be neglected. Eq. (2.9) then simplifies to:

$$\Delta V(\Delta r) = V(\Delta r) - V(0) = \frac{1}{2} k \Delta r^2 \text{ where } k = \left(\frac{d^2V}{d\Delta r^2}\right) \qquad (2.10)$$

i.e. the potential energy for a linear harmonic oscillator. The corresponding energies of the vibrational levels are

$$E_v = (v + \frac{1}{2})\hbar\omega \qquad (2.11)$$

where v is the vibrational quantum number and ω is the vibrational frequency. The latter depends on the force constant k and the reduced mass μ of the bond:

$$\omega = \sqrt{\frac{k}{\mu}} \qquad (2.12)$$

A more realistic, but still highly approximate, function is the Morse potential energy, which correctly describes the strong repulsion of the nuclei at small internuclear distances and the dissociation at large:

$$V(\Delta r) = hcD_e(1 - e^{-a\cdot\Delta r})^2 \text{ where } a = \left(\frac{k}{2hcD_e}\right)^{1/2} \qquad (2.13)$$

h and c are Plancks constant and speed of light, respectively, and D_e is the depth of the potential energy curve. Due to the asymmetry of the Morse potential, the energy separation between the different vibrational level is not constant, but decreases with increasing vibrational quantum number (see fig. 2.7). However, for the first few vibrational levels the deviation from that of a linear harmonic oscillator is insignificant.

Figure 2.9 gives an example of a transition following the Franck-Condon principle, where the lower and upper part represent the energy diagram for a diatomic molecule in its unperturbed and excited electronic states, respectively.

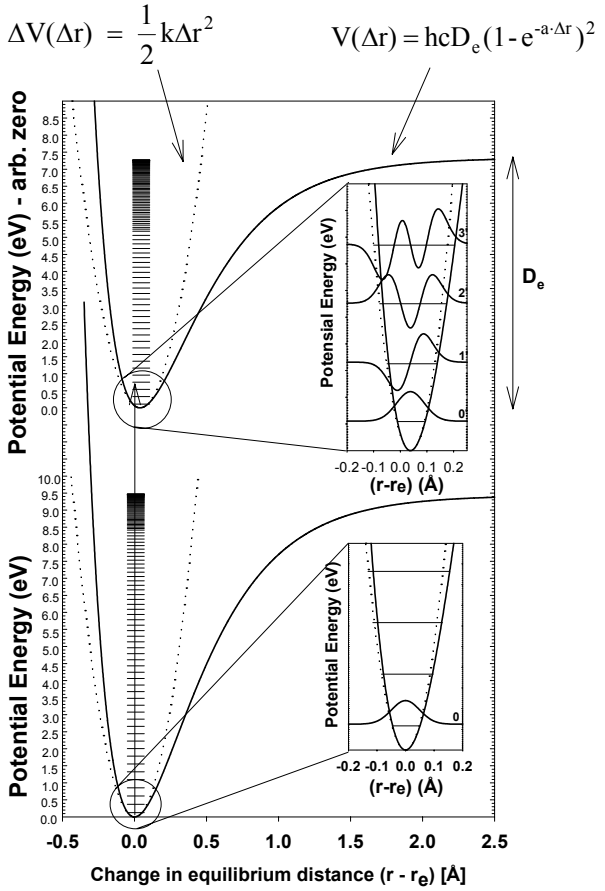

Figure 2.9: Illustration of the Franck-Condon principle. A diatomic molecule undergoes a vertical electronic transition from the unperturbed state to an excited state. Due to the redistribution of electronic charge the molecule seeks a new equilibrium position, represented as a displacement of the potential energy curve. For comparison both the harmonic potential (dotted lines) and the Morse potential (full lines) are given. The inset figures show the harmonic wavefunctions for the first vibrational levels.

The dotted curves describes the potential for a linear harmonic oscillator (eq. (2.10)), valid for small displacements of the nuclei, while the Morse potential (eq. (2.13)) is shown as full lines. For the latter, the corresponding vibrational energy levels are illustrated as horizontal marks. The convergence of the levels reflects the gradual decrease of confinement at high excitations. From the figure it is directly seen that a harmonic oscillator potential is a very good approximation for the first few vibrational energy levels. These are the vibrational levels that can be observed using high-resolution photoemission spectroscopy and NEXAFS. The validity of such an approximate potential is thus well justified. For the excited electronic state the first

four harmonic wavefunctions are calculated and shown in the upper inset figure. For temperatures at or below room-temperature the initial state in the photoemission process is the vibrational ground state of the unperturbed molecule. Hence in the lower inset in fig. 2.9 just the ground state wavefunction is shown. The Franck-Condon principle states that during an electronic transition the internuclear distance can be assumed constant. Therefore only those vibrational states of the excited electronic state can be reached in a "vertical" transition from the vibrational ground state whose wavefunction have a finite overlap with those of the electronic ground state.

As an example of such a vibrational progression the C 1s core-level spectrum of CO adsorbed in on-top sites on Co(0001) is displayed in Figure 2.10.

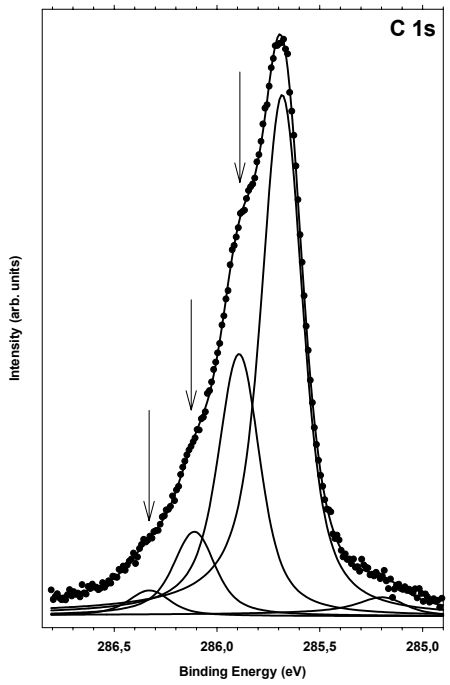

Figure 2.10: Normal emission C 1s photoelectron spectrum from the Co(0001)-($\sqrt{3}\times\sqrt{3}$)R30°-CO overlayer. The spectrum was recorded at a photon energy of 321 eV and with a resolution ≤ 60 meV. Filled circles: experimental data, lines: individual components of the decomposition and the resulting fit for the adsorbate spectrum.

The C 1s core level spectrum is decomposed using Doniach-Šunjić [42] line profiles convoluted by a Gaussian function [47]. The peaks at 285.89 eV, 286.11 eV and 286.33 eV (marked with arrows in the figure) are shown to originate from excitation of the first, second and third harmonic CO stretch vibrations, respectively.

Change in equilibrium bond length for diatomic molecules

The quantum mechanical description of the Franck-Condon process is based on the evaluation of the transition dipole moment between the ground vibronic state, |εν>, and the upper vibronic state |ε'ν'>. The dipole electric moment operator for a molecule depends on the positions and charges of the electrons ($\vec{r}_i$,-e) and the nuclei ($\vec{R}_n$,Z_ne):

$$\bar{\mu} = \bar{\mu}_e + \bar{\mu}_N = -e\sum_i \bar{r}_i + e\sum_n Z_n \bar{R}_n \tag{2.14}$$

The Born-Oppenheimer approximation allows the vibronic state |εν> to be rewritten as the product of the electronic and nuclear wavefunctions, i.e. $|\varepsilon\nu\rangle = \psi_\varepsilon(\vec{r};\vec{R})\psi_\nu(\vec{R})$, where $\vec{r}$ and $\vec{R}$ denote the electronic and nuclear coordinates[3]. Within this approximation the following expression of the transition moment is deduced:

$$\begin{aligned}\left\langle \varepsilon'\nu' \middle| \bar{\mu} \middle| \varepsilon\nu \right\rangle = {} & \int \psi^*_{\nu'}(R)\left\{\int \psi^*_{\varepsilon'}(r;R)\bar{\mu}_e\psi_\varepsilon(r;R)d\tau_e\right\}\psi_\nu(R)d\tau_N \\ & + \int \psi^*_{\nu'}(R)\bar{\mu}_N\left\{\int \psi^*_{\varepsilon'}(r;R)\psi_\varepsilon(r;R)d\tau_e\right\}\psi_\nu(R)d\tau_N\end{aligned} \tag{2.15}$$

The final term is zero since the electronic states are orthogonal to one another for each value of $\vec{R}$. The remaining integral over electronic coordinates is the electrical dipole moment for a certain separation $\vec{R}$. If the nuclei are not displaced by a large amount from equilibrium, r_e, this dipole moment can be approximated by a constant $\bar{\mu}_{\varepsilon'\varepsilon}$. The resulting transition moment between |εν> and |ε'ν'> is:

$$\left\langle \varepsilon'\nu' \middle| \bar{\mu} \middle| \varepsilon\nu \right\rangle = \bar{\mu}_{\varepsilon'\varepsilon} S(\nu',\nu) \tag{2.16}$$

$$\text{where } S(\nu',\nu) = \int \psi^*_{\nu'}(\bar{R})\psi_\nu(\bar{R})d\tau_N \tag{2.17}$$

Eq. (2.17) is the overlap integral between the two vibrational states in their respective electronic states, integrated over all nuclear coordinates. Hence the largest transition moment is obtained when the vibrational states have the greatest overlap. A graphic representation of eq. (2.17) is shown in Figure 2.11 for the specific case of core-ionised CO adsorbed in on-top site on Rh(100).

[3] For each nuclear arrangement there is a separate electronic wavefunction. Hence the electronic wavefunction depends parametrically on the nuclear coordinates.

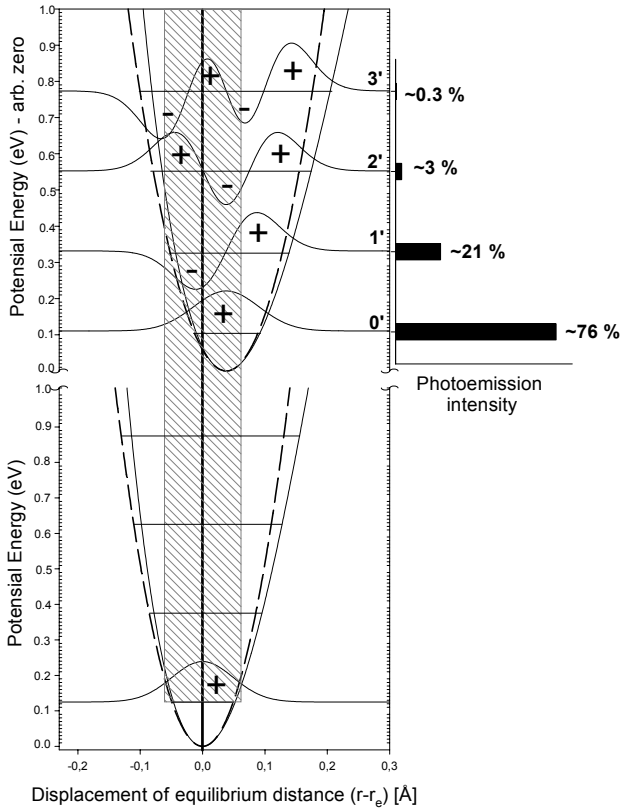

Figure 2.11: Graphic representation of the wavefunction overlap intergral given in eq. (2.17). As in figure 2.9 the curves shown as full and short dashed lines are the Morse- and linear harmonic oscillator potential, respectively. The first four vibrational energy levels are given, together with the resultant harmonic wavefunctions. The range of internuclear distances spanned by ~80 % of the ground state vibrational wavefunction is shaded. The horizontal bars on the left display the intensity distribution due to the wavefunction overlap.

If no changes in the equilibrium distance take place, the wavefunctions will be close to orthogonal and most of the transitions go to the ground state of the excited molecule. However, a displacement from the equilibrium position introduces non-orthogonality, and hence significant transitions to higher vibrational levels can occur. These transitions are observed as a series of peaks in the electronic spectrum as observed in fig. 2.10 and illustrated by the horizontal bars on the left in fig. 2.11. The relative intensities of the peaks are proportional to the square of the transition dipole moment, $|S(\nu',\nu)|^2$, a value commonly known as the *Franck-Condon factor*. For linear molecules as CO the displacements of the nuclei are only along the molecular bond, and the calculation can therefore be considered as a one-dimensional problem.

The Franck-Condon factor for transition to any vibrational state in the excited molecule then takes the form

$$|S(\nu',0)|^2 = \left(\int_{-\infty}^{\infty} \psi^*_{\nu'}(x - \Delta r)\psi_{\nu}(x)dx \right)^2 \tag{2.18}$$

where $\psi_{\nu'}$ and ψ_{ν} are the vibrational states for the excited and unperturbed electronic states, respectively and Δr is the increase of the equilibrium distance for the excited state relative to the unperturbed. In fig. 2.9 the harmonic oscillator potential was seen to be a good approximation for the first vibrational levels. Therefore the normalised ground state vibrational wavefunctions for the initial and ionised molecule can be employed [48]:

$$\psi_0 = \left(\frac{2\alpha_u}{\pi}\right)^{1/4} e^{-\alpha_u x^2} \quad \text{and} \quad \psi_{0'} = \left(\frac{2\alpha_e}{\pi}\right)^{1/4} e^{-\alpha_e (x \mp \Delta r)^2} \text{ with } \alpha_i = \frac{\mu\omega_i}{2\hbar} \tag{2.19}$$

μ is the effective mass of the diatomic molecule and ω_i is the angular frequency of the vibration for the two electronic states. The subscripts u and e signify unperturbed and excited states, respectively. The effective mass is assumed constant before and after chemisorption onto the substrate. The integral in eq. (2.18) can be calculated analytically using the wavefunction in eq. (2.19), giving the following expression for the change of the equilibrium distance:

$$\Delta r = \sqrt{\frac{(\alpha_u + \alpha_e)}{2\alpha_u\alpha_e} \ln\left(\frac{2(\alpha_u\alpha_e)^{1/2}}{|S(0,0)|^2(\alpha_u + \alpha_e)} \right)} \tag{2.20}$$

For the specific case of CO adsorbed in on-top site on Rh(100) the intensity of the adiabatic[4] peak relative to the total is found to be 0.76, i.e. $|S(0,0)|^2 = 0.76$. The extracted vibrational energy splitting ($\hbar\omega_e$) is 221 meV. From Electron Energy Loss Spectroscopy (EELS) measurements performed by others [49] the corresponding energy splitting for the unperturbed molecule ($\hbar\omega_u$) is reported to be ~250 meV. Inserting these values in eq. (2.20) a change of equilibrium distance of 3.8 pm is deduced. Since the vibrational frequency is reduced for the core-ionised molecule, the direction of the change is to higher bond length, i.e. the core-ionisation process lead to an elongation of the C-O bond.

The linear coupling model

The derived equation for the change of equilibrium distance (eq. (2.20)) is only valid for diatomic molecules. Therefore a more general model is needed when studying the vibrational structure of more complex molecules. If the potential energy surfaces of the unperturbed and

excited molecule are assumed to differ only in linear terms, a model for the internal molecular vibrations known as the linear coupling model is applicable [50]. In this approximation the intensities of the vibrational components in the photoemission spectrum follow a Poisson distribution:

$$I(0-\nu_1,\ldots,0-\nu_n) = I(0-0,\ldots 0-0)\cdot\prod_{i=1}^{n}\frac{S_i^{\nu_i}}{\nu_i!} \qquad (2.21)$$

where I(0 - ν') is the photoemission intensity for a transition between the ground state of the unperturbed molecule and the final state ν' in the excited molecule. The S-factor in the Poisson distribution is obtained from experiment simply by taking the ratio between the first vibrational component and the adiabatic component in a photoemission spectrum. The multiplication is done over all excited vibrational modes. Eq. (2.21) confines the intensity distribution of the vibrational progression, and together with the constant separation of the harmonic vibrational energy levels, it can be used to connect the intensities and energy positions of the different components in the vibrational fine structure. This has been employed for the study of C_2H_2 on Co(0001) (Paper I) and CO on Rh(100) and Co(0001) (Paper III).

For a single symmetric stretch mode the S-factor in eq. (2.21) can be expressed as

$$S = \frac{m}{2}\cdot\frac{\mu\omega}{\hbar}\left(\frac{\omega'}{\omega}\Delta r\right)^2 \qquad (2.22)$$

where Δr is the change in equilibrium position, m is the number of identical bonds[5] and μ is the effective mass of the nuclei involved in the vibrational mode. In addition a factor $(\omega'/\omega)^2$ is included to take into account the difference in vibrational frequency for the unperturbed (ω) and excited (ω') molecule [51]. Hence the linear coupling model gives an S-factor which is proportional to the effective mass. This is also the case for the energy separation ΔE between the vibrational components for a harmonic oscillator (eq. (2.11)). For the specific case of hydrocarbons this dependency can be used to determine if the structure seen in a spectrum is due to internal molecular vibration of the C-H bond. By replacing the hydrogen with deuterium the only effect will be an increase of the effective mass. Using eq. (2.12) and (2.22) the following ratios of the frequencies and S-factors of the hydrocarbon molecule and its deuterated counterparts are therefore obtained:

$$\varpi_D \approx \frac{1}{\sqrt{2}}\varpi_H \qquad (2.23)$$

[4] Adiabatic means here excitations to the ground state of the excited molecule.
[5] E.g., for the C-H stretch mode in ethylene (C_2H_4), m ≡ 2

$$S_D \approx \sqrt{2} S_H \quad (2.24)$$

The relations are highly approximate. However the overall trend of reduced energy separation and increased S-factor for the deuterated molecule should be observed. Figure 2.12 shows the C1s spectra of acetylene and deuterated acetylene, where such an effect is clearly seen.

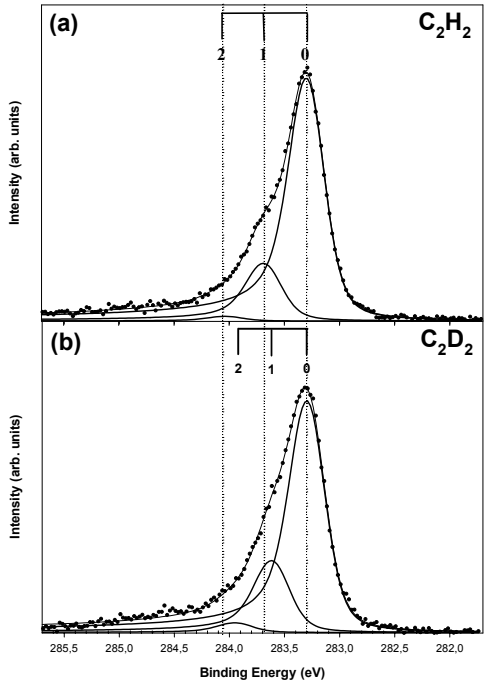

Figure 2.12: C 1s photoemission spectra after a saturation exposure of (a) acetylene (C_2H_2) and (b) deuterated acetylene (C_2D_2) on Co(0001). Both spectra were measured at a photon energy of 320 eV and with a resolution ≤ 111 meV. The fine structures of both the C-H and C-D stretch vibrations are marked with vertical lines.

2.4.4. Photoelectron diffraction

In solids, when an electron is emitted from a core level of an atom, components of the electron wavefield may scatter elastically by the nearby atoms. The interference of the scattered and directly emitted parts of the electron waves is determined by the position of the emitting atom relative to the surrounding scattering atoms. The result is a variation of the core level peak intensity with emission angle and photon energy, which contains information on the local geometry around the emitter. For atoms in the same structural environment, the same diffraction behaviour should be observed. Hence by simply varying the angle of the sample or the energy of the incoming photons chemical shifts due to different adsorption sites can be

verified [52-54]. An example of such an effect is given in figure 2.13, which shows the intensity variation due to two adsorption sites of CO on Co(0001).

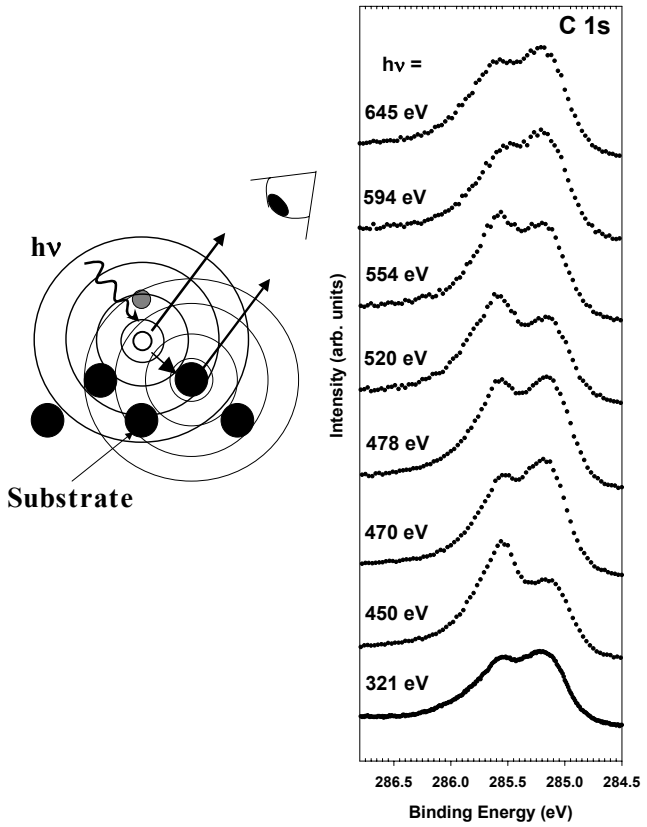

Figure 2.13:

On the left: Schematic illustration of electron diffraction in core level photoemission. The black circles represent the substrate, the white and grey circles the carbon and oxygen atoms, respectively, constituting the CO molecule.

On the right: Photon energy dependence of the two C 1s components in the Co(0001)-2√3×2√3-CO system measured at normal emission. The overlayer is prepared by exposing 10 L CO on the Co(0001) surface at 90 K.

The high binding energy component has been verified as due to CO adsorbed in on-top site [55, 56]. The other component is still unresolved but is suggested to be either bridge or three-fold hollow site [57]

In the case of quantitative estimations diffraction effects may lead to wrong results, especially at low electron kinetic energies. By using higher photon energies, this effect can be minimised. In fig. 2.13 a clear stabilisation of the intensity ratio is seen for photon energies above ~600 eV. However, increasing the photon energy will influence negatively on other

experimental parameters, such as lower photon flux with lower energy resolution, and decreasing photoionisation cross section [58].

2.5. Near-edge X-ray absorption fine structure (NEXAFS)

2.5.1. General

In NEXAFS (near edge x-ray absorption fine structure), photon energies close to the K-edge of one constituent atom are used to investigate bound and continuum state resonances of molecules [59-61]. In general this technique is not as surface sensitive as photoemission spectroscopy since the electrons that are detected are secondary electrons which originates from typically the top ~50 Å of the surface layer (fig. 2.1). However, by careful normalisation and background corrections [62] important properties of the adsorbates can be extracted. Figure 2.14 shows the principles of NEXAFS using a schematic diagram of the potential wells in a diatomic molecule. The figure shows the electronic states for a diatomic molecule in gas-phase. The most prominent are the π^* and σ^* molecular states, as exemplified in the C-K shell spectrum on the right. The former corresponds to a transition of a 1s electron into an empty or partially filled antibonding π^* orbital ($1s \rightarrow 2\pi^*$ in CO) which is pulled below the vacuum level by the electron-hole Coulomb interaction. The σ^* resonance (commonly called the shape resonance) is located at energies typically 5-20 eV higher than π^* and represent transitions from 1s into a quasi-bond state located immediately above the vacuum level (see figure text). In addition, the Schrödinger equation predicts empty Rydberg states just below the vacuum level and a continuum of empty states above. Usually NEXAFS is used in connection with studies of adsorbed molecules on crystal surfaces. For strongly chemisorbed molecules one would expect pure Rydberg resonances to be quenched since electrons from the substrate would populate these states, and can thus serve as an indicator of the degree of hybridisation. The spectrum on the right of fig. 2.14, CO on Co(0001), is an example of a system showing a strong chemisorption.

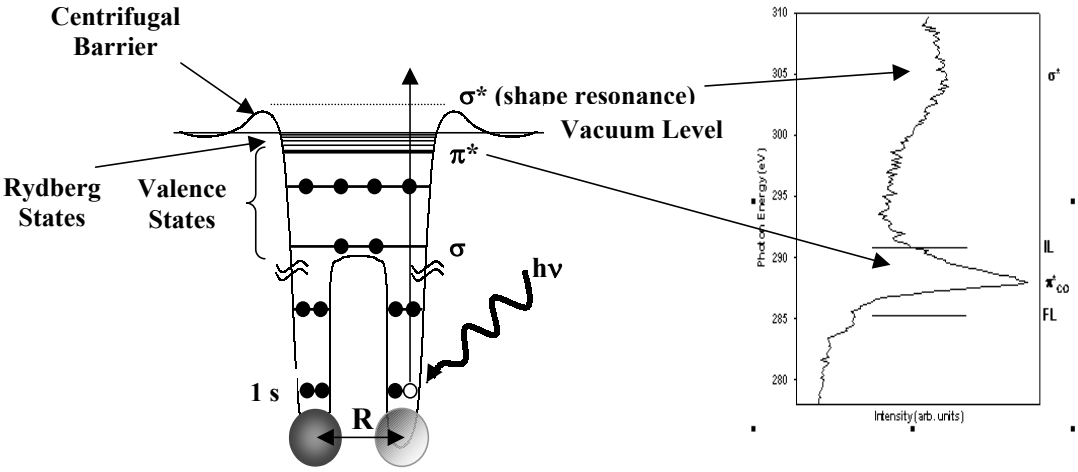

Figure 2.14: Potential wells in a diatomic potential displaying the bound states below the vacuum level and the σ* resonance above [62]. The effective potential includes a centrifugal term proportional to $l(l+1)/r^2$, where l is the angular momentum of the molecule. R is the equilibrium bond length between the two atoms. This term gives rise to a barrier above the vacuum level that may "trap" an excited electron for enough time to be measured. The spectrum to the right shows the carbon K-shell NEXAFS spectra of the Co(0001)-($\sqrt{3}\times\sqrt{3}$)R30°-CO overlayer for a X-ray incidence angle of 45°. FL and IL denote the C 1s binding energies and ionisation limits, respectively (see paper III).

2.5.2. Molecular Orientation and Hybridisation Strength

In the study of CO and NO chemisorption on Ni(100), J. Stöhr et al. [63, 64] showed that the intensity of the dominant π* and σ* resonances have a strong angular dependence with the electric field vector ***E***. The polarised nature of the synchrotron radiation can thus be used to extract information about the molecular orientation on a surface. This is achieved by rotating the sample with the molecule bonded to its surface in the photon beam, thereby changing the orientation of the molecule relative to the ***E*** vector. Since the K-shell NEXAFS resonance intensities are governed by the dipole selection rules *the resonance intensity associated with a specific molecular orbital final state is largest if the* ***E*** *vector points in the direction of that molecular orbital, and the intensity vanishes if* ***E*** *is perpendicular to the direction of the orbital* (quote from [62] p. 170). An example of such a polarisation dependence between the intensities of the π* and σ* resonances and the E vector is given in Figure 2.15 for acetylene chemisorbed on Co(0001).

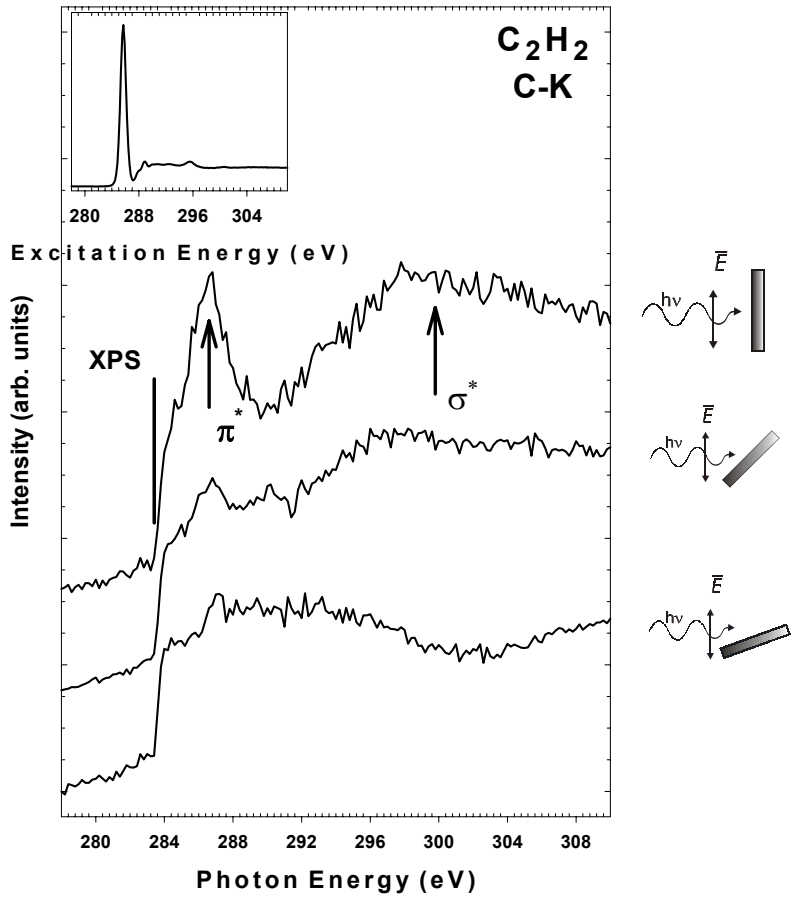

Figure 2.15: Polaization-dependent Carbon K-shell NEXAFS spectra of acetylene (C_2H_2) chemisorbed on Co(0001) recorded at 110 K for X-ray incidence angles of 90°, 45° and 20°, relative to the surface plane. The spectra are all normalized by the intensity of the Fermi edge with maximum at ~283.7 eV. Inset figure: ISEELS K-shell spectra of gaseous acetylene [65]

The triple bond in gaseous acetylene is a combination of one σ-bond and two π-bonds. Their antibonding orbitals are oriented perpendicular to each other, with the σ* orbital located along the C-C bond. From fig. 2.15 it is seen that this orbital reaches the highest intensity when the E-vector is in the surface plane. Hence, according to the dipole selection rules described above the carbon-carbon bond of the acetylene molecule has close to parallel orientation with respect to the surface.

If the acetylene molecule is weakly hybridised with the surface one would expect a strong contribution at grazing incidence from the π* orbital perpendicular to the surface. Such a contribution is not seen in the case of C_2H_2 on Co(0001), which is interpreted as due to

substrate electrons populating this orbital during the hybridisation process. Comparing with ISEELS data from gaseous acetylene (inset in fig. 2.15) it is clear that the other π* orbital, i.e. parallel to the surface, is also strongly modified. Hence, by adsorbing acetylene molecules on Co(0001), the initial sp-hybridisation is changed to a state near sp^3.

Figure 2.16 further confirms the ability of NEXAFS to reveal the hybridisation strength between an adsorbate and the substrate.

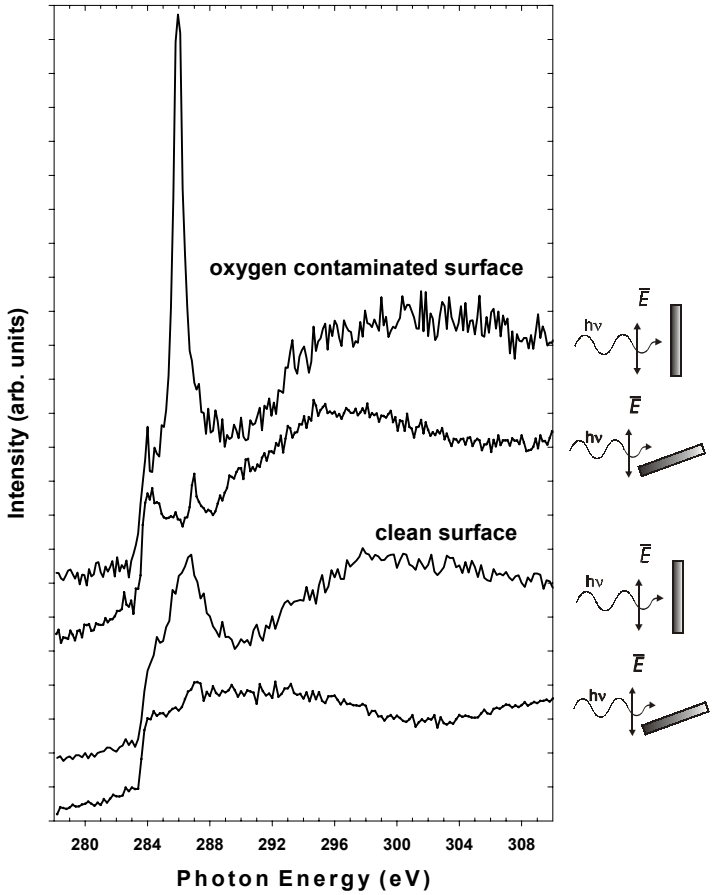

Figure 2.16: Carbon K-edge NEXAFS spectra for acetylene on Co(0001) at ~110 K as a function of X-ray incidence (normal and grazing). The upper two spectra show the result from an oxygen-contaminated surface while the two lower spectra are the results from exposure on a clean surface.

By contaminating the cobalt-surface with some oxygen prior to acetylene exposure the component of the π* orbital parallel to the surface is more preserved, and the acetylene experience a weaker hybridisation than the case for clean Co(0001).

In addition to the height, the width of the π* resonance contains information about the degree of hybridisation. For strongly chemisorbed molecules the excited electron can decay into the conduction band, and the reduced lifetime of the excited state cause a broadening of the resonance. This effect is clearly seen in fig. 2.16 for the spectra recorded with normal X-ray incidence where the FWHM (full width at half maximum) for the π* resonance of clean and oxygen-contaminated Co(0001) are found to be 1.7 eV and 0.6 eV, respectively.

2.5.3. σ* Resonance Position and Bond Length

Since the early 1980s till today the question of a correlation between the σ* resonance position and the molecular bond length has been the subject of extensive discussions. As seen in the schematic representation of the effective potential in fig. 2.14 the σ* resonances are related to the details of the atomic or molecular potential, hence a correlation with the bond length is intuitively clear. A more comprehensive investigation of this correlation was performed by J. L. Dehmer et al. [66] using Xα MS calculations to study the nuclear motion effects in N_2. By calculating the cross section for photoionisation of the $3\sigma_g$ valence level of N_2 in the excitation region of the σ* resonance he showed that the energy position of σ* is very sensitive to the internuclear distance.

In the following years this observation has been thoroughly examined [67-71]. In particular attempts of relating the position of the σ* resonance to the C-C bond length of unsaturated hydrocarbons has been given special attention [72-77] due to their fundamental significance. In 1984 J. Stöhr and co-workers proposed the so-called "bond-length with a ruler" [72], i.e. a simple relation to find the C-C bond length (Figure 2.17).

The validity of using the σ* resonance to give a quantitative estimate of the bond length of adsorbed molecules has been a target of criticism [79]. In addition, it has been claimed that the broad feature in the photoabsorption cross section of gaseous C_2H_2, centred at ~310 eV, is largely due to satellite contributions [80], i.e. the true σ* resonance predicted in theory [81] is weak. However, this has been contradicted in more recent publications [82- 84].

If a σ* resonance is present in a molecule it seems clear that for its energy position there exist a trend of decreasing bond length with increasing energy position relative to the ionisation limit. Hence, including this effect with the broadening and decrease of the π* resonance commented earlier, NEXAFS is a powerful technique to measure the strength of hybridisation of an adsorption system.

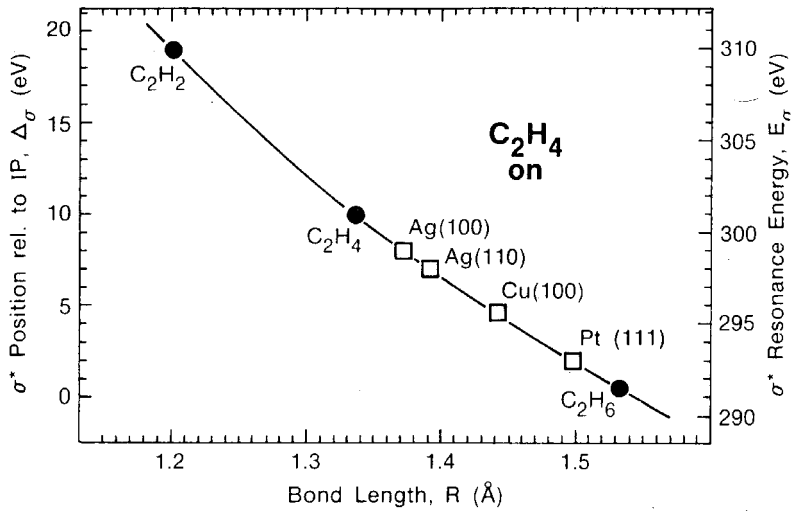

Figure 2.17: σ* resonance position versus carbon-carbon bond length for acetylene, ethylene and ethane gas (solid cicles) and resonance positions observed for ethylene chemisorbed on some metal surfaces (open squares) [62]. The data points have been plotted as a function of either Δ_σ, the σ* resonance position relative to the ionisation limit (IP*) (left ordinate*), or E_σ, the absolute σ* resonance position (*right ordinate*). The solid curve corresponds to an inverse quadratic ($\propto 1/R^2$) relationship, obtained by Gustafsson et al. [78].

2.6. Scanning Tunneling Microscopy (STM)

The STM was invented and developed by Gerd Binnig, Heinrich Rohrer and coworkers at the IBM research laboratories in Zürich, Switzerland, in the early 1980s [85-87]. In July 1982 topographic pictures of surfaces on an atomic scale were presented in Physical Review Letters for (110) surfaces of $CaIrSn_4$ and Au [86,87], which demonstrated the instruments powerful quality as a surface analysis tool. For this pioneering work they were awarded the Nobel price in physics in 1986.

The principle of STM is quite simple. In a conductor the electron wavefunction at the Fermi level leak out of the confining potential wells described with a characteristic exponential inverse decay length κ

$$\kappa = \hbar^{-1}\sqrt{2m_e\varphi} \tag{2.25}$$

where m_e is the electron mass and φ is the effective local work function. By bringing two conductors sufficiently close together these wavefunctions overlap and quantum mechanical tunneling of electrons are permitted across the gap. If a bias voltage V_t is applied to the sample, these tunneling electrons produce a current I_t in the nano-ampere regime flowing from the tip to the sample or vice versa, depending on the polarity of V_t. Figure 2.18 gives a schematic

illustration of how the tunneling current is set up by the electron wavefunction overlap. In this case the direction of the current will go from the occupied states of the tip into the empty states of the sample. (marked with an arrow). Within the limit of small V_t and assuming the tip as spherical with a radius of curvature R, Tersoff and Hamann developed a fairly simple expression for the tunneling conductance [88]:

$$G_t \equiv \frac{I_t}{V_t} \approx 0.1 R^2 e^{2\kappa R} \rho_S(\bar{r}_t, E_F)$$

$$\rho_S(r_t, E_F) \equiv \sum_v \left|\psi_v(r_t)\right|^2 \delta(E_v - E_F) \qquad (2.26)$$

where $\rho_S(\bar{r}_t, E_F)$ is the local density of states (LDOS) of the sample at the Fermi level calculated at the centre position $\bar{r}_t$ of the tip and κ is the decay length of the wave function in vacuum given in eq. (2.25).

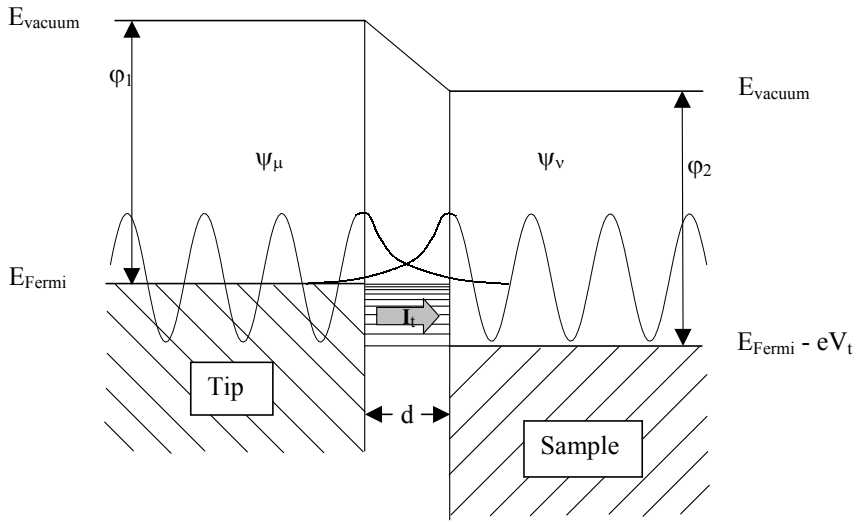

Figure 2.18: Energy diagram illustrating the tunneling between two conductors

In the model of Tersoff and Hamann the STM topographs can be interpreted as contours of constant $\rho_S(\bar{r}_t, E_F)$ of the surface, i.e. constant LDOS at the Fermi-level.

By substituting $\left|\psi_v(r_t)\right|^2 \propto e^{-2\kappa(R+d)}$ in eq. (2.26) the tunnel conductance can be expressed as

$$G_t = \frac{I_t}{V_t} \propto e^{-2\kappa d} = e^{-1.025\sqrt{\varphi}d} \qquad (\varphi \text{ in eV and d in Å}) \qquad (2.27)$$

i.e. an exponential decay of the conductance with increasing distance d between the tip and the surface. Eq. (2.27) can be used to find estimates of important factors which limit the atomic resolution in STM. For a typical value of 4 eV for φ a change of the tip-sample distance d by 1 Å results in a variation of a factor of ten in I_t. As a consequence only the atoms closest to the sample contribute to the tunneling current.

Figure 2.19 shows a practical implementation of an STM setup. A tip (typically W or PtIr) is brought to ~5-10 Å of the sample. Three dimensional motion at a sub-Ångström level is accomplished using three orthogonal piezoelectric transducers.

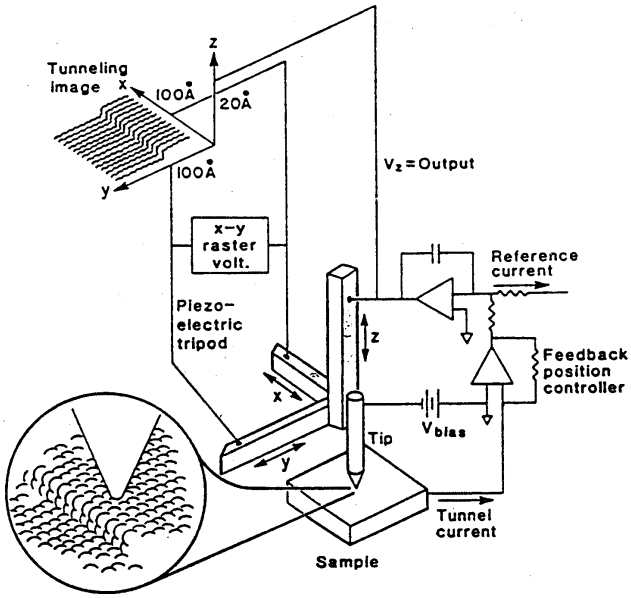

Figure 2.19: Principle of operation of the scanning tunneling microscope [89]

The tunneling current I_t is then produced by applying the voltage V_t (V_{bias} in fig. 2.17) between the tip and sample. By scanning the tip across the sample, an image of the sample topography is achieved. Characteristic values for the tunneling current and voltage are 0.1 - 10 nA and 1 mV - 1 V respectively for metal surfaces. One way to avoid tip-sample contact is to adjust the height continuously to maintain a constant tunneling current using a feedback loop (fig. 2.19). By recording the tip height as a function of lateral position, z(x,y), a constant-current image of the surface is obtained. This “constant current mode” is the most common way to operate the STM. Another way of achieving sample topography is keeping the tip at constant position relative to the surface and scanned with virtually no feedback while monitoring the variation in I_t. In this work only the constant current mode has been utilised.

Figure 2.20 show examples of STM images for the case of ~0.2 ML[6] La deposited on Rh(100) at 300 K. The large image is of size 1000×1000 Å^2, and the two small on the right are both 50×50 Å^2. At this coverage La islands of varying size and shapes are formed, ranging from a few atoms up to a length ~100 Å. In addition a step is observed in the high crystallographic direction of Rh(100) (fig. 2.20a).

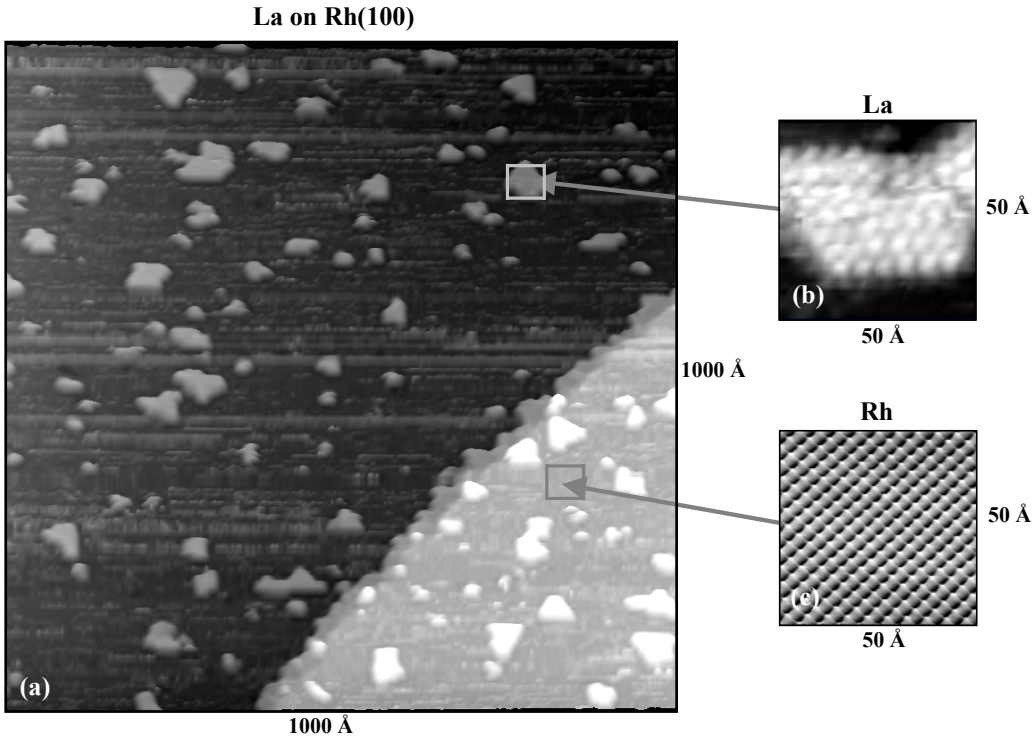

Figure 2.20: STM images of submonolayer coverage of La on Rh(100). (a) 1000 × 1000 Å^2 image of ~0.2 ML La deposited at room-temperature on Rh(100). (b) and (c) 50 × 50 Å^2 images of an La island and the clean Rh(100) substrate, respectively. Their references to the squares in image (a) are meant for illustrations only, and do not represent actual positions. The horizontal lines seen between the La islands are caused by a high reactivity between the La atoms and the tungsten tip.

The fact that islands of size up to 100 Å can be observed shows that the deposited La-atoms have some mobility on the rhodium surface at 300 K.. In general, STM has proved to be a powerful technique to explore the dynamics of growth. For instance in paper VII STM

[6] 1 ML (monolayer) is here defined as a single complete atomic layer.

measurements have been employed to reveal a high degree of anisotropic diffusion during the homoepitaxial growth of Co on $Co(11\bar{2}0)$.

2.7. Low energy electron diffraction (LEED)

Low Energy Electron Diffraction is the oldest technique, which gives access to the atomic structure of surfaces. Its history goes back to 1927 when C. J. Davisson and L. H. Germer observed (accidentally) the electron diffraction pattern from a Ni crystal [90,91]. These findings give an experimental proof of the wave nature of electrons. However, due to the presence of adsorbed species on the surface the reproducibility of these first studies was poor and not improved before the start of the UHV technologies in the sixties (sec. 2.3).

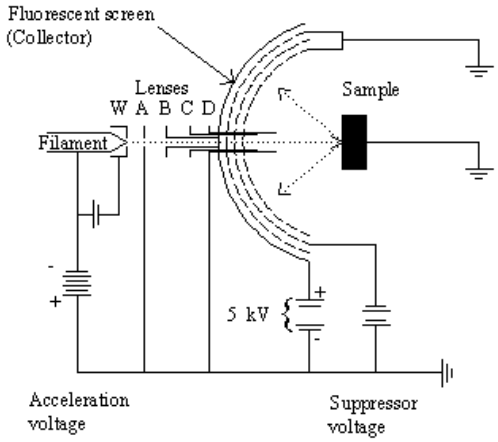

Figure 2.21: Schematic of a LEED display system.

Figure 2.21 shows a schematic illustration of a typical LEED apparatus. The main elements are an electron gun providing a collimated beam of electrons in the range 20-500 eV, a sample holder, retarding grids and a hemispherical fluorescent screen on which the diffracted electrons are observed. The first grid is connected to earth ground to provide an essentially field-free region between the sample and the first grid. A suitable negative potential is applied to the second grid (suppressor) to restrict the transmission to the fluorescent screen to involve only a narrow range of elastically scattered electrons. Also the third grid is usually grounded to reduce field penetration of the suppressors by the screen voltage when a potential of a few kilovolts is applied to the screen in order to accelerate the diffracted electrons.

In the energy range specified the de Broglie wavelengths of the electrons are in the same order of magnitude as the typical interatomic distances in crystals. In addition the electron mean

free path is near its minimum, i.e. ~5-10 Å (see fig. 2.1 in sec. 2.1), restricting the outgoing elastic electrons to only the first few layers.

If long range ordering is present on the surface a diffraction pattern as the example shown in Figure 2.22 can be observed.

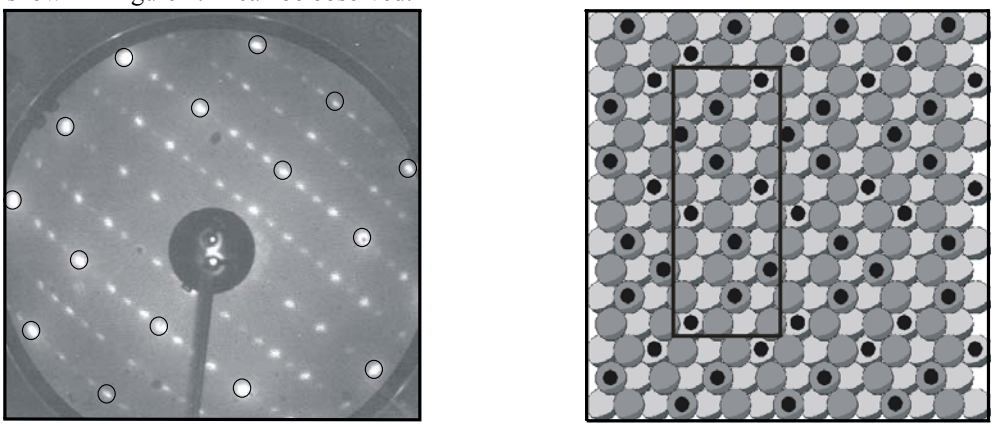

Figure 2.22: The LEED pattern (reciprocal space) for 0.25 ML carbon on $Co(11\bar{2}0)$ showing a (5×2) periodicity. The circles indicate the location of the substrate LEED spots. On the left a hard sphere model of the $Co(11\bar{2}0)$ surface with a proposed carbon overlayer is displayed. The (5×2) unit cell is indicated as a black rectangular frame.

The LEED pattern displays the surface reciprocal space with the consequence that only the unit cell of an overlayer structure can be determined directly. The pattern does not reveal the arrangement of the atoms or molecules within the unit cell. This is however possible using quantitative LEED, a technique not performed in this work. This is done by measuring the intensities of the LEED spots as a function of electron energy (I-V measurements) and comparing those with calculated intensities using different geometrical models.

To describe the overlayer structures the most common notation is the one proposed by E. A. Wood [92] where the relation between the overlayer lattice and the substrate lattice in real space is expressed by

$$\left(\frac{\left|\vec{b}_1\right|}{\left|\vec{a}_1\right|} \times \frac{\left|\vec{b}_2\right|}{\left|\vec{a}_2\right|} \right) R\alpha \qquad (2.28)$$

where $\vec{a}_1$ and $\vec{a}_2$ are the basis lattice vectors of the substrate unit cell, $\vec{b}_1$ and $\vec{b}_2$ are the basis lattice vectors of the adsorbate unit cell and $R\alpha$ specify a possible rotation of the unit cell of the overlayer by an angle α. Using the Wood notation the structure in fig. 2.22 is described as

$$Co(1\bar{1}\bar{2}0)\text{-}(5\times2)R0^{o}\text{-}C \qquad (2.29)$$

A more general way of describing the overlayer structure involves a simple vectorial construction [93]. If the primitive translation vector of the substrate are $\vec{a}_1$ and $\vec{a}_2$ and those of the adsorbate are $\vec{b}_1$ and $\vec{b}_2$, then these can be related by

$$\begin{pmatrix} \vec{b}_1 \\ \vec{b}_2 \end{pmatrix} = \bar{G} \begin{pmatrix} \vec{a}_1 \\ \vec{a}_2 \end{pmatrix} \qquad (2.30)$$

where $\bar{G}$ is a 2×2 matrix relating the adsorbate and substrate meshes.

In this work LEED will only be used in a qualitative way to determine the surface overlayer structure and ordering. For a more detailed description of the LEED technique, see e.g. [94]

2.8. Thermal programmed desorption (TPD)

When a metal sample is heated in a vacuum, gas is desorbed from the surface. Measurements of the gas pressure may reveal several temperatures for which the evolution rate goes through a relative maximum. Careful analyses of these peaks provides information of surface-adsorbate interactions. Since the initial work of F. Urbach in 1930 [95] rate measurements at continuously changing temperatures have been widely applied. The reason can be partly attributed to the relatively simple setup of the experiment. The sample must be placed in UHV environment to avoid unsolicited species from ambient atmosphere. Then the adsorbate overlayer is prepared, followed by a heating at a constant, known rate. Measurement of changes in the adsorbate pressure is recorded using a well calibrated mass spectrometer.

Figure 2.23 show examples of TPD for CO desorbing from a clean Rh(100) single crystal surface (bottom), La covered Rh(100) surface and La-Rh(100) surface alloy (top). The temperature range shown is from 200 to 1150 K.

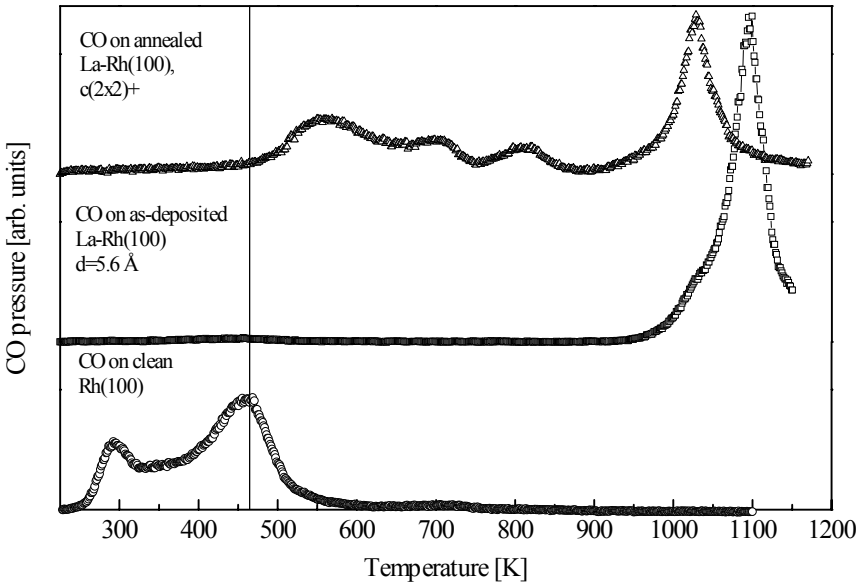

Figure 2.23: Recorded TPD traces from CO on clean Rh(100) (bottom figure), CO on as-deposited La-Rh(100), and CO on annealed La-Rh(100). The effective thickness from the as-deposited layer was d=5.6 Å. The LEED pattern observed for the annealed layer was a c(2x2) with fractional spots.

In the TPD trace from CO on clean Rh(100) (bottom spectrum) two distinct peaks appear originating from CO in on-top and bridge sites, respectively [37, 38]. The middle curve in fig. 2.23 shows the recorded TPD traces of CO after deposited a ~5.6 Å thick La layer on Rh(100). The layer shows mainly a single TPD peak at ~1080 K, with a weak shoulder at ~1040 K. Hence the TPD spectrum reveals a stronger CO chemisorption with the surface in present of deposited La layers. Finally, the top spectrum in fig. 2.23 shows the TPD traces of CO-on-annealed-La-Rh(100), creating a surface alloy. It is observed that the desorption trace is somewhere in between what is observed from pure Rh(100) and as-deposited La-Rh(100). Hence the creation of a surface alloy forms new chemical binding states that are a mixture of La and Rh in terms of desorption energy. The results show that TPD is a powerful technique in order to study the change in electronic structure upon alloying and to distinguish different adsorption sites.

2.9. Experimental equipments

In this section the main equipments employed for the experiments are described briefly.

2.9.1. The MAX-lab synchrotron radiation facility

Figure 2.24 shows a sketch of MAX-lab, a laboratory in Lund, Sweden, built around three storage rings for electrons (MAX I, II and III) at which several experimental stations are placed. MAX I and MAX II, which have been in operation for some time, store electrons with energies 550 MeV and 1500 MeV, respectively. Synchrotron radiation is produced by acceleration of the relativistic electrons through either bending magnets or insertion devices (undulators or wigglers) that are placed in straight sections of the storage rings. The radiation is led from the storage ring to an experimental chamber via a beamline (straight lines in figure 2.24). During the experiments performed for this thesis beamlines from both storage rings have been used, and are indicated by names and thick lines in the figure. Included is also the new 700 MeV storage ring MAX III with the intention of providing synchrotron radiation in the UV spectral region. The first injections into MAX II will take place in 2002.

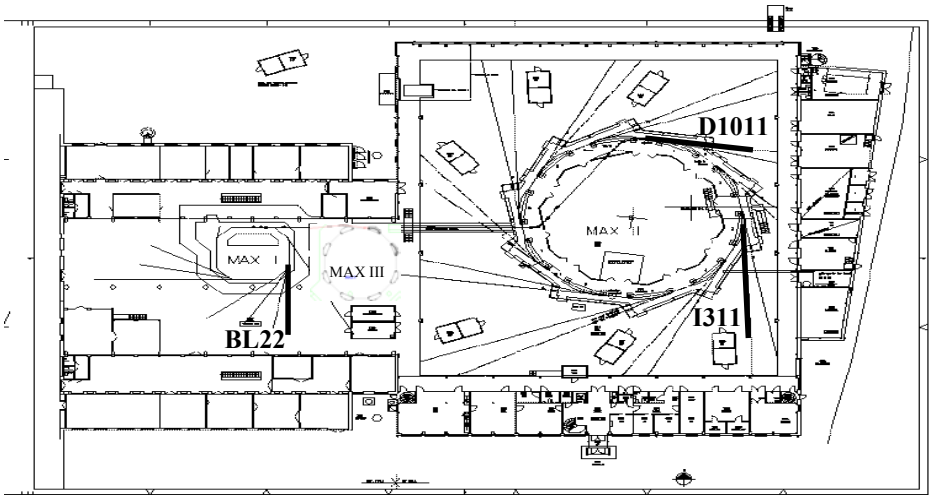

Figure 2.24: A top view of the MAX-lab synchrotron radiation facility, with the 550 MeV MAX I storage ring to the left and the 1500 MeV MAX II ring to the right. The position of the new 700 MeV MAX III storage ring is as indicated.

BL22 and D1011

Beamline 22 was operational until 1999 when both the monochromator and the experimental station were relocated to MAX II under the name D1011. For many years it was situated at one of the bending magnets of the MAX I with an utilisable photon energy range of

20 eV to 1000 eV. However, due to the decreasing photon flux at higher energies it was problematic to use energies above 500 eV for photoemission measurements. This has been improved significantly after the relocation to a bending magnet at MAX II, giving an energy range from 20 eV up to 1500 eV. In addition, energy resolution tests of the monochromator show an improvement of about a factor of two as compared to BL 22 at MAX I. The smaller beam size in MAX II and the up-grade of the focussing mirror in the monochromator are the major reasons for this improvement. The photon flux on the sample is in the range ~ 10^{10} - 10^{11} photons/sec..

The monochromator is of a modified Zeiss SX-700 plane grating (PGM) type [96, 97] and an experimental station [97], which is especially designed for surface science experiments.

I311

Beamline I311 is a VUV, soft X-ray beamline [98] connected to the MAX II storage ring, providing photons in the energy range from 30 eV to ~1500 eV. The radiation source is a 2.65 m. undulator containing 32 magnetic periods producing a beam of ~10^{11} - 10^{13} photons/sec., i.e. about two orders of magnitude higher than for D1011. Figure 2.25 shows a schematic layout of the I311 beamline.

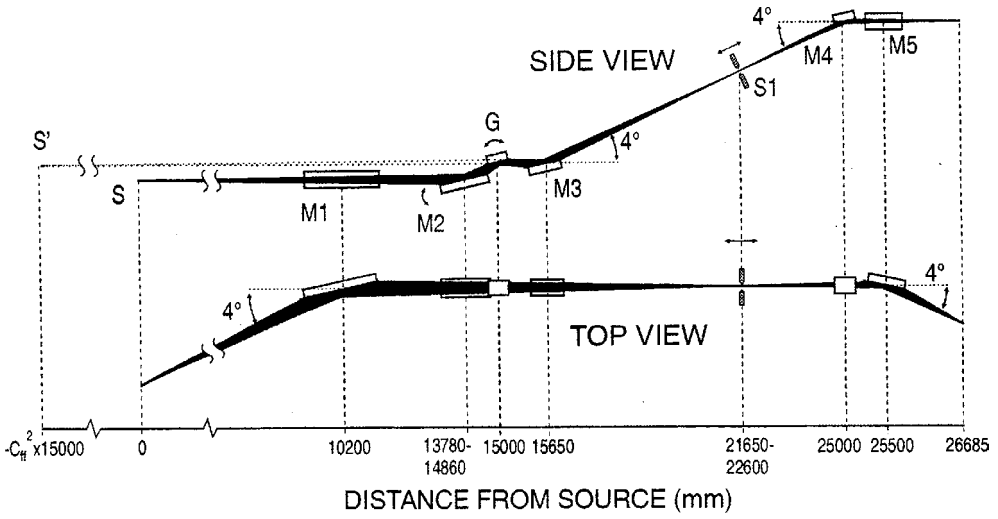

Figure 2.25: Layout of the I311 beamline. The optical elements are (from left to right): M1, horizontally focusing pre-mirror, M2, rotatable plane mirror, G, plane grating, M3, spherical focusing mirror, M4 and M5, spherical re-focusing mirrors. S1 is a movable exit slit. The actual source is at position S while the virual monochromatic source is at S' [98].

The monochromator is a modified SX-700 with 1220 l/mm grating, spherical focusing mirror and movable exit slit. The experimental end station includes a hemispherical electron energy analyser of type Scienta SES-200 [99] for photoemission spectroscopy.

2.9.2. The STM-lab in Trondheim

All the STM experiments presented were performed using an Omicron UHV STM 1 situated at NTNU in Trondheim, which allows room-temperature measurements only. The maximum allowed scan range for the mounted tripod piezoscanner is 12000 × 12000 $Å^2$. Two UHV chambers are available separated with an UHV valve, which makes it possible to perform sample preparations on two different materials simultaneous. The base pressure of both chambers is $<1\times10^{-10}$ mbar. For cleaning, preparing and characterising the surfaces the system is also equipped with ion sputtering guns, LEED and Auger optics.

3. Summary of papers

In this section a brief summary is given of the most important findings in papers I to VII. The details of the investigations can be found in the respective papers.

Paper I: *Hybridisation and vibrational excitation of C_2H_2 on Co(0001)*

A thorough investigation of acetylene adsorption on Co(0001) has been performed at low temperature (~110 K) using near edge x-ray absorption fine structure (NEXAFS) and high-resolution core level photoemission spectroscopy. From polarisation dependent NEXAFS spectra it was concluded that acetylene adsorb molecularly with its carbon-carbon bond close to parallel orientation with respect to the surface. A comparison with gas-phase measurements revealed a state of hybridisation close to sp^3, considerably higher than previously reported. In the C 1s photoemission spectra of adsorbed C_2H_2 an additional contribution at a binding energy located 389 meV higher in energy side that the main peak was observed. Comparisons with the deuterated counterpart of C_2H_2, C_2D_2 showed that the structure arises from excitations of the internal C-H molecular vibrational mode. The S-factor of the CH-vibrational mode was determined to be ~0.17, a quite surprising results since experimental and theoretical investigations for gaseous acetylene predicts a negligible contribution from this mode in the core-level photoemission process.

Paper II: *Acetylene adsorption on cobalt single crystal surfaces*

The acetylene chemisorption and thermal decomposition on $Co(11\bar{2}0)$ single crystal surface has been studied with high-resolution core level photoemission spectroscopy, NEXAFS, LEED and STM. For comparison similar photoemission measurements were presented for the system C_2H_2 on Co(0001). It was concluded that acetylene chemisorb molecularly at ~110 K on the anisotropic $Co(11\bar{2}0)$ surface and dissociate at ~200 K, which is significantly lower than for C_2H_2 on Co(0001). NEXAFS measurements showed that acetylene hybridises strongly with the $Co(11\bar{2}0)$ surface, forming antibonding states below the ionisation limit, which are not present in the gas-phase. In the temperature region from ~200 K to ~300 K a dehydrogenated fragment, possibly of the form C_2H or C_2, was found to co-exist with molecular acetylene. Further heating to ~450 K led to decomposition of this fragment to graphitic carbon, while an ordered (5×2) carbon overlayer started to form at the expensive of molecular acetylene. At ~570 K this ordered overlayer was fully developed. By combining results from photoemission spectroscopy measurements, LEED and STM, a hard sphere model

for the carbon overlayer relative to the Co substrate was proposed. Above ~600 K a substantial decrease in the amount of ordered carbon atoms was seen, leaving mainly graphitic carbon on the Co($1\,1\bar{2}0$) surface.

Paper III: *Molecular vibrations in core-ionised CO adsorbed on Co(0001) and Rh(100)*

High-resolution core-level photoemission has been used to study the vibrational fine structures of core-ionised CO adsorbed on Co(0001) and Rh(100). For CO in on-top site on Co(0001) the vibrational splitting was determined to be (210 ± 4) meV from the adiabatic C1s peak. By including the measured intensities and comparing with similar data from EELS-experiments the change in the equilibrium distance between the initial state and the ionised state was deduced to (4.7 ± 0.2) pm. Evidence for a non-Franck-Condon behaviour of the vibrational fine structure using photon energies 16 eV above the shape resonance was reported. For CO on Rh(100) the vibrational fine structure of two adsorption sites, on-top and bridge, were analysed. Vibrational splittings of (221 ± 4) meV for the on-top site and (174 ± 11) meV for the bridge site were found with changes in the equilibrium distances of (3.8 ± 0.2) pm and (5.3 ± 0.3) pm, respectively. Comparing the results found in this report with previous studies showed that the trend of decreasing vibrational splitting with increasing co-ordination is also applicable for screened core-ionised CO.

Paper IV: *Vibrationally resolved C 1s photoemission from CO adsorbed on Rh(111): The investigation of a new chemically shifted C 1s component.*

High resolution core level photoemission and electron energy loss spectroscopy have been used to study the different overlayers formed by CO on Rh(111), at coverages ranging from 0.2 ML to the saturation coverage of 0.75 ML. The CO molecules were reported earlier only to adsorb in on-top positions up to a coverage of 0.33 ML. At higher coverage an increasing amount of three-fold hollow sites are populated leading to a saturation coverage with the unit cell containing one CO molecule in an on-top position and two in hollow-positions. Fine structure components due to vibrational excitation of the C-O stretch mode were clearly resolved in the emission peak from each site. The vibrational splittings and intensity ratios were found to be different for the different adsorption sites, in consistency with the findings on Rh(100). A third C 1s component, which had not been resolved earlier, was found at intermediate CO coverages. Some possible explanations for the origin of this extra component

were discussed. For this reason high-resolution electron energy loss spectroscopy spectra were measured for different CO coverages and the photoelectron diffraction behaviour was analysed.

Paper V: *Investigation of the La-Rh(100) surface alloy*

Paper V contains a study of the La-Rh(100) surface alloy formed when La on Rh(100) is annealed to 1350 K. The experimental methods were high resolution photoemission spectroscopy, low energy electron diffraction (LEED), and temperature programmed desorption (TPD). Anneal of a sub-monolayer of La deposited on Rh(100) led to a LEED pattern with streaked fractional order spots appears. By increasing the La coverage a more ordered c(2×2) structure with split fractional order were observed in LEED. The fractional spots were suggested to originate from anti-phase domains on the surface. Analyses of the photoemission spectra of the Rh $3d_{5/2}$ and La 5p core-levels showed that an ordering takes place in going from the as-deposited to the annealed system, which resulted in a Rh terminated surface. TPD experiments of CO adsorbed on the annealed La/Rh(100) system showed CO desorption peaks at significantly lower temperature than CO on the as-deposited La/Rh(100), but still higher than the desorption peaks found for CO on Rh(100). From these results it was concluded that a true, ordered surface alloy is formed with new electronic states.

Paper VI: *Study of CO adsorption on La-Rh(100) surface alloys*

A strong modification of the surface electronic properties and the bonding of CO to the La-Rh(100) surface alloy, has been demonstrated for both sub-monolayer and monolayer coverages of La/Rh(100). The TPD spectrum for CO/La-Rh(100) shows a mixture of desorption temperatures between those of CO/Rh(100) and CO on as-deposited La/Rh(100).

In particular, it has been found that CO partly dissociates at low temperatures on the La-Rh(100) surface alloy, due to the presence of La in the near surface region. The photo emission spectra of C1s, O1s, La 5p, Rh 3d and valence band region, has been correlated to the peaks in the TPD spectra, and to the LEED patterns. Different atomic carbon and atomic oxygen adsorption sites have been observed and commented, with proposed correlation with the TPD peaks. In addition, adsorbate interactions were thought to be responsible for a 100 K lowered desorption temperature in case of the sub-monolayer alloy. At higher temperatures a c(4x4) LEED pattern was the preferred structure for dissociated CO on the c(2x2) monolayer alloy. The sub-monolayer alloy showed here a ring pattern, superposed on a (10x10) superstructure and streaks.

A semi-quantitative analysis of the temperature dependent partial CO and C+O coverages have been demonstrated based on LEED, core level photoemission spectroscopy and TPD.

Paper VII: *Homoepitaxial growth of Co on $Co(11\bar{2}0)$ studied by STM*

The homoepitaxial growth of Co on $Co(11\bar{2}0)$ has been studied by scanning tunnelling microscopy (STM). Elongated Co islands were observed to form along the [0001] direction, indicating anisotropic growth. A plot of the auto-correlation function confirmed the anisotropy. To investigate the growth further, the substrate temperature and deposition rate were varied at a constant coverage of ~(5 ± 1)%. The size distribution of the Co islands deposited was found to be very sensitive to the substrate temperature. Larger and fewer islands were observed for higher temperatures.

References:

[1] G. A. Somorjai and P. Chen, Solid State Ionics, 141-142 (2001) 3.

[2] T. P. Beebe, Jr., D. W. Goodman, B. D. Kay and J. T. Yates, Jr., J. Chem. Phys. 87 (1987) 2305.

[3] H. Papp, Surf. Sci. 129 (1983) 205.

[4] K. A. Prior, K. Scwaha and R. M. Lambert, Surf. Sci. 77 (1978) 193.

[5] J. C. C. Geerlings, M. C. Zonnevylle and C. P. M. de Groot, Surf. Sci. (1991) 241.

[6] F. Besenbacher, I. Chorkendorff, B. S. Clausen, B. Hammer, A. M. Molenbroek, J. K. Nørskov, I. Stensgaard, Science, 279 (1998) 1913.

[7] K. B. Rider, K. S. Hwang, M. Salmeron and G. A. Somorjai, Phys. Rev. Lett. 86 (2001) 4330.

[8] L. Österlund, P. B. Rasmussen, P. Thostrup, E. Lægsgaard, I. Stensgaard and F. Besenbacher, Phys. Rev. Lett. 86 (2001) 460.

[9] J.A. Jensen, K.B. Rider, Y. Chen, M. Salmeron and G.A. Somorjai, J. Vac. Sci. Technol. B 17 (3) (1999) 1080.

[10] J.A. Jensen, K.B. Rider, M. Salmeron and G.A. Somorjai, Phys. Rev. Lett. 80 (6) (1998) 1228.

[11] D. W. Goodman, Surf. Sci. 299/300 (1994) 837.

[12] G. A. Somorjai, Surf. Sci. 299/300 (1994) 849.

[13] U. Gelius, S. Svensson, H. Siegbahn, E. Basilier, Å. Faxälv and K. Siegbahn, Chem. Phys. Lett. 28 (1974) 1

[14] S. J. Osborne, A. Ausmees, S. Svensson, A. Kivimäki, O. P. Sairanen, A. N. De Brito, H. Aksela and S. Akseal, J. Chem. Phys. 102 (1995) 7317, and references therein

[15] J. N. Andersen, A. Beutler, S. L. Sorensen, R. Nyholm, B. Setlik and D. Heskett, Chem. Phys. Lett. 269 (1997) 371.

[16] A. Föhlisch, N. Wassdahl, J. Hasselström, O. Karis, D. Menzel, N. Mårtensson and A. Nilsson, Phys. Rev. Lett. 81 (1998) 1730.

[17] G. A. Somorjai, Introduction to surface chemistry and catalysis (Wiley, New York, 1994)

[18] J. J. C. Geerlings, M. C. Zonnevylle and C. P. M. de Groot, Surf. Sci. 241 (1991) 302.

[19] D. P. Woodruff, T. A. Delchar, Modern Techniques of Surface Science, Cambridge Solid State Science Series, 2. ed. (1994)

[20] A. Zangwill, Physics at surfaces, Camrbidge University Press, Cambridge (1988)

[21] M. Prutton, Introduction to surface physics, Oxford University Press, Oxford (1994)

[22] D. J. O'Connor, B. A. Sexton and R. St. C. Smart (Eds.), Surface Analysis Methods in Materials Science, Springer-Verlag, Berlin (1992)

[23] I. Lindau and W. E. Spicer, J. of Electron Spectrosc. 3 (1974) 409.,

[24] M. P. Seah and W. A. Dench, Surface and Interface Analysis 1 (1979) 2.

[25] C. R. Brundle, Surf. Sci. 48 (1975) 99.

[26] Cobalt Monograph, edited by Batelle Institut (Centre d'Information du Cobalt, Paris (1960)

[27] B. W. Lee, R. Alsenz, A. Ignatiev and M. A. van Hove, Phys. Rev. B, 17 (1978) 1510.

[28] R. L. Toomes and D. A. King, Surf. Sci. 349 (1996) 1.

[29] M. R. Albert and L. G. Sneddon, Surf. Sci. 147 (1984) 127.

[30] E. W. Plummer, W. R. Salaneck and J. S. Miller, Phys. Rev. B18 (1978) 1673.

[31] F. Greuter, D. Heskett, E. W. Plummer and H. J. Freund, Phys. Rev. B27 (1983) 7117.

[32] C. D. Wagner, W. M. Riggs, L. E. Davis, J. F. Moulder and G. E. Muilenberg, Handbook of X-ray photoelectron spectroscopy, Perkin-Elmer Corporation, Minnesota (1979)

[33] N. Mårtensson and A. Nilsson, J. Electron Spectrosc. Relat. Phenom. 75 (1995) 209.

[34] S. Hagström, C. Nordling and K. Siegbahn, Phys. Lett., 9 (1964) 235.

[35] H. Antonsson, A: Nilsson, N. Mårtensson, I. Panas and P. E. M. Siegbahn, J. Electron Spectrosc. Relat. Phenom., 54/55 (1990) 601.

[36] A. Nilsson, H. Antonsson, A. Sandell and N. Mårtensson in S. Y. Tong, M. A. van Hove, K. Takayanagi and X. D. Xie (Eds.), The Structure of Surfaces III, Vol. 24, Springer-Verlag, Berlin (1991) 467.

[37] A. Baraldi, L. Gregoratti, G. Comelli, V. R. Dhanak, M. Kiskinova and R. Rosei, Appl. Surf. Sci. 99 (1996) 1.

[38] F. Strisland, A. Ramstad, T. Ramsvik and A. Borg, Surf. Sci. 415 (1998) L1020.

[39] A. Borg, C. Berg, S. Raaen and H. J. Venvik, J. Phys. Cond. Matt. 6 (1994) L7.

[40] B. Johansson and N. Mårtensson, Phys. Rev. B 21 (1980) 4427.

[41] A. Rosengren and B. Johansson, Phys. Rev. B 22 (1980) 3706.

[42] S. Doniach and M. Šunjić, J.Phys. C3 (1970) 285.

[43] G. D. Mahan, Phys. Rev. 163 (1967) 612.

[44] P. Nozières and C. T. DeDominicis, Phys. Rev. 178 (1969) 1097.

[45] P. H. Citrin and G. W. Wertheim, Phys. Rev. B, 16 (1977) 4256.

[46] see e.g. P. W. Atkins and R. S. Friedman: Molecular Quantum Mechanics, third edition, 1997

[47] Curve fitting routine, FITXPS, developed by D. L. Adams at the Institute of Physics and Astronomy, University of Århus, Denmark

[48] see e.g. E. Merzbacher, Quantum Mechanics, Wiley International Edition, 2nd edition (1970)

[49] B. A. Gurney, L. J. Richter, J. S. Villarrubia and W. Ho: J. Chem. Phys. 87 (1987) 6710.

[50] L. S. Cederbaum and W. Domcke, J. Chem. Phys. 64 (1976) 603.

[51] W. Domcke, L. S. Cederbaum, H. Köppel and W. von Niessen, Mol. Phys. 34 (1977) 1759.

[52] D. P. Woodruff, D. Norman, B. W. Holland, N. V. Smith, H. H. Farrell, M. M. Traum, Phys. Rev. Lett. 41 (1978) 1130.

[53] S. D. Kevan, D. H. Rosenblatt, D. Denley, B. C. Lu and D. A. Shirley, Phys. Rev. Lett. 41 (1978) 1565.

[54] C. H. Li and S. Y. Tong, Phys. Rev. Lett. 42 (1979) 901.

[55] H. Papp, Surf. Sci. 129 (1983) 205.

[56] J. Lahtinen, J. Vaari, K. Kauraala, E. A. Soares and M. A. Hove, Surf. Sci. 448 (2000) 269.

[57] J. Lahtinen, J. Vaari and K. Kauraala, Surf. Sci. 418 (1998) 502.

[58] J. J. Yeh and I. Lindau, Atomic Data and Nuclear Data Tables 32 (1985) 1.

[59] J. Stöhr, K. Baberschke, R. Jæger, R. Treichler and S. Brennan, Phys. Rev. Lett. 47 (1981) 381.

[60] J. Stöhr and R. Jæger, Phys. Rev. B 26 (1982) 4111.

[61] J. Stöhr, Z. Phys. B 61 (1985) 439.

[62] J. Stöhr: In NEXAFS Spectroscopy, Springer Series in Surface Sciences Vol. 25 (Springer, Berlin, Heidelberg, New York 1992)

[63] J. Stöhr, K. Baberschke, R. Jæger, T. Treichler, S. Brennan, Phys. Rev. Lett. 47 (1981) 381.

[64] J. Stöhr and R. Jæger, Phys. Rev. B 26 (1982) 4111.

[65] A.P. Hitchcock and C. E. Brion, J.El.Spec. 10 (1977) 317.

[66] J. L. Dehmer, D. Dill and S. Wallace, Phys. Rev. Lett. 43 (1979) 1005.

[67] F. Sette, J. Stöhr and A. P. Hitchcock, J. Chem. Phys. 81 (1984) 4906.

[68] C. R. Natoli: In EXAFS and Near Edge Structure, ed. By A. Bianconi, L. Incoccia and S. Stipcich, Springer Ser. Chem. Phys. Vol. 27 (Springer, Berling, Heidelberg 1983)

[69] J. Sheehy, T. J. Gil, C. L. Winstead, R. E. Farren and P. W. Langhoff, J. Chem. Phys. 91 (1989) 1796.

[70] A. P. Hitchcock, S. Beaulieu, T. Steel, J. Stöhr and F. Sette, J. Chem. Phys. 80 (1984) 3927.

[71] A. P. Hitchcock and J. Stöhr, J. Chem. Phys. 87 (1987) 3253.

[72] J. Stöhr, F. Sette and A. L. Johnson, Phys. Rev. Lett. 53 (1984) 1684.

[73] D. Arvanitis, U. Döbler, L. Wenzel, K. Baberschke and J. Stöhr, Surf. Sci. 178 (1986) 696.

[74] D. Arvanitis, K. Baberschke, L. Wenzel and U. Döbler, Phys. Rev. Lett. 57 (1986) 3175.

[75] D. Arvanitis, L. Wenzel and K. Baberschke, Phys. Rev. Lett. 59 (1987) 2435.

[76] J. Störh, D. A. Outka, K. Baberschke, D. Arvanitis and J. A. Horsley, Phys. Rev. B 36 (1987) 2967.

[77] D. Arvanitis, H. Rabus, L. Wenzel and K. Baberschke, Z. Phys. D - Atoms, Molecules and Clusters 11 (1989) 219.

[78] T. Gustafsson and H. J. Levinson, Chem. Phys. Lett. 78 (1981) 28.

[79] see e.g. M. N. Piancastelli, J. of Electron Spect. and Related Phenomena 100 (1999) 167.

[80] H. Kempgens, H. M. Köppe, A. Kivimäki, M. Neeb, K. Maier, U. Hergenhahn and A. M. Bradshaw, Phys. Rev. Lett. 79, (1997) 35. and references therein

[81] R. E. Farren, J. A. Sheehy and P. W. Langhoff, Chem. Phys. Lett. 177 (1991) 307.

[82] N. Haack, G. Ceballos, H. Wende, K. Baberschke, D. Arvanitis, A. L. Ankudinov and J. J. Rehr, Phys. Rev. Lett. 84, (2000) 614.

[83] D. Arvanitis, N. Haack, G. Ceballos, H. Wende and K. Baberschke, J. of Electron Spect. and Related Phenomena 113 (2000) 57.

[84] T. D. Thomas, N. Berrah, J. Bozek, T. X. Carroll, J. Hahne, T. Karlsen, E. Kukk and L. J. Sæthre, Phys. Rev. Lett. 82 (1998) 1120.

[85] G. Binnig, H. Rohrer, Ch. Gerber and E. Weibel, Physica (Utrecht) 107B+C, 1335 (1981), Proceedings of the Sixteenth International Conference on Low-Temperature Physics, Los Angeles, 19-25 August 1981

[86] G. Binnig, H. Rohrer, Ch. Gerber and E. Weibel, Appl. Phys. Lett. 40 (1981) 178.

[87] G. Binnig, H. Rohrer, Ch. Gerber and E. Weibel, Phys. Rev. Lett. 49 (1982) 57.

[88] J. Tersoff and D. R. Hamann, Phys. Rev. Lett. (1983) 1998.

[89] J. A. Golovochenko, Science 232 (1986) 48.

[90] C. J. Davisson and L. H. Germer, Nature (London) 119 (1927) 558.

[91] C. J. Davisson and L. H. Germer, Phys. Rev. 29 (1927) 908.

[92] E. A. Wood, J. Appl. Phys. 35 (1964) 1306.

[93] R. L. Park and H. H. Madden Jr., Surf. Sci. 11 (1968) 188.

[94] M.A. van Hove, W. H. Weinberg, C.-M. Chan, Low-Energy Electron Diffraction, Springer-Verlag (1986)

[95] F. Urbach, Sitzber. Akad. Wien, Math.-Naturw. Kl. Abt. Iia, 139, (1930) 363.

[96] R. Nyholm, S. Svensson, J. Nordgren and S. A. Flodström, Nucl. Instrum. Methods A 246 (1986) 267.

[97] J. N. Andersen, O. Björneholm, A. Sandell, R. Nyholm, J. Forsell, L. Thånell, A. Nilsson and N. Mårtensson, Synchrotron Radiat. News 4 (4) (1991) 15.

[98] R. Nyholm, J. N. Andersen, U. Johansson, B. N. Jensen and I Lindau, Nucl. Instr. & Meth. in Phys. Res A, in press

[99] N. Mårtensson, P. Balzer, P. A. Brühwiler, J. O. Forsell, A. Nilsson, A. Stenborg and B. Wannberg, J. Electron Spectrosc. Relat. Phenom. 70 /1994) 117.

Paper I

Hybridisation and vibrational excitation of C_2H_2 on Co(0001)

T. Ramsvik, A. Borg, T. Worren and M. Kildemo

Submitted to Physical Review B

HYBRIDISATION AND VIBRATIONAL EXCITATION OF C_2H_2 ON Co(0001)

T. Ramsvik, A. Borg, T. Worren and M. Kildemo,
Department of Physics, Norwegian University of Science and Technology,
N-7491 Trondheim, Norway

Abstract

The chemisorption of acetylene on the Co(0001) crystal surface have been studied using high resolution core level photoemission, x-ray absorption spectroscopy and low energy electron diffraction. At low temperatures (≤300 K) acetylene forms a strong chemisorption bond to the substrate, creating a state of hybridisation close to sp^3. The molecules are confirmed to be oriented with the C-C axis parallel to the surface. The vibrational splitting in the photoemission spectra due to excitation of the C-H stretch vibration is determined to be (389 ± 8) meV, which is ~6 % lower then the reported C-H stretch vibration frequency for gaseous acetylene. The S-factor of the C-H-vibrational mode is determined to be (0.17 ± 0.02), considerably higher than those reported for other systems.

1. INTRODUCTION

Studies of the bonding and reactivity of unsaturated hydrocarbon molecules adsorbed on transition metal single crystal surfaces are important for a molecular-level understanding of heterogeneous hydrocarbon catalysis.

Near edge x-ray absorption fine structure (NEXAFS) has shown to be a powerful tool to extract important information concerning the geometry and electronic nature of hydrocarbon adsorbates [1]. Among the capabilities are the ability to detect the presence of specific bonds in molecules (e.g. C-C, C=C, C≡C, and C-H bonds in hydrocarbon) and the derivation of the orientation of molecules and functional groups on surfaces or in solids. In addition, by comparing the spectra of free and chemisorbed molecules NEXAFS can reveal the strength of hybridisation between adsorbates and substrate.

High resolution photoemission spectroscopy is routinely utilised to identify and distinguish between different chemical species at surfaces. An important type of chemical shift is the splitting in the core-level binding energy for adsorbates due to different adsorbate sites. In recent years, due to improved instrumental resolution, it has been possible to observe the additional structure of the core level peak profile due to internal molecular vibrations of chemisorbed molecules. The information that can be derived from analysis of this vibrational structure has become a valuable tool in the identification of hydrocarbon species on a surface [2]. For ethylidyne (CCH_3) on Rh(111), J. Andersen et al. were able to identify the CH_3 group by relating a resolved contribution on the high binding energy side of the main C 1s peak to the C-H vibrational mode. These conclusions were later supported by observations of the CH_3O on Cu(100) system[3].

The adsorption and decomposition of acetylene on metal surfaces have been studied extensively the last 30 years, particularly by vibrational spectroscopy (for a review, see e.g. ref. 4). Normally, at temperatures below 300 K, acetylene adsorbs molecularly with its carbon-carbon bond parallel to the surface. The thermally induced decomposition results in several types of fragments depending on both the initial coverage and the substrate. However, exceptions from these trends exist: an example which has received considerable attention is acetylene adsorbed on Pd(111) where partial desorption (20 to 35 %) was found due to benzene formation on the surface[5,6]. For the specific case of Co(0001) acetylene has been determined to adsorb in a laying position [7,8].

Thermal decomposition occurs at 400 K, which results in a carbonaceous overlayer consisting mainly of graphitic carbon but with a small amount of carbon in a carbidic form [8]. The hybridisation with the substrate was found to be approximately $sp^{1.5}$ based on valence band photoemission results [7] which implies a rather weak hybridisation for the C_2H_2/Co(0001) system.

In this paper the adsorption of C_2H_2/Co(0001) is studied using high resolution core level spectroscopy, near-edge X-ray absorption fine structure (NEXAFS) and LEED to investigate the hybridisation and vibrational excitations of this system. It is confirmed that acetylene adsorbs with its carbon-carbon bond in a near parallel orientation with respect to the cobalt surface. The charge transfer to the acetylene molecule from Cobalt is shown to be substantial after chemisorption, giving a state of hybridisation close to sp^3. It is further seen that the carbon-carbon bond length is elongated relative to the gas phase. Based on the new energy position of the shape resonance, this elongation is estimated to be (14 ± 3) %. The vibrational fine structure of the core level spectra reveals a C-H vibrational energy of (389 ± 8) meV for the core ionised C_2H_2 molecule. For the corresponding S-factor indications of a considerable increase relative to the gas phase is observed. This corresponds to a significantly larger change in the carbon-hydrogen bond length between the neutral and ionised molecule than what is found for acetylene in the gas phase.

2. EXPERIMENTAL

The photoemission and x-ray absorption spectroscopy experiments were performed at the soft X-ray beamline BL22 at the MAX I and beamline D1011 at the MAX II storage rings at the Max-lab facility in Lund, Sweden. These beamlines are equipped with a modified Zeiss SX-700 monochromator and a large Scienta-type hemispherical photoelectron energy analyser [9,10]. The total experimental resolutions were ~170 meV for BL22 and ~124 meV for D1011 in the energy range 320-380 eV. The NEXAFS spectra were measured in the constant final state (CFS) mode with the kinetic energy set to collect electrons from the surface sensitive C KVV Auger transition using the hemispherical energy analyser for detection.

The Co(0001) single crystal was cleaned by cycles of sputtering with 0.5 keV Ar^+ ions at ~570 K and subsequent annealing at ~630 K in UHV. The annealing temperature was kept well below ~700 K, to avoid the Co hcp $\rightarrow$ fcc phase transition. The C_2H_2 and C_2D_2 overlayers were prepared by exposing the surface to 10 L of gas molecules at a substrate temperature of about 110 K. This procedure produced a fully saturated overlayer corresponding to a coverage of about 0.3 ML, as deduced from the variations in the Co 2p spectra. The acetylene gas was provided by L'Air Liquide (99.0 % purity) and the deuterated isotope was prepared in a laboratory at Fysikum in Lund, Sweden. All measurements of the adsorbate C 1s core-level spectra and the C K-shell NEXAFS spectra were performed at a sample temperature of 110 K in order to reduce the broadening due to low-energy vibrational modes.

3. RESULTS AND DISCUSSION

The polarisation dependent NEXAFS spectra at the C 1s absorption edge for a saturated C_2H_2 layer on Co(0001) are shown in Figure 1.

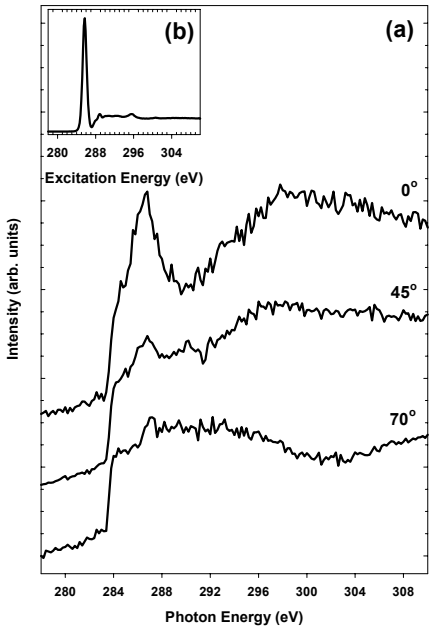

Figure 1: (a) Polarization dependent carbon K-shell NEXAFS spectra of acetylene chemisorbed on Co(0001) recorded at 110 K for X-ray incidence angle of 0^o, 45^o and 70^o b) ISEELS K-shell spectrum of gaseous acetylene [11].

The spectra are all normalised by the intensity of the Fermi edge with maximum at ~283.7 eV. The σ* resonance, at a photon energy of around 299 eV, reaches the highest intensity when the ***E***-vector is in the surface plane. This clearly indicates that the carbon-carbon bond of the acetylene molecule has close to parallel orientation with respect to the surface, in accordance with the results obtained by both Albert et al. [7] and Vaari et al.[8].

Comparison with ISEELS experiments of gaseous acetylene (insert in figure 1) shows that there is a high degree of hybridisation with the substrate where both π* antibonding orbitals contribute to the chemisorption bond. At normal incidence the π* component arises from the strongly modified $\pi_{\|}$* orbital, while at grazing incidence a weak component at slightly higher photon energy (~0.7 eV) is observed. The latter may be due to contribution from an incompletely filled $\pi_{\perp}$ * orbital and/or transition to a new acetylene-cobalt resonance.

In figure 1(a) a pronounced Fermi edge located at ~283.3 eV is seen, corresponding to the C 1s binding energy of the adiabatic peak (see Table 1). According to J. Stöhr (see Ref. 1) transitions to unoccupied metal orbitals can only take place if the molecular states hybridise with the substrate. In

addition the height of the Fermi edge increases with the strength of the binding with the adsorbates. Furthermore, the fact that the Fermi edge is located at lower excitation energy than the π* resonance is also an indication of strong hybridisation since it requires that the screening of the created core hole from the substrate electrons is more effective than the screening from the molecule itself. A quantification of the degree of hybridisation with the Cobalt substrate is possible by comparing the adsorption modified π* resonance intensity for X-ray incidence angle of 45 degrees (figure 1a) with the unperturbed π* resonance intensity of gaseous acetylene (figure 1b) [12]. E.g., if the chemisorption results in a sp^2 hybridisation, the π* intensity should be reduced to one half of its original value. From the almost complete disappearance of the π* state at 45 degrees it can be deduced that the

charge transfer from the Cobalt substrate to the molecule results in a state of hybridisation of about $sp^{2.8}$, i.e. close to sp^3. This is considerably stronger than what has been reported earlier [7]. The X-ray angle of incidence of 45 degrees has been chosen since the measured intensity distribution at this angle is nearly independent of the molecular orientation and thus is more comparable to the gaseous phase spectra.

An approximately linear relation between the absolute σ* resonance position and bond length for C-C bonds in unsaturated hydrocarbons has been reported in literature [13-16]. In our experiments a σ* energy position of (299 ± 2) eV was found (see figure 1 a). A rather high uncertainty is stated to take into account the broad characteristic of the σ* resonance. In addition, for acetylene the existence of multielectron peaks with noticeable intensity above the ionisation potential is well known [1]. These shake-up excitations are broad and overlap with the σ* resonance which is shifted due to the adsorption induced change of the C-C bond length. However, the most prominent multielectron peak located at 295 eV (see figure 1b) has a final state of the type $(1s)^{-1}1\pi^{-1}(2\pi^*)^1(\text{Ryd.})^1$ i.e. proportional to the π* transition intensity. For this particular system this peak should not influence the position of the π* resonance significantly. The validity of using the σ* resonance to give a quantitative estimate of the bond length of adsorbed molecules has been a subject of discussion in literature [17]. In addition, it has been claimed that the broad feature in the photoabsorption cross section of gaseous C_2H_2, centred at ~310 eV, is largely due to satellite contributions [18], i.e. the true shape resonance predicted in theory [19] is weak. However, this has been contradicted in more recent publications [15,20]. If the observed resonance position is used to find a quantitative estimate of the carbon-carbon bond length, according to the proposed linear relation, our experimental results imply a new equilibrium length of (1.37 ± 0.04) Å for C_2H_2 on Co(0001). In comparison, NEXAFS studies of the system C_2H_2/Pd(111) performed by Hoffmann et

al. [5] reveal a π*-modification slightly stronger than the present findings, and with a σ*-resonance position located at about 1 eV lower excitation energy. According to the proposed relation this corresponds to a C-C bond length for

C_2H_2/Pd(111) of ~1.39 Å. In a later study of C_2H_2/Pd(111) by Baddeley et al. using photoelectron diffraction [21], this length was found to be (1.34 ± 0.10) Å. Within the experimental uncertainty, both values are consistent with the bond length found for C_2H_2/Co(0001) in the present work. Other examples of systems that show strong rehybridisation are C_2H_2/Cu(111) [22] and C_2H_2/Ni(111) [23-25], where the C-C bond lengths have been determined by photoelectron diffraction to be (1.48 ± 0.10) Å and (1.44 ± 0.10) Å, respectively. Also in the case of C_2H_2/Co(0001) the strong hybridisation with the substrate surface leads to a substantial increase of the bond length as compared to acetylene in the gas phase (1.203 Å) [26]. With the length determined from our data, (1.37 ± 0.04) Å, it corresponds to an elongation of ~(14 ± 3) %.

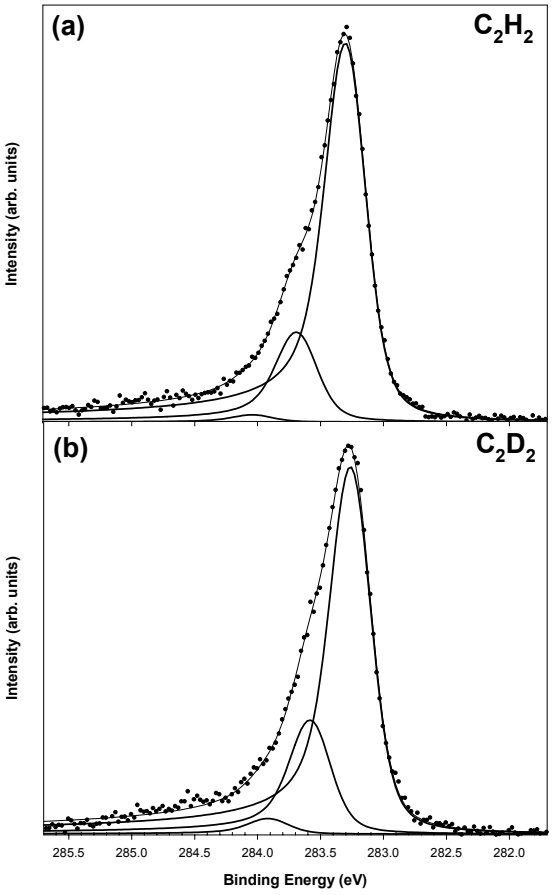

Figure 2: C 1s photoemission spectra after a saturation exposure of (a) acetylene (C_2H_2) and (b) deuterated acetylene (C_2D_2) on Co(0001). Both spectra were measured at a photon energy of 320 eV and with a resolution ≤ 124 meV.

Figure 2a shows the C 1s core level spectrum after a saturation exposure of C_2H_2 on Co(0001) at 110 K. LEED experiments only revealed the substrate (1×1) pattern, indicating a lack of long-range order in the C_2H_2 overlayer. The C 1s core level spectrum is decomposed using Doniach-Šunjić line profiles [27] convoluted by a Gaussian function [28]. Decomposition of the C 1s spectrum of Figure 2a gives two components at binding energies 283.28 eV and 283.67 eV, respectively, and a corresponding energy splitting of (389 ± 8) meV. These two peaks are also observed at higher photon energies. Traditionally, such energy shifts have been interpreted as changes in the total energy (final and initial states) for two different chemical species [29]. Such shifts can arise if equivalent atoms occupy sites with different chemical environments. It has been concluded, both in literature [7,8] and in this paper, that the C_2H_2 molecule has its carbon-carbon bond parallel to the surface. If the observed shift has its origin from unequal sites for the two carbon atoms, one would expect an intensity ratio between the two contributions of about 1.0 for high kinetic energies of the photoemitted electrons. This is not observed for the present system. At high photon energies the intensity ratio is found to be ~0.17, i.e. far from unity. From our experimental data it is therefore considered unlikely that the two contributions originate from such chemical shifts. J. C. Dunphy et al. [30] have studied acetylene on Pd(111) with variable temperature STM. In this system the acetylene molecules where imaged in a laying position with the two carbon atoms located at identical sites. This has also been shown to be the case for the systems C_2H_2/Ni(111) [24,25] and C_2H_2/Cu(111) [22].

To investigate further the origin of the two components in figure 2a, the cobalt surface was exposed to the same amount of deuterated acetylene (C_2D_2). By comparing the C 1s spectra of C_2H_2 and C_2D_2 possible vibrational contributions to the spectra can be identified [2]. During exposure the substrate was kept at the same temperature as for C_2H_2, i.e. 110 K. Assuming that the vibrational motion of the atoms can be described by an harmonic oscillator potential and that the intensities of the different vibrational components in the photoemission spectrum follow a Poisson distribution [31], approximate relationships between the frequencies and S-factors for the C-H stretch vibration and the C-D vibration can be found:

$$\varpi_H \approx \sqrt{2}\varpi_D$$

$$S_D \approx \sqrt{2}S_H$$

The S-factor is here the intensity ratio between the first vibrational components and the adiabatic peak. The resulting C 1s spectrum after C_2D_2 exposure is shown in Figure 2b. The decomposition gives two components at 283.23 eV and 283.55 eV. This gives an energy shift of (321 ± 11) meV, i.e.

a factor of (1.21 ± 0.05) lower than for non-deuterated acetylene. Likewise, it is found that the intensity ratios for C_2H_2 and C_2D_2 between the low and high intensity components are (0.24 ± 0.01) and (0.31 ± 0.02), respectively. The ratio of the two S-factors is thus (1.29 ± 0.10). Both ratios are somewhat lower than the theoretically predicted values. However, the overall trend, i.e. higher S factor and lower energy split for C_2D_2 compared to C_2H_2, is clearly observed. For both acetylene and deuterated acetylene the second vibrational peak is also included based on the same assumptions given for the above-mentioned relationships. The resulting energy position, E_B, of the adiabatic peak and the energy of the single vibrational loss, $\hbar\omega$, are summarised in Table 1 along with the corresponding S-factors.

Table 1: Results from the decompositions of the spectra in Fig. 2. E_B refers to the energy positions of the adiabatic peaks. The uncertainties are deduced directly from the decomposition (see text).

	E_B	$\hbar\varpi$	S
	eV	meV	%
C_2H_2 on Co(0001)	283.28	389 ± 8	24 ± 1
C_2D_2 on Co(0001)	283.23	321 ± 11	31 ± 2

In the decompositions only the intensity and energy position were assumed to be different for C_2H_2 and C_2D_2. In addition, the Lorentzian and Gaussian width plus the asymmetry function were kept identical for each vibrational succession. If the shift to the high binding energy side had its origin from different chemical sites, one should not see any difference in the two spectra. It is hence concluded that the high binding energy components in Figure 2a are due to vibrational excitation of the C-H stretching mode within the molecule, where the peak at 283.53 eV is determined as the contribution from the first vibrational mode. This implies that the two C atoms of C_2H_2/Co(0001) occupy similar adsorption sites as observed for Pd(111), Ni(111) and Cu(111).

If the excitation energy approaches the ionisation limit, the shape resonance or multiple excitations can influence the S-factor. Recent measurements [32] have shown that such effects can significantly influence the S-factor for CO on Co(0001) at photon energies 16 eV above the location of the shape resonance. The S-factor stated in Table 1 is recorded with a photon energy of 320 eV. Hence, to make sure that an S-factor is obtained where no such effects are present, similar analyses of the C 1s spectrum of acetylene at 300 K have been performed at a photon energy of 380 eV at which an S-factor of (0.17 ± 0.02) is found. This is a somewhat surprising result since experimental and theoretical results for gaseous acetylene [33] predicts a negligible contribution from this mode in the

core-level photoemission process. R. Denecke and co-workers have recently shown that this also is the case for acetylene chemisorbed on Ni(100) [34,35]. If the interpretation above is correct, hybridisation with the Co(0001) surface leads to a substantial increase in the S-factor. Since the S-factor is a measure of the change in the normal coordinates between the ground state and the ionised state (here along the C-H bond), such an increase implies that the potential surface for the final state has been altered along this direction in a larger degree than what is found for gaseous acetylene. The reason for this change is not clear from the available data. One can speculate that the significant electron exchange between cobalt and acetylene, verified by NEXAFS, alters the potential surface of the final state. Increase in the S-factor after adsorption has been reported earlier for methyl groups. M. Wiklund et al. observed an increase of up to 27 % for ethylidyne (C_2H_3) on Rh(111) [36] and 18 % for methoxy (CH_3O) on Cu(100) [3].

For the specific case of small hydrocarbons the C-H stretch vibrational energy has about the same value, around 400 meV, independent of the number of hydrogen bonds [33,37]. The energy split found for acetylene (~389 meV) is in good agreement with this value. However, some influence of the strong C-C stretch mode found at about 240 meV in gaseous acetylene [38] is expected. For gaseous acetylene Kempgens et al. [38] obtained a vibrational energy split of (415 ± 15) meV, i.e. ~6 % higher the value measured in this study.

It should be emphasised that the vibrational data measured here cannot be compared directly to other vibrational spectroscopy techniques (infrared spectroscopy, electron energy loss spectroscopy, etc.) since these methods probe the initial state. In our case the photoemission process leads to a fully screened final state which is equivalent to that of the neighbouring atom to the right in the periodic table, i.e. the atom of atomic number Z is replaced by one having an atomic number (Z+1). This means that C_2H_2 adsorption should be compared to vibrational spectroscopy studies of CNH_2, which are not available.

4. CONCLUSIONS

The adsorption of acetylene on Co(0001) has been investigate using near edge x-ray absorption fine structure (NEXAFS) and high-resolution core level photoemission spectroscopy. Acetylene is molecularly adsorbed on Co(0001) at 110 K with saturation coverage of around 0.3 ML. The NEXAFS spectra show that acetylene adsorbs with the carbon-carbon bond close to parallel orientation with respect to the surface. A comparison with ISEELS K-shell spectrum of gaseous acetylene reveals a strong degree of hybridisation of the C atom close to sp^3. In the C 1s spectra of adsorbed C_2H_2 a shoulder at the high binding energy side with a splitting of (389 ± 8) mV is observed. By comparison with the deuterated counterpart of C_2H_2, C_2D_2, it is suggested that the

structure arises from excitations of the internal C-H molecular vibrational mode. The S-factor of the CH-vibrational mode is determined to be (0.17 ± 0.02), which is considerably higher than those reported for other systems.

ACKNOWLEDGEMENTS

The assistance of the MAX-lab staff is gratefully acknowledged. We also acknowledge financial support from the Norwegian Research Council. MAX-lab is supported by the European Community - Access to Research Infrastructure action of the Improving Human Potential Programme. The authors thank Dr. L. Sæthre and Dr. S. Sorensen for valuable discussions.

REFERENCES

[1] see e.g.: J. Stöhr: NEXAFS Spectroscopy Springer Series in Surface Science 25

[2] J. N. Andersen, A. Beutler, S. L. Sorensen, R. Nyholm, B. Setlik and D. Heskett, Chem. Phys. Lett. 269 (1997) 371.

[3] M. Wiklund, A. Jaworowski, F. Strisland, A. Beutler, A. Sandell, R. Nyholm, S. L. Sorensen and J. N. Andersen, Surf. Sci. 418 (1998) 210.

[4] N. Sheppard, Annual Rev. Phys. Chem. 39 (1988) 589.

[5] H. Hoffmann, F. Zaera, R. M. Ormerod, R. M. Lambert, J. M. Yao, D. K. Saldin, L. P. Wang, D. W. Bennett and W. T. Tysoe, Surf. Sci. 268 (1992) 1.

[6] W. T. Tysoe, G. L. Nyberg, R. M. Lambert, Surf. Sci. 135 (1983) 128.

[7] M. R. Albert, L. G. Sneddon, E. W. Plummer, Surf. Sci. 147 (1984) 127.

[8] J. Vaari, J. Lahtinen and P. Hautojärvi, Catalysis Letters 44 (1997) 43.

[9] R. Nyholm, S. Svensson, J. Nordgren and S. A. Flodström, Nucl. Instrum. Methods in Phys. Res. Sect. A 246 (1986) 267.

[10] J. N. Andersen O. Björnholm, A. Sandell, R. Nyholm, J. Forsell, L. Thånell, A. Nilsson and N. Mårtensson, Synchrotron Radiat. News 4 (4) (1991) 15.

[11] A.P. Hitchcock and C. E. Brion, J.El.Spec. 10 (1977) 317.

[12] The height of the π^* state is measured from the peak intensity to the step edge intensity for gaseous acetylene and to the Fermi-edge intensity for acetylene adsorbed on Co(0001)

[13] J. Stöhr, F. Sette and A. L. Johnson, Phys. Rev. Lett. 53 (1984) 1684.

[14] D. Arvanitis U. Döbler, L. Wenzel and K. Baberschke, Surf. Sci, 178, (1986) 686.

[15] N. Haack, G. Ceballos, H. Wende, K. Baberschke, D. Arvanitis, A. L. Ankudinov and J. J. Rehr, Phys. Rev. Lett. 84, (2000) 614.

[16] T. D. Thomas, N. Berrah, J. Bozek, T. X. Carroll, J. Hahne, T. Karlsen, E. Kukk and L. J. Sæthre, Phys. Rev. Lett. 82 (1998) 1120.

[17] see e.g. M. N. Piancastelli, J. of Electron Spect. and Related Phenomena 100 (1999) 167.

[18] H. Kempgens, H. M. Köppe, A. Kivimäki, M. Neeb, K. Maier, U. Hergenhahn and A. M. Bradshaw, Phys. Rev. Lett. 79, (1997) 35.

[19] R. E. Farren, J. A. Sheehy and P. W. Langhoff, Chem. Phys. Lett. 177 (1991) 307.

[20] T. D. Thomas, N. Berrah, J. Bozek, T. X. Carroll, J. Hahne, T. Karlsen, E. Kukk and L. J. Sæthre, Phys. Rev. Lett. 82 (1998) 1120.
[21] C. J. Baddeley, A. F. Lee, R. M. Lambert, T. Gieβel, O. Schaff, V. Fernandez, K.-M. Schindler, A. Theobald, C. J. Hirschmugl, R. Lindsay, A. M. Bradshaw and D. P. Woodruff, Surf. Sci. 400 (1998) 166.
[22] S. Bao, K.-M. Schindler, Ph. Hofmann, V. Frizsche, A. M. Bradshaw, D. P. Woodruff, Surf. Sci. 291 (1993) 295.
[23] S. Bao, Ph. Hofmann, K.-M. Schindler, V. Frizsche, A. M. Bradshaw, D. P. Woodruff, C. Casado, M. C. Asensio, J. Phys. Condens. Matter 6 (1994) L93
[24] S. Bao, Ph. Hofmann, K.-M. Schindler, V. Frizsche, A. M. Bradshaw, D. P. Woodruff, C. Casado, M. C. Asensio, Surf. Sci. 307-309 (1994) 722.
[25] S. Bao, Ph. Hofmann, K.-M. Schindler, V. Frizsche, A. M. Bradshaw, D. P. Woodruff, C. Casado, M. C. Asensio, Surf. Sci. 323 (1995) 19.
[26] Handbook of Chemistry and Physics, edited by D. R. Lide (CRC Press, Boca Raton, 1994)
[27] S. Doniach and M. Šunjić, J. Phys. C3 (1970) 285.
[28] Curve fitting routine developed by D. Adams at the Institute of Physics and Astronomy, University of Århus, Denmark
[29] N. Mårtensson and A. Nilsson, J. of Electron Spectroscopy and Related Phenomena, 75 (1995) 209.
[30] J. C. Dunphy, M. Rose, S. Behler, D. F. Ogletree, M. Salmeron and P. Sautet, Phys. Rev. B 57 (1997) 12705.
[31] L. S. Cederbaum and W. Domcke, J. Chem. Phys. 64 (1976) 603.
[32] T. Ramsvik, A. Borg, M. Kildemo, S. Raaen, A. Y. Matsuura, A. J. Jaworowski, T. Worren and M. Leandersson, Surface Science 492 (2001) 152.
[33] S. J. Osborne, S. Sundin, A. Ausmees, S. Svensson, S. L. Sorensen, L. J. Sæthre, O Sværen, J. Végh, J. Karvonen, S. Aksela and A. Kikas, J. Chem. Phys. 106 (1997) 1661.
[34] The acetylene overlayer was prepared by exposing ethylene at low temperature, with a subsequent dehydrogenation through annealing
[35] R. Denecke, R. Neubauer, C. Whelan, H.-P. Steinrück, to be published.
[36] M. Wiklund, A. Beutler, R. Nyholm and J. N. Andersen, Surf. Sci. 461 (2000) 107.
[37] L. Sæthre, O. Sværen, S. Svensson, S. J. Osborne, T. D. Thomas, J. Jauhiainen and S. Aksela, Phys. Rev. A 55 (1997) 2848.
[38] B. Kempgens, H. Köppel, A. Kivimäki, M. Neeb, L. S. Cederbaum, and A. M. Bradshaw, Phys. Rev. Lett. 79 (1997) 3617.

Paper II

Acetylene adsorption on cobalt single crystal surfaces

T. Ramsvik, A. Borg, M. Kildemo, and F. Hansteen

Submitted to Surface Science

ACETYLENE CHEMISORPTION AND DECOMPOSITION ON COBALT SINGLE CRYSTAL SURFACES

T. Ramsvik[†], A. Borg[†], H. J. Venvik[‡], F. Hansteen[†], M. Kildemo[†] and T. Worren[†]

[†] *Dept. of Physics, Norwegian University of Science and Technology, N-7491 Trondheim, NORWAY*

[‡] *SINTEF Applied Chemistry, N-7465 Trondheim, NORWAY*

Abstract

Acetylene chemisorption and dissociation on the Co(0001) and Co(11$\bar{2}$0) surfaces has been studied using high-resolution core level photoemission spectroscopy, near-edge x-ray absorption fine structure (NEXAFS), low energy electron energy diffraction (LEED) and scanning tunneling microscopy (STM). For chemisorption on Co(0001) dissociation to carbidic and graphitic carbon occurs at temperatures above 300 K. Below this temperature acetylene adsorb molecularly with its carbon-carbon bond parallel to the surface. Acetylene chemisorption on the anisotropic Co(11$\bar{2}$0) surface lead to dissociation at ~200 K, i.e. significantly lower than for C_2H_2 on Co(0001). NEXAFS measurements show that acetylene hybridise strongly with the Co(11$\bar{2}$0) surface, forming antibonding states below the ionisation limit which are not present in the gas-phase. In the temperature region from ~200 K to ~300 K a dehydrogenated fragment, possibly of the form C_2H or C_2, is found to co-exist with molecular acetylene. Further heating to ~450 K leads to decomposition of this fragment to graphitic carbon, while an ordered (5×2) carbon overlayer starts to form at the expensive of molecular acetylene. At ~570 K this ordered overlayer is fully developed. By combining results from photoemission spectroscopy measurements, LEED and STM, a hard sphere model for the carbon overlayer relative to the Co substrate is proposed. Above ~600 K a substantial decrease in the amount of ordered carbon atoms is seen, leaving mainly graphitic carbon on the Co(11$\bar{2}$0) surface.

1. INTRODUCTION

Studies of the bonding and reactivity of unsaturated hydrocarbon molecules adsorbed on transition metal single crystal surfaces are important for a molecular-level understanding of heterogeneous hydrocarbon catalysis. The adsorption and decomposition of acetylene on metal surfaces has been studied extensively the last 30 years, particularly by vibrational spectroscopy (for a review, see e.g. ref. [1]). Normally, at temperatures below room 300 K, acetylene adsorbs molecularly with its carbon-carbon bond parallel to the surface. The thermal induced decomposition produces several types of fragments depending on both the initial coverage and the substrate. However, exceptions from these trends exist: an example which has received considerable attention is acetylene adsorbed on Pd(111) where partial desorption (20 to 35 %) was found due to benzene formation on the surface [2,3].

In the present work, we present a comparative study of chemisorption and decomposition of C_2H_2/Co(0001) and $C_2H_2/\mathrm{Co}(11\bar{2}0)$. C_2H_2/Co(0001) has been extensively investigated previously using numerous surface analysis techniques, while, to our knowledge, investigations of $C_2H_2/\mathrm{Co}(11\bar{2}0)$ have not been reported in literature. For the C_2H_2/Co(0001) system, acetylene adsorbs with its carbon-carbon bond in a near parallel orientation with respect to the cobalt surface for temperatures below 320 K [4, 5, 6]. In this temperature region acetylene forms a strong chemisorption bond to the substrate, creating a state of hybridisation close to sp^3 [6]. Thermal decomposition occurs at 400 K, which results in a carbonaceous overlayer consisting mainly of graphitic carbon but with a small amount of carbon in a carbidic form [5].

In this work, high resolution core level photoemission spectroscopy, near-edge X-ray absorption fine-structure (NEXAFS), LEED and Scanning Tunneling Microscopy (STM) have been used to study the chemisorption and decomposition of C_2H_2 adsorbed on the Co(0001) and $\mathrm{Co}(11\bar{2}0)$ single crystal surfaces as function of temperature. It is confirmed that acetylene starts to decompose on Co(0001) above ~300 K, which results in two peaks interpreted earlier as due to carbidic and graphitic carbon. On $\mathrm{Co}(11\bar{2}0)$, NEXAFS measurements show a strong hybridisation between the acetylene molecules and the substrate at ~120 K, creating additional states below the ionisation limit. The adsorbed acetylene starts to decompose at ~200 K, i.e. at a significantly lower temperature than for Co(0001). The decomposition fragments below 300 K are suggested to involve C_2 or C_2H in coexistence with molecular acetylene. Further heating lead to a decomposition of the dehydrogenated fragment to graphitic carbon, and formation of an ordered (5×2) overlayer [7,8]. By combining results from STM, LEED and core-level

photoemission spectroscopy measurements, a structural model for the ordered carbon overlayer is proposed.

2. EXPERIMENTS

The core-level photoemission and NEXAFS experiments were performed at the soft X-ray beamline 22[1] at the MAX I and beamline D1011 at the MAX II synchrotron sources. These beamlines are equipped with a modified Zeiss SX-700 monochromator and a large Scienta-type hemispherical photoelectron energy analyser [9, 10]. The total experimental resolutions were ~ 170 meV for BL22 and ~160 meV for D1011 in the energy range 320 – 380 eV. The NEXAFS spectra were measured in the partial electron yield mode.

The cobalt single crystals were cleaned by repeated cycles of Ar+ sputtering at ~570 K, heating in oxygen at 5×10^{-8} mbar in the temperature range 300 K to 600 K, and annealing at ~639 K in UHV. Residual oxygen was removed by additional cycles of sputtering and annealing.

The C_2H_2 overlayer was prepared by exposing the Co(0001) and Co(11$\bar{2}$0) surfaces to 10 L and 6 L of gas molecules, respectively, at substrate temperature below 120 K. The acetylene gas was provided by L'Air Liquide (99.0 % purity). All measurements of the adsorbate C 1s core-level spectra and the C K-shell NEXAFS spectra were performed at a sample temperature of 110 K in order to reduce the broadening due to low-energy vibrational modes. For each temperature LEED patterns were recorded to determine possible ordered overlayer structures.

The STM studies were performed in a separate home laboratory, with an UHV STM from Omicron Vakuumphysik GmbH. The STM measurements can be done at room temperature only, and the instrument is equipped with a tripod piezoscanner. The probe tip was prepared from tungsten wire. The STM measurements were carried out in the constant current mode with bias voltages from 7 mV to 350 mV and tunnel currents between 5.6 to 6.4 nA. All the images are presented as greyscale images, with the darkest colours representing the lowest levels. The STM laboratory also allows for standard LEED measurements.

The (5×2) carbon overlayer on Co(11$\bar{2}$0) was obtained in two ways: By adsorbing small amount of C_2H_2 ($\leq$ 3L) with a following heating of the sample to ~570 K for 5 minutes, or exposing up to 20 L of ethylene (C_2H_4) with the sample kept between 470 to 520 K. Before STM measurements were performed, the sample was cooled to 300 K.

[1] This beamline has been moved from MAX I to MAXII and is now called D1011.

3. RESULTS AND DISCUSSION

3.1. C_2H_2 on Co(0001)

Acetylene decomposition on Co(0001) has been reported earlier [4, 5]. However, due to the superior resolution obtained by using high-brilliance light from synchrotron storage rings a reinvestigation of the results is well justified.

Figure 1 shows the C 1s core level spectra after heating 10 L C_2H_2 adsorbed on Co(0001) at 110 K to temperatures in the range 150 K – 650 K.

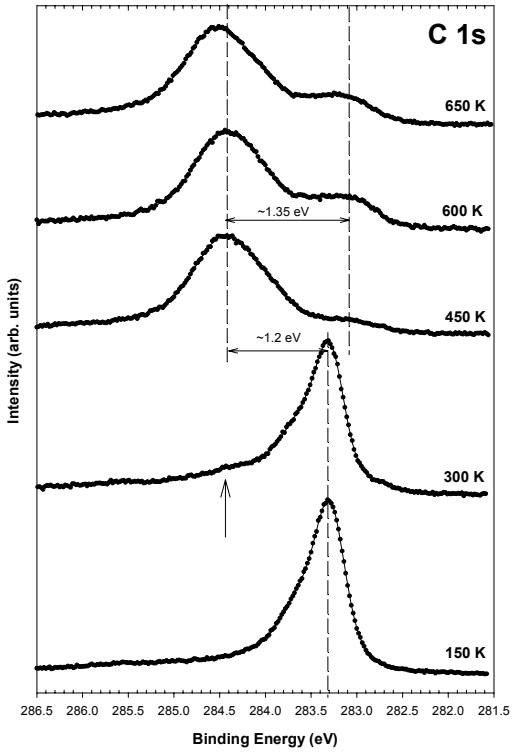

Figure 1: C 1s photoemission spectra after a saturation exposure of acetylene (C_2H_2) on Co(0001) at 110 K, followed by heating up to 650 K. All spectra were measured at a photon energy of 380 eV and with resolution ≤ 170 meV.

The overlayer corresponds to a coverage of about 0.3 ML, as deduced from the variations in the Co 2p spectra. At 150 K acetylene is still adsorbed molecularly on the Co(0001) surface with the carbon-carbon bond parallel to the surface, resulting in only one adiabatic peak at ~283.3

eV. NEXAFS experiments showed that acetylene forms a strong chemisorption bond to the substrate at these temperatures, creating a state of hybridisation close to sp^3 [6]. At 300 K most acetylene molecules are intact, but at ~284.5 eV a small contribution corresponding to a beginning decomposition can be seen (marked with an arrow in figure 1). The shoulder on the high binding energy side of the adiabatic peak is due to vibrational losses from the C-H stretch mode [6]. Heating to 450 K causes the acetylene to decompose completely, and two broad spectral contributions to appear at ~284.5 eV and ~283.1 eV. Only a minor decrease in the integrated C 1s intensity is observed from 150 K to room temperature, indicating negligible desorption. However, from room temperature to 650 K a 21% increase is observed which is interpreted as additional carbon segregating from the bulk. Based on the work by J. Nakamura et al. [11] the low and high binding energy contributions were suggested to originate from carbidic and graphitic carbon, respectively. The C 1s photoemission spectra reported here confirm the experimental findings by Vaari et al. [5] with some minor variations. The fact that only the substrate (1×1) pattern is observed for these temperatures indicates that the graphitic carbon, i.e. chemically inert carbon atoms, do not form ordered 6-fold graphite rings. Such rings have been observed for other systems. [12-14], but after annealing to considerably higher temperatures. The small shift of ~0.1 eV seen for the both the high- and low binding energy peaks between 600 K and 650 K may indicate minor changes in the carboneous layer upon heating. However, a shift caused by instability in the beam cannot be excluded.

3.2. C_2H_2 on Co(11$\bar{2}$0)

Figure 2a shows the polarisation dependent NEXAFS spectra at the C K-shell absorption edge after a 6 L C_2H_2 exposure of Co(11$\bar{2}$0) at 119 K. The measurements where recorded at 90° and 54.7° incidence angles and with a total experimental resolution of ~0.46 eV. At this temperature acetylene adsorbs molecularly, as verified by a single peak in the core level photoemission spectra (see fig. 3 and later discussions). The $\pi_{C\text{-}C}$* resonance peak is observed at ~286 eV, i.e. a shift of 0.5 eV to higher excitation energy compared to the gas phase [15]. The $\pi_{C\text{-}C}$* resonance and the apparent $\sigma_{C\text{-}C}$* shape resonance (~296 eV) are nearly identical in intensity. Changing the incidence angle leads to only a minor change in the intensities of the two states. The sample was mounted with the troughs of the anisotropic Co(11$\bar{2}$0) surface at ~45° relative to the incoming electrical field vector (***E***) (see figure 4).

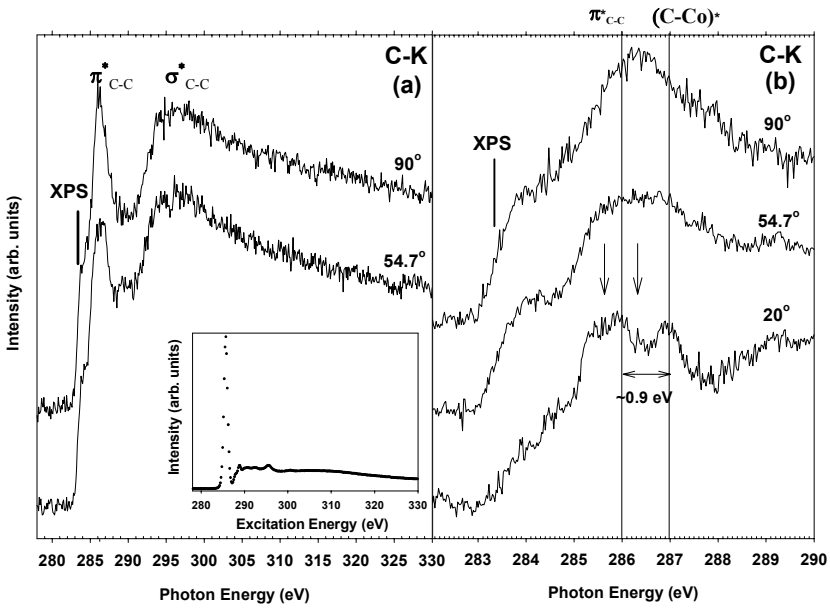

Figure 2:

(a) Carbon K-shell NEXAFS spectra of 6 L C_2H_2 on Co(11$\bar{2}$0) at 119 K, recorded at normal (90°) and magic (54.7°) incidence angles. The total instrumental resolution was ≤ 460 meV. The inset figure shows ISEELS K-shell spectrum of gaseous acetylene [15].

(b) The Carbon K-shell NEXAFS spectra around the π* resonance recorded at normal, magic and grazing (20°) incidence angles. The resolution was ≤ 200 meV.

If one assumes that the C-C bond is either parallel or perpendicular to these troughs, the components of the E-vector will give contributions of similar magnitude, independent of the incident angles. For the systems C_2/Ag(110) [16] and C_2H_2/Ni(110) [17] the C-C bonds have been determined to lay along the substrate troughs. However, any unambiguous determinations of the acetylene geometry require additional experiments where the azimuthal angle of either the electrical field or the sample is allowed to vary.

It has been claimed that the broad feature in the photoabsorption cross section of gaseous C_2H_2, centred at ~310 eV, is largely due to satellite contributions [18], i.e. the true shape resonance predicted in theory [19] is weak. However, this has been contradicted in more recent publications [20,21]. If the broad peak seen at ~296 eV in fig. 2a is a true shape resonance (σ_{C-C}*) its energy location is at significantly lower excitation energy as compared to the position of this resonance for the system C_2H_2/Co(0001) (299 eV) [6]. A shift of the shape resonance toward the ionisation limit relative to the Co(0001) surface indicates a stronger

hybridisation on $Co(11\bar{2}0)$. This is not surprising since the more open, trough like structure of $Co(11\bar{2}0)$ may give more complex hybridisation with the substrate.

Comparison with ISEELS experiments of gaseous acetylene (insert in fig. 2a) further confirms that there is a high degree of hybridisation with the substrate where both π* antibonding orbitals ($\pi_\perp$* and $\pi_\parallel$*) contribute to the chemisorption bond. For chemisorbed acetylene the FWHM for the π* resonance recorded at 54.7° (magic angle) is ~2.9 eV, which is considerably larger than for gaseous acetylene of ~1 eV [15]. Such an effect has also been observed for the system C_2H_2/Co(0001) [6]. This is partly attributed to the increased natural linewidths for the adsorbed molecule, reflecting the additional decay channels for the core-excited molecule when the substrate is present [22]. However, a closer inspection of the π* resonance reveals a change in shape going from magic to normal incidence angle. This is not expected if an increase in natural linewidth is the only cause. To further investigate this, additional NEXAFS measurement around the π* resonance have been recorded at normal (90°), magic (54.7°) and grazing (20°) incidence angels, with a total experimental resolution of ~0.2 eV. The resulting spectra are given in Figure 2b. Here the change of shape is more apparent. Particularly the spectrum obtained for grazing incidence shows additional structures that were not observed for the long energy scan measurements. A distinct peak is seen at an excitation energy of ~286.9 eV, ~0.9 eV higher than the position of the π* resonance. Such a peak is not present for C_2H_2 in gas- [15] or solid-phase [22]. Hence it is likely that the peak represents transition to a new acetylene – cobalt resonance. This resonance is expected to have its C-Co bond in a near upright position relative to the surface. The reduced intensity at 286.9 eV for normal incidence supports this interpretation. A similar adsorption induced state displaced 1.3 eV from the π* resonance has been suggested by F. Matsui et al. [23] who studied the system C_2H_2/Si(100)2×1 by NEXAFS and UPS. In a theoretical study of a C_2/Ag_6(110) cluster by P. A. Stevens et al. [16] a new (C_2-Ag)* orbital was assigned ~2 eV above the π* resonance. This resonance was also deduced for ***E*** along the C-C bond direction, and hence contains some σ character. Since our experiment did not permit variations of the azimuthal angle, any assignment of π or σ character is not possible. In fig. 2b this resonance is marked (C-Co)*, where the star signify its antibonding nature. A similar carbon-cobalt induced antibonding state located ~0.7 eV above π* resonance has been suggested for the system C_2H_2/Co(0001) [6]. It is not totally excluded that the observed peak originates from the $\sigma_{C\text{-}H}$* resonance. For both gaseous acetylene [15] and acetylene chemisorbed on Ag(100) [24, 25] this resonance is found

at ~289 eV, i.e. ~3.5 eV above its π* resonance. A higher degree of charge transfer from the cobalt substrate to the C-H* state compared to the weakly chemisorbed system C_2H_2/Ag(100) is expected. Thus some energy shift would not be surprising. However, a shift of ~2.6 eV to lower energies is substantial and seems unlikely. For the system C_2H_2/Si(001)2×1, which forms a stronger hybridisation than C_2H_2/Ag(100), a shift of just ~0.1 eV to higher energies was observed [23].

In the energy region 287.4 to 290 eV the spectrum for the grazing incidence shows additional structure. This is the region where the $\sigma_{C\text{-}H}$* resonance is expected to be located. The structure observed in the lower spectrum of fig. 2b may therefore be partly explained by a broad $\sigma_{C\text{-}H}$*, though any determination of such a resonance is problematical due to the low signal-to-noise ratio.

The π* resonance observed at grazing incidence is located at 285.7 eV, i.e. ~0.7 eV lower than the peak recorded at normal incidence (marked with arrows in the fig. 2b). Due to the different hybridisation with the cobalt substrate, the two π* resonances, $\pi_{\|}$* and $\pi_{\perp}$*, are not degenerate as the case for gaseous acetylene. By increasing the incidence angle the high energy side of the π* resonance becomes more dominant, as apparent from the different shoulders at low energies for magic and normal incidence. Due to the strong hybridisation any significant contribution from the $\pi_{\perp}$* orbitals is not expected. A possible interpretation could therefore be that the structure is caused by a splitting of the $\pi_{\|}$* and $\pi_{\perp}$* orbitals, with approximate positions marked with arrows in fig. 2b. The arrow at lower photon energy marks the position of the π* resonance perpendicular to the Co(11$\bar{2}$0) surface. The vertical line represent the energy position of the π* resonance and is taken as the mean of the apparent $\pi_{\|}$* and $\pi_{\perp}$* positions.

Figure 3 shows a series of C 1s photoemission spectra after 6 L exposure of acetylene at 119 K, followed by heating to temperatures up to 640 K.. At the lowest temperature only one component is observed at binding energy ~283.3 eV, interpreted as acetylene adsorbed with its C-C bond parallel to the cobalt surface. Compared to the total instrumental resolution (≤ 160 meV) the Gaussian broadening is large, indicating a high degree of disorder. This is supported by LEED, which only shows the substrate (1×1) pattern.

From Fig. 3 it can be seen that acetylene starts to decompose at ~200 K, which is at considerably lower temperature than observed for the C_2H_2/Co(0001) system (see section 3.1). This is in agreement with the NEXAFS measurements. In the temperature region from ~200 K to ~450 K a contribution at around 284.0 eV is observed.

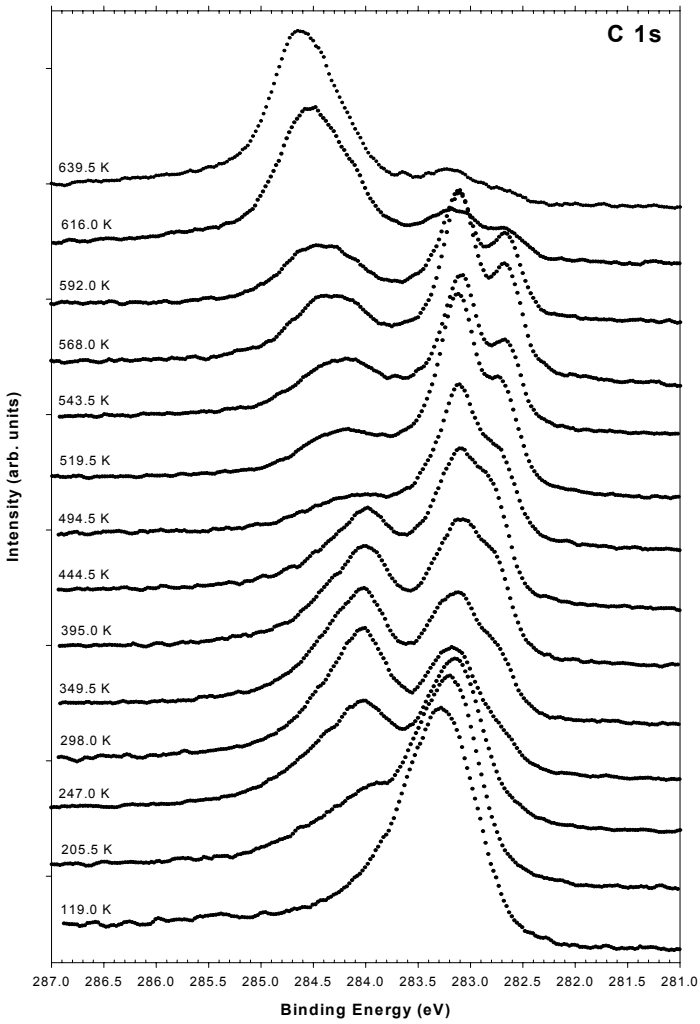

Figure 3: C 1s photoemission spectra after a 6 L exposure of C_2H_2 on Co(11$\bar{2}$0) at 119 K**,** followed by heating to the specified temperatures. All the spectra were recorded with a photon energy of 380 eV. The total resolution was ≤ 160 meV.

The photoemission data alone do not give any definite identification of the peak's origin. However, polarisation dependent NEXAFS spectra have been recorded also at 298 K, where the intermediate fragment has its strongest intensity. The spectra show a close resemblance to the spectra obtained at ~119 K, where only acetylene with its C-C bond parallel to the substrate is present. The most prominent difference is a shift of the $\pi^*_{C\text{-}C}$ peak of ~0.8 eV to higher excitation energies, which is close to the measured binding energy difference between the two

species observed at 298 K in Fig. 3 (~0.84 eV). Therefore it is considered most likely that the contribution at ~284.0 eV originates from dehydrogenated acetylene where its C-C bond is maintained, i.e. either as C_2H or C_2.

Above 450 K three peaks are observed in the photoemission spectra of Fig. 3 and identified as being due to carbon in two different environments. The two peaks with lowest binding energies start to develop at ~300 K, as deduced from the shift of the acetylene related peak to ~283.1 eV and a small contribution at ~282.8 eV. By increasing the temperature to ~590 K, the contribution at 283.1 eV is constant while a minor shift from ~282.8 to 282.7 eV is seen for the other. For both peaks the FWHM are significantly reduced for elevated temperatures. These contributions are caused by an ordered (5×2) carbon overlayer, as observed by LEED (Figure 4).

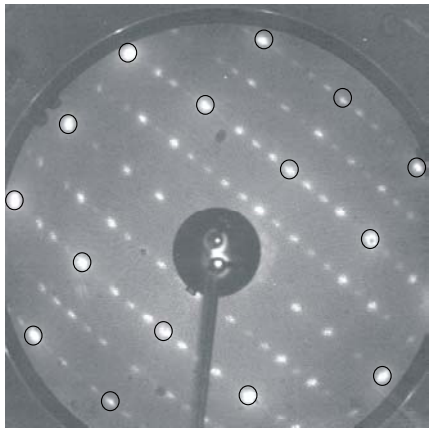

Figure 4: (5×2) LEED pattern recorded at 160 eV after a 6 L C_2H_2 exposure on the $Co(11\bar{2}0)$ surface at 119 K, followed by a heating of the sample to ~570 K for 5 minutes. The circles indicate the location of the substrate LEED spots. The direction of the "missing spots" corresponds to the [0001] direction in real space.

Such overlayer has been reported earlier by adsorption and thermal decomposition of ethylene on $Co(11\bar{2}0)$ [7, 8]. Based on STM results a model with carbon atoms occupying equal chemisorption sites was proposed [8]. Our results show two distinct peaks, which is in contradiction to these conclusions.

Figure 5 a) and b) display 40×40 nm^2 size STM images of the ordered overlayer where the $Co(11\bar{2}0)$ surface has been exposed for 0.75 L and 3 L of C_2H_2, respectively.

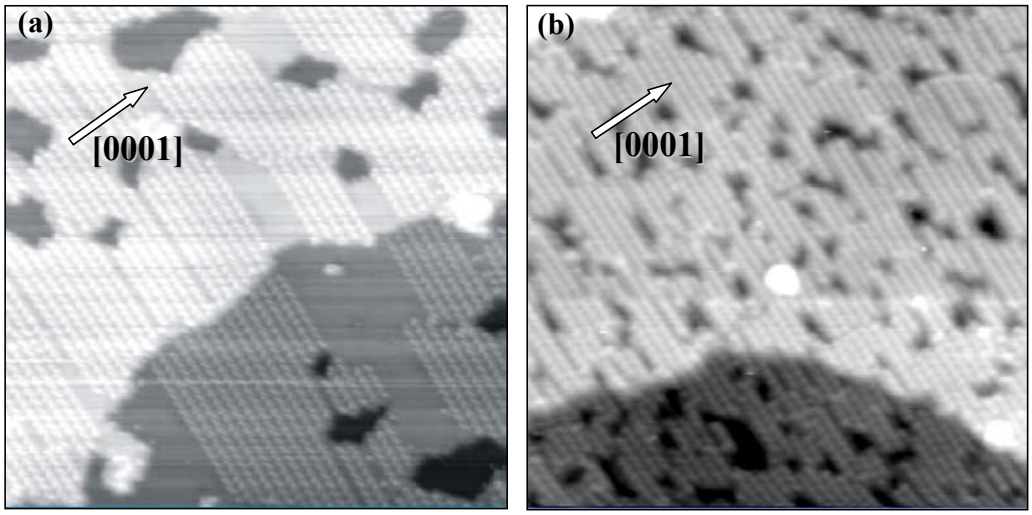

Figure 5: 40× 40 nm^2 STM images of the (5×2) carbon overlayer. The [0001] direction is indicated as white arrows in both images.

(a) 0.75 L C_2H_2, areas exposing the clean $Co(11\bar{2}0)$ surface. Greyscale range: 0.258 nm.

(b) 3 L C_2H_2, leading to a saturated surface. Greyscale range: 0.214 nm.

As seen in both images the carbon atoms are forming chains running perpendicular to the [0001] direction, with mismatch defects of varying density and size, as reported earlier [8]. After an exposure of 0.75 L (Fig. 5a) the (5×2) carbon overlayer coexists with domains of the clean (1×1) surface. Increasing the amount of C_2H_2 to 3 L leads to a fully saturated surface. Figure 6 a) and b) display atomically resolved STM images of the clean $Co(11\bar{2}0)$ surface and the (5×2) carbon overlayer, respectively.

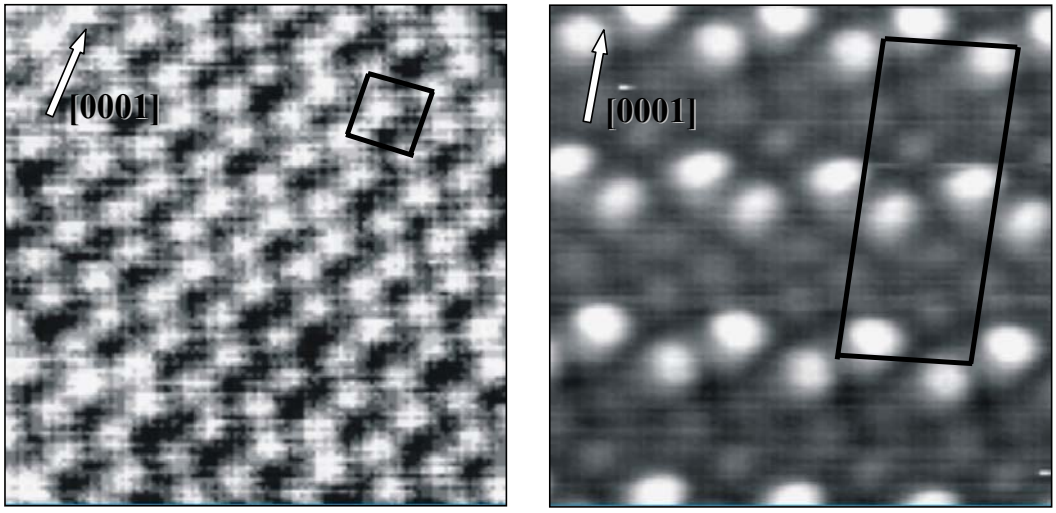

Figure 6: Atomically resolved STM images, 3.22×3.22 nm^2. For both images the unit cells are indicated as black, rectangular frames.

(a) The clean $Co(11\bar{2}0)$ surface with the zigzag chains of atoms running along [0001]. The size of the indicated unit cell is 0.407×0.435 nm^2. Greyscale range: 0.030 nm.

(b) The (5×2) carbon overlayer with buckled rows of spherical protrusions perpendicular to [0001], with a unit cell of 2.035×0.870 nm^2. Greyscale range: 0.134 nm.

The two images are of equal sizes, with the zigzag chains of cobalt atoms running along the [0001] direction. H. J. Venvik et al. [8] suggested that the buckled rows of spherical protrusions seen in Fig. 6b correspond to carbon atoms, while the spherical features appearing with darker greyscale originate from top layer Co atoms. If the $Co(11\bar{2}0)$ surface is considered composed of the first and second layer Co atoms the carbon overlayer, would according to this model, correspond to a coverage of 0.1 ML.

From the decrease of the Co 2p core-level intensity from clean to acetylene covered $Co(11\bar{2}0)$ surface, a rough estimate of ~0.3 ML of carbon atoms is found. ~76 % of these carbon atoms contribute to the two narrow peaks in Fig. 2, originating from the (5×2) carbon overlayer. The resulting effective overlayer coverage is thus ~0.23 ML. A proper deconvolution of the two peaks using Doniach-Šunjić line profiles [26] convoluted by a Gaussian function [27] gives an intensity ratio of 0.69 at high photon energies, i.e. where

diffraction effects should be insignificant[2]. Based on the additional information from the photoemission spectroscopy measurements a new structural model is suggested, and is presented in Figure 7.

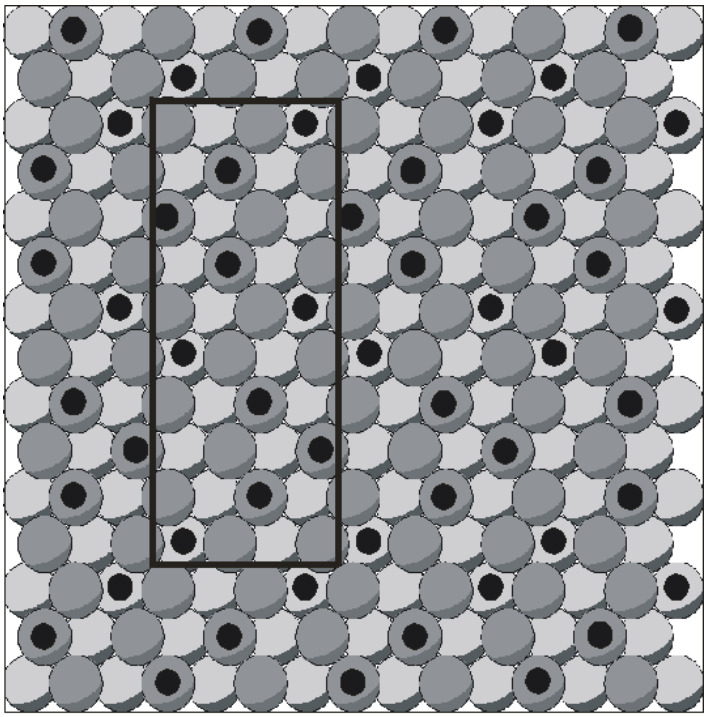

Figure 7: Suggested structural model of the (5×2) carbon overlayer on $Co(11\bar{2}0)$. The (5×2) unit cell is indicated as a black rectangular frame. The dark- and light gray spheres represent the first and second Co layer, respectively, while the carbon atoms are illustrated as black, filled spheres. The carbon coverage for this model is 0.25 ML (see text).

The (5×2) unit cell (indicated in the figure) now consist of 10 carbon atoms, where 6 and 4 are located on-top of Co-atoms in the first and second layer, respectively. This model gives a ratio of 4/6 (=0.67), which agrees well with the results obtained from the photoemission spectroscopy measurements. Also the coverage, 0.25 ML, is more in accordance with experiments. According to this model all the spherical features observed in Fig. 6b are due to carbon atoms. The darkest appearing features in the STM image are consequently carbon sitting

[2] By changing the photon energy considerable variations in the peaks ratio are obtained, showing that they originate from carbon atoms adsorbed at sites with different chemical environments.

on-top of first layer cobalt atoms. The different appearance of the carbon atoms at the two different sites in the STM images may be due to electron effects.

The new, broad contribution observed at ~284.1 eV at ~500 K increases in both intensity and binding energy as the temperature is raised. At ~640 K its binding energy is ~284.6 eV, which coincide with the contribution obtained at high temperature for the system C_2H_2 on Co(0001) (see section 3.1). Also for C_2H_2 on Co(11$\bar{2}$0) only the (1×1) LEED pattern is seen for the highest temperatures. It is therefore suggested that a disordered layer of graphitic carbon similar to the one found on the more close-packed surface is formed. The two low-intensity peaks appearing at the highest temperatures are most likely caused by residual carbon atoms from the ordered overlayer. In contrast to the system C_2H_2/Co(0001) no evidence of any formation of carbidic carbon is found.

4. CONCLUSIONS

The acetylene chemisorption and decomposition on Co(0001) and Co(11$\bar{2}$0) single crystal surfaces have been studied with high-resolution core level photoemission spectroscopy, NEXAFS, LEED and STM. For the system C_2H_2/Co(0001), acetylene adsorbs molecularly with its carbon-carbon bond parallel to the surface at 110 K. Above 300 K decomposition takes place, most probably to carbon atoms in carbidic and graphitic form. The results are in accordance with previous investigations.

From photoemission spectroscopy and NEXAFS measurements it is concluded that acetylene also adsorbs molecularly on the Co(11$\bar{2}$0) surface at low temperatures (< ~200K), with its C-C bond in a near parallel orientation relative to the surface. Polarisation dependent NEXAFS measurements show a considerable reduction in the $\pi_{C\text{-}C}$* resonance compared to the gas phase demonstrating that there is a high degree of hybridisation with the substrate. An apparent $\sigma_{C\text{-}C}$* shape resonance at ~296 eV confirms this interpretation. From NEXAFS measurements recorded below the ionisation limit with higher resolution, additional structures are observed. It is suggested that the pronounced peak located ~0.9 eV higher than the $\pi_{C\text{-}C}$* resonance is caused by a new acetylene-cobalt antibonding state.

The adsorbed acetylene starts to decompose at ~200 K, i.e. at significantly lower temperature than for C_2H_2/Co(0001). The decomposition fragments below 300 K are suggested to involve C_2 or C_2H in coexistence with molecular acetylene. Further heating lead to a decomposition of the dehydrogenated fragment to graphitic carbon, and formation of an ordered (5×2) overlayer. By combining results from STM, LEED and core-level photoemission

spectroscopy measurements, a structural model for the carbon atoms relative to the Co substrate is proposed. Above ~600 K a considerable decrease of the ordered overlayer is observed leaving predominantly graphitic carbon in the $Co(11\bar{2}0)$ surface.

ACKNOWLEDGEMENTS

The assistance of the MAX-lab staff is gratefully acknowledged. We also acknowledge financial support from the Norwegian Research Council. MAX-lab is supported by the European Community - Access to Research Infrastructure action of the Improving Human Potential Programme.

REFERENCES

[1] N. Sheppard: Annual Rev. Phys. Chem. 39 (1988) 589-644

[2] H. Hoffmann, F. Zaera, R. M. Ormerod, R. M. Lambert, J. M. Yao, D. K. Saldin, L. P. Wang, D. W. Bennett and W. T. Tysoe: Surf. Sci. 268 (1992) 1.

[3] W. T. Tysoe, G. L. Nyberg, R. M. Lambert: Surf. Sci. 135 (1983) 128.

[4] M. R. Albert, L. G. Sneddon, E. W. Plummer, Surf. Sci. 147 (1984) 127.

[5] J. Vaari, J. Lahtinen and P. Hautojärvi, Catalysis Letters 44 (1997) 43.

[6] T. Ramsvik, A. Borg, T. Worren and M. Kildemo, submitted to Phys. Rev. B

[7] A. Atrei, U. Bardi, G. Rovida, M. Torrini and E. Zanazzi, J. Vac. Sci. Technol. A 5 (1987) 1006.

[8] H. J. Venvik and A. Borg, Applied Physics A 66 (1998) S491.

[9] R. Nyholm, S. Svensson, J. Nordgren and S. A. Flodström, Nucl. Instrum. Methods in Phys. Res. Sect. A 246 (1986) 267.

[10] J. N. Andersen O. Björnholm, A. Sandell, R. Nyholm, J. Forsell, L. Thånell, A. Nilsson and N. Mårtensson, Synchrotron Radiat. News 4 (4) (1991) 15.

[11] J. Nakamura, I. Toyoshima and K. Tanaka, Surf. Sci. 201 (1988) 185.

[12] B. Lang, Surf. Sci. 53 (1975) 317.

[13] R. P. Merrill and D. L. Smith, Surf. Sci. 21 (1970) 203.

[14] E. Janin, M. Göthelid and U. O. Karlsson, Appl. Surf. Sci. 162-163 (2000) 184.

[15] A.P. Hitchcock and C. E. Brion, J. El. Spec. 10 (1977) 317.

[16] P. Stevens, T. H. Upton, J. Stöhr, R. J. Madix: Phys. Rev. Lett. 67 (1991) 1653.

[17] M. Weinelt, W. Huber, P. Zebisch, H.-P. Steinrück, P. Ulbricht, U. Birkenheuer, J. C. Boettger and N. Rõsch, J. of Chem. Physics, 102 (1995) 9709.

[18] H. Kempgens, H. M. Köppe, A. Kivimäki, M. Neeb, K. Maier, U. Hergenhahn and A. M. Bradshaw, Phys. Rev. Lett. 79 (1997) 35.

[19] R. E. Farren, J. A. Sheehy and P. W. Langhoff, Chem. Phys. Lett. **177**, 307 (1991).

[20] N. Haack, G. Ceballos, H. Wende, K. Baberschke, D. Arvanitis, A. L. Ankudinov and J. J. Rehr, Phys. Rev. Lett. 84 (2000) 614.

[21] T. D. Thomas, N. Berrah, J. Bozek, T. X. Carroll, J. Hahne, T. Karlsen, E. Kukk and L. J. Sæthre, Phys. Rev. Lett. 82 (1998) 1120.

[22] H. Rabus, D. Arvanitis, M. Domke and K. Baberschke, J. Chem. Phys. 96 (1992) 1560.

[23] F. Matsui, H. W. Yeom, I. Matsuda and T. Ohta, Phys. Rev. B, 62 (2000) 5036.

[24] D. Arvanitis, K. Baberschke, L. Wenzel, U. Döbler, Phys. Rev. Lett. 105 (1986) 3175.

[25] D. Arvanitis, H. Rabus, L. Wenzel, K. Baberschke, Z. Phys. D 11 (1989) 219.

[26] S. Doniach and M. Šunjić, J. Phys. C3 (1970) 185.

[27] Curve fitting routine developed by D. Adams at the Institute of Physics and Astronomy, University of Århus, Denmark

Paper III

Molecular vibrations in core-ionised CO adsorbed Co(0001) and Rh(100)

T. Ramsvik, A. Borg, M. Kildemo, S. Raaen, A. Y. Matsuura,
A. J. Jaworowski, T. Worren and M. Leandersson

Surface Science 492 (2001) 152.

MOLECULAR VIBRATIONS IN CORE-IONISED CO ADSORBED ON Co(0001) AND Rh(100)

T. Ramsvik, A. Borg, M. Kildemo, S. Raaen, A. Y. Matsuura*, A. J. Jaworowski*, T. Worren and M. Leandersson*

Dept. of Physics, Norwegian University of Science and Technology, N-7491 Trondheim, NORWAY

**Dept. of Synchrotron Radiation Research, Institute of Physics, Lund University, Box 118, S-221 00 Lund, SWEDEN*

ABSTRACT

Previous studies of CO on Ni(100) by Föhlisch et al. (Phys. Rev. Lett. 81 (1998) 1730) have shown that the intramolecular stretch vibration mode observed in the C1s photoelectron lines depends strongly on the chemical state of the adsorbate. In the current investigation analogous analyses have been done for CO on Co(0001) and Rh(100). CO adsorbs in on-top sites on Co(0001) resulting in a vibrational splitting of (210 ± 3) meV from the adiabatic C 1s peak. Including the measured intensities and comparing with similar data from EELS-experiments the change in the equilibrium distance between the initial state and the ionised state has been deduced to (4.7 ± 0.2) pm. For CO on Rh(100) two adsorption sites, on-top and bridge, are populated. Similar analyses of the vibrational fine structure gives a vibrational splitting of (221 ± 4) meV for on-top site and (174 ± 11) meV for bridge site. The respective changes in the equilibrium distances are (3.8 ± 0.2) pm and (5.6 ± 0.3) pm. These results are compared with available data in literature.

1. INTRODUCTION

Chemical shifts in photoemission spectroscopy were unambiguously observed for the first time in 1964 by Hagström and co-workers [1]. Since then observation of such shifts has developed into a routine technique to identify and distinguish between different chemical species in a system. An important type of chemical shift is the splitting in the core-level binding energy for adsorbates due to different adsorbate sites. In the recent years, however, it has been possible to go beyond the chemical shift and observe the additional structure of the core level peak profile due to internal molecular vibrations of chemisorbed molecules. Andersen et al. showed that for adsorbates with hydrocarbon functional groups it is feasible to resolve vibrational fine structure with large splittings [2]. Soon afterwards Föhlisch et al. presented vibrational resolved core-level photoelectron spectra of adsorbed CO on Ni(100) [3]. By combining former results on the systems CO/Ni(100) and CO/H/Ni(100) they were able to measure the vibrational fine structure of CO adsorbed in three different adsorption sites: on-top, two-fold bridge and four-fold hollow sites. A lowering of the vibrational splitting in the C 1s line was observed with increasing coordination. This trend has been a rule of thumb for CO (and NO) for analyses of EELS spectra for a long time [4], and attempts have been made to assign the measured vibrational frequencies to adsorption sites. However, it has been shown that such a general method is unreliable [5].

In this paper the vibrational fine structure is reported and discussed for CO adsorbed on Co(0001) and Rh(100). For the latter substrate it was possible to distinguish the vibrational contributions from two different chemical states, on-top and bridge sites. The validity of using the equilibrium core approximation to predict the adsorption site for NO of a metallic substrate based on the knowledge of vibrational fine structure of core-ionised CO is also discussed.

2. EXPERIMENTAL

The high-resolution photoemission measurements were performed at beamline I311 at the synchrotron radiation facility Max-Lab at the University of Lund, Sweden. The beamline is an undulator based VUV, soft X-ray beamline aimed at high resolution XPS. It is equipped with a modified Zeiss SX-700 monochromator and a large Scienta-type hemispherical photoelectron energy analyser [6]. In the present experiment the overall resolution for C 1s is estimated to be in the range ~60 to ~70 meV, as determined from the width of the Fermi edge.

The X-ray absorption spectroscopy experiments were performed at the soft X-ray beamline BL22[1] at the MAX I storage ring. This beamline was equipped with the same type of monochromator and analyser as beamline I311. The spectrum was measured in the constant final state (CFS) mode with the kinetic energy set to collect electrons from the surface sensitive C KVV Auger transition using the hemispherical energy analyser for detection.

Both the Co(0001) and Rh(100) crystals were mounted on a 0.5 mm W-wire, and were heated by passing current through the support wires or cooled with liquid nitrogen to ~100 K. The temperature was measured by a Chromel-Alumel thermocouple that was spot-welded to the rear of the sample. The Rh(100) crystal surface was cleaned by repeated cycles of Ar^+ sputtering (15 min room temperature and 15 min 1100 K), oxygen annealing at 1×10^{-8} mbar at 1075 K in 5 minutes, and flash annealing to 1350 K in UHV. The surface cleanliness was checked by monitoring the core-level regions of likely contaminants and by measuring valence-band spectra at photon energies close to the Cooper minimum in the Rh 4d photoionisation cross section [7]. The Co(0001) single crystal was cleaned by cycles of sputtering with 0.5 keV Ar^+ ions at ~570 K and subsequent annealing at ~630 K in UHV. The annealing temperature was kept well below ~700 K, to avoid the Co hcp $\rightarrow$ fcc phase transition. The ordering of the surfaces were checked by low energy electron diffraction (LEED). The Co(0001)-($\sqrt{3}$x$\sqrt{3}$)R30°-CO phase was obtained by exposing the cobalt crystal to 10 L CO at ~90 K and subsequently annealing the sample to ~300 K for 5 minutes. The Rh(100)-c(2x2)-CO phase was obtained by keeping the Rh crystal at ~350 K during a 3 L CO exposure.

[1] This beamline has been moved from MAX I and is now connected to the third generation storage ring MAX II under the name D1011.

3. RESULTS AND DISCUSSION

In Figure 1a the C 1s spectrum for the Co(0001)-(√3x√3)R30°-CO structure is shown.

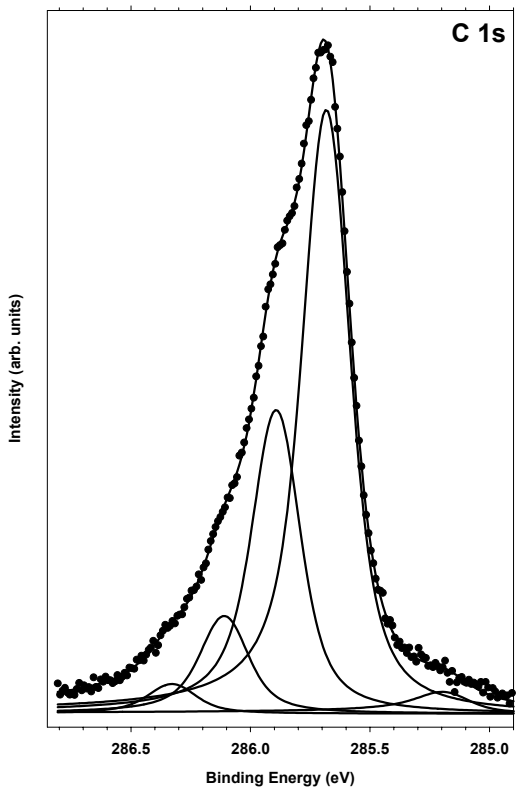

Figure 1: Normal emission C 1s photoelectron spectrum from the Co(0001)-(√3×√3)R30°-CO overlayer. The spectrum was recorded at a photon energy of 321 eV and with a resolution ≤ 60 meV. Filled circles: experimental data, lines: individual components of the decomposition and the resulting fit for the adsorbate spectrum (see text).

An excitation energy of 321 eV was used, giving a total resolution of ~58 meV. The C 1s core level spectrum is decomposed using Doniach-Šunjić [8] line profiles convoluted by a Gaussian function [9]. The Doniach-Šunjić line-shape accounts for the broadening due to the finite lifetime of the created core hole by a Lorentzian function and the creation of electron-hole pairs at the Fermi edge by introducing an asymmetric parameter. The Gaussian function represents the experimental bandwidth, with additional broadening mainly due low-energy vibrational modes, e.g. frustrated translations of the molecule along the surface. The decomposition shows that the largest (main) peak is located at 285.68 eV, ~0.1 eV lower than previously reported in literature [10]. On the high binding energy side three shoulders are observed at 285.89 eV,

286.11 eV and 286.33 eV, giving energy splittings from the main peak of (210 ± 3) meV, (427 ± 7) meV and (646 ± 14) meV, respectively. In addition, a small peak contributing with around 2 % of the total intensity is seen at 285.17 eV due to a beginning population of an additional CO adsorption site [11,12]. It is shown [11, 13] that the (√3x√3)R30° structure consist ideally only of molecular CO adsorbed in on-top sites. It is therefore concluded that the three high energy contributions are due to excitation of the first, second and third harmonic CO stretch vibrations. The corresponding S-factor[2] is found to be 0.50 ± 0.02. The decomposition spectrum gives a lifetime broadening of 140 meV at FWHM, and an asymmetry parameter of ~0.03. Additional Gaussian contribution of ~150 meV is needed to correctly decompose the spectrum. This is considerably larger than the experimental bandwidth of 58 meV, suggesting that the additional broadening from the low energy vibrational modes is significant. In the decomposition the line profile is assumed identical for each vibrational succession.

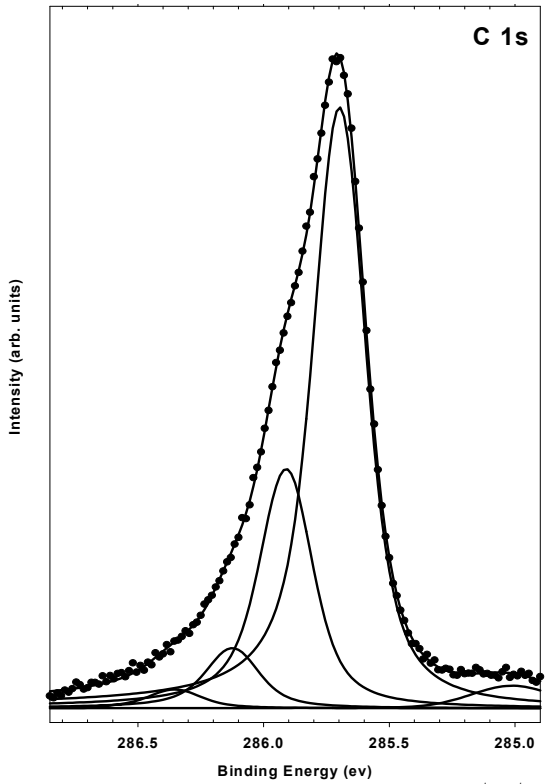

Figure 2: C 1s normal emission photoelectron spectrum from the Co(0001)-(√3×√3)R30°-CO overlayer, recorded at a photon energy of 380 eV and with a resolution ≤ 70 meV. Filled circles: experimental data, lines: individual components of the decomposition and the resulting fit for the adsorbate spectrum (see text).

[2] The S-factor is the ratio of the intensity of the first peak in the vibrational progression to the intensity of the adiabatic peak

Figure 2 shows the same CO overlayer as described above for figure 1, but measured at higher photon energy, 380 eV. The overall resolution was in this case ~70 meV. Also here one can clearly observe shoulders at the high binding energy side of the main peak corresponding to the first vibrational losses. One does not expect the energy splitting, lifetime broadening and asymmetry index to vary significantly with increasing photon energy. The decomposition of the spectrum in figure 2 was therefore performed keeping these parameters equal to those deduced in figure 1 letting only the intensities and the Gaussian broadening vary. The result is an S-factor of 0.40 ± 0.02, that is, considerably smaller than in figure 1. Larger S-factors for low photon energies have been observed previously. An extensive photoemission spectroscopy study of the vibrational fine structure of the C1s main lines of adsorbed CO was performed by Föhlisch et al. [14] on Ni(100) and Ru(0001) surfaces as a function of photon energies. On the Ru substrate a broad but defined maximum of the vibrational excitation was found ~5 eV above the shape resonance followed by an equalisation after a further 6 eV increase in the photon energy. The location of the shape resonance of CO on Co(0001) can be deduced from carbon K-shell XAS spectra. Such measurements have been performed, and the XAS spectrum recorded at 45^{o} X-ray incidence angle is displayed in Figure 3. Both the π^*-resonance, corresponding to the C 1s$\rightarrow 2\pi^*$ transition, and the shape resonance (σ^*) are clearly seen with peak positions at ~288 eV and ~305 eV, respectively. In the figure the measured core-level binding energy at 285.7 eV (XPS) and the ionisation limit[3] at 291.7 eV (IL) are inset. From these results and the XPS data it is hence found that at an energy of 16 eV above the location of the shape resonance the vibrational excitation still has not reached the values predicted by a Franck-Condon process. The reason for this large S-factor is suggested to be a superposition of the influences of the shape resonance, and of intermediate multiple excitations spread over a wide range [14].

[3] The energy of the ionisation limit for the system Co(0001)-($\sqrt{3}$x$\sqrt{3}$)R30°-CO is obtained as the corresponding core-level binding energy relative to the Fermi level, plus the work function [12]

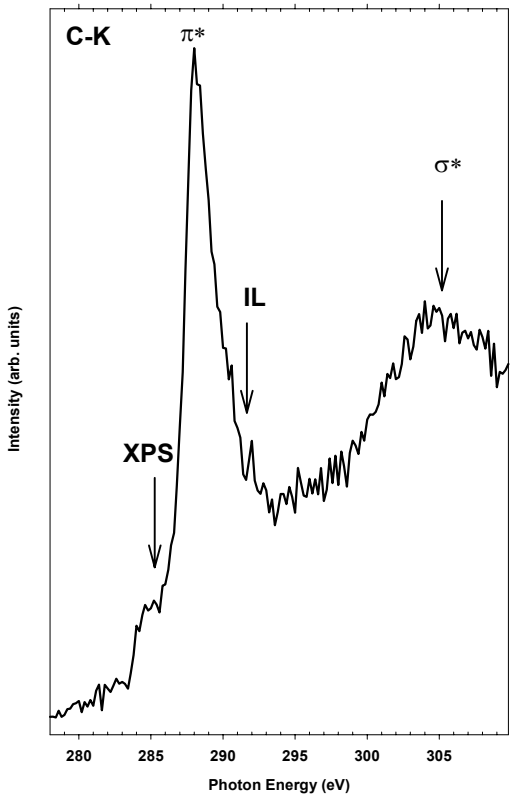

Figure 3: Carbon K-shell NEXAFS spectra of the Co(0001)-($\sqrt{3}\times\sqrt{3}$)R30°-CO overlayer for a X-ray incidence angle of 45°. XPS and IL denote the C 1s binding energies and ionisation limits, respectively.

Figure 4 shows the C 1s core level spectrum after exposing 3 L of CO on Rh(100) at 380 K, resulting in a sharp c(2x2) LEED-pattern. The photon energy is 340 eV giving a total resolution of ~68 meV. The decomposition is carried out in the same way as for CO on Co(0001). Two main components are located at binding energies 285.78 eV and 285.41 eV, which have been shown [15,16] to originate from on-top and bridge sites, respectively. Similar to the spectra of figure 1 extra contributions corresponding to the CO vibrational stretch modes can be directly observed at the high binding energy side of the on-top peak. The decomposition gives 286.00 eV and 286.22 eV for the first and second harmonic vibrational loss, respectively, corresponding to energy splittings from the main, adiabatic peak of (221 ± 4) meV and (437 ± 17) meV. To obtain a reasonable fit to the spectrum, an extra peak located between the two main peaks is needed. This is justified by the well-deduced line profile of the adiabatic peak for bridge site. By recognising the extra peak as the first vibrational component of the bridge site

its line profile can be assumed to be identical to its main peak. One then obtains a height and energy position with a fairly high accuracy.

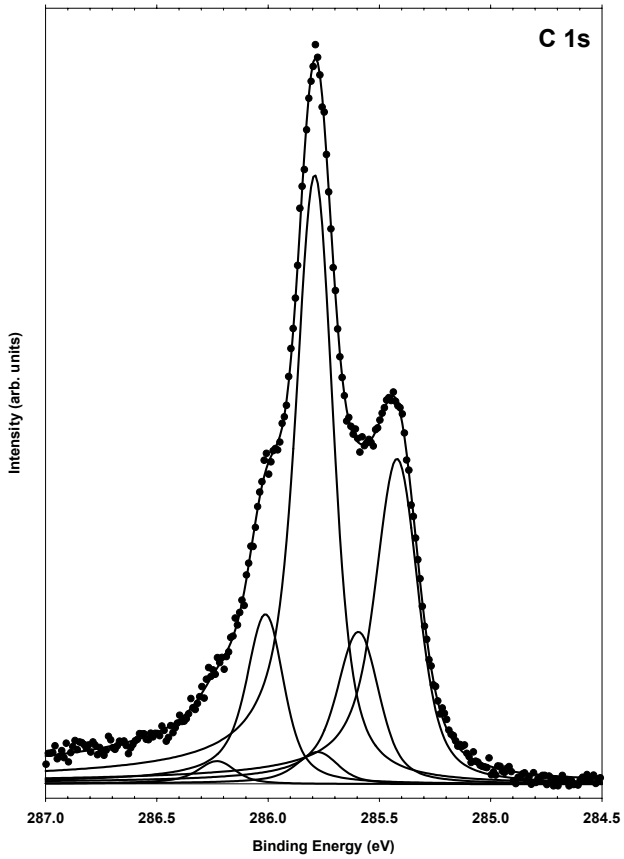

Figure 4: C 1s normal emission photoelectron spectrum from the Rh(100)-c(2×2)-CO overlayer. The spectrum was recorded at a photon energy of 340 eV and with a resolution ≤ 70 meV. Filled circles: experimental data, lines: individual components of the decomposition and the resulting fit for the adsorbate spectrum (see text).

The result is an energy splitting from the main bridge peak of (174 ± 11) meV. For both sites no significant diffraction effects are seen when the excitation energy is increased, and hence it is concluded that the extra contributions are true vibrational fine structure of the C1s main lines. For the same reasons potential non-Franck-Condon effects or influence of the shape resonance is ruled out. To extract more reliable vibrational data the contribution from the second harmonic of the CO stretch vibration must be taken into consideration. For a diatomic molecule like CO a good approximation for the lowest vibrational mode is to assume that the vibrational motions is described by an ideal harmonic oscillator potential and that the photoemission spectrum follows a Poisson distribution [17]. Then an intensity and energy

position for the second harmonic contribution of CO in bridge sites can easily be estimated, based on its energy splitting and S-factor. The most pronounce effect of including this second harmonic peak is an increase of the on-top S-factor of about 6 %. The resulting S-factors are found to be 0.28 ± 0.01 and 0.48 ± 0.06 for on-top and bridge sites, respectively. The Gaussian contributions (experimental bandwidth + low energy frustrated translational modes) are found to be 128 meV for on-top and 154 meV for bridge. The corresponding lifetime broadenings are 92 meV and 114 meV. The asymmetry parameter is assumed equal for both adsorption sites, amounting to 0.08. Due to the ability to resolve vibrational contributions the energy positions found here are slightly lower than what has been reported previously in literature [16]. As for CO on Co(0001) a larger S-factor is found for an excitation energy of 320 eV. However, the difference is less pronounced in the case of CO on Rh(100).

In Table I the branching ratios[4] and energy splittings for both Co(0001) and Rh(100) are summarised.

Table I: Summary of C 1s photoemission data for Rh(100) and Co(0001). The results are taken from figure 1, 2 and 4.

	Vibrational splitting E_{vib} (meV)		Branching ratio $\frac{\nu_0 \rightarrow \nu_i^{\mid}}{\nu_0 \rightarrow \nu_0^{\mid}}$ for i = 1,2	Δr (pm)
	Initial state EELS / infrared	C 1s ionised XPS	Experiment	
CO/Rh(100) c(2×2)				
On top	248 - 251 [18]	221 ± 4	0.28 ± 0.02	3.8 ± 0.2
		437 ± 17	0.04 ± 0.01	
Bridge	235 [18]	174 ± 11	0.48 ± 0.06	5.3 ± 0.3
		-	-	
CO/Co(0001) (√3×√3)R30°				
On top	248.5 [19] - 250 [20]	210 ± 3	0.40 ± 0.02	4.7 ± 0.2
		427 ± 7	0.10 ± 0.02	

The latter values are here compared with the C-O stretching frequency for CO adsorbed on identical substrates and sites, probed in its initial state. It is seen that the splittings are significantly reduced after core ionisation, in consistency with earlier reports [3]. A reduced vibrational splitting implies an increase of the equilibrium distance, Δr, between the carbon and oxygen atom. This is a general trend in diatomic molecules since excitation of electrons generally introduces more antibonding character in the molecular orbitals. To quantify this

[4] i.e. the intensity ratio between the two first harmonic peaks and the adiabatic peak

increase in equilibrium distance, a few approximations are commonly made: The transition between two different electronic states is much faster than the nuclear motion (Born-Oppenheimer approximation) giving a vertical transition in the energy diagram. In addition, the electronic part of the dipole operator is assumed independent of the internuclear distance. Then the transition dipole moment is proportional to the overlap integral between the vibrational states in their respective electronic states [21]:

$$<\varepsilon'\nu'|\mu|\varepsilon\nu> \propto \int \psi^*_{\nu'}(\mathbf{R})\,\psi_{\nu}(\mathbf{R})d\tau_N = S(\nu',\nu) \qquad (1)$$

Here $|\varepsilon'\nu'>$ and $|\varepsilon\nu>$ are the ionised and initial vibronic states, respectively, and $\underset{\sim}{\mu}$ is the electric dipole moment operator. $\psi_{\nu'}$ and ψ_{ν} represent the wavefunctions for the vibrational parts of the ionised and initial states, i.e. independent of the electronic coordinates. The integral is taken over all nuclear coordinates. For linear molecules as CO the displacements of the nuclei are only along the molecular bond, and the calculation can therefore be considered as a one-dimensional problem. The square of this overlap integral, $|S(\nu',\nu)|^2$, is the *Franck-Condon factor*, which determines the intensities of each vibrational mode. As mentioned previously, a harmonic oscillator is assumed sufficient to describe the potential energy curve for both electronic states. One can then apply the simple oscillator ground state eigenfunctions for both the initial and ionised molecule, displaced from each other by a separation Δr, i.e. the increase of the equilibrium distance. The Franck-Condon factor for transition to the ground state ($\nu' = 0$) in the ionised molecule than takes the form[5]

$$|\,S(0,0)\,|^2 = \left(\int_{-\infty}^{\infty} \psi^*_{0'}(x - \Delta r)\psi_0(x)dx \right)^2 \qquad (2)$$

where ψ_0 and $\psi_{0'}$ represent the normalised ground state vibrational wavefunctions for the initial and ionised molecule. The effective mass of CO is assumed constant before and after chemisorption onto the substrate. The experimental intensity measured for the adiabatic peak relative to the total intensity of the photoemission spectra then determines the increase, Δr, for each substrate and adsorption site. The results are given in the rightmost column in Table I. For adsorption in on-top sites on Rh(100) the increase in equilibrium distance is similar to the value of 3.9 pm found by Föhlisch et al. for CO in on-top sites on Ni(100). For CO in bridge sites, however, the increase is significantly larger, 4.5 pm for CO on Ni(100) and 5.3 pm in this study. If one compares the result on Co(0001) with Ru(0001) [14] the difference is even higher,

[5] for temperatures relevant in this paper the initial state in the photoemission process is the vibrational ground state of the neutral molecule

4.7 pm and 5.7 pm, respectively. Since Δr is sensitive to change in the electronic structure, as the apparent variation with co-ordination indicates, it is not surprising to find such differences going from one material to another. In Table II the S-factors and vibrational splittings reported for CO on different substrates and in different adsorption sites are summarised, together with those obtained in this paper.

Table II: Vibrational energies and S-factors of the C-O stretch mode for core-ionised CO adsorbed on a number of transition metals.

	Rh(100)		Ni(100) [3]		Co(0001)		Ru(0001) [14]		Rh(111) [22]	
	$\hbar\omega_{CO}$ meV	S	$\hbar\omega_{CO}$ meV	S	$\hbar\omega_{CO}$ meV	S	$\hbar\omega_{CO}$ meV	S	$\hbar\omega_{CO}$ meV	S
On top	221	0.28	217.8	0.305	210	0.40	213	0.62[7]	232-235 [8]	0.24 - 0.23 [8]
Bridge	174	0.47	183.0	0.379	-	-	-	-	192 [9]	0.53
Hollow	-	-	156.6	0.624	-	-	-	-	171-173 [8]	0.58

For CO in on-top sites the vibrational splittings show little variations for all the surfaces given, ranging from 213 meV for CO on Ru(0001) to 235 meV for CO on Rh(111)[6]. Within the same orientations and crystal structures the correspondences are very good. For CO on Rh(100) and Ni(100) similar vibrational energies are observed, and likewise for Co(0001) and Ru(0001). For bridge site the variations are surprisingly small in view of the different coordination number between the (111) surface of Rh and the (100) surfaces of Rh and Ni. For CO adsorbed in hollow sites the higher vibrational splitting found for Rh(111) (three-fold hollow) compared to Ni(100) (four-fold hollow) are more in accordance with the expectations due to the different co-ordination number. Despite the small amount of data available today the trend of reduced vibrational splitting with increasing coordination is evident. A clear tendency of increasing S-factor with increasing coordination is also seen, however the quantitative agreements are poorer in this case.

The fact that CO vibrational fine structure is observed on both Co(0001) and Rh(100) can be taken as evidence for major hybridisation of the CO 2π orbital and the metal d bands (3d

[6] The CO molecule experience different hybridisation from one substrate to another. Some variations are therefore expected. In addition the CO coverages are not equal in Table II.
[7] Determined by the author reading directly from a graph which presents the intensity of the different vibrational modes as a function of photon energy.
[8] Vibrational splittings of 235 meV and 173 meV correspond to a saturation CO coverage of 0.75 ML, 232 meV to 0.2 ML and 171 meV to ~0.5 ML
[9] The adsorption site is questionable, but is considered most likely to be in bridge site

for cobalt and 4d for rhodium) upon chemisorption. It is well established that weakly chemisorbed CO exhibits pronounced core-level satellites, and that the satellite intensities decrease for increasing adsorption strength [23]. For example, in the weakly chemisorbed system c(2x2)-CO/Cu(100) large shake-up intensities smear out any vibrational fine structure in the main line completely [24]. Shake-up contributions exist if the lowest-energy configuration of the ion and the ground state are dissimilar [25]. In the case of strong hybridisation between the CO 2π orbital and the metal d band the relative difference between the initial state bonding level and the final state bonding level is small. Hence weak shake-up intensities are expected. For the systems $(\sqrt{3}\times\sqrt{3})R30^{o}$-CO/Co(0001) and c(2×2)-CO/Rh(100) the chemisorption is strong, and consequently it is possible to observe the molecules internal vibrations. The somewhat lower asymmetry parameter for Co(0001) (0.03) compared to Rh(100) (0.08) indicates that the chemisorption strength is weaker in the former case. From earlier studies adsorption energies of 30 kcal/mol and 32 kcal/mol have been found for CO on Co(0001) and Rh(100), respectively [26].

According to the equivalent core approximation [27], the intramolecular vibrational stretch energies between C1s ionised CO and initial state NO should be comparable if complete screening of the ionised state is achieved. Based on the discussion above, it is likely that such screening is achieved. Villarrubia et al. [28,19] studied the NO/Rh(100) system using electron energy loss spectroscopy (EELS) and found two vibrational energies at 114 meV and 196 meV. The latter was suggested to be the N-O stretch vibration of molecularly adsorbed NO in an upright position in a bridge site. This was later supported theoretically [29] using tight-binding band calculations of the extended Hückel type. When comparing the intramolecular stretch vibration energies of the C1s ionised CO and the initial state NO molecules, the different atomic masses have to be corrected for. By doing this a renormalised initial state vibration of NO/Rh(100) is found to be 205.5 meV, i.e. 15 % higher than the stretch energy for the bridge site given in Table I. Using our experimental result from C1s XPS measurements, a NO vibrational stretch energy on Rh(100) bridge site is predicted to be ~166 meV. Föhlisch et al [3] found the equivalent core approximation to be applicable for on-top, bridge and hollow sites. Also for the system CO/Rh(111) [22] good agreements for CO in on-top sites are found, while for hollow site the vibrational splitting for the core-ionised CO is ~12% lower than for the renormalised initial state vibration of NO/Rh(111). It was suggested that this discrepancy can be due differences in vibrational energies between core-ionised CO surrounded by neutral CO molecules and NO molecules surrounded by other NO molecules. In addition, Zasada et al. [30] suggested that the site-frequency relations can be doubtful for NO and CO adsorbed at

high coverages on metal surfaces due to interactions with the adsorbate. These lead to an upward shift of the N-O and C-O stretch frequency. In our case, CO on Rh(100), the coverage of CO was ~0.3 ML which is about half of the saturation layer (0.62 ML) of NO studied by Villarrubia et al. [28, 19] From this reasoning it is not surprising that a higher vibrational stretch energy is found for this system. Such a comparison can not be made for CO on Co(0001) since, to our knowledge, the initial state vibrational energies of NO on Co(0001) have not been determined.

4. CONCLUSIONS

The vibrational fine structures of core-ionised CO adsorbed on Co(0001) and Rh(100) have been studied by high-resolution core-level photoemission. For CO in on-top site on Co(0001) the vibrational splitting is determined to be (210 ± 4) meV from the adiabatic C1s peak. Including the measured intensities and comparing with similar data from EELS-experiments the change in the equilibrium distance between the initial state and the ionised state has been deduced to (4.7 ± 0.2) pm. For CO on Rh(100) the vibrational fine structure of two adsorption sites, on-top and bridge, are analysed. Vibrational splittings of (221 ± 4) meV for the on-top site and (174 ± 11) meV for the bridge site are found with changes in the equilibrium distances of (3.8 ± 0.2) pm and (5.3 ± 0.3) pm, respectively. Comparing the results found in this report with previous studies show that the trend of decreasing vibrational splitting with increasing co-ordination is also applicable for screened core-ionised CO. However, the available data is still limited.

ACKNOWLEDGEMENT

The assistance of the MAX-lab staff is gratefully acknowledged. We also acknowledge financial support from the Norwegian Research Council. MAX-lab is supported by the European Community - Access to Research Infrastructure action of the Improving Human Potential Programme.

REFERENCES

[1] S. Hagström, C. Nordling and K. Siegbahn, Phys. Lett., 9 (1964) 235.

[2] J. N. Andersen, A. Beutler, S. L. Sorensen, R. Nyholm, B. Setlik and D. Heskett, Chem. Phys. Letter 269 (1997) 371.

[3] A. Föhlisch, N. Wassdahl, J. Hasselström, O. Karis, D. Menzel, N. Mårtensson and A. Nilsson, Phys. Rev. Lett. 81 (1998) 1730

[4] N. Sheppard and N. T. Nguyen, Adv. IR Raman Spectr. 5 (1978) 67.
[5] K.-M. Schindler, P. Hoffmann, K.-U. Weiβ, R. Dippel, P. Gardner, V. Fritzsche, A. M. Bradshaw, D. P. Woodruff, M. E. Davila, M. C. Asensio, J. C. Conesa and A. R. González-Elipe, J. Electron Spectrosc. Relat. Phenom. 64/65 (1993) 75.
[6] R. Nyholm, J. N. Andersen, U. Johansson, B. N. Jensen and I. Lindau, Nucl. Instr. and Meth. in Phys. Res. A, in press
[7] J. J. Yeh and I. Lindau, Atomic Data and Nuclear Data Tables **32** (1985) 1.
[8] S. Doniach and M. Šunjić, J.Phys. C3 (1970) 285.
[9] Curve fitting routine, FITXPS, developed by D. L. Adams at the Institute of Physics and Astronomy, University of Århus, Denmark
[10] G. F. Cabeza, P. Légare and N. J. Castellani, Surf. Sci. 465 (2000) 286.
[11] H. Papp, Surf. Sci. 129 (1983) 205
[12] J. Lahtinen, J. Vaari, K. Kauraala, Surf. Sci. 418 (1998) 502.
[13] J. Lahtinen, J. Vaari, K. Kauraala, E. A. Soares and M. A. Hove, Surf. Sci. 448 (2000) 269.
[14] A. Föhlisch, J. Hasselström, O. Karis, P. Väterlein, N. Mårtensson, A. Nilsson, C. Heske, M. Stichler, C. Keller, W. Wurth and D. Menzel, Chem. Phys. Lett. 315 (1999) 194.
[15] A. Baraldi, L. Gregoratti, G. Comelli, V. R. Dhanak, M. Kiskinova and R. Rosei, Appl. Surf. Sci. 99 (1996) 1.
[16] F. Strisland, A. Ramstad, T. Ramsvik and A. Borg, Surf. Sci. 415 (1998) L1020
[17] L. S. Cederbaum and W. Domcke, J. Chem. Phys. 64, 603 (1976)
[18] B. A. Gurney, L. J. Richter, J. S. Villarrubia and W. Ho: J. Chem. Phys. 87 (1987) 6710
[19] J. S. Villarrubia, W. Ho: J. Chem. Phys. 87 (1987), 750 - 64
[20] G. A. Beitel, A. Laskov, H. Oosterbeek, E. W. Kuipers: J. Chem. Phys. 100 (1996) 12494.
[21] P. W. Atkins and R. S. Friedman, Molecular Quantum Mechanics, 3rd edition, Oxford University Press (1997)
[22] M. Smedh, A. Beutler, T. Ramsvik, R. Nyholm, M. Borg, J. N. Andersen, R. Duschek, M. Sock, F. P. Netzer and M. G. RamseySurface Science 491 (2001) 99.
[23] H. Tillborg, A. Nilsson, N. Mårtensson, J. El. Spec. Rel. Phenom. 62 (1993) 73 and references therein.
[24] A. Föhlisch, J. Hasselström, O. Karis, D. Menzel, N. Mårtensson and A. Nilsson, J. El. Spec. Rel. Phenom. 101-103 (1999) 303.
[25] H.-J. Freund and E. W. Plummer, Phys. Rev. B 23 (1981) 4859.
[26] S. Ishi, Y. Ohno and B. Viswanathan, Surf. Sci. 161 (1985) 349. and references therein
[27] B. Johansson and N. Mårtensson, Phys. Rev. B 21 (1980) 4427.
[28] J. S. Villarrubia, L. J. Richter, B. A. Gurney and W. Ho, J. Vac. Sci. Technol. A 4, (1986) 1487.
[29] D. L. Vučković, S. A. Jansen, R. Hoffman, Langmuir 6 (1990) 732.
[30] I. Zasada, M.A. van Hove and G. A. Somorjai, Surf. Sci. 418 (1998) L89.

Paper IV

Vibrationally resolved C 1s photoemission from CO adsorbed on Rh(111): The investigation of a new chemically shifted C 1s component

M. Smedh, A. Beutler, T. Ramsvik, R. Nyholm, M. Borg, J. N. Andersen, R. Duschek, M. Sock, F. P. Netzer and M. G. Ramsey

Surface Science 491 (2001) 99.

VIBRATIONALLY RESOLVED C 1S PHOTOEMISSION FROM CO ADSORBED ON Rh(111): THE INVESTIGATION OF A NEW CHEMICALLY SHIFTED C 1S COMPONENT

M. Smedh[1], A. Beutler[1], T. Ramsvik[2], R.Nyholm[3], M. Borg[1], J. N. Andersen[1], R. Duschek[4], M. Sock[4], F. P. Netzer[4], M. G. Ramsey[4]

[1]*Department of Synchrotron Radiation Research, Institute of Physics, Lund University, P.O. Box 118, S-22100 Lund, Sweden*

[2]*Department of Physics, Norwegian University of Science and Technology, NTNU, N-7034 Trondheim, Norway*

[3]*MAX-lab, Lund University, Box 118, S-221 00 Lund, Sweden*

[4]*Institut für Experimentalphysik, Karl-Franzens Universität Graz, Universitätsplatz 5, A-8010 Austria*

Abstract

High resolution core level photoemission at an energy resolution better than the intrinsic width of the C 1s level has been used to study the CO/Rh(111) overlayer system. C 1s spectra have been measured in a large CO coverage range; from low coverages, where the CO molecules only adsorb in on-top positions, to saturation coverage, where CO molecules occupy both on-top and three-fold hollow sites. Fine structure components due to vibrational excitation of the C-O stretch mode are clearly resolved in the emission peak from each site. The vibrational splittings and intensity ratios are found to be different for the different adsorption sites. A third C 1s component, which has not been resolved earlier, is found at intermediate CO coverages. Some possible explanations for the origin of this extra component are discussed. For this cause high resolution electron energy loss spectroscopy spectra were measured for different CO coverages and the photoelectron diffraction behavior was analyzed.

1. INTRODUCTION

The overlayer system which we present in this study, CO molecules adsorbed on the Rh(111) surface, has been extensively studied previously by several different surface science techniques such as electron energy loss spectroscopy (EELS) [1], low energy electron diffraction (LEED) [2,3], high resolution core level photoemission (HRCLS) [4,5], and surface x-ray diffraction [6].

This adsorption system is rather complicated in the sense that several different ordered overlayer structures are formed depending on the CO coverage and sample temperature (see references 4 and 5). Based on the previous investigations, the following picture has emerged. At low temperature and low coverages, up to a third of a monolayer (0.33 ML), the CO molecules adsorb only in the on-top positions of the rhodium surface. At intermediate coverages up to about 0.5 ML, a small amount of three-fold hollow sites become occupied, while at higher coverages the three-fold hollow positions are filled quickly, at the expense of the on-top positions. At the saturation coverage of 0.75 ML each unit cell contains one CO molecule in an on-top position and two CO molecules in hollow positions [3,4,5,6]. At coverages above ~ 0.4 ML the occupation of on-top and hollow positions also depends on the sample temperature (see ref. 5). Up to ~ 0.54 ML the relative amount of CO molecules adsorbed in three-fold hollow sites increases with increasing sample temperature whereas at coverages above ~ 0.54 ML the three-fold hollow coverage decreases with increasing temperature. As long as the temperature stays below the (coverage dependent) desorption temperature these site changes are reversible.

Our previous core-level photoemission studies of the CO/Rh(111) system [4,5] were performed at beamline 22 at the MAX I storage ring (MAX-lab, Sweden). MAX I is a second generation synchrotron radiation source still in use, where the radiation is mainly produced in the bending magnets and the resolution is below that obtained at newer sources. Due to the substantial previous knowledge about the CO/Rh(111) overlayer system we chose it as a test system for a new beamline, I311, at the third generation storage ring MAX II. There the radiation comes from an insertion device and both the photon flux and the energy resolution are much higher than at MAX I. Our aim was to obtain new information from these measurements,

e. g. details about the vibrations in the C 1s ionized CO molecule[1], since we expected to be able to resolve the core-level splitting caused by excitations of the C-O stretch vibration during the photoemission process.

The fact that excitations of localized internal molecular vibrations can give rise to split core levels in photoemission spectra from adsorbed molecules is a quite recently observed phenomenon. The first example of resolved vibrational fine structure in a chemisorbed molecule was a study of ethylidyne chemisorbed on Rh(111) [7]. At that time the C-H stretch vibration, with a vibrational splitting of about 400 meV, could be resolved in the C 1s spectra. The C-O stretch vibration has only about half that vibrational energy, approximately 200 meV. The design of new experimental equipment with increasingly better resolution has just recently made it possible to resolve this vibration in core level photoemission spectra from CO molecules adsorbed on metal surfaces [8].

Due to the improvement of the resolution we expected to find vibrational fine structure in the C 1s photoemission spectra from CO adsorbed on Rh(111), which previously [4,5] showed only two peaks arising from on-top and three-fold hollow adsorbed CO molecules, respectively. That is, we expected the on-top and the hollow emission peaks to each contain one C-O stretch vibrational progression. However, the overlayer system CO/Rh(111) turned out to be more complicated than expected. The fine structure components of the C 1s emission peak from CO molecules adsorbed in on-top positions behaved as expected: they have the same energy and intensity distribution for all different CO coverages, as expected for a vibrational progression. This, however, is not the case for the fine structure of the emission peak in the hollow region of the spectrum, whose intensity distribution apparently changes significantly both for different CO exposures and for different sample temperature. To obtain a physically plausible interpretation of this anomalous behavior of the photoemission intensity a third C 1s component had to be introduced in the decomposition of the spectra. The origin of this third component is discussed and we argue that it is most likely due to CO molecules adsorbed in bridge sites.

[1] These are not equal to the initial state vibrational energies, which have been measured for the ground state molecule for many years using the electron energy loss and infrared spectroscopy methods. In most discussions below we will ignore this fact for simplicity and only refer to it as C-O stretch vibration.

2. EXPERIMENTAL DETAILS

2.1 Experimental equipment and sample preparation

The high resolution core level photoemission measurements were performed at beamline I311 at the synchrotron radiation facility MAX-lab in Lund, Sweden. At this beamline the radiation comes from an undulator in the MAX II storage ring. The undulator consists of 38 magnetic periods, has a period length of 66 mm, and a total length of 2.65 m. The monochromator [9] is a modified SX-700 with a 1220 l/mm grating, spherical focusing mirror, and a movable exit slit. The electron energy analyzer is a hemispherical SCIENTA SES 200 analyzer [10]. In the present C 1s measurements the total (photons plus electrons) energy resolution was about 50 meV, as determined from the width of the Fermi edge. The measurements were done at a temperature of 100 K in order to reduce temperature dependent broadening. All spectra were measured at normal emission and a typical measuring time for a spectrum was about 15 minutes.

The Rh(111) crystal was mounted on 0.5 mm tungsten wires, and could be heated by sending a current through these support wires or be cooled to 100 K. The temperature was measured by Chromel-Alumel thermocouples spot-welded to the side of the crystal. The Rh(111) surface was cleaned by Ar^+ sputtering at a temperature of 900 K, and subsequently annealed at 1400 K in order to restore the surface structure. Any residual carbon contamination was removed by heating of the crystal in 10^{-8} Torr O_2 followed by a flash to 1300 K in vacuum. Photoemission spectra for the likely contaminants were measured to check the cleanliness. The ordering of the surface was checked by low energy electron diffraction (LEED).

CO can form several different overlayer structures on Rh(111) depending on CO coverage and sample temperature [4,5]. The main focus of this study is on the case of low temperature (around 100 K): At low coverages the CO molecules only occupy the on-top positions of the rhodium surface, forming first a (2×2) LEED pattern at around 0.25 ML [4,5] and then a (√3×√3)R30° at around 0.33 ML [2]. At higher coverages the three-fold hollow positions start to become occupied and a (4×4) pattern forms at around 0.5 ML followed by a region of split (2×2) structures and then finally a sharp (2×2) at saturation [4,5]. At the saturation coverage of 0.75 ML each unit cell consists of two CO molecules in hollow positions

(hcp and fcc) and one CO molecule in the on-top position [4,5,3,6] (this structure is denoted (2×2)-3CO).

The adsorption temperature does not seem critical, as long as it is high enough that the CO molecules are mobile on the surface. Most CO overlayers were prepared at a sample temperature of around 160-190 K in an CO pressure of about 10^{-8} Torr. The saturation coverage was prepared with the sample at about room temperature in a CO pressure of around 10^{-5} Torr, and then quickly cooled down to 100 K. The exposure[2] of CO on the Rh(111) surface is measured in Langmuir (L) = 10^{-6} Torr · s. The ordering of the overlayer structures was checked by LEED.

The high-resolution EELS measurements were performed at the Surface Science Division, Institute of Experimental Physics, Karl-Franzens-Universität Graz, Austria. These measurements were conducted on the same crystal in a 2-chamber UHV-System [11], dedicated to high resolution electron energy loss spectroscopy. The cleaning of the Rh(111) crystal was performed in the same way as described above except for the heating of the sample, which was accomplished by electron bombardment from behind the crystal. All the EELS spectra were measured at room temperature. The energy resolution, determined from the peak elastically reflected in the specular direction, was about 3.5 meV.

2.2 Curve fitting and data analysis procedure

In order to analyze the C 1s photoemission spectra we use a least squares fitting routine developed in the MatLab [12] programming environment. The spectra are decomposed into several different components, each with a certain binding energy and intensity, to simulate the experimental data. The line shape of the individual components consists of a Doniach-Šunjić profile [13] convoluted with a Gaussian distribution, which represents unresolved vibrations, many-body effects [14] and the experimental broadening. The Doniach-Šunjić profile contains a Lorentzian distribution, which represents the natural lifetime broadening, and an asymmetry, which accounts for electron-hole pair excitations at the Fermi level for metallic systems. A linear background is included in the fit. In an ordinary fitting procedure the background parameters and the parameters describing the different C 1s components, i.e. the intensity, the binding energy, and the three lineshape parameters, are varied. In the case of a complicated spectrum this gives a large amount of free parameters. For example, excitations to the

[2] The pressure is taken from the ion gauge without any correction for the sensitivity towards CO.

vibrational levels of a core-ionized molecule may, if the splitting of these levels is sufficiently large, lead to several observable vibrational fine structure components in the corresponding core level photoemission spectrum. In the case of such vibrationally split core levels the number of free parameters can often be reduced, which simplifies the fitting of the spectrum.

Within the harmonic approximation the energy separation of vibrational levels, and hence between the fine structure components due to a certain vibrational mode in the photoemission spectrum, is constant:

$$E_v = \left(v + \tfrac{1}{2}\right)\hbar\omega \ , \tag{1}$$

where E_v is the energy of the vibrational level with quantum number v and ω is the vibrational frequency of the core ionized molecule. This frequency and thereby the vibrational energy depends on the force constant k and the reduced mass μ for the bond:

$$\omega = \sqrt{k/\mu} \tag{2}$$

Therefore, for the case of a single vibrational mode, if the vibrational energy of this mode is large enough to be resolved, the spectrum should show a number of equidistant components separated by the final state vibrational energy. In the fitting procedure the lineshape parameters are set equal for all of these components reducing the number of free parameters significantly.

A further simplification of the curve fitting is to use the so-called linear coupling model [15] for the analysis of the vibrational progression. This model is valid if the potential energy surfaces describing the vibrational motion in the initial (ground) state and the final (ionized) state only differ in linear terms. Then the intensities of the vibrational components follow a Poisson distribution,

$$I\left(0-v_1,...,0-v_q\right) = I\left(0-0,...,0-0\right)\cdot\prod_{r=1}^{q}\frac{S_r^{v_r}}{v_r!}, \tag{3}$$

where v_r is the vibrational quantum number for the mode r and S_r is termed the S factor. In this expression it is assumed that the initial neutral molecule is in its vibrational ground state, which is appropriate at low temperatures for internal molecular vibrational modes with high vibrational energies ($\Delta E_{C\text{-}O} \sim 200$ mV). For a single stretch vibrational mode the S factor depends on the change in bond length Δr upon ionization:

$$S = \frac{\mu\omega}{2\hbar} \cdot \Delta r^2 . \qquad (4)$$

This S factor, which is a measure of the strength of the vibrational excitation, is easily deduced from the experimental data as the intensity ratio between the first vibrational component ($v = 1$) and the adiabatic peak ($v = 0$). In the linear coupling model, which is frequently used in gas phase studies, there is therefore only two free parameters for each vibrational progression; the vibrational energy and the S factor. This gives useful physical constraints on the decomposition of the core level photoemission spectra.

3. RESULTS AND DISCUSSION

In the discussion about the C 1s photoemission spectra from the different overlayers of CO adsorbed on Rh(111) we will start with the extremes; low CO coverages with only on-top adsorption and saturation coverage containing 0.75 ML of CO adsorbed in on-top and three-fold hollow positions. After this we will turn to the intermediate region of CO coverages between about 0.5 ML and saturation coverage, which is the most complex coverage region. Finally, the lineshape parameters used for the decomposition of the spectra will be discussed in section 3.4 in connection with a comparison to the old HRCLS studies.

3.1 Low CO coverage

The C 1s photoemission spectrum from about 0.2 ML of CO on Rh(111) is shown in Figure 1. The result from a decomposition of the spectrum is included in the figure, and the corresponding parameter values are tabulated in the first row of Table 1. This spectrum is fairly simple since it only contains emission at around 286 eV due to CO molecules adsorbed in on-top positions (for the site determination, see references 4 and 5). This emission can be decomposed into three fine-structure components, i.e. the adiabatic peak and the first and the

second vibrational component of the C-O stretching mode. The adiabatic C 1s peak, for CO in on-top positions, has a binding energy of 286.04 eV. The simple theory discussed above seems well suited to describe the intensity distribution of the vibrational progression, which follows a Poisson distribution described by an S factor of around 0.24 and a constant energy separation of around 232 meV, i.e. ~20 meV lower than the ground state vibrational energy.

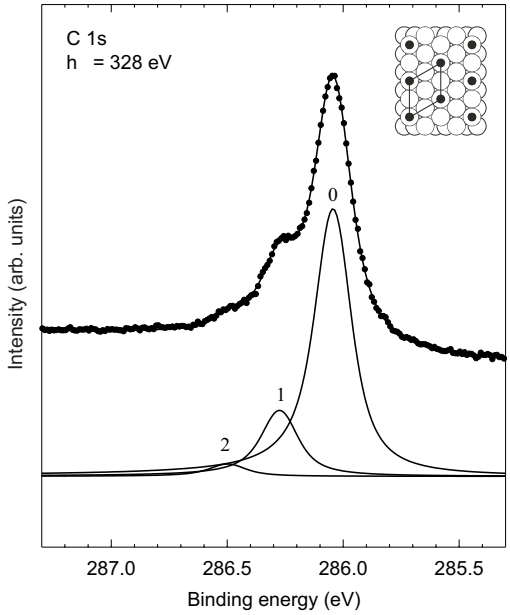

Figure 1.
The C 1s spectrum of a low coverage CO overlayer, about 0.2 ML, on Rh(111) measured at a photon energy of 328 eV. A decomposition of the spectrum is included, with final state vibrational quantum number indicated for the respective component.

The spectrum in Figure 1 is measured at a photon energy of 328 eV for the following reasons. The S factor of the C-O stretch shows small differences between spectra measured at different photon energies. Especially at low photon energies, the influence on the vibrational intensity distribution from a so-called shape resonance is noticeable, which also was found for CO adsorbed on Ni(100) and Ru(0001) [16]. The presence of a shape resonance above the ionization threshold induces strong coupling between vibrational and electronic motion [17], which can lead to a non-Franck-Condon distribution of the vibrational components. For C 1s photoionization of CO in gas phase this was demonstrated in the beginning of the 1990's [18]. Then again, at higher photon energies, where there is no influence of the shape resonance, the C 1s photoemission signal decreases due to the decreasing photoemission cross section. We found that at a photon energy of 328 eV there is both a fairly strong photoemission signal, the intensity ratio between the on-top and the three-fold hollow components is approximately equal

to the relative occupation of these two sites, and the S factors are similar to those obtained from measurements at higher photon energies.

Table 1: The C 1s binding energy of CO adsorbed in on-top respective three-fold hollow positions on Rh(111) for three different CO coverages. The S factor and vibrational energy of the C-O stretch mode is also given for each case.

CO coverage	C 1s component	E_B (eV)	S factor	$\hbar\omega$ (meV)
Low	on-top	286.04	0.24 ± 0.02	232 ± 2
Saturation	on-top	285.99	0.23 ± 0.02	235 ± 5
	hollow 1	285.29	0.58 ± 0.02	173 ± 5
Intermediate (3 L)	on-top	286.03	0.24 ± 0.02	233 ± 6
	hollow 1	285.25	0.58 ± 0.05	171 ± 10
	hollow 2	285.42	0.53 ± 0.05	192 ± 20

In the neutral ground state of CO adsorbed in on-top positions on Rh(111) the C-O stretch vibrational energy is 247-257 meV as previously found by EELS [1,2]. In our own high-resolution EELS measurements we obtain a C-O stretch vibrational energy of 254 meV, see the first row of Table 2. The vibrational splitting found in photoemission is however not directly comparable to an EELS energy loss, as mentioned above in Footnote 1, since the core hole must be taken into consideration. A core-ionized molecule can in many cases be likened by its (Z + 1)-equivalent [19], that is, the influence of the core hole on the valence electrons is approximated by adding one extra nuclear charge to the ionized atom. For C 1s ionized CO adsorbed on Rh(111), the Z+1 equivalent is NO adsorbed on the same surface. From this we expect a lower vibrational energy, since the bond strength of NO is weaker than that of CO. The NO on Rh(111) system has fortunately also been investigated previously with EELS [20,21]. Contrary to CO, the NO molecules adsorb only in hollow positions at low coverages, while the on-top positions become occupied only at higher coverage[3]. The saturation unit cell is identical for NO and CO adsorbed on Rh(111). In these EELS studies [20,21] the N-O stretch energy loss for NO in on-top positions on Rh(111) was found to be 228 meV, which is indeed very close to our C 1s photoemission value for the C-O stretch[4].

[3] In reference 20 the two loss peaks were attributed to bridge- and top-bonded NO. In a later paper (ref. 21) the structure was reanalyzed and the low-energy loss peak was instead attributed to NO adsorbed in three-fold hollow positions.

[4] It is in amazingly good agreement considering that our on-top vibrational energy comes from isolated C^*O molecules while the NO on-top vibrational energy comes from a densely packed NO overlayer. In this context we also neglect the small discrepancy due to the different reduced masses of C^*O and NO.

Table 2. HREELS results: The energy loss due to the C-O vibration and the full width at half maximum (FWHM) of the peaks for CO molecules adsorbed in on-top respective three-fold hollow positions on the Rh(111) surface.

Adsorption site	Energy loss	FWHM (meV)
on-top	254 ± 1	5 ± 1
hollow	227 ± 3	12 ± 2

3.2 Saturation coverage

The C 1s spectrum from the saturation (2×2)-3CO overlayer measured at a photon energy of 328 eV is shown in Figure 2. This spectrum is a little more complicated than the low-coverage spectrum shown in Figure 1. The (2×2)-3CO unit cell contains one CO molecule in an on-top position, one in the hcp three-fold hollow position and one in the fcc three-fold hollow position [4,5,3,6]. However, the result of the decomposition of the C 1s spectrum in Figure 2 reveals only emission from two chemically inequivalent CO molecules: The emission with an adiabatic peak at the binding energy of 285.99 eV comes from the CO molecules adsorbed in on-top positions and the emission at lower binding energy, with the adiabatic peak at 285.29 eV, is due to the CO molecules adsorbed in three-fold hollow positions[5]. This assignment was made in refs. 4 and 5. Thus, at the present resolution and due to the intrinsic line width of C 1s we are not able to distinguish between the fcc and hcp hollow positions. We will therefore not make any distinction between these two sites.

The C 1s emission from both on-top and hollow adsorbed CO contains vibrational fine structure from excitation of the C-O stretch mode. The on-top vibrational fine structure, with an S factor of 0.23 and a separation of 235 meV, is very similar to the low coverage case. On the other hand, the hollow vibrational fine structure differs substantially from that of the on-top component. The vibrational components are much more intense, with an S factor of 0.58, and the separation is smaller, 173 meV.

There is a rule of thumb for CO (and NO) adsorbed in different sites on metal surfaces that higher coordination to the surface lowers the vibrational energy of the C-O (and N-O) stretch, which has been used in analyses of EELS spectra for a long time [22]. A more recent discussion of this rule, and the dangers of assigning adsorption sites only by the vibrational

frequencies, is given in reference 23. From the discussion above about the Z+1 approximation this rule of thumb can be expected to work for C 1s photoemission studies of CO as well.

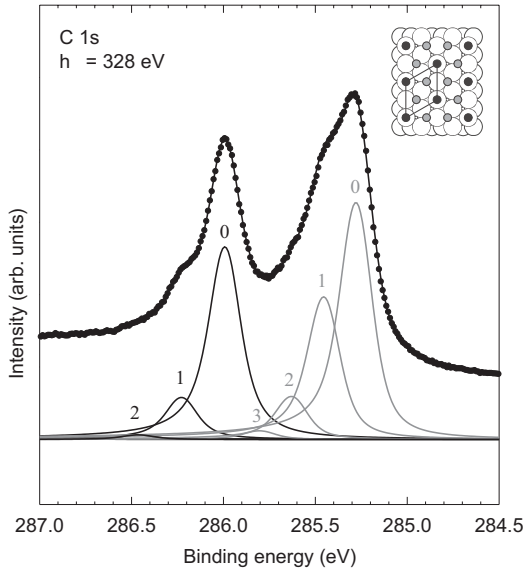

Figure 2.
The C 1s spectrum of the saturated CO overlayer on Rh(111) measured at a photon energy of 328 eV. A decomposition of the spectrum is included, with final state vibrational quantum number indicated for respective component.

Accordingly, we find the hollow vibrational energy to be about 60 meV lower than the on-top vibrational energy. In the previous subsection the vibrational energy of the on-top vibrational mode was compared to the EELS energy loss for the same mode in NO (the Z+1 equivalent to CO) adsorbed on Rh(111). The same comparison is valid for the three-fold hollow mode. At high coverage the N-O three-fold hollow vibrational mode has an energy of 188 meV [20]. This is close to, but somewhat higher[6], than 173 meV, which we find for the C-O stretch mode of the C 1s ionized CO molecules adsorbed in the three-fold hollow sites. Still, the vibrational energy is similar enough that it may be used as a fingerprint of adsorption site, but of course with the precautions given by reference 23 in mind.

---

[5] The ratio between the total intensity for the hollow components respective the total intensity of the on-top components is about 1.8, which differs somewhat from the factor of 2 expected from the number of adsorption sites per unit cell. This is due to diffraction of the photoelectrons [4,5].

[6] Judging only from the difference in reduced mass the C^*O vibrational energy should be larger than for NO, not smaller as in this case. Apparently the fact that the NO molecule is surrounded by other NO molecules, whereas the C^*O molecule is surrounded by neutral CO molecules, has some effect on the vibrational energies.

That the S factor for the hollow C-O vibrational progression would turn out to be so much larger than for the on-top progression is not immediately obvious. According to eq. 4 the S factor could be expected to decrease if the vibrational energy $\hbar\omega$ decreases. However, both the reduced mass μ of the C-O bond and the change in bondlength upon ionization Δr could be different for different adsorption sites. On the other hand, to a first approximation, if the substrate is considered to have infinite mass the reduced mass of the C-O bond should be equal for the hollow and on-top adsorbed CO molecules. Therefore, in this case, the change in bond length upon C 1s ionization must be considerably larger for the CO molecules adsorbed in the hollow positions compared to CO in on-top positions.

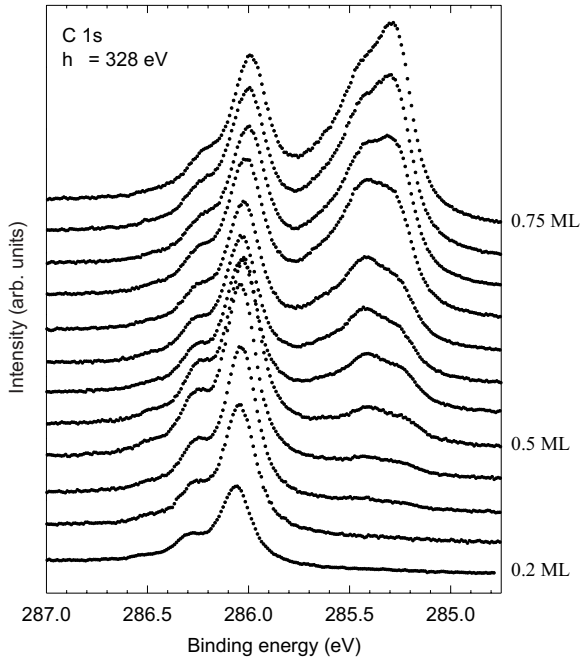

Figure 3.
The C 1s spectrum from the CO on Rh(111) overlayer system as a function of increasing CO coverage between 0.2 ML and saturation coverage. The spectra are normalized to the background at the low binding energy side.

3.3 Intermediate CO coverage

C 1s spectra for CO coverages in the whole range between 0.2 and 0.75 ML on Rh(111) are shown in Figure 3. At intermediate coverages (0.5 ML < θ < 0.75 ML) both on-top and three-fold hollow positions are occupied [4,5]. The CO overlayers show a (4×4) LEED pattern at around 0.5 ML and at higher coverages a split (2×2) pattern, with spots that gradually coalesce with increasing coverage to pure (2×2) spots at saturation. One might expect the

spectra in this intermediate region to be more or less a simple interpolation between the results from the low coverage and the saturation case. This, however, turned out not to be the case.

The emission peak from the CO molecules adsorbed in on-top positions is similar for all different coverages, including the low-coverage and the saturation case as discussed above. In Table 1 the C-O stretch S factor and the vibrational splitting for on-top adsorbed CO is shown for a 3 L exposure of CO, as well as for low and saturation coverage, and S factors for several different exposures are shown in the first row of Table 3.

Table 3. The "S factor", i.e. the intensity ratio between the first vibrational component and the adiabatic peak, for the C-O stretch mode of CO molecules adsorbed in on-top respective three-fold hollow positions on the Rh(111) surface (in the case of decomposing the spectra with only these two C 1s components).

CO dose:	1.3	2 L	3 L	4 L	5 L	10 L	20 L	50 L	Saturation
I_1/I_0(on-	0.24	0.24	0.24	0.24	0.24	0.23	0.24	0.23	0.23 ± 0.02
I_1/I_0(hollo	-	1.44	1.28	1.25	1.22	0.95	0.77	0.65	0.58 ± 0.02

However, an unexpected behavior is found if the intermediate-coverage spectra are fitted in the same way as the saturation-coverage spectrum, that is, with one vibrational progression for the on-top emission and one vibrational progression for the three-fold hollow emission. The intensity ratio between the first vibrational component and the adiabatic peak of the hollow emission is found to depend strongly on the CO coverage, as seen from the raw data in Figure 3 and shown in the second row of Table 3. I_1/I_0 decreases from above 1.4 at low coverage to about 0.6 at saturation. Furthermore, the decomposition of the different intermediate-coverage spectra shows that these fine-structure components do not follow a Poisson distribution, as expected from the simple theory for molecular vibrations described above.

Moreover, the intensity distribution of the hollow fine structure not only changes with different CO coverage, but also with sample temperature. Figure 4 is an example, for a CO coverage of just above a half monolayer, of how the hollow region of the C 1s spectrum (binding energies between 285 eV and 286 eV) varies with temperature. Similar behavior is observed for all CO coverages in the intermediate coverage region. The spectrum in the lowest panel is measured at 100 K whereas the middle and top panel show spectra from the same overlayer measured at sample temperatures of 170 K and 250 K, respectively. Already at 100 K component one (binding energy of about 285.43 eV) is stronger than component zero (binding energy of about 285.26 eV), with an intensity ratio of $I_1/I_0 = 1.3$ (compare to $I_1/I_0 = 0.58$ for the

saturation coverage). This intensity ratio increases with increasing temperature; at 170 K it is 1.6 and at 250 K it is 1.9. This is in contrast to the fine structure of the on-top component, which has the same intensity ratio independent of both CO coverage and sample temperature. It should finally be noted that these changes are reversible; cooling down restores the initial intensity ratio.

In the search for an explanation of the changing intensity ratio we first rule out any effects from initial state vibrations. Increasing the temperature could certainly give vibrational excitations in the initial state molecule. However, the spectra in Figure 4 are measured at temperatures below room temperature where thermal excitations to the vibrational levels of the C-O stretch mode ($\Delta E = \hbar\omega \sim 0.2$ eV) are negligible.

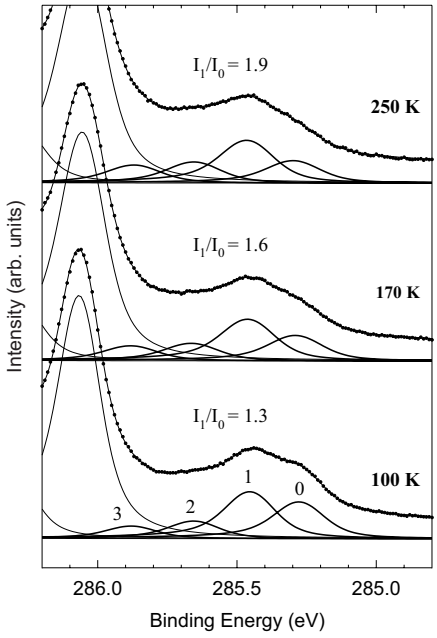

Figure 4.
The C 1s spectrum of about 0.55 ML CO on the Rh(111) surface at different sample temperatures measured at a photon energy of 328 eV. The spectrum is decomposed using the same number of components as for the saturation spectrum in Figure 2.

Then the only temperature effect would be broadening of the peaks due to many-body effects and excitations to low-energy vibrational modes, e. g. phonons. Therefore the C-O stretch intensity distribution should not differ between these spectra, which indeed was seen to be true for the on-top components. The conclusion is that trying to represent the C 1s emission from an intermediate coverage CO overlayer in the same manner as for the case of CO saturation

coverage, with one vibrational progression for the on-top emission and one vibrational progression for the three-fold hollow emission, is not physically correct.

To solve this problem we then tried, instead of using only one vibrational progression, to fit the binding energy region between 285 and 286 eV with two Poisson progressions, shifted about the same amount as the C-O three-fold hollow stretch vibrational energy. To be able to perform such a decomposition, with many overlapping components, it is absolutely necessary to understand how vibrational excitations affect photoemission spectra since physically correct constraints must be applied to the fitting parameters (see section 2.2). As an example, the result for a CO coverage of about 0.55 ML is shown in Figure 5 and Table 1. As seen in Figure 5 the low binding energy emission around 285.5 eV can be described by two vibrational progressions; one with an adiabatic binding energy of about 285.25 eV and one shifted about 170 meV towards higher binding energy, to about 285.42 eV. The component at 285.25 eV has almost the same binding energy as the three-fold hollow component found in the saturation coverage spectrum (285.29 eV) and their vibrational fine structures are also similar. The S-factor is 0.58 and the vibrational splitting is 171 meV for the 285.25 eV component in the intermediate coverage spectrum, as compared to 0.58 and 173 meV for the saturation case.

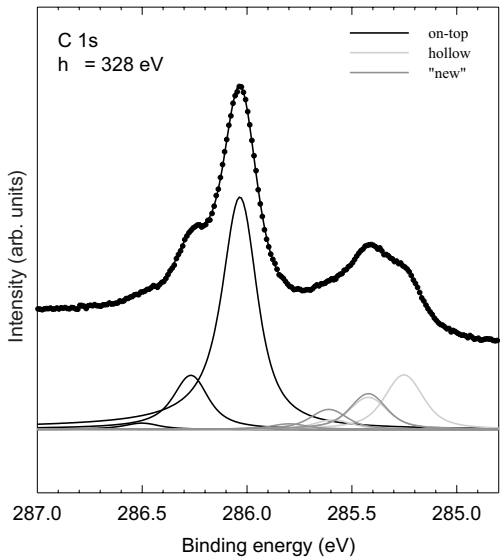

Figure 5.
The C 1s spectrum of an intermediate coverage CO overlayer, about 0.55 ML, on Rh(111) measured at a photon energy of 328 eV. A decomposition of the spectrum using three vibrational progressions is included.

We believe that this component is due to emission from the three-fold hollow CO molecules just as the low binding energy component in the saturation C 1s spectrum. The vibrational fine

structure of the "new" component at 285.42 eV, which is not observable in the saturation spectrum, is rather similar to that of the three-fold hollow component. However, the vibrational energy, 192 meV, is slightly higher, and the S factor, 0.53, slightly lower. There is no obvious assignment of this component in terms of a CO adsorption site. A discussion of possible assignments will be given below.

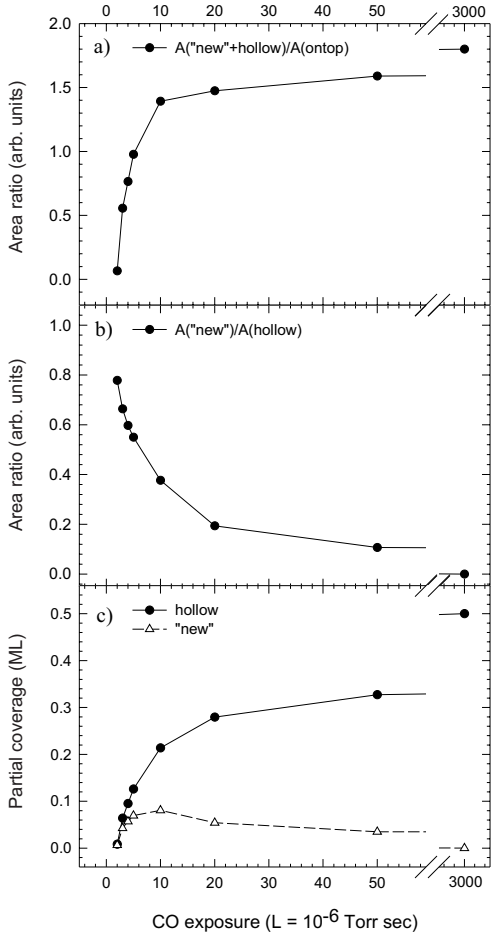

Figure 6.
a) The intensity ratio between the sum of the "new" plus the hollow components and the on-top component versus CO exposure.
b) The intensity ratio between the new component at a binding energy of 285.42 eV and the hollow component versus CO exposure. The area of the components includes all vibrational components corresponding to the respective modes.
c) The partial coverage as a function of CO exposure for the "new" component and the hollow component.

The parameters for the vibrational progressions found for the 0.55 ML CO overlayer may be used to decompose the C 1s spectra measured at other intermediate CO coverages and higher sample temperatures. The only parameter that changes is the intensity ratio between the "new" component and the hollow component, which is plotted in Figure 6b as a function of CO

dosage. The relative intensity of the “new” component is strongest at low coverage and decreases rapidly as the three-fold hollow to on-top ratio grows, see Figure 6a. In Figure 6c the partial coverage versus CO exposure is shown for the three-fold hollow and the “new” component. The amount of this “new” CO species is quite small in the whole range of CO exposures.

The maximum is reached after a CO dose of about 5–10 L, which corresponds to a total overage of around 0.6 ML, and even then the partial coverage is below 0.1 ML. In Figure 7 we show the temperature variation of the “new” component relative to the three-fold hollow component for three different CO coverages. Clearly the “new” component becomes more pronounced at higher sample temperature.

Before we start speculating about the possible origin of the “new” C 1s component we summarize its behavior: It is most pronounced at low intermediate coverages, just above 0.5 ML, where the three-fold hollow positions start to become occupied by CO molecules. Its relative intensity compared to the three-fold hollow component increases with increasing temperature, see Figure 7. Finally, the C-O stretch vibrational energy is somewhat higher than for the three-fold hollow vibrational progression but significantly lower than for the on-top progression.

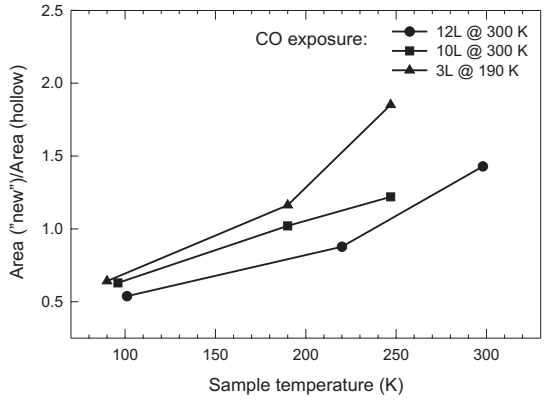

Figure 7.
The intensity ratio (total area for the vibrational progressions) between the “new” and the hollow C 1s components at binding energies of 285.42 eV and 285.25 eV, respectively.

A most natural thought is that the extra C 1s component could be due to CO molecules adsorbed in a different adsorption site, for instance a bridge site, even though the previous EELS spectra [1] only showed two peaks arising from CO adsorbed in different sites. However, since the EELS resolution has improved since then, we decided to test the bridge hypothesis

with this method. We therefore measured high-resolution EELS spectra for a number of CO coverages on Rh(111), in which we obtained a primary peak with a FWHM of about 3.5 meV, significantly below the width of 11 meV (90 cm^{-1}) obtained in ref. 1. In Figure 8a the energy loss spectrum of a CO-covered Rh(111) surface is shown. This spectrum consists of a very intense primary peak due to elastically scattered electrons, a peak at about 50 meV due to the CO-metal stretch mode, and a couple of peaks at around 250 meV due to the C-O stretch mode. In Figure 8b-e loss spectra for the C-O stretch region between 220 meV and 280 meV are shown for CO exposures of 1 L, 2 L, 3 L and 60 L. These HREELS spectra are measured at room temperature as opposed to the HRCLS spectra, which are measured at about 100 K. However, as can be seen in Figures 4 and 7 the new C 1s component is enhanced at higher temperature. Still, in the HREELS spectra in Figure 8 only two distinct C-O energy loss components are seen, at 227 meV and 254 meV, which represent the vibrational energies for the C-O stretch mode in CO molecules adsorbed in three-fold hollow and on-top positions, respectively, see also the results specified in Table 2. There is no clear sign of a third component from a bridge site neither in the shown specular nor in off-specular geometry (not shown). Such a component would be expected to show up between the hollow and on-top component according to the coordination rule of EELS [22,23] mentioned above. However, the hollow loss peak at 227 meV is very broad, with about twice the width of the on-top peak (12 meV respective 5 meV) and it cannot be excluded that this peak actually contains two components. We therefore argue that the present HREELS measurements cannot rule out the possible occupation of a bridge site by CO molecules.

Furthermore, it has recently come to our knowledge that a very recent EELS measurement [24], with even higher resolution, found that a weak bridge component was present at all coverages above 0.2 ML. The bridge component was explained to be due to CO molecules in domain boundaries on the surface.

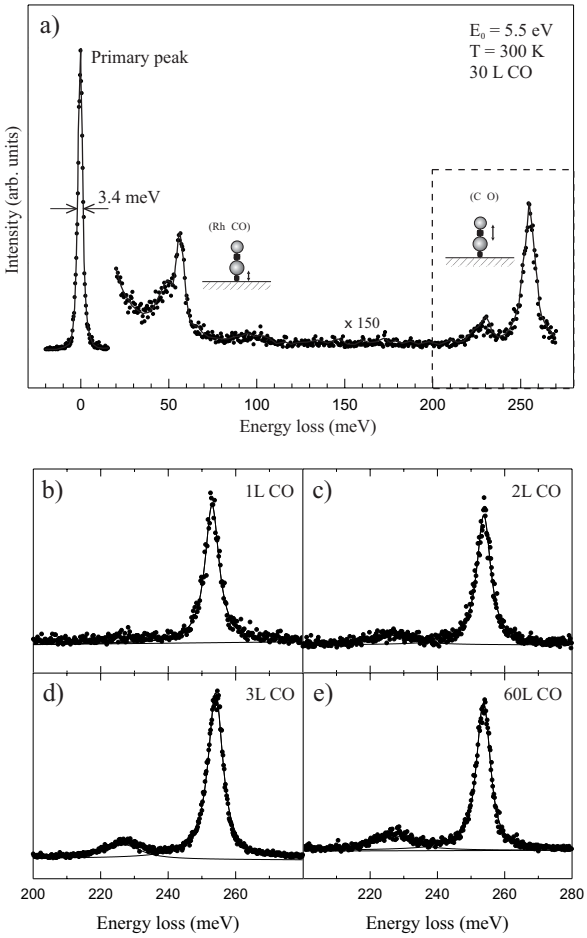

Figure 8.
a) Overview HREELS spectrum measured for CO on Rh(111) at room temperature.
b)–e) HREELS spectra over the C-O stretch energy region measured for four selected CO exposures of Rh(111).

The photoemission intensity variation as a function of photon energy caused by photoelectron diffraction [25,26,27,28] may be used as a fingerprint of adsorption sites. This diffraction effect is due to interference between the scattered and directly emitted photoelectrons, and is dependent on the adsorption geometry. In the case of CO on Rh(111) this results in large variations of the on-top to three-fold hollow C 1s intensity ratio versus photon energy as demonstrated in references 4 and 5. If the "new" component was due to CO molecules in bridge sites its intensity variation with photon energy should differ from that of the on-top and bridge components. We therefore measured C 1s spectra with different photon energies for CO coverages where the "new" component is strong. We find that the

photoemission diffraction behavior of C 1s spectra[7] measured at such intermediate CO coverages is rather similar to the diffraction behavior for saturation. The two components below 286 eV have about the same intensity variation, which is similar to the intensity variation of the three-fold hollow component in the (2×2)-3CO spectra. This may be taken to indicate that the "new" component is due to CO molecules in three-fold hollow sites. However, we believe that such a conclusion has to be made with much caution. Firstly, although the intensity variation of the "new" component is similar to that of the three-fold hollow component it is very difficult to establish that it is identical. Secondly, these C 1s spectra are measured at the best possible resolution which results in typical measurement times of ~15 min. These lengthy measurement times and the strong variation of the relative intensities of the two components below 286 eV with CO coverage limits the number of photon energies, which may be measured without influence from further CO adsorption. As a result, the data set is limited making it difficult to draw any definite conclusions from the diffraction behavior of the "new" component.

From the present measurements we therefore cannot make a conclusive decision about the origin of the "new" C 1s component. However, we can give a few suggestions to what it might be[8]. The first possible cause is CO adsorbed in bridge positions at domain boundaries, as suggested in Ref. 24. The intensity variation of the "new" component is consistent with such an explanation. Also, preliminary theoretical *ab-initio* calculations [29] show that the C 1s binding energy of a CO molecule in a bridge site should be in between that of the on-top and the three-fold hollow components, consistent with our determination of a binding energy of 285.42 eV for the "new" component. Furthermore, the vibrational energy determined from the progression of the "new" component is 192 meV, i.e. higher than that of the three-fold hollow but lower than that of the on-top component. This in combination with the mentioned rule of thumb [22,23] for vibrational energies of adsorbed molecules is indicative of a bridge site.

A second suggestion is that the "new" C 1s component might be due to CO molecules in three-fold hollow positions with a different number of CO neighbors than at saturation coverage. The "new" component could, for instance, arise from CO molecules in three-fold hollow sites, where some of the neighboring hollow sites of the (2x2)-3CO overlayer are not filled by other CO molecules, contrary to the situation in the saturation-coverage overlayer (see

[7] All spectra are measured at normal emission.

the structure model in Fig. 2). The existence of CO molecules with such a less dense CO surrounding is a clear possibility at intermediate coverages either as an integral part of the "split" 2x2 structure or as defects in the overlayer. Such an explanation would be consistent with the intensity variation of the "new" component. However, this hypothesis has also been checked by *ab-initio* calculations [29] of the C 1s binding energy. From these calculations it is found that the three-fold hollow binding energy is largely independent of the CO surroundings making it unlikely that the "new" component is due to a chemical shift of the three-fold hollow component.

Based on these considerations we propose that the "new" C 1s component at intermediate coverages is due to CO molecules adsorbed in bridge positions on the Rh(111) surface. This assignment is consistent with the suggestion based on HREELS measurements in ref. 24 that bridge adsorbed CO molecules may be found at domain boundaries in the CO overlayer at intermediate coverages.

3.4 Comparison to previous HRCLS studies

With increasing CO coverage, the C 1s binding energy of the on-top component shifts slightly towards lower binding energy, from 286.04 eV at low coverage to 285.99 eV at saturation coverage, see Table 1 and Figure 3. This was observed in the earlier HRCLS study as well (ref. 5), where the on-top binding energy was found to be 286.07 eV at low coverage and 286.00 eV at saturation.

The three-fold hollow component shifts towards higher binding energy with increasing CO coverage from 285.25 eV at low coverage (exposure = 3 L) to 285.29 eV at saturation. In the previous measurements (ref. 5) the binding energy of the hollow component instead seemed to decrease for increasing coverage, from 285.38 eV at low coverage to 285.35 eV at saturation. Furthermore, increasing the sample temperature was reported to cause a C 1s binding energy shift towards higher energy for the three-fold hollow component in the spectra from a (4×4)-overlayer structure at about 0.5 ML. The present measurements show no temperature dependent energy shift. At first the previous and present findings for the three-fold hollow component therefore might seem to be contradictory. The reason for this apparent conflict is that the "new" (bridge) component at a binding energy of around 285.42 eV, which

[8] The two components below 286 eV are not simply due to CO molecules adsorbed in the fcc and hcp sites. In that case we would detect both of these in the saturation coverage spectrum as well.

in the present study is treated as a separate component, was not resolved in the previous measurements. As mentioned above, see Figure 6b, at low coverage this extra component is stronger compared to the three-fold hollow component than at higher coverages, and at saturation it is not visible at all. It is also enhanced for higher sample temperatures, see Figures 4 and 7. Since this component has a higher binding energy than the three-fold hollow component its presence will cause the total C 1s emission, in the binding energy region below 286 eV, to shift towards higher binding energy. As also can be noted, the binding energies for both the on-top and three-fold hollow components, even at saturation, stated in reference 5 are slightly higher than those obtained in the present study. This is again due to the difference in instrumental resolution. The C-O stretch vibrational components were not resolved at that time, which gave much broader and more asymmetric peaks leading to erroneous binding energies.

Table 4: Lineshape parameters for the on-top respective hollow C1s components.

Adsorption site	Γ (meV)	σ (meV)	α	FWHM
on-top	140 ± 20	90 -110	0.04 ± 0.02	190 - 210
hollow	120 ± 20	130 -140	0.04 ± 0.02	~ 210

As mentioned in section 2.2 the lineshape parameters (Table 4) were kept fixed for all components belonging to the same vibrational progression during the decomposition of the C 1s spectra. To obtain a proper Lorentzian width Γ the fit has to be good at the low binding energy side of the photoemission peak and, at the same time, the fit at the high binding energy side has to be good to obtain the proper asymmetry parameter α. Therefore the Lorentzian width and the asymmetry parameter for the on-top component are determined from the low coverage spectrum, where no hollow component is present. The Lorentzian width and the asymmetry for the hollow components are determined from the saturation coverage spectrum. The Lorentzian width for the on-top progression is determined to about 140 meV and the asymmetry parameter to about 0.04. For the hollow components the Lorentzian width is about 120 meV, and the asymmetry is the same as for the on-top component. The line shape parameters of the bridge component is set equal to those of the three-fold hollow component. These parameters are then used for fitting the spectra at other CO coverages. The Gaussian[9]

[9] The values of the Gaussian broadening given here are for the low temperature measurements (about 100 K). At higher temperatures the Gaussian width is increased due to thermal broadening, i. e. excitation of low energy vibrations and many-body effects.

widths can differ between the overlayers due to different levels of disorder and are varied to obtain the best fits. In the case of the on-top component the Gaussian width is smaller, about 90 meV, for the low coverage regime with only on-top emission, than for the overlayers with CO adsorbed in both on-top and three-fold hollow positions. $\sigma_{\text{on-top}} \approx 110$ meV for the saturation coverage. The Gaussian width of the three-fold hollow components is about 130 meV for the saturation coverage and about 140 meV for the intermediate coverages.

We obtain C 1s Lorentzian widths for both the on top and the hollow components, which are broader than for CO in gas phase (about 100 meV [30]), contrary to what reference 8 uses for CO adsorbed on Ni(100). However, our experience from adsorbed molecules on metal surfaces (see for example references 4,5,7,31 and 32) is that the C 1s Lorentzian width generally is larger than for corresponding molecule in gas phase indicating shorter lifetimes due to more decay channels for the adsorbate molecule.

In the previous photoemission measurements (references 4 and 5) a Lorentzian of 0.14 eV and an asymmetry parameter of 0.12 were used for both the on-top and the hollow components. The previously obtained Gaussian widths were about 0.3 eV higher than the present. Since the experimental broadening was about 0.2 eV larger at that time, the presence of the unresolved C-O vibrational progressions caused an extra Gaussian broadening of about 0.1 eV. The much larger asymmetry parameter is also due to the unresolved C-O vibrational progressions. For highly excited vibrations the Poisson distribution approaches a symmetric Gaussian, which is often the case for low energy phonons. For the C-O stretch mode in CO adsorbed on Rh(111), however, only the lowest vibrational levels are excited during the photoemission process and the intensity distribution is a highly asymmetric Poisson distribution, leading to a too large Doniach-Šunjić asymmetry parameter if the vibrational progression is not included.

4. CONCLUSIONS

The knowledge of how internal molecular vibrations affect photoemission spectra is necessary for the understanding of complicated core-level spectra from molecules adsorbed on metal surfaces. Without such knowledge the decomposition of the C 1s spectra from CO on Rh(111) could not have been done in a proper way. In addition to deriving information about the vibrations in the core-ionized CO molecules, which differ between the CO molecules adsorbed in different sites on the Rh(111) surface, the understanding of vibrational excitations

in core level spectra also allowed the identification of a new C 1s component at intermediate CO coverages. Different possible origins of this "new" component were discussed. Even though the experimental findings are not conclusive, we suggest that the "new" C 1s component is due to a small amount of CO molecules adsorbed in bridge positions.

It is noteworthy that this third kind of CO molecule could be seen with core level photoemission spectroscopy, when it was not detected by electron energy loss spectroscopy at an energy resolution of 3.5 meV. With photoemission this component could even be followed quantitatively while increasing the coverage of the CO/Rh(111) overlayer and it was found to have the greatest influence on the C 1s spectra at low coverages, when the occupation of the three-fold hollow positions starts.

ACKNOWLEDGEMENTS

The assistance of the MAX-lab staff is gratefully acknowledged. We thank R. Linke for communicating the results of ref. 24 prior to publication. This work has been financially supported by the Swedish Natural Science Research Council.

REFERENCES

[1] L.H. Dubois and G.A. Somorjai, Surf. Sci. 91 (1980) 514.

[2] P. A. Thiel, E. D. Williams, J. T. Yates, and W. H. Weinberg,
Surf. Sci. 84 (1979) 54.

[3] M. Gierer, A. Barbieri,M.A. van Hove, G.A. Somorjai, Surf. Sci. 391 (1997) 176.

[4] A. Beutler, E. Lundgren, R. Nyholm, J.N. Andersen, B. Setlik, and D. Heskett, Surf. Sci. 371 (1997) 381.

[5] A. Beutler, E. Lundgren, R. Nyholm, J.N. Andersen, B. Setlik, and D. Heskett, Surf. Sci. 396 (1998) 117.

[6] E. Lundgren, X. Torrelles, J. Alvarez, S. Ferrrer, H. Over, A. Beutler, and J. N. Andersen, Phys. Rev. B 59 (1999) 5876.

[7] J. N. Andersen, A. Beutler, S. L. Sorensen, R. Nyholm, B. Setlik, and D. Heskett, Chem. Phys. Lett. 269 (1997) 371.

[8] A. Föhlisch, N. Wassdahl, J. Hasselström, O. Karis, D. Menzel, N. Mårtensson, and A. Nilsson, Phys. Rev. Lett. 81 (1998) 1730

[9] R. Nyholm, J.N. Andersen, U. Johansson, B.N. Jensen and I. Lindau, Nucl. Instr. & Meth. in Phys. Res. A, in press. Additional information can be found at http://www.maxlab.lu.se/beamline/max-ii/i311/i311.htm

[10] N. Mårtensson, P. Baltzer, P. A. Brűhwiler, J. O. Forsell, A. Nilsson, A. Stenborg, and B. Wannberg, J. Electron Spectrosc. Relat. Phenom. 70 (1994) 117.

[11] I. Kardinal, F.P. Netzer, and M.G. Ramsey, Surf. Sci. 376 (1996) 229.

[12] MatLab, The Mathworks, Massachusetts, USA.

[13] S. Doniach and M. Šunjić, J. Phys. C 3 (1970) 185.

[14] C.-O. Almblad and P. Minnhagen, Phys. Stat. Sol. 85 (1978) 135.
[15] L. S. Cederbaum and W. Domcke, J. Chem. Phys. 64 (1976) 603.
[16] A. Föhlisch, J. Hasselström, O. Karis, P. Väterlein, N. Mårtensson, A. Nilsson, C. Heske, M. Stichler, C. Keller, W. Wurth, and D. Menzel,
Chem. Phys. Lett. 315 (1999) 194.
[17] J. L. Dehmer, D. Dill, S. Wallace, Phys. Rev. Lett. 43 (1979) 1005.
[18] K. J. Randall, A. L. D. Kilcoyne, H. M. Köppe, J. Feldhaus, A. M. Bradshaw, J.-E. Rubensson, W. Eberhardt, Z. Xu, P. D. Johnson and Y. Ma,
Phys. Rev. Lett. 71 (1993) 1156.
[19] B. Johansson and N. Mårtensson, Phys. Rev. B 21 (1980) 4427.
[20] C.-T. Kao, G.S. Blackman, M.A. van Hove, G.A. Somorjai, and C.-M. Chan, Surf. Sci. 224 (1989) 77.
[21] I. Zasada, M.A. van Hove, G.A. Somorjai, Surf. Sci. 418 (1998) L89.
[22] N. Sheppard and N. T. Nguyen, Adv. IR Raman Spectr. 5 (1978) 67.
[23] K.-M. Schindler, Ph. Hofmann, K.-U. Weiß, R. Dippel, P. Gardner, V. Fritzsche, A. M. Bradshaw, P. D. Woodruff, M. E. Davila, M. C. Asensio, J. C. Conesa, and A. R. González-Elipe, J. Electron Spectrosc. Relat. Phenom. 64/65 (1993) 75.
[24] R. Linke, D. Curulla, M. J. P. Hopstaken, and J. W. Niemantsverdriet, private communication and submitted to J. Chem. Phys.
[25] D. P. Woodruff, D. Norman, B. W. Holland, N. V. Smith, H. H. Farrell, M. M. Traum, Phys. Rev. Lett. 41 (1978) 1130.
[26] S. D. Kevan, D. H. Rosenblatt, D. Denley, B. C. Lu, and D. A. Shirley, Phys. Rev. Lett. 41 (1978) 1565.
[27] C. H. Li and S. Y. Tong, Phys. Rev. Lett. 42 (1979) 901.
[28] D. P. Woodruff, Surf. Sci. 166 (1986) 377.
[29] M. Birgersson *et al*, to be published.
[30] S. J. Osborne, A. Ausmees, S. Svensson, A. Kivimäki, O.-P. Sairanen, A. Naves deBrito, H. Aksela, and S. Aksela, J. Chem. Phys. 102 (1995) 7317.
[31] M. Wiklund, A. Jaworowski, F. Strisland, A. Beutler, A. Sandell, R. Nyholm, S. L. Sorensen, and J. N. Andersen, Surf. Sci. 418 (1998) 210.
[32] M. Wiklund, A. Beutler, R. Nyholm, and J. N. Andersen, Surf. Sci. 461 (2000) 107.

Paper V

Investigation of the La-Rh(100) surface alloy

M. Kildemo, T. Ramsvik and S. Raaen

Surface Science 490 (2001) 1.

INVESTIGATION OF THE La-Rh(100) SURFACE ALLOY

M. Kildemo, T. Ramsvik, and S. Raaen
Department of Physics
Norges teknisk-naturvitenskapelige universitet, NTNU
N-7491 Trondheim; Norway

Abstract

In the present work surface alloy formation when La on Rh(100) is annealed to 1350 K is investigated by photoelectron spectroscopy, low energy electron diffraction (LEED), and temperature programmed desorption (TPD). When a sub-monolayer of La deposited on Rh(100) is annealed, a LEED pattern with streaked fractional order spots appears. By increasing the La coverage a modified c(2×2) structure is formed. In this case split fractional order spots indicative of anti-phase domain effects are observed in LEED. Analyses of the photoemission spectra of the Rh $3d_{5/2}$ and La 5p core-levels show that an ordering takes place in going from the as-deposited to the annealed system, which results in a Rh terminated surface. TPD experiments of CO adsorbed on the annealed La/Rh(100) system show CO desorption peaks at significantly lower temperature than CO on the as-deposited La/Rh(100), but still higher than the desorption peaks found for CO on Rh(100). From these results it is concluded that a true, ordered surface alloy is formed with new electronic states.

1. INTRODUCTION

The objective of this work is to investigate changes in electronic properties at the surface of an alloy that is formed by annealing a thin overlayer of a low work function material on a transition metal substrate. Presently, overlayers of La on Rh(100) of thicknesses near one monolayer are studied after annealing to form surface alloys. The role of electronic promoters in heterogeneous catalysis has been well documented [1,2]. The low work function rare earth elements may be good choices for the overlayer material when studying catalytic promotion [3]. The presence of a low workfunction element at the surface has the effect of lowering the electrostatic potential and thus influencing the bonding of gas molecules. Both structural and electronic changes have to be considered in such overlayer systems.

Rare earths may also be well suited to be used as dopants in catalysts since they have low surface free energies [4]. They therefore have a tendency to be located at or near the surface in an actual catalytic system, and will thus directly influence adsorption and desorption of various gas molecules. Frequently simple model systems give useful insight into real catalytic processes as well as fundamentals of adsorption and desorption of different gas molecules. Previous experiments have shown that solid state reactions occur when rare earths are deposited on a variety of metallic substrates even at ambient temperatures [5,6,7]. In a recent work, the formation of an ordered La-Pt(111) surface alloy when a La on Pt overlayer system was annealed to 900 K was observed. An analysis of thermal desorption spectra of CO from Pt and La-Pt showed that the desorption energy was considerably lower in the case of the surface alloy [8]. The large reduction in reactivity of CO on the La-Pt(111) surface alloy was argued to be related to the existence of strong resonant interactions of the Pt 5d-band with the CO 5σ orbital that give rise to a pronounced 5σ donor contribution to the CO-Pt bond [9]. As the La-Pt(111) surface alloy was formed, the d-band moves to lower binding energies and the Pt 5d – CO 5σ interaction is no longer resonant, resulting in a significantly suppressed CO-PT bond. On this background, other rare earth – transition metal systems are of interest. This work presents aspects of the formation of La-Rh(100) surface alloys as well as some structural and electronic properties of these alloys.

2. EXPERIMENTAL

The high-resolution photoemission measurements were performed at beamline I311 at the synchrotron radiation facility Max-lab in Lund, Sweden. The beamline is an undulator based VUV, soft X-ray beamline aimed at high resolution XPS. The monochromator is a modified SX-700 with a 1200 l/mm grating, spherical focusing mirror, and a movable exit slit. The electron energy analyser is a hemispherical SCIENTA SES 200 analyser. In the present experiment the total (energy) resolution for Rh $3d_{5/2}$ and La 5d is estimated to be 100 and 40 meV respectively, as determined from the width of the Fermi edge. Binding energies were calibrated by measuring the position of the Fermi edge after each spectrum. The Rhodium crystal was cooled to below 150 K during photoemission measurements to reduce the vibrational broadening, and all spectra were measured at normal emission.

The Rh(100) crystal was mounted on a 0.5 mm W-wire, and were heated by sending current through the support wires or cooled with liquid nitrogen to ~100 K. The temperature was measured by a Chromel-Alumel thermocouple that was spot-welded to the rear of the sample.

The Rh(100) crystal surface was cleaned by repeated cycles of Ar^+ sputtering (15 min room temperature and 15 min 1100 K), oxygen annealing at $1*10^{-8}$ at 1075 K in 5 minutes, and flash annealing to 1350 K in UHV. The surface cleanliness was checked by monitoring the core-level regions of likely contaminants and by measuring valence-band spectra at photon energies close to the Cooper minimum in the Rh 4d photo-ionisation cross section [10] The ordering of the surface was checked by low energy electron diffraction (LEED).

La was deposited from a water-cooled evaporation source that consisted of a thermally heated tungsten basket that was thoroughly out-gassed before use. The deposition was performed with the Rh substrate cooled below 150 K. During deposition the pressure did not exceed $1*10^{-9}$ Torr. The photoelectron spectra were recorded immediately after deposition-hereby defined as; “as-deposited layer”, and the Rh $3d_{5/2}$ core level photoemission measurement were used to estimate the “as-deposited thickness”. The photoemission intensity for all spectra was normalised to the background. Finally, the alloys were formed by slowly heating the samples to 1350 K.

The TPD spectra were recorded using a Transpector H100M quadropole mass-spectrometer from Leybold-Inficon that was interfaced to a personal computer. The heating rate was 2 K/s, controlled using a Eurotherm temperature controller.

3. RESULTS AND DISCUSSION

The experimental results related to formation of La-Rh(100) surface alloys are presented below. The deposited thickness of La was in the range 0.4 to 2.2 monolayers (ML). The experimental techniques used were high-resolution photoelectron spectroscopy, LEED and TPD.

3.1. LEED

No LEED pattern was observed for the La-Rh(100) surface deposited at liquid Nitrogen temperatures, and prior to annealing. Deposition at room temperature resulted in a partly mixed interface, as is commonly well known to other rare earth on transition metal systems [5-7]. The main focus is on the annealed "surface alloy" throughout the paper.

Figure 1 shows the LEED patterns observed after evaporating La on the Rh(100) surface at as-deposited thicknesses of 1.0 Å (Fig. 1a) and 2.8 Å (Fig. 1b), followed by an anneal to ~1350 K.

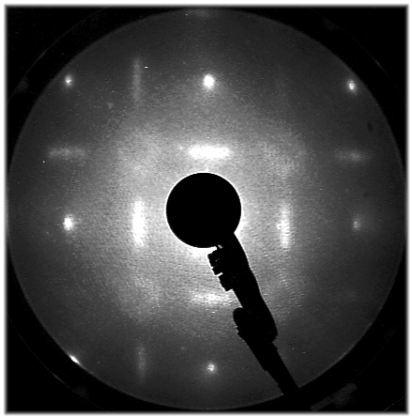

Fig. 1a. E=80 eV. d=1.0 Å.

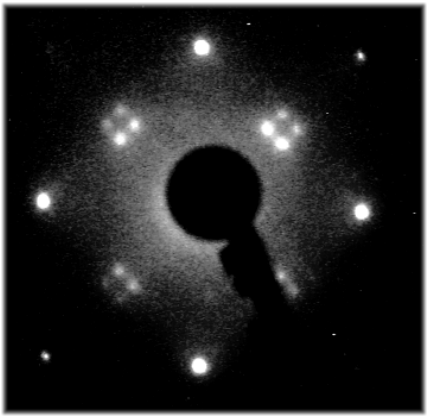

Fig 1b. E=112 eV. d=2.8 Å.

Figure 1. The figure shows the LEED patterns recorded from the annealed La-Rh(100) surface alloy. In the right figure 1a, the deposition time for the layer was 2 minutes, with an effective "as-deposited" thickness of d=1.0 Å. The LEED pattern was recorded with Electron beam energy of 80 eV. The LEED pattern is approximately (1x1) with additional features. In the right figure 1b, the deposition time was 5 minutes, with d=2.8 Å. The LEED pattern is approximately c(2x2) with the additionally split spots , as seen in the figure.

It is seen from figure 1a, that the LEED pattern of the sub-monolayer alloy shows a modified (1x1) pattern with additional streaks. This structure will be denoted as (1x1)+ throughout the paper. The layer in figure 1a seems to be incomplete and in a transition phase towards c(2x2). In fact, weak spots of half-integer order can be observed at this thickness.

When the thickness of the La-layer exceeds 2 Å (approaches 1 ML), a modified c(2x2) pattern appears. It can be seen from figure 1b that every second spot in the $b_1^*=0.5(a_1^*+a_2^*)$ and $b_2^*=0.5(-a_1^*+a_2^*)$ directions are split into four satellite spots, with no centre spot, where a_1^* and a_2^* are the reciprocal lattice vectors for the (1x1) substrate structure. This structure will be denoted as c(2x2)+ where it is understood that satellite spots are present such as is observed from figure 1b. The split spots in the c(2x2)+ structure in figure 1b makes approximately a square with spot splitting of approximately $\Delta a_1^* \approx \Delta a_2^* \approx 0.193a1^*$.

However, some preliminary arguments may be proposed based on the nearest neighbour distances in Rh (100) surface (a_{Rh}=2.8 Å) and the allotropic variations of La. There exist three phases of La, hcp (300 K), fcc (T>613 K), and bcc (T>1100 K), with nearest neighbour distances in the range 3.75 Å (fcc) and 3.77 Å (hcp) [11], giving approximately a smallest nearest neighbour distance of $1.34*a_{Rh}$. It is therefore not too surprising that at low coverages, we observe a (1x1) structure in transition towards a c(2x2) structure at higher coverages.

Since the split spots are of fractional order, the anti-phase domain effect is expected to be the main cause for the splitting of the spots [12]. The LEED structure in figure 1b, may be interpreted by considering the "form-factor" envelope of a c(2x2) domain (of spot width Δa_1^*) multiplied by a (5x5) LEED super-structure [12]. We note that the real space wavelength of the structure in figure 1b corresponds approximately to 14 Å. If we neglect domain disorder, one may present an ideal schematic diagram of the structure, such as in figure 2.

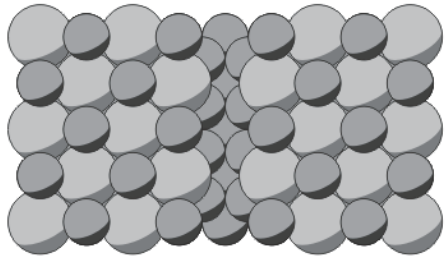

Figure 2. Simplified real space schematic diagram of the c(2x2)+ surface alloy, as estimated from LEED (see figure 1) and photoemission spectroscopy (see figure 3). The figure 2 shows two (5x5) superstructure domains. Each domain consist of a c(2x2) structure terminated by Rh atoms. The small balls represent Rh atoms, while the large balls represent La atoms. The domain shapes are largely simplified.

Each domain consists thus of a c(2x2) La layer on the fcc Rh(100) substrate. The surface is believed to be terminated by Rh atoms in a c(2x2) structure, as will be thoroughly discussed in section 3.2.1. The thickest structure studied in this paper (denoted 6 minutes of deposition time)

shows an approximate spot splitting of $0.173a_1$*, approaching a (6x6) domain structure, with a real space wavelength of 16.8 Å.

The weak spot splitting observed in the sub-monolayer regime in figure 1a is found to be approximately $0.25a_1$*. The latter corresponds to a (4x4) repetition of the structure, or a real space wavelength of 11.2 Å. Furthermore, the streaks running in the a_1*, a_2* directions, between the split half order spots, is proposed to be caused by scattering from the domain walls in the sub-monolayer alloy. Such an explanation has previously been reported in the literature in case of small anti-phase domains of various phases of Au adsorbed Si(111) [13]. In the latter work zigzagging domain walls following a 6-fold symmetry were directly observed with STM. One could thus speculate that in the La-Rh(100) sub-monolayer case, the domains grow in four fold symmetry along the principal directions of the Rh(100) substrate. The streaks may thus represent an amorphous organisation of the domains, which appears in the sub-monolayer regime, while the c(2x2) with split spot represent a higher crystalline state or domain superstructure for the monolayer regime.

The bulk La-Rh phase diagram shows a large number of La-Rh compounds [14], in the current temperature range (1000-1400 K). Some of these structures have large unit cells from 8 to 18 Å. It is therefore likely, that a competition between the energetically favourable surface structure and the stable bulk structure, is responsible for the domain super-structure giving the split spots. Complex surface restructuring has been reported for rare earth-transition metal systems [15], and the relation to known structures was evaluated based on LEED, Scanning Tunnelling Microscopy (STM) and photoemission studies. However it is out of the scope of the current paper to relate the current structure to a known structure.

3.2 Core level spectra Rh 3d and La5p

3.2.1 Rh 3d and thickness of alloy

The core level spectra of Rh 3d can be used to investigate the shifts in the core levels as the surface alloy is formed, and to estimate the thickness of the as-deposited layer.

Figure 3 shows the Rh $3d_{5/2}$ level, of clean Rh(100), as deposited La-Rh(100), and annealed La-Rh(100) alloy.

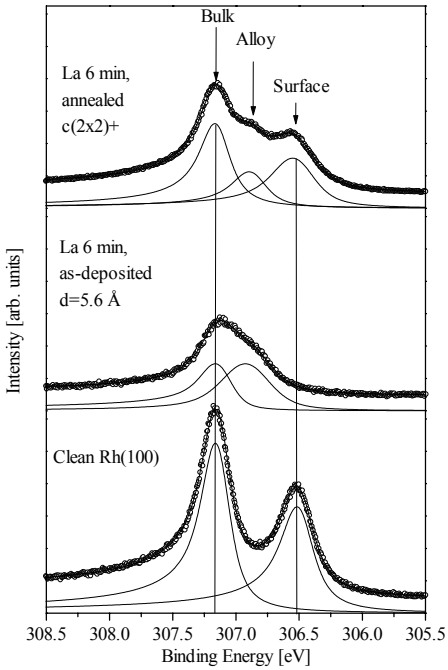

Figure 3. Rh $3d_{5/2}$ core levels for the clean Rh(100) sample (bottom figure), the as-deposited layer (middle figure), with 6 minutes deposition time corresponding approximately to 5.6 Å of as-deposited thickness, and the corresponding annealed sample (top figure). The clean Rh(100) sample has bulk Rh 3d core level at 307.13 eV and SCLS at 306.49 eV, while the annealed layer consist of the bulk Rh component, and a Rh-La component at 306.88 eV. The experimental data is shown as hollow circles, while the full lines show the fitted lineshapes. The photon energy for all spectra were 400 eV.

The bottom figure shows the clean Rh(100), with its characteristic bulk peak and surface peak, at 307.13 eV and 306.48 eV respectively, thus having a surface core level shift (SCLS) in accordance with previous results of 0.65 eV in case of a clean surface [16]. The middle figure shows the "as-deposited layer", with thickness 5.6 Å of deposited La. In particular, it is observed that the surface peak has disappeared, and that an additional peak at 306.91 eV has appeared. This latter peak is caused by a chemical shift appearing due to Rh in contact with La (or La co-ordination).

The observed shift towards *higher* binding energy for the Rh surface atoms after deposition of La and prior to annealing, can possibly be explained by a final state effect. After the creation of a core hole, an additional electron in the valence 4d shell will screen the Rh-atom [17]. The antibonding nature of this electron will increase the final state energy in the system, and hence give higher ionisation energy. The result would consequently be a positive

shift relative to the surface peak. However, it is shown in literature [18] that initial state effects can be the major features of the core-level shifts. Therefore, the true origin of the shift is uncertain. The top figure 3 shows a spectrum recorded after annealing. It is observed that a peak reappears at the position of the surface peak, i.e. 307.13 eV, and that the middle La-Rh peak becomes narrower. The former contribution is interpreted as Rhodium atoms that have reappeared as true surface atoms, but now in contact with Lanthanum atoms. Hence, this contribution will also be referred to as the surface peak. The mid peak is assumed to have the same origin as for the as-deposited layer, i.e. lower level Rh atoms in contact with La atoms, but now in the more ordered alloy. For this particular thickness, corresponding to the c(2x2)+ LEED patterns, the La-Rh peak is located at ~ 306.88 eV. Hence, the energy position La-Rh peak seems unaffected by the creation of a surface alloy.

The total area of the Rh $3d_{5/2}$ bulk core level was used to extract the thickness of the as deposited alloy. In addition, decomposition of the spectra using the Doniach-Šunjić line profiles [19] convoluted by a Gaussian function, supplied areas corresponding to the bulk and surface contributions of the Rh $3d_{5/2}$ peak.

The photoemission intensity from the substrate with an overlayer thickness in the monolayer regime, may be estimated by assuming epitaxial growth:

$$I_{sub} = I_{sub}^{0}\left[(1-\theta) + X\theta\right], \qquad (1)$$

where $X = e^{-\frac{d}{\Lambda}}$, θ is the fractional overlayer coverage, and Λ is the electron mean free path in the metal, at the given kinetic energy. In case of Rh $3d_{5/2}$ the kinetic energy in this study was E_{kin}=93 eV giving approximately $\Lambda = 6$ Å from the general inelastic mean free path curve, and I_{sub}^{0} is the recorded intensity from the clean Rh(100) substrate. For one full monolayer, θ = 1, and eq. (1) may therefore be rewritten as the following expression:

$$d = \Lambda \ln(I^{0}_{sub}/I_{sub}), \qquad (2)$$

Figure 4 shows $\Lambda\ln(I^{0}_{sub}/I_{sub})$ for La depositions of 1,2,4 and 6 minutes, for as-deposited and annealed samples, using the entire area under the Rh $3d_{5/2}$ peak to estimate the intensities. Clearly, alloying has taken place, as witnessed by the increased Rh intensity.

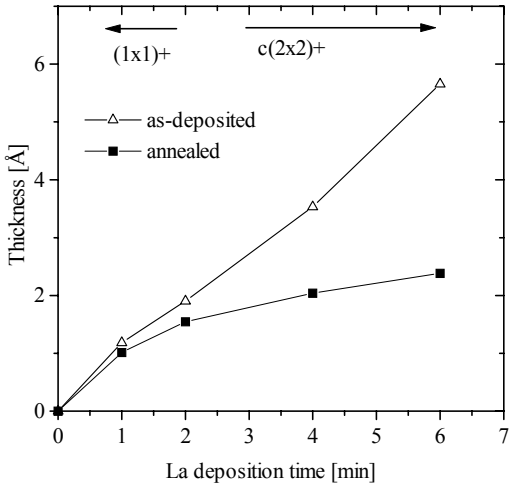

Figure 4. The figure shows $d = \Lambda \ln(I^0_{sub}/I_{sub})$ calculated from the entire area underneath the Rh $3d_{5/2}$ peak in figure 1 (see text for details). The hollow triangles correspond to the as-deposited layer, whereas the solid triangles correspond to effective thicknesses after annealing.

An approximate conversion to coverages in monolayers can be obtained by choosing the thickness (d) to be 3.1 Å in equation (1) (in case of submonolayer epitaxial growth), and adapting the appropriate formulas for epitaxial growth above one monolayer. The thickness for the second and third monolayer was chosen as 2.1 Å. All thicknesses were here chosen as the minimum thickness based on purely geometric considerations using the hard sphere approximation. The coverages corresponding to figure 4 are then estimated to be 0.45, 0.68, 1.25 and 2.25 ML, for 1, 2, 4 and 6 minutes of deposition respectively. Since the choice of thickness (d) is uncertain, particularly with respect to a possible layer intermixing, and that no LEED pattern was observed for the as-deposited structure, the as-deposited thicknesses calculated from equation (2) will be used throughout the paper. However, we note that the above estimated coverages are also found to be in reasonable correspondence to the disappearance at about 1 ML of the surface peak in the Rh 3d spectrum for the as-deposited layer.

The progression of the Rh 3d core level spectra resulting from the annealed layer, as a function of La deposition time, or as-deposited thickness, is shown in figure 5.

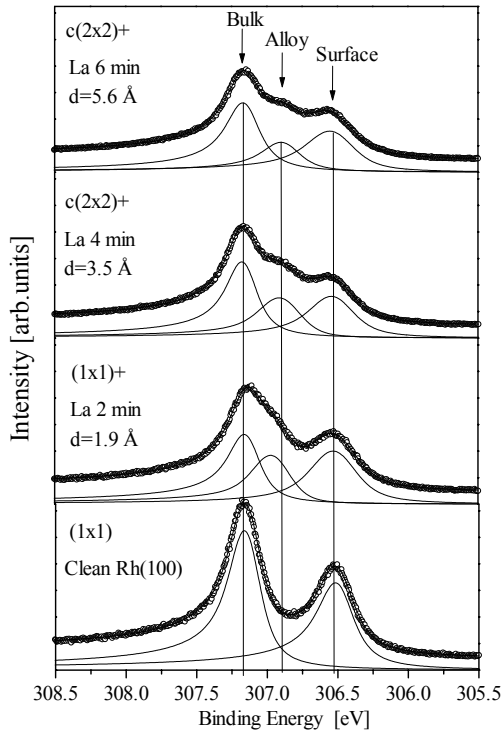

Figure 5. Rh $3d_{5/2}$ core levels recorded from annealed La-Rh(100) layers, as a function of La deposition time. The bottom figure shows clean Rh(100). The evaporation time, as-deposited thickness (d) and LEED pattern is indicated in the left hand side of the figure. The experimental data is shown in hollow circles, while the fitted DS lineshape functions are shown in full lines. The photon energy was 400 eV.

The bottom figure 5 shows the core level spectrum of clean Rh(100). The next spectrum shows the submonolayer alloy, resulting from "as-deposited-thickness" d = 1.9 Å. The corresponding LEED image in figure 1a showed a (1x1)+ LEED pattern. The next two figures shows the Rh 3d level appearing for d=3.53 and 5.64 Å, both showing the c(2x2)+ LEED pattern as in figure 1b. The bulk peak shifts slightly with approximately 0.02 eV to higher binding energies with increasing deposition thickness, i.e. below the estimated instrumental resolution. The alloy peak shifts by ~ 0.09 eV to lower binding energies, probably due to a more compressed alloyed layer. The position of the surface peak remains approximately constant with increasing deposition time.

It is interesting to note the relative areas of the surface peak and the alloy shifted peak extracted from the decomposition. The "surface peak" areas were normalised to 1 for clean Rh(100), and gave then approximately 0.6 for the thin layer, and 0.5 for the thicker layer. One

could speculate that the reduction of the "surface peak" ratio towards 0.5, indicates that the surface is thus terminated by "surface" Rh atoms in a c(2x2) structure. It is further extracted from figure 5, that the alloy peak signal is attenuated with increasing deposited thickness, again indicating that La is not terminating the surface for the thicker alloys. These observations are the main reasons for proposing the c(2x2) Rh termination in the schematic diagram in figure 2. A Rh termination is in contradiction to the fact that La have lower surface free energy than Rh [4], and is therefore an indication that the surface composition may also be a strong function of the heat of mixing of La-Rh [20].

3.2.2 La5p Core level

Figure 6 shows the La 5p level of the as-deposited and annealed layer with a deposition time of 6 minutes. The resulting lineshapes upon annealing of the as-deposited layer, are narrowed and shifted substantially to lower binding energies (approximately 0.2 eV).

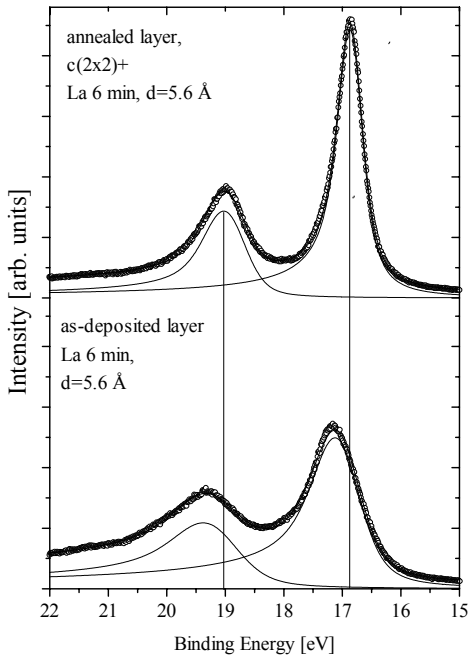

Figure 6. La 5p core level spectra, for La evaporation times 6 minutes. The bottom spectra is recorded on the as-deposited layer, while the upper spectrum represent the annealed layer. The fitted DS lineshapes for each spectrum are also shown in the figure. The left-hand side of the figure denotes the corresponding LEED structure, evaporation time and effective as-deposited thickness. The photon energy was 130 eV. The core level positions of the annealed layer are; 16.84 for La $5p_{3/2}$, and 18.94 for La $5p_{1/2}$. The as-deposited core levels are located at 17.03 eV and 19.18 eV respectively. The La $5p_{3/2}$ FWHM of the annealed and as-deposited layer are 0.56 and 1.15 eV respectively. The DS parameter α is 0.10 and 0.20 for the annealed and as-deposited layer respectively.

In particular, the FWHM of the annealed layer is reduced to 0.55 from 1.15 of the as-deposited layer. This is a strong indication of increased ordering. Furthermore, the asymmetry parameter used in the DS lineshape fit, is reduced from 0.2 to 0.1 upon annealing. In a previous paper, the latter was taken as an indication of change in co-ordination, and a change in La VB DOS around the Fermi level due to hybridisation between La and Rh 5d states [8 and references therein].

Figure 7 shows the La 5p core level of the annealed La-Rh(100) surface alloy as a function of deposited thickness. The annealed core levels shifts 0.18 eV towards lower energies on going from (1x1)+ sub-monolayer structure to c(2x2)+ monolayer structure. The asymmetry parameter is reduced with increasing La in the sub-monolayer regime, while it is considerably increased on going to the c(2x2)+ regime.

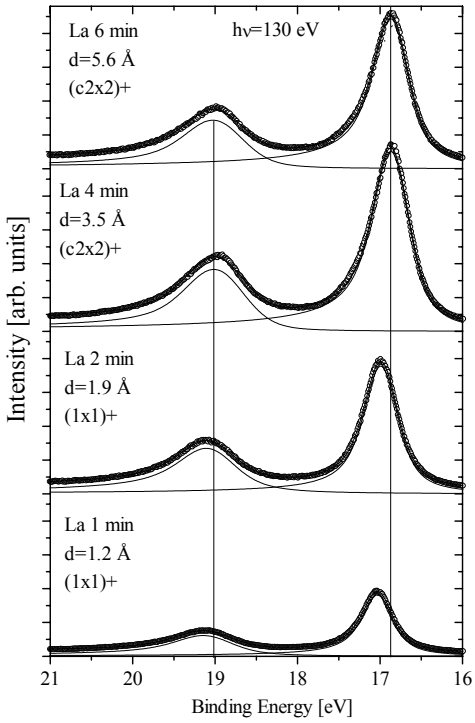

Figure 7. La 5p core level spectra of annealed La-on-Rh(100) surface alloy, for La evaporation times of 1, 2, 4 and 6 minutes from the bottom to top respectively. The fitted DS lineshapes for each spectrum are also shown in the figure. The left hand side of the figure denotes the LEED structure, evaporation time and effective as-deposited thickness (d). The photon energy was 130 eV. The La $5p_{3/2}$ core levels are 17.02, 16.98, 16.84 and 16.84 eV from bottom to top respectively. The asymmetry parameters are 0.06, 0.06, 0.10 and 0.10 from bottom to top respectively. The areas of the La $5p_{3/2}$ peaks are 11.0, 24.1, 37.3 and 31.2 from bottom to top (in arbitrary units).

The increased core level shift is an indication of increased Rh-coordination as a function of deposition time. As above, the radical change in asymmetry parameter is also an indication of considerable changes in interactions with Rh with deposition time, and further changes in La VB DOS near the Fermi level, as will be further discussed with respect to the photoemission VB spectra.

Going back to figure 6, the shift of ~ 0.2 eV to lower binding energy can be explained by an increase of the coordination to Rh atoms. Such a shift is commonly seen in the lanthanides when they are alloyed to electronegative transition metals [17,21][1], and can be explained in an analogous way as for the Rh 3d shift. By removing a core electron from La, the bonds of an atom that has essentially only s-type valence electrons are broken. For the final screened state, however, there will be an additional d-electron which contribute to the formation of strong bonds to the lattice. The result is therefore a stabilization of the final state and thus a lower ionization energy.

3.3 Valence Band spectra

The photoemission valence band spectra of the clean Rh(100), annealed-La-Rh(100) with evaporation times of 2,4 and 6 minutes, corresponding to as-deposited thicknesses of 1.9, 3.5 and 5.6 Å respectively, are shown in figure 8. It is observed that new electronic valence band states (VB-DOS) are formed upon annealing. The structural features observed in the spectra may be summarised as follows; The VB-DOS at the Fermi level is reduced with increasing La thickness, particularly going from the (1x1)+ to the c(2x2)+ structure. The two VB DOS peaks at approximately 1.36 and 2.6 eV in the clean Rh(100) spectrum seem to be replaced by a single broad and intense VB DOS peak at around 2.6 eV, with an additional weak state at 0.53 eV plus a weak state at 1.93 in case of d = 3.5 Å. There is thus an indication that the electronic density of states has shifted towards higher binding energies, i.e. away from the Fermi level.

[1] This is opposite to a simple charge transfer interpretation, which shows that shifts due to final state effects are significant.

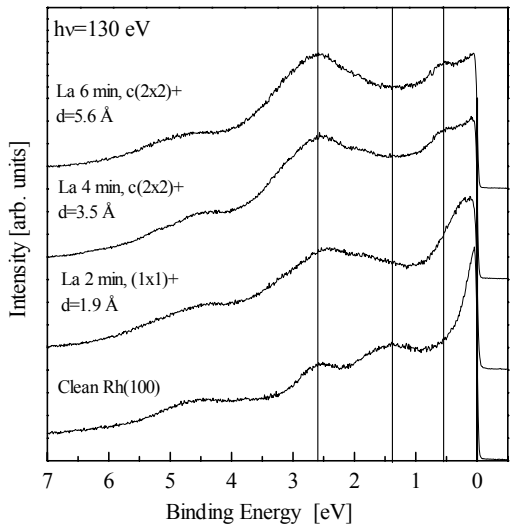

Figure 8. Photoemission valence band spectra of annealed La-on-Rh(100), with deposition times 2, 4 and 6 minutes. The bottom figure also shows the valence band spectrum of clean Rh(100). The photon energy was hν,=130 eV.

Figure 9 shows the photoemission valence band spectra of the clean Rh(100), as-deposited- La-Rh(100) and annealed-La-Rh(100), for deposition time of 6 minutes.

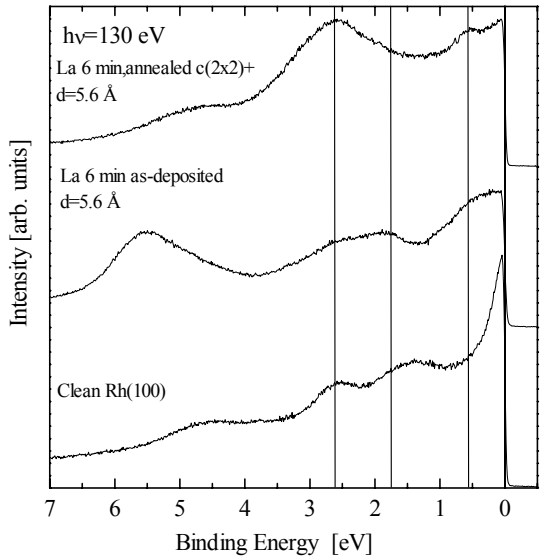

Figure 9. Photoemission valence band spectra of clean Rh(100) (bottom figure), as-deposited La-on-Rh(100) (middle figure) and annealed La-on-Rh(100) (upper figure) The photon energy was hν=130 eV.

It is demonstrated that the disordered (or polycrystalline) as deposited layer turns into a surface alloy upon annealing. The peak at around 5.6 eV in the as-deposited layer (middle figure 9) is due to oxygen contamination during evaporation, which further desorbs upon annealing.

We speculate that the feature at 0.53 eV is related to La covering Rh "surface" atoms, thus directly related to the alloy peak in the Rh 3d core level (see the discussion in section 3.2.1), which was found shifted towards higher binding energies with respect to the surface peak. Similarly, we speculate, that the reappearance of the near Fermi-level valence band density of states (DOS) (approximately 0-0.3 eV) is related to the reappearance of the surface Rh local DOS, recalling that we estimated in section 3.2.1 surface Rh atoms to reappear over the La atoms after annealing. The 0.53 eV peak is thus present in both the as-deposited valence band spectra (middle figure 9), but narrowed probably due to higher ordering in the valence band spectra for the annealed layer (top figure 9).

3.4 TPD traces of CO on as-deposited La layer and annealed La-on-Rh(100) surface alloy.

The use of TPD traces in order to study the formation of the La-on-Pt(111) alloy was previously shown to be a powerful technique to fingerprint the change in electronic structure upon alloying [8]. In this work, 6L of CO was dosed (saturation of surface) on the La-Rh(100) layer at 110 K.

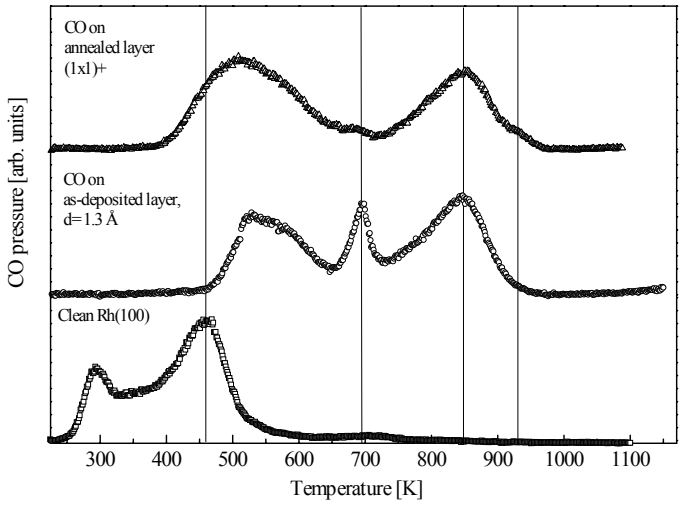

Figure 10. The figure shows the recorded TPD traces from CO on clean Rh(100) (bottom figure), CO on as-deposited La-Rh(100), and CO on annealed La-Rh(100). The effective thickness from the as-deposited layer was d= 1.3 Å. The LEED pattern observed for the annealed layer was (1x1)+ (similar to figure 1a).

TPD traces were then recorded for CO on both the as-deposited layer and on the annealed layer (alloy).

Figure 10 and 11 show the TPD spectra for CO on the thin (1x1)+ La-Rh(100) layer, and the thicker c(2x2)+ La-Rh(100) layer respectively. In all the TPD spectra, a linear background was subtracted, and then further normalised to the total area under the trace.

The bottom figure 10 shows the reference TPD trace for CO on clean Rh(100). The middle figure 10 shows the recorded TPD trace of CO on the as-deposited layer, with effective "as-deposited" layer thickness of 1.25 Å. It is seen from the middle curve of figure 10, that the as-deposited layer seems already to have lost the Rh(100) character indicating a early development of an alloy. Finally, the top figure 10 shows the TPD traces of CO-on-annealed-La-Rh(100) having a (1x1)+ LEED pattern. It is observed that considerable changes in the desorption spectra takes place, indicating corresponding changes in electronic structure.

The middle curve in figure 11 shows the recorded TPD traces of CO on the thicker as-deposited layer, with effective as-deposited layer thickness of 5.6 Å.

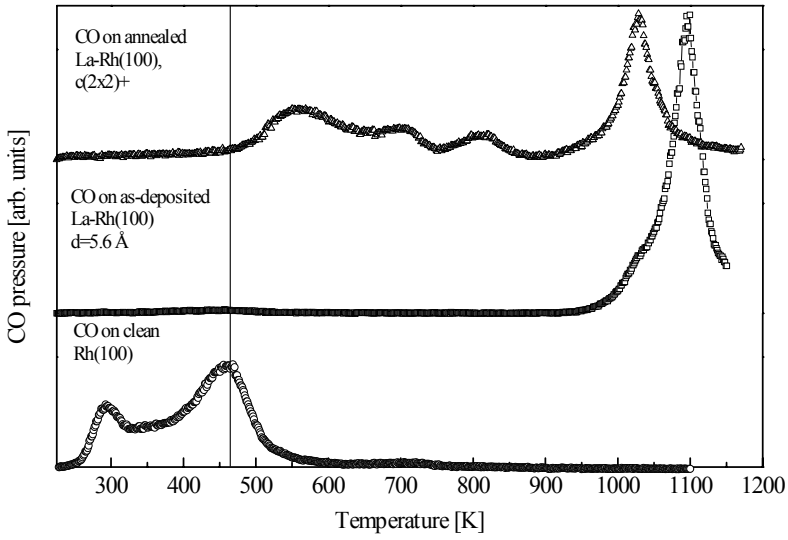

Figure 11. The figure shows the recorded TPD traces from CO on clean Rh(100) (bottom figure), CO on as-deposited La-Rh(100), and CO on annealed La-Rh(100). The effective thickness from the as-deposited layer was d=5.6 Å. The LEED pattern observed for the annealed layer was c(2x2)+.

The layer shows mainly a single TPD peak at 1080 K, with a much weaker feature around 400-500 K. Finally, the top curve in figure 11 shows the TPD traces of CO-on-annealed-La-Rh(100). The alloy showed in this case a c(2x2)+ LEED pattern. It is observed from the top figure 11 that the desorption trace is somewhere in between what is observed from pure

Rh(100) (bottom figure 11) and as-deposited La-Rh(100) (mid figure 11). New chemical binding states appears that are a mixture of La and Rh in terms of desorption energy. Recall that such new states were also observed in the photoemission Valence Band spectra.

Recently, a simple model expression for the d-band contribution to the CO chemisorption ($E_{d\text{-}hyb}$) was proposed by Hammer et al. [22]. We will assume that $E_{d\text{-}Hyb}$ is proportional to the desorption energy (E_D). According to this model, in case of a dominant coupling between the d-band and the $2\pi*$ orbitals of CO (due to a nearly full d-valence), a shift of the centre of gravity of the d-band towards higher binding energies (away from the Fermi level), would cause a lower desorption energy. This contradicts the observations made in this study. However, in a recent paper investigating the formation of the La-Pt(111) alloy [8], the centre of the d-band shifted towards the Fermi level, while the CO desorption energies were in fact reduced with respect to the pure CO/Pt(111) system. In terms of the model of Hammer et al.[22], these results could only be explained by a strong coupling of the d-band with the 5σ orbital of CO [8]. A similar interpretation could in principle also be proposed here, where the VB spectra indicates an apparent shift of the centre of gravity of the d-band of Rh(100) towards higher binding energies for La-Rh(100), thus making $E_{d\text{-}hyb}$ stronger through stronger coupling to the 5σ band of CO.

The experimental results relating TPD and photoemission spectroscopy can be summarised as follows; TPD for the CO/La-Rh/Rh(100) alloy show a mixture of desorption energies between those of CO/Rh(100) and CO/La. The valence band spectra show a shift of the centre of gravity towards higher binding energies compared to the clean Rh(100) surface. Furthermore, the high resolution core level binding energy of Rh $3d_{5/2}$ show a peak (alloy peak) between the bulk Rh peak and the clean Rh(100) surface peak (thus one may regard it as the surface peak shifted to higher binding energies). The La 5p core level of the annealed alloy is shifted towards lower binding energies compared to the La 5p core level of the as-deposited layer. The observations of the core level shifts may also be related to the shift in valence band spectra, and hence change in chemical reactivity, as described in Ref. 23. A detailed investigation of CO on the La-Rh(100) surface alloy will be reported in a separate work [24].

4. SUMMARY

The formation of surface alloy in the La-Rh(100), where La was deposited on Rh(100) in sub-monolayer and monolayer thicknesses has been studied by LEED photoemission spectroscopy, and CO-La-Rh(100) TPD traces. The LEED pattern shows the formation of an

incomplete (1x1) structure in the sub-monolayer regime, while a modified c(2x2) structure with split spots appears for as-deposited thicknesses closer to a monolayer and thicker layers. The split spots were explained by antiphase domains of (4x4), (5x5) and (6x6) superstructures, with increasing as-deposited thickness. The Rh $3d_{5/2}$ core levels show the appearance of an alloy-peak due to La coordination. In addition, the surface peak of the Rh $3d_{5/2}$ core level reappears upon annealing, which is taken as an indication that a large amount of the surface becomes Rh terminated upon annealing. The La 5p core level shows a narrowing probably due to increased ordering, and a shift to lower energies, probably due to higher Rh coordination upon annealing.

The valence band spectra show a reduced density of states near the Fermi level, and the appearance of a more intense state shifted to higher binding energies with respect to clean Rh(100). The TPD traces for the CO/La-Rh/Rh(100) alloy show a mixture of desorption energies between those of CO/Rh(100) and CO/La.

ACKNOWLEDGEMENTS

The assistance of the MAX-lab staff is gratefully acknowledged. We also acknowledge financial support from the Norwegian Research Council. MAX-lab is supported by the Swedish Natural Science Research Council.

REFERENCES:

[1] see, e.g, R.J. Madix, in *The Chemical Physics of Solid Surfaces and Heterogeneous Catalysis, Vol 4: Fundamental Studies of Heterogeneous Catalysis*, edited by D.A. King and D.P. Woodruff (Elsevier, Amsterdam - Oxford - New York, 1982), pp.1-23

[2] see, e.g., J.W.A. Sachtler and G.A. Somorjai, J. Catalysis 81 (1983) 77.

[3] J. Lehmann, P. Roos, and E. Bertel, Phys. Rev. B 54 (1996) R2347.

[4] L.Z. Mezey and J. Giber, Jpn. J. Appl. Phys. 21 (1982) 169.

[5] R.B. Schwarz and W.L. Johnson, Phys. Rev. Lett. 52 (1983) 415.

[6] S. Raaen, C. Berg, and N.A. Braaten, Surf. Sci. 269/270 (1992) 953, and references cited therein.

[7] D.M. Wieliczka and C.G. Olson, J. Vac. Sci. Technol. A 8 (1990) 891.

[8] A. Ramstad and S. Raaen, Phys. Rev. B. 59 (1999) 15935.

[9] E. Bertel, N. Memmel, G. Rangelov, and U. Bischler, Chemical Physics 177 (1993) 337.

[10] J. J. Yeh and I. Lindau, Atomic Data and Nuclear Data Tables 32 (1985) 1.

[11] Landholt-Börnstein, New Series IV/5J.

[12] M. A. Van Hove, W. H. Weinberg, C. M. Chan, *Low Energy Electron Diffraction*, (Springer, 1986) 84.

[13] T. Nagao, C. Voges, H. Pfnuer, M. Henzler, S. Ino, F. Shimokoshi, S. Hasegawa, Appl. Surf. Sci. 130-132 (1998) 47-53.

[14] A. Palenzona, J. of Alloys and Comp. 190 (1992) 13.

[15] C. J. Baddeley, A. W. Stephenson, C. Hardacre, M. Tikhov and R. M. Lambert, Phys. Rev. B 56 (1997) 12 589-12598.

[16] A. Borg, C. Berg, S. Raaen and H. J. Venvik, J. Phys. : Condens. Matter 6, (1994) L7.

[17] A. Nilsson, B. Eriksson, N. Mårtensson, J. N. Andersen and J. Onsgaard, Phys. Rev. B 38 (1988) 10357.

[18] M. Weinert and R. E. Watson: Phys. Rev. B 51 (1995) 17168.

[19] S. Doniac and M. Sunjic, J. Phys. C3 (1970) 285.

[20] P. Wynblatt and R.C. Ku, Surf. Sci 65 (1977) 511.

[21] N. Mårtensson and A. Nilsson, J. of El. Spec. and Rel. Phen. 75 (1995) 209.

[22] B. Hammer, Y. Morikawa and J. K. Nørskov, Phys. Rev. Lett. 76 (1996) 2142.

[23] D. Hennig and M. V. Ganduglia-Pirovano and M. Scheffler, Phys. Rev. B 53 (1996) 10344.

[24] M. Kildemo, T. Ramsvik and S. Raaen, Surf. Sci. (in press, 2001)

APPENDIX:

INVESTIGATION OF THE La-Rh(100) SURFACE ALLOY BY SCANNING TUNNELING MICROSCOPY

T. Ramsvik, A. Borg, M. Kildemo and S. Raaen

Dept. of Physics, Norwegian University of Science and Technology, N-7491 Trondheim, NORWAY

In the study of Kildemo et al. [1] the formation of a true surface alloy was firmly established using a combination of high-resolution photoemission spectroscopy, LEED and TPD. The sub-monolayer alloy showed a (1x1) LEED pattern with streaks, which transforms to a c(2x2) pattern with four ways split fractional order spots at higher coverages. The split spots were interpreted as due to small anti-phase domains [2] each exhibiting a c(2x2) structure. The streaks in the LEED pattern for the sub-monolayer was proposed to represent a low order organisation of the domains. Based on the reappearance of the surface peak in the Rh 3d core-level spectrum, the c(2×2) domains were proposed terminated by surface Rh atoms [1].

As a further investigation of these proposals, STM measurements have been performed of the La-Rh(100) surface alloy using a room temperature Omicron UHV STM. All images presented are recorded in constant current mode, using tunneling currents and bias voltages in the range 1.8 - 3.2 nA and 12 - 447 mV, respectively. The Rh(100) single crystal was cleaned by cycles of argon sputtering with the sample kept at room temperature, heating in oxygen (~1000 K - 1100 K at 1×10^{-8} mbar), and annealing in vacuum (~ 1350 K). The surface was considered clean when atomically resolved STM images were obtained without detectable traces of contaminants. La was deposited from a resistively heated tungsten basket. The deposition was performed with the Rh substrate kept at 300 K, and the alloys were formed by slowly heating the samples to 1350 K.

Figure A.1 shows a sequence of STM images with increasing “as-deposited” coverages of La. The displayed areas for all images are 418 × 418 $Å^2$. Fig. A.1a presents an image including a monoatomic step of the surface alloy after depositing and annealing ~ 0.2 ML of La. Randomly distributed domains, 10 - 13 Å in diameter, are observed, covering ~50 % of the surface. LEED measurements reveal the (1×1) substrate unit cell with weak streaks. The inset figure in the upper right corner displays an atomically resolved STM image of size 50×50 $Å^2$. The average spacing between the atoms is consistent with that expected for a clean rhodium surface (~2.7 Å) [3]. At these low La coverages the surface corrugation is small, and no evidence for any local c(2×2) structure is found. Furthermore, photoemission spectroscopy measurements indicate that the surface is rhodium terminated [1]. Hence, a likely scenario

could be that the larger La atoms penetrate the rhodium crystal beyond the first surface layer. Such an effect has been reported earlier for the Re-Pt(111) surface alloy formation [4].

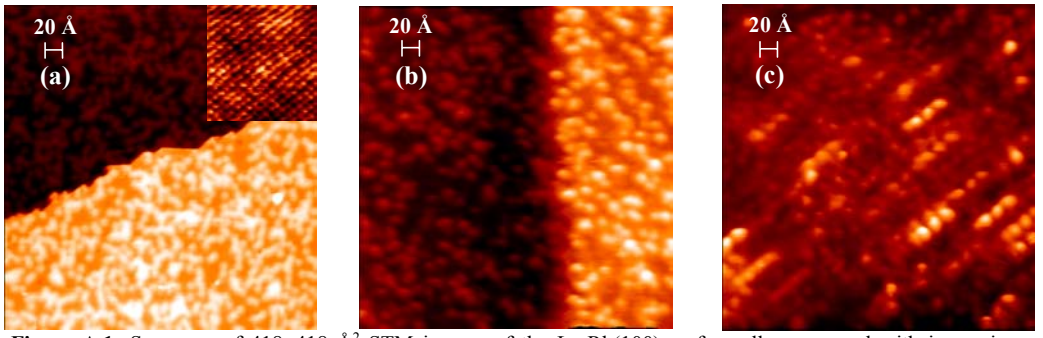

Figure A.1: Sequence of 418×418 Å^2 STM images of the La-Rh(100) surface alloy prepared with increasing amount of La. The images (a) to (c) displays surface alloys with initial "as-deposited" La coverages of ~0.2 ML, ~0.8 ML and ~1.6 ML, respectively. The inset image in figure A.1a shows an atomically resolved STM image of size 50×50 Å^2.

Figure A.1b shows an STM image after annealing the surface with ~0.8 ML of "as-deposited" La. Also at this coverage a high degree of disorder is found.

A further increase of "as-deposited" La to ~1.6 ML leads to highly corrugated surface alloy with domains in the range 13 - 17 Å (fig. A.1c). An apparent ordering of the domains in the high symmetry directions is seen. This is confirmed by LEED, which reveals a c(2×2) pattern with split spots. Such a LEED pattern can be found in figure 1b of ref. 1. The distance between the split spots corresponds to a real space wavelength of ~14 Å, i.e. within the range of domain sizes found from the STM measurements. Due to the high corrugation, images with atomic resolution were not obtained. Verification of a local c(2×2) structure on the domains are therefore not feasible. In the specific image displayed here the domains seem to have a preferred alignment in one of the high symmetry directions, an observation not supported by LEED. Since STM is a highly local probe it cannot be excluded that the overall surface has a domain distribution that differs from the one shown in fig. A.1c.

As a general conclusion these STM investigations do support the structural proposals given in ref. 1.

References:

[1] M. Kildemo, T. Ramsvik, and S. Raaen, Surf. Sci. 490 (2001) 1.

[2] see e.g. M. A. Van Hove, W. H. Weinberg, C. M. Chan, *Low Energy Electron Diffraction*, (Springer, 1986) 84.

[3] Landholt-Börnstein, New Series Volume III/6: Structure Data of Elements and Intermetallic Phases

[4] A. Ramstad, F. Strisland, S. Raaen, T. Worren, A. Borg and C. Berg, Surf. Sci. 425 (1999) 57.

Paper VI

Study of CO adsorption on La-Rh(100) surface alloys

M. Kildemo, T. Ramsvik and S. Raaen

Accepted for publication in Surface Science

STUDY OF CO ADSORPTION ON La-Rh(100) SURFACE ALLOYS

M. Kildemo, T. Ramsvik, and S. Raaen
Department of Physics, Norges teknisk-naturvitenskapelige universitet, NTNU,
N-7491 Trondheim; Norway

Abstract

Adsorption of carbon monoxide on La-Rh(100) surface alloys has been studied by photoelectron spectroscopy, low-energy electron diffraction (LEED) and temperature programmed desorption (TPD). The surface alloys were formed by depositing overlayers of La in the monolayer regime on a Rh(100) substrate, and by subsequent annealing to about 1350 K. Carbon-monoxide was dosed to saturation at various temperatures. The LEED-pattern of the dissociated CO overlayer shows a c(4x4) structure with respect to the Rh(100) substrate. The LEED structure for the sub-monolayer alloy takes on a ring structure superposed on a (1x1) structure. At higher temperatures an apparent (10x10) superstructure is superposed on the ring structure.

The TPD results shows that 4 different peaks are present in the desorption traces. From the core level spectroscopic data it is argued that the two first peaks are a combination of direct CO desorption, CO dissociation and associative CO desorption. The remaining two peaks are assumed to be related to associative desorption from atomic carbon and oxygen in a combination of different bonding states and different adsorbate interactions.

Rh 3d core level spectra show that the two peaks related to the surface atoms are shifted towards the bulk peak for CO on the alloy. The La 5p core level spectra show the splitting of the core level into two peaks for CO and dissociated CO on the alloy. The 4σ and $5\sigma/1\pi$ molecular levels of CO on the alloy are observed in the valence band spectra, with similar binding energies as for CO on a disordered La layer. In particular, a stronger rehybridization of the CO 4σ state with the electronic states of the surface alloy as compared to CO on clean Rh(100), is argued to be responsible for dissociation of CO on the alloy at low temperatures.

1. INTRODUCTION

The reactivity of a surface may be changed dramatically by depositing a thin layer of a material on the surface and subsequently annealing the system to form a surface alloy. In this work we study CO adsorption on a La-Rh(100) surface alloy. This alloy has been characterised in a previous work [1]. Lanthanum may be well suited to be used as overlayer material due to the low surface free energy [2]. La therefore has a tendency to be located at or near the surface when the surface alloy is formed and will thus strongly influence the adsorption and desorption properties of gas molecules, like carbon-monoxide in this case. This study was further motivated by the idea that simple model systems may give useful insight into real catalytic processes as well as fundamentals of adsorption and desorption of various gas molecules. The role of electronic promoters in heterogeneous catalysis has been well-documented [3,4]. In addition, the low work function rare earth element La may be a good choice for the overlayer material since its presence at the surface has the effect of lowering the electrostatic potential and thus influencing the bonding of gas molecules. Previous experiments have shown that solid state reactions occur when rare earths are deposited on a variety of metallic substrates even at ambient temperatures [5,6,7], and that these systems tend to form ordered surface alloys [8,9]. Naturally, both structural and electronic changes have to be considered in such overlayer systems.

In a recent work, the formation of an ordered La-Pt(111) surface alloy when a La on Pt overlayer system was annealed to 900 K was observed [9]. An analysis of thermal desorption spectra of CO from Pt and La-Pt showed that the desorption energy was considerably lower in the case of the surface alloy [9]. The large reduction in reactivity of CO on the La-Pt(111) surface alloy was argued to be related to the existence of strong resonant interactions of the Pt 5d-band with the CO 5σ orbital that give rise to a pronounced 5σ donor contribution to the CO-Pt bond [10]. As the La-Pt(111) surface alloy was formed, the d-band moves to lower binding energies and the Pt 5d – CO 5σ interaction is no longer resonant, and the CO-Pt bond is significantly suppressed. On this background, other rare earth – transition metal systems are of interest. This work presents aspects of the adsorption of CO on La-Rh(100) surface alloys, which were formed by depositing overlayers of La in the monolayer regime on a Rh(100) substrate, and by subsequent annealing to about 1350 K.

2. EXPERIMENTAL

The photoemission measurements were performed at beamline I311 at the Max-lab synchrotron radiation facility in Lund, Sweden. The experimental details are previously described in Ref. [1]. In the present experiment the total resolutions for Rh 3d and La 5p are estimated to be 100 meV and 40 meV respectively, while the total resolution for C1s and O1s are estimated to be 100 meV and 200 meV respectively, as determined from the width of the Fermi edge. Binding energies were calibrated by measuring the position of the Fermi edge after each spectrum. The Rhodium crystal was cooled to below 150 K during photoemission measurements.

The Rh(100) crystal was mounted on a 0.5 mm W-wire and heated by sending current through the support wires. A liquid nitrogen reservoir in thermal contact with the W-wire allowed for cooling the crystal to ~100 K. The crystal temperature was measured by a Chromel-Alumel thermocouple which was spot-welded to the rear of the sample. The Rh(100) crystal surface was cleaned by repeated cycles of Ar^+ sputtering (15 min at room temperature and 15 min. at 1100 K), oxygen annealing at $1*10^{-8}$ mbar at a temperature of 1075 K for 5 minutes, and flash annealing to 1350 K.

La was deposited from a water-cooled evaporation source that consisted of a thermally heated tungsten basket. The deposition was performed with the Rh substrate cooled below 150 K. The photoelectron spectra were recorded immediately after deposition, hereby defined as "as-deposited layer", and the Rh $3d_{5/2}$ core level photoemission measurement were used to estimate the "as-deposited thickness" [1]. The photoemission intensity for all spectra was normalised to the background. The "as-deposited thickness" or effective thickness (d) was calculated from $d = \Lambda \ln(I^0_{sub}/I_{sub})$, where I^0_{sub} and I_{sub} denote the total emission from the Rh $3d_{5/2}$ core level before and after deposition of La. Here, Λ is the electron free mean path in the metal, estimated to 6 Å in the current experiments. Finally, the alloying were performed by slowly heating the sample to 1350 K.

For all experiments the overlayer structures were formed by dosing the crystal with 6 L of CO, corresponding to a CO-saturated surface, with the crystal held at 150 K. The sample was then heated slowly (approximately 2K/s), while monitoring the LEED screen. At the appearance of new visible LEED structures, the sample was cooled to 150 K, were all photoemission measurements were performed. The procedure was then repeated by heating the sample to a higher temperature.

The TPD spectra were recorded in a separate system in the home laboratory, using a Transpector H100M quadropole mass-spectrometer from Leybold-Inficon. The heating rate was 2 K/s. The LEED structure and the as-deposited thickness from XPS, as described in detail previously [1], was used in order to compare to the results from the high-resolution photoelectron measurements performed at the synchrotron radiation facility.

3. RESULTS AND DISCUSSION

In this work we study CO on two different La-Rh alloys, sub-monolayer La coverage and above one monolayer. The main focus will be on the latter. We first review the structural findings of the two surface alloys previously described [1]. The sub-monolayer alloy showed a (1x1) LEED pattern with streaks (thus denoted (1x1)+), in transition towards a c(2x2) pattern with four ways split half order spots, which corresponds to the surface alloy. The split spots were interpreted as c(2x2) anti-phase domains [1,11]. The streaks in the LEED pattern for the sub-monolayer was thus proposed to represent a low order organisation of the domains, while the c(2x2) with split spots represent a higher crystalline state or domain superstructure for the monolayer regime [1 and references therein]. The c(2x2) domains of La-Rh were proposed terminated by surface Rh atoms [1], based on the reappearance of the surface peak in the Rh 3d core level spectrum.

In section 3.1, the experimental results are presented for CO on the monolayer regime alloy. In section 3.2 we briefly discuss the experimental results corresponding to CO on the sub-monolayer La-Rh.

3.1 CO on monolayer regime La-on-Rh(100) surface alloy

The experimental data from CO/[c(2x2)+]-La-Rh(100) alloy is presented in sections 3.1.1-3. In section 3.1.4 the areas extracted from the TPD traces and core levels are put together in order to summarise the experimental data.

3.1.1. TPD and LEED

Figure 1 shows the TPD Traces for CO/[c(2x2)+]-La-Rh(100) alloy.

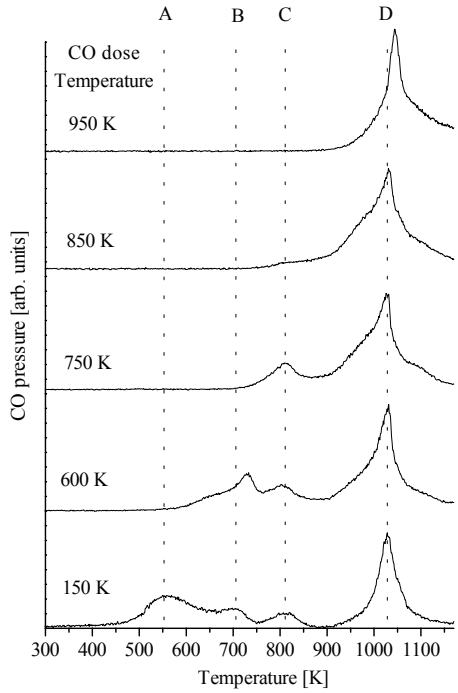

Figure 1: TPD trace of CO/La-Rh(100) alloy. The figures from bottom to top shows the TPD traces after dosing 6L CO at 150, 600, 750, 850 and 950 K. The vertical lines indicate the positions of the TPD peaks, located at approximately; A=561 K, B=697 K, C=810 K and D=1028 K.

The thickness of the as-deposited layer was estimated to 5.7 Å, corresponding to a coverage of approximately 2 monolayers (ML) [1]. Figure 1 shows from the bottom to the top the TPD traces after a CO saturation exposure at 150, 600, 750, 850 and 950 K. The TPD traces show 4 distinct peaks, which we denote A, B, C and D, as shown in figure 1, corresponding to 561, 697, 810 and 1028 K respectively. Some additional contributions are apparent within peak D. Its position remain constant up to an exposure temperature of 850 K, while at 950 K a significant shift to higher desorption temperature is observed. Note that dosing CO at higher temperatures gives lower coverages [9]. This shift of the upper peak is towards higher temperatures. This may be an indication of reduced repulsive interactions with lower coverages, giving an increase in activation energy for CO desorption from the surface. However, due to the large complexity of the present system, structural changes may also give rise to the observed effects. The composition of peak D will be further discussed in relations to the valence band spectra.

Figure 2a shows the clean La-Rh(100) alloy, with the characteristic c(2x2) structure with split spots [1]. Figures 2b to 2e show the LEED images recorded after a saturation CO exposure on La-Rh at 150 K, and a subsequent heating to 600 K (2b), 730K (2c) and 830 K (2d).

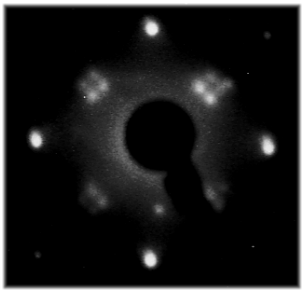

2a. Clean La-Rh(100) alloy. c(2x2)+. E=112 eV

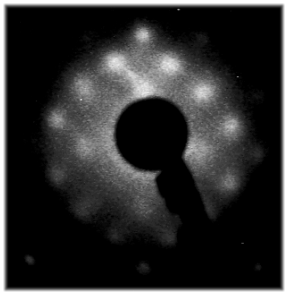

2b. 600K CO/La-Rh(100) E=80 eV

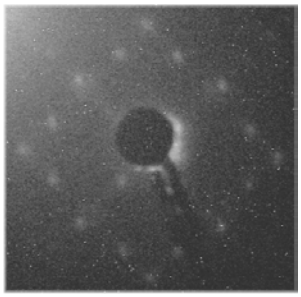

2c. 730 K CO/La-Rh(100) 65 eV

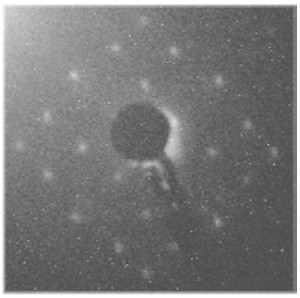

2d. 830 K CO/La-Rh(100) E=65 eV

Figure 2: The figure shows the LEED pattern recorded from CO on La-Rh(100) alloy with a c(2x2)+ structure and 2.75 Å as deposited thickness (approximately 1 ML). Figure 2a shows the clean La-Rh(100) alloy, with the characteristic c(2x2) structure with split spots (thus denoted c(2x2)+. Figure 2b, shows CO/La-Rh(100) heated to 600 K. The structure is disordered c(4x4) with reference to clean Rh(100). The structure is (2x2) with reference to the alloy. Figure 2c, shows CO/La-Rh(100) heated to 730 K. The structure matrix with reference to clean Rh(100) is given in the text, or (2x1) with reference to the alloy. Figure 2d shows CO/La-Rh(100) heated to 830 K. The structure is again an ordered c(4x4) with reference to clean Rh(100) or (2x2) with reference to the alloy. The LEED images 2c and 2d also show partially spot splitting.

At 600 K (2b) a diffuse c(4x4) overlayer forms. We will discuss this in relation to the photoemission data, which shows a presence of both dissociated and molecular CO at this temperature. In particular, the LEED pattern can in principle be caused by either CO, atomic Carbon or Oxygen in a c(4x4) structure. It is also possible that the structure is a superposition of two c(2x2) structures, one of atomic carbon or oxygen, and one of CO. The LEED pattern

seen in figure 2b is the structure obtained between peaks A and B in the TPD spectrum in figure 1.

Figure 2c shows CO/La-Rh(100) heated to 730 K. This corresponds to the low temperature side of peak C in the TPD spectra in figure 1. At this temperature most of the CO molecules are dissociated, as will be later described in the photoemission spectra. The structure may be approximated by $M = \begin{bmatrix} 1 & 1 \\ -1 & 3 \end{bmatrix}$ with reference to clean Rh(100), or (2x1) with reference to the c(2x2) alloy. We will denote this structure (2x1)/c(2x2)+ throughout the paper.

Figure 2d shows CO/La-Rh(100) heated to 830 K. The structure is again an ordered c(4x4) with reference to clean Rh(100) or (2x2) with reference to the alloy in figure 2a. This corresponds to the high temperature side of peak C in the TPD spectra in figure 1. In principle the LEED pattern can occur from a combination of atomic Carbon or atomic Oxygen forming a c(4x4) structure. We estimate the coverage in monolayers (ML) by counting the effective number of adsorbate molecules per surface Rhodium atoms caused by the c(4x4) LEED pattern. The latter supply a coverage of atomic Carbon plus Oxygen (θ_{C+O}) of 0.125 ML which we will show later is unrealistically low (see section 3.1.3). However, if the LEED pattern is caused by diffraction from only atomic Carbon or atomic oxygen, then this number becomes a more reasonable fractional coverage ($\theta_{C,O}$). It has previously been reported that at lower coverages of O_2 adsorbed (and dissociated) on clean Rh(100, a (2x2) or a c(2x2) structure is formed at 125^{o}C [12], depending of coverage. In addition, by dissociation of acetylene, they showed that atomic carbon forms graphite rings on Rh(100). Based on these observations, it seems more likely that the LEED patterns in figures 2c and 2d are caused by electron diffraction from ordered atomic oxygen.

Finally, a close inspection of the LEED pattern in figure 2d, shows that the spot splitting reappears also for CO/La-Rh(100). This indicates that atomic carbon and oxygen are also affected by the anti-phase domain structure.

3.1.2 Photoelectron Spectroscopy

The “as-deposited thickness” of the La layer studied was approximately 5.6 Å (approximately 2 Monolayers) [1], while the spot splitting in the LEED pattern is speculated to indicate a (6x6) domain super structure, thus nearly identical to the alloy studied by TPD in the previous section.

C1s and O1s core levels

Figure 3 shows the C1s core level as a function of temperature.

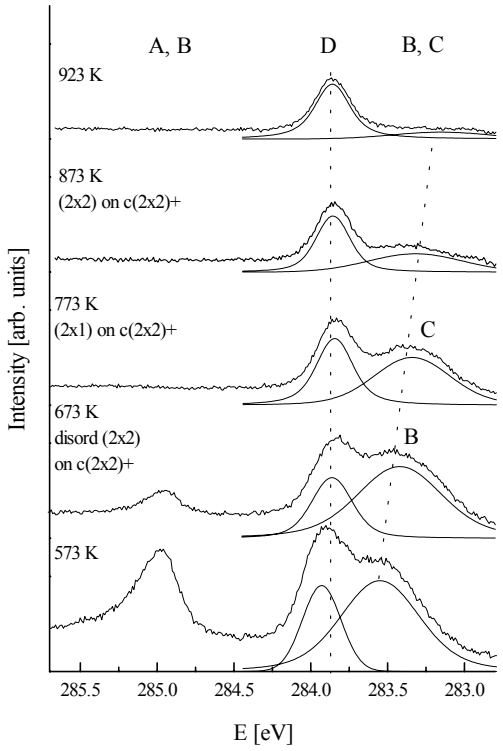

Figure 3: The figure shows C1s recorded from CO/La-Rh(100) heated to 573, 673, 773, 873 and 923 K from the bottom to the top. The photon energy was 360 eV. The peaks are labelled A, B, C and D with relation to the TPD spectra in figure 1.

It is observed from the bottom figure (after heating the sample to 573 K), that a mixture of CO (in the region 284.5-286 eV) and atomic Carbon (in the region 283-284.5 eV) is present on the surface. Figure 3 further shows that the atomic Carbon is composed of one narrow peak located at 283.9 eV with FWHM of 0.3, and one large (disordered) peak with FWHM of 0.6. The latter large peak is located at 283.5 eV at 573 K, and is shifted to 283.3 eV at 873 K. Due to the large FWHM, the latter peaks may be composed of unresolved peaks or represent disorder.

The C1s core level peaks from CO dosed at 100 K on the as-deposited La layer on Rh(100), showed that CO partly dissociates at low temperatures on the as-deposited La layer. It is shown earlier that CO does not dissociate on clean Rh(100) [13], and we may conclude that the presence of La promotes the dissociation of CO.

The line profile of the CO peak in figure 3 (denoted A,B) indicates that it also consist of other unresolved sub peaks. LEED shows a diffuse (1x1) pattern, which suggest some disorder on the surface. The unusual low binding energy for C1s in CO on the La-Rh(100) surface alloy, is not fully understood, but may presumably be due to both initial and final state effects. The designation of the peaks will be explained below.

As the sample is further heated towards 773 K, the CO peak disappears, and only the two peaks due to dissociated CO are present. The site denoted with peak D seems to be located around the high binding energy (B.E.) peaks of C/Rh(100) (283.8 eV) and C/as-deposited La sites (284.0 eV), while the broad peak denoted C is moving towards an average position between the low B.E. positions of C/Rh(100) (283.1 eV) and C/as-deposited La (283.6 eV). The B.E.'s of C1s of atomic Carbon on "clean" Rh(100) were estimated from traces of atomic carbon after an incomplete oxygen annealing step. Similarly the C1s B.E.'s of atomic carbon on as-deposited La were estimated from traces of carbon prior to annealing of the sample. Note, that we cannot entirely rule out subsurface carbon in the reference measurements. Given the latter reservations, the C1s B.E.'s from atomic Carbon on the La-Rh(100) surface alloy, appears to act in a "true alloy" manner with B.E.'s in between those of their La and Rh(100) counterparts.

As the sample is further heated to 923 K, peak C disappears, leaving only peak D. These observations are thus related to peaks A-D in the TPD spectrum as will be further discussed below. However, it is not possible to firmly dedicate the TPD peak B only to associative desorption. Therefore we have denoted this peak both to the CO peak and the atomic carbon peak for the two lowest energies, as shown in figure 3.

Figure 4 shows the O1s core-level measured for the same coverages as for figure 3.

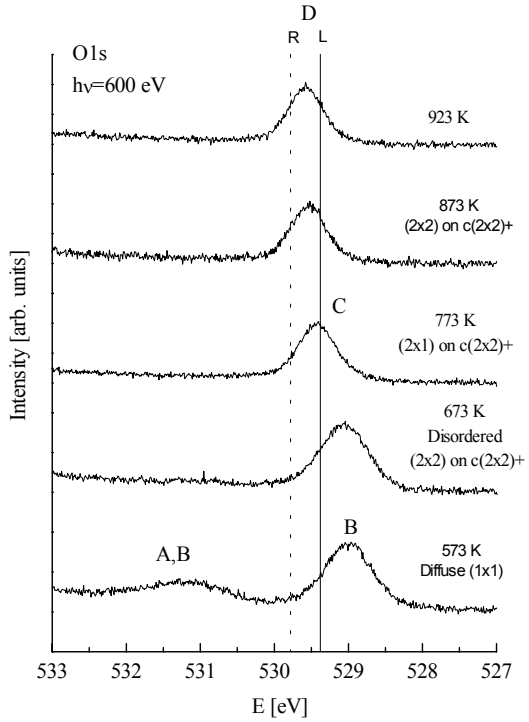

Figure 4: O1s core level recorded from CO/La-Rh(100) heated to 573, 673, 773, 873 and 923 K as indicated on the right hand side of the figure. The photon energy was 600 eV. The peaks are labelled A, B, C and D with relation to the TPD spectra in figure 1. The CO peak is located at approximately 531.2 eV, while the atomic oxygen peaks denoted A,B are located approx. at 529.0 eV. Peak C at 529.4 eV and peaks D at 529.6 eV. The vertical lines denoted R and L, represent atomic oxygen on "clean" Rh(100) and La/Rh(100) prior to annealing.

It is seen from figure 4, as in the case of the C1s core level peaks, that CO is present on the surface and disappears when heating the sample. Furthermore, a distinct shift of the B.E. position, accompanied by a narrowing of the FWHM, takes place as the CO disappears (dissociates or desorbs) when heating from 673 to 773 K. A small additional shift appears as the sample is further heated to 873 K. As indicated by the letters in figure 4 we can relate the specific peaks to the positions A-D in the TPD traces. As in the case for C1s, the high temperature peak is located between the peak positions of O/Rh(100) (denoted R in figure 4) and O/as-deposited La (denoted L in figure 4), in a "true alloy" fashion. The shift in the O1s B.E. takes place after CO desorption, and as an ordered structure appears in the LEED pattern (c.f. the (2x1)/c(2x2)+ in figure 2c). The latter shift may be caused by different binding sites, but it may also be caused by the reduction in adsorbate interactions.

In conclusion, the above observations show that the peaks denoted A from the C1s and O1s core-level spectra seem to be involved in the CO desorption from the TPD traces denoted A (corresponding to direct CO desorption). For dissociated CO two distinct peaks are found at lower B.E. in the C1s spectra. It is suggested that the one with highest B.E. of these two consist only of Carbon with one chemical state throughout the whole temperature range (denoted D), while the other consist of two states up to 773 K (B and C). Above this temperature only Carbon of type C gives a contribution. Also here the designation are chosen to correspond to the observed peaks in the TPD spectrum. For the O1s spectra the different chemical states are observed as shift towards higher binding energies.

La5p and Rh3d core levels

Figure 5 shows the La 5p core level spectra recorded after CO exposure as described for figures 3 and 4.

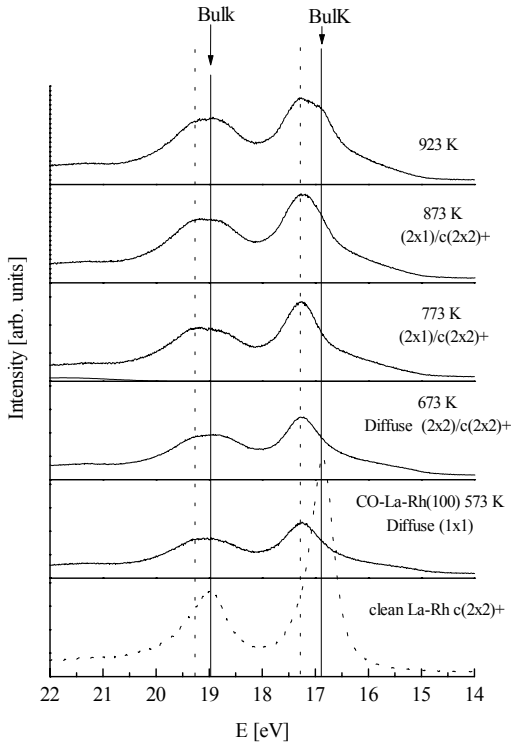

Figure 5: The figure shows the La 5p core level emission from CO on La-Rh(100). The photon energy was 130 eV. The bottom figure shows clean La-Rh(100) surface alloy. The remaining figures show 6L of CO on La-Rh(100) heated to the temperatures indicated on the right hand side. The full vertical lines are located at the clean alloy core levels for La 5 $p_{3/2}$=16.84 eV and La $5p_{1/2}$=18.94 eV. The dotted vertical lines are the proposed shifted components due to change in co-ordination upon CO and atomic C and O adsorption.

It is clearly observed from the La $5p_{3/2}$ core level (lower component), that a distinct shifted component appear at 0.37 eV on the high B.E. side of the core level peak relative to the "clean" alloy core level. The full vertical lines in the figure indicate the clean alloy components in the core level, and the dotted vertical lines the possible positions of the shifted components. On the extremities of both the high and low B.E. sides, we observe additional shoulders, not present in the clean alloy component.

The core level components of the clean La-Rh alloy were previously reported to be located at 18.95 eV and 16.85 eV for La$5p_{1/2}$ and La $5p_{3/2}$ respectively [1], while the core level positions for the as-deposited alloy were located at 19.18 and 17.03 eV.

Thus the peaks are shifted to lower B.E. by 0.23 eV for La$5p_{1/2}$ and 0.18 eV for La$5p_{3/2}$ when the La-Rh alloy is formed. This shift was related to the change in Rh-coordination [1]. Such a shift is commonly seen in the lanthanides when they are alloyed to electronegative transition metals [14,15]. By removing a core electron from La, the bonds of an atom that has essentially only s-type valence electrons are broken. For the final screened state, however, there will be an additional d-electron which contribute to the formation of strong bonds to the lattice. The result is therefore a stabilisation of the final state and thus a lower ionisation energy. Based on the latter arguments, one possible explanation for the current shift to higher B.E.'s, is that the new high B.E. component of La5p is caused by CO and C+O adsorption on the Rh sites in contact with La. This reduces the co-ordination effect obtained upon annealing, since the d electrons supplied from Rh that stabilised the final states are no longer available due to bonding to CO+C+O.

Figure 6 shows the core level intensity of Rh $3d_{5/2}$.

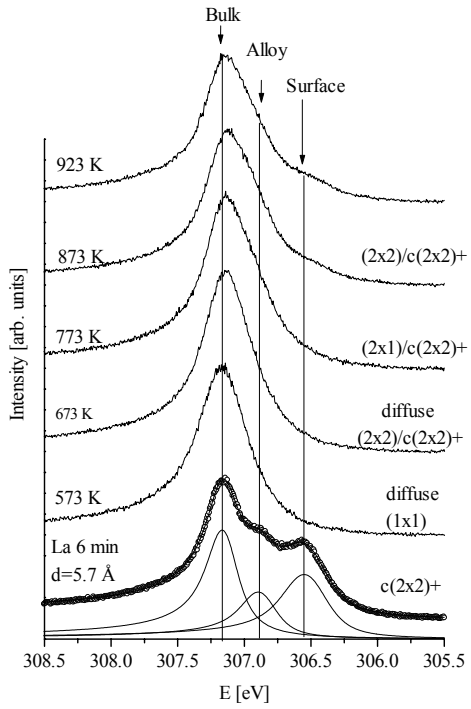

Figure 6: The figure shows Rh $3d_{5/2}$ core level photo-emission spectra from CO dosed on the La-Rh(100) alloy. The photon energy was 400 eV. The bottom figure shows the clean La-Rh(100) alloy, with as-deposited thickness of 5.7 Å (approximately 2 ML), and the c(2x2)+ LEED pattern. The full vertical lines represent the core level positions denoted bulk peak, alloy and surface peak [1]. The remaining figures show the core level spectra as a function of heating, with the temperature indicated on the left-hand side. The right hand side shows the LEED pattern observed.

It is observed that for the CO-covered alloy surface at low temperatures, the bulk peak is broad compared to the one for the clean alloy. In addition, the alloy and surface peak previously described [1] and shown in the bottom figure are damped out completely. As the temperature is increased, the surface peak weakly reappears, while the alloy peak still remain small. Chemical shifted components related to CO on Rh(100) has previously been reported to be located close to the bulk Rh peak, only shifted by approximately 0.05 eV towards lower B.E.'s [13, 16] accompanied by a damping out (or shift towards bulk) of the surface component. For atomic Oxygen on Rh(100) it has been reported to damp out the surface peak (or shift towards bulk), thus giving a new component shifted 0.25 eV towards lower B.E.'s with respect to the bulk peak [16]. Figure 6 shows a small shift towards lower B.E. and an additional shoulder appearing on the low B.E. side of the bulk peak, as all CO is dissociated.

3.1.2.3 Valence Band Spectra

Figure 7 shows the valence band spectra recorded in the same way as for figure 6.

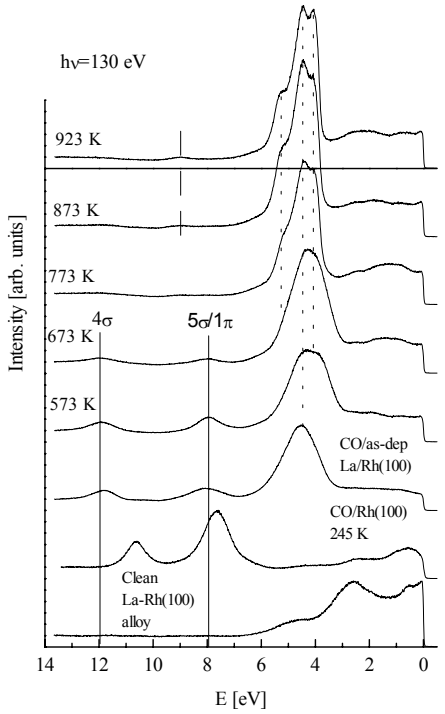

Figure 7. The bottom figure shows the clean c(2x2)+ La-Rh(100) alloy. The next figure up, shows the valence band spectrum of CO/Rh(100) heated to 245 K. The next figure up shows CO/as-deposited La on Rh(100) surface, i.e. prior to annealing. The remaining figures shows CO/La-Rh(100) heated to 573, 673, 773, 873 and 923 K, similar to figures 3-6. The molecular orbitals of CO on clean Rh(100) are located at $4\sigma \approx 10.7$ eV, and $5\sigma/1\pi \approx 7.6$ eV. The molecular orbitals of CO on as-deposited La on Rh(100) are located at $4\sigma \approx 11.8$ eV, and $5\sigma/1\pi \approx 8.1$ eV, while the molecular orbitals of CO on annealed La-Rh(100) are located at; $4\sigma \approx 11.9$ eV, and $5\sigma/1\pi \approx 8.0$ eV. The structure around 4.5 eV, are the O2p levels on La-Rh(100). At higher temperatures (lower coverages), these levels split into 3 components at 4.1 eV, 4.5 eV and 5.2 eV.

The bottom figure 7 shows as a reference the valence band spectrum of clean c(2x2)+ La-Rh(100) surface alloy. The next figure up, shows as a second reference the valence band spectrum of CO/Rh(100) heated to 245 K, with the CO molecular orbitals 5σ/1π and 4σ located at 7.6 eV and 10.6 eV, respectively . The next figure up shows CO dosed on as-deposited La/Rh(100) (i.e. prior to annealing), with CO molecular orbitals located at 8.1 eV and 11.8 eV. The remaining spectra show CO/La-Rh(100) heated to 573, 673, 773, 873 and 923 K. The molecular orbitals of CO on the latter annealed La-Rh(100) alloy are located at 11.9 eV,

and 8.0 eV, for 4σ and $5\sigma/1\pi$, respectively. With respect to the clean Rh(100), the 4σ molecular orbital of CO on the alloy is shifted with 1.3 eV towards higher binding energies. A smaller, but similar shift is seen for the $5\sigma/1\pi$ molecular orbitals of 0.3 eV. With respect to the as-deposited La layer, the 4σ molecular orbital of CO on the alloy is shifted 0.1 eV towards higher binding energies, while the $5\sigma/1\pi$ molecular orbitals are shifted 0.1 eV towards lower B.E.'s.

It is thus evident that CO on the alloy behaves more like CO on La than CO on clean Rh(100), and we conclude that the presence of La atoms near the surface is clearly responsible for a low temperature dissociation of CO on the alloy. The fact that the 4σ level shifts substantially more than the 5σ level towards higher B.E.'s, may be and indication of some tilting of the molecule from the upright position commonly seen for CO adsorbed on metal surfaces. On the other hand, the latter observations may simply show that the CO molecular levels on the alloy are similar to the molecular orbital levels on La. However, we envisage that NEXAFS spectra could show whether, the CO molecule tilts on this surface. Furthermore, a stronger interaction of the 4σ orbital of CO with the surface alloy, may also be the clue to why CO readily dissociates on this surface alloy.

At temperatures above 773 K the 4σ and $5\sigma/1\pi$ molecular orbitals have disappeared, confirming that the CO molecules have undergone a complete dissociation. The disappearance of peak B in the TPD spectrum in figure 1, indicates that complete dissociation has taken place at around 750 K. Note that the photo-emission spectra has been recorded at 100 K temperature intervals.

The peak observed around 4.5 eV is due to Oxygen 2p levels on La-Rh(100). At higher temperatures (lower coverages), this level split into 3 components at 4.1 eV, 4.5 eV and 5.2 eV. The Oxygen 2p levels on clean Rh(100) has been reported to be located at approximately 5.2 eV [16]. From partly dissociated and disordered CO on the as-deposited layer, we extract an approximate O2p/La level of 4.5 eV (see figure 7), which corresponds to the middle O2p peak of O/La-Rh(100) alloy. The lower peak seem thus to be an O2p level, characteristic of the alloy. The broadening of the peak at lower temperatures is expected to be due to disorder, while the above analysis indicates thus three different orbital levels for Oxygen on La-Rh at lower coverages (or higher temperatures). We may further compare the O2p discrete levels in the valence band with the peak D in the TPD spectrum in figure 1. Peak D seems to be composed of 3 different components. Finally, it is noted that the structure in the valence band spectra at 9.0 eV, is most likely C2p.

3.1.3 Analysis and estimation of Temperature dependent coverages.

In this section we try to make a synthese and summary of the information obtained in the previous sections, and apply it to a semi-quantitative description of the temperature dependent partial CO and C+O coverages. We attempt to formalise how the coverages and core level intensities may be presented in a practical manner in order to compare and combine TPD and core level intensities.

The coverage from the TPD trace may be estimated by [17]:

$$\frac{\theta(T)}{\theta^0} \approx \frac{A_t - A(T)}{A_t}, \qquad (1)$$

where $\theta(T) \approx \theta_{CO}(T) + \theta_{C+O}(T)$ and $A(T) = \int_{T_1}^{T} P(\tau) d\tau$. Here P(τ) is the partial CO pressure at temperature τ, and T_1=150 K. Further, $A_t = A(T_{max})$ is the total area under the TPD trace, where T_{max}=1180 K in our set of measurements. Furthermore, θ^0 is the initial coverage, i.e. obtained below 150 K. We will assume that $\theta_{C+O}(T) \equiv \theta_C(T) + \theta_O(T) \approx 2\theta_C(T)$.

The ratio of CO/C coverages can be estimated from the C1s intensities for atomic I_C(T) and molecular Carbon I_{CO}(T), giving

$$\frac{\theta_{CO}}{\theta_C} = \frac{I_{CO}(T)}{I_C(T)} \qquad (2)$$

where the ratio of the cross sections for emission from the atomic carbon and molecular carbon sites has been neglected in the current work. The latter ratio is not expected to be very different from unity, due to the relative similarity of the sites. However, the different CO sites and the different atomic carbon sites, will in principle all have different photo-emission cross-sections.

The bottom figure 8 shows the uncalibrated θ(T) calculated from equation (1), together with the recorded TPD spectrum (from figure 1).

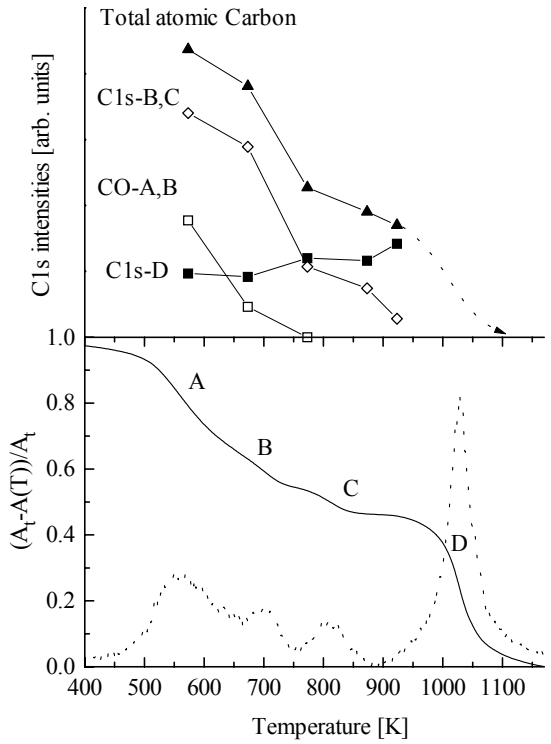

Figure 8: The bottom figure shows the total coverage estimated from equation (1), before calibration. The figure also shows the TPD trace as a reference (dotted line). The top figure shows the C1s core level intensities (normalised). The hollow squares is the C1s-CO intensity, while the hollow diamonds correspond to the high binding energy component of C1s of atomic Carbon in figure 3. The full squares correspond to the low binding energy component of C1s of atomic carbon in figure 3. The full triangles denote the total atomic Carbon C1s intensity.

The top figure 8 shows the normalised C1s core level intensities (see figure 3). The intensities are denoted CO-A,B, C1s-B,C and C1s-D, with respect to the CO and atomic carbon peaks in figure 3. It is observed that the fraction of CO/C is approximately 0.40 and 0.12 at 573 K and 673 K respectively, while all CO have desorbed or dissociated at 773 K (as previously discussed in figure 3). Furthermore, it is seen from figure 8, that the total C1s core level intensity follows the trend of the coverage estimated from TPD. A thermally programmed XPS study has previously been reported in the literature [18], and seems to be well suited for future studies of CO desorption and adsorption on the current structure. However, a careful calibration of the coverage from the core level intensities, and calibration of the difference in scattering cross-section for all sites is required.

The initial coverage in equation (1), can be corrected for using the c(4x4) LEED pattern observed at 873 K. It was noted in section 3.1.1, that this pattern could be due to either atomic carbon, atomic oxygen or both, and that the c(4x4) pattern corresponds to a coverage of 0.125 ML. If we first assume that the LEED pattern is caused by θ_{C+O}=0.125, and then calibrates the TPD spectrum, we obtain an unreasonably low initial total coverage of θ^0=0.25 ML (as can be seen by inspection of the bottom figure 8). On the other hand, assuming $\theta_{C,O}$=0.125, the initial coverage comes out as θ^0=0.5 ML, which corresponds approximately to a (1x1) structure with reference to the clean c(2x2) surface alloy. The latter seems reasonable, and is applied in order to calibrate the temperature dependent coverage. The full line in figure 9 thus shows the total calibrated coverage $\theta(T) \approx \theta_{CO}(T) + \theta_{C+O}(T)$, calculated using equation (1).

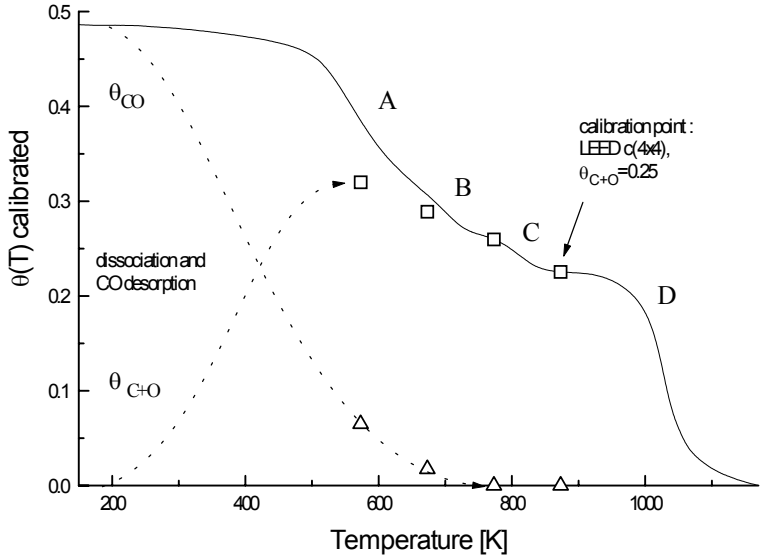

Figure 9. The figure shows the estimated coverage from equation (1), calibrated to 0.25 at 873 K, from the LEED structure. The hollow triangles shows the CO coverage and the hollow squares the C+O coverage, both estimated from the C1s intensities, and the calibrated $\theta(T)= \theta_{CO}(T)+ \theta_{C+O}(T)$ from TPD. It is particularly clear that the C and D states are two different C+O states, while the A and B states are a combination of associate desorption, and direct CO desorption. The dotted lines indicate how the dissociation may take place.

The calibration point from the c(4x4) structure is indicated in the figure. We stress here that the origin of the c(4x4) pattern remains unknown, and therefore these coverage estimates must be regarded as somewhat speculative.

By further using equation (2), and the temperature dependent CO and atomic carbon core level intensities in the top figure 8, it is possible to produce an estimate of the temperature

dependent partial C+O ($\theta_{C+O}(T)$) and CO coverages ($\theta_{CO}(T)$). The hollow squares and triangles in figure 9, give the C+O coverage and CO coverage. Furthermore, the dotted lines show how we believe the partial CO and C+O coverage to vary as a function of temperature. We envisage that the fine details of the dotted lines in figure 9 can be obtained in a thermally programmed XPS study, such as in Ref.18.

3.2 CO on sub-monolayer La-on-Rh(100) surface alloy

This section briefly discusses the different experimental data from CO/[(1x1)+]-La-Rh(100) alloy. This alloy was previously shown to be more characteristic of a sub-monolayer alloy [1]. In particular the different TPD traces, the LEED strucures of CO/(1x1)+ alloy, and the C1s levels are discussed and differences to the c(2x2)+ structure in section 3.1 are emphasised.

Figure 10 shows the TPD traces for CO dosed on the (1x1)+ La-Rh(100) sub-monolayer alloy, with as-deposited thickness of 1.25 Å (approximately 0.5 Monolayers).

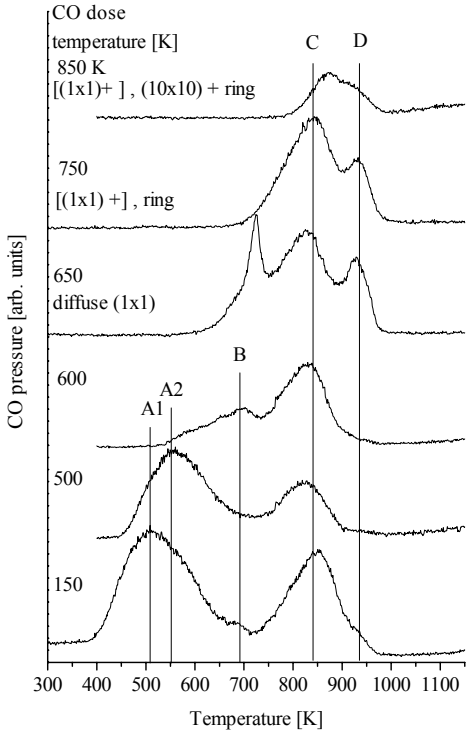

Figure 10: TPD trace of CO/La-Rh(100) alloy, with La as–deposited thickness of 1.25 Å (approximately 0.5 ML). The curves, from bottom to top, show the TPD traces after dosing 6L CO at; 150, 500, 600, 650, 750, and 850 K. The vertical lines indicate the positions of the TPD peaks. These are located at; A1=510 K, A2=558 K, B=695 K, C=823 K and D=928 K.

TPD spectra resulting from CO dosed at temperatures 150, 500, 600, 650, 750, and 850 K are shown from the bottom to top in the figure. The vertical lines indicate the positions of the TPD peaks, located at approximately at; A1=510 K, A2=558 K, B=695 K, C=823 K and D=928 K. The main lower peak A2 corresponds to peak A in figure 1. However, we observe that a new peak, marked A1, has appeared. This peak corresponds well to the high temperature desorption peak of CO on clean Rh(100). The latter peak is thus expected to appear from patches of the clean Rh(100) substrate (due to low La coverage). Peak B and C in figure 10 is located at approximately same position as peaks B and C in figure 1 for the c(2x2)+ alloy. Finally, one major difference is that peak D in figure 10 is lowered by 100 K with respect to the corresponding peak D of the c(2x2)+ alloy in figure 1.

Figure 11a, shows as a reference the clean (1x1)+ alloy, with as-deposited thickness of 1.9 Å (approximately 0.65 ML).

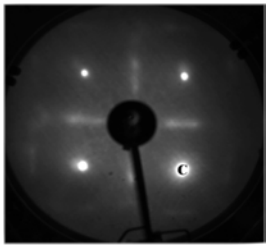

11a. Clean (1x1)+ La-Rh(100)

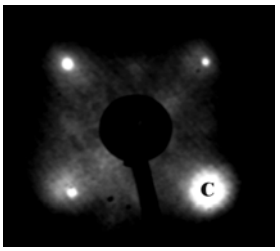

11b. CO on (1x1)+ 573

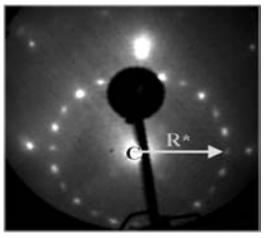

11c. CO on (1x1)+,

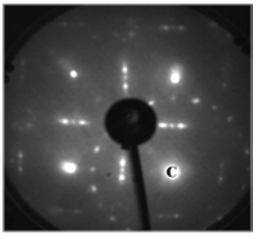

12d. CO on (1x1)+,

Figure 11: The figure shows the LEED pattern recorded for clean (1x1)+, and CO dosed at 150 K and heated. All figures are recorded at 150 K, using 80 eV electron beam energy. The (0,0) spot is located in the right bottom corner and denoted “centre” or “C”, in the figure. Figure 11a shows the clean La-Rh(100) alloy, with the characteristic (1x1) structure with streaks and partially split spots (thus denoted c(1x1)+). Figure 11b shows CO dosed on the (1x1)+ surface alloy, and heated to 573 K, giving the diffuse (1x1) pattern. Figure 11c shows the CO dosed surface, after heating to 773 K. The main spots appears as a diffuse (1x1) structure. An additional ring structure appears. The ring consists of 24 spots, with radius denoted R* in figure 11c, of 0.76a1*. Figure 11d shows the CO dosed surface, after heating to 873 K. The structure appears as in figure 11a, but with additional spots with splitting corresponding to a (10x10) superstructure. Superposed on the latter is the ring pattern as in figure 11c.

The structure is (1x1) with streaks, interpreted as disordered c(2x2) domains [1]. A close inspection shows a weak spot splitting, which in the anti-phase domain interpretation would approach a (4x4) superstructure. Figure 11b-e show the LEED images recorded for 6L CO dosed on the La-Rh alloy at 150 K, then heated to 573 K (11b), 773 K (11c) and 873 K (11d). The pictures were taken as above after re-cooling to 150 K, and recorded with 80 eV beam energy. Note that the (0,0) spot is not centred, but located as indicated in the right bottom corner. In particular, figure 11b shows CO dosed on the (1x1)+ surface alloy (i.e. figure 11a), and heated to 573 K. The LEED image appears as a diffuse (1x1) structure. This corresponds to the high temperature side of peak A2 in the TPD spectra. The VB photoemission spectrum (at 573 K) shows here a mixture of CO and atomic C and O on the surface. Figure 11c shows the CO dosed surface, after heating to 773 K. The main spots appear as a diffuse (1x1) pattern, while an additional ring structure appears. The ring consists of 24 spots, with radius (denoted R* in figure 11c) of $0.76a_{Rh}$*, where a_{Rh}* is the reciprocal unit vector for the clean Rh(100) surface. At an electron beam energy of 140 eV, we observe additionally a second most intense ring of $1.58a_{Rh}$* i.e. approximately 2(R*). Such a structure has been proposed to be related to either a compressed liquid [19], or islands with a statistical distribution (the so-called Henzler rings) [20,21, and references therein]. In both cases a diffuse ring appears in the diffraction pattern, with the ring radius related to the average island separation or average separation of atomic Carbon or atomic Oxygen. It is here argued, in accordance with the interpretation of the coverage estimated from the LEED pattern of C+O on the monolayer alloy, that the ring pattern is electron diffraction by either atomic oxygen, or atomic carbon, but not both.

It is more natural to choose the island interpretation of Bardotti et al. [20] due to the low C+O coverages at these temperatures. This model described in the literature relates the ring radius in reciprocal space (defined as a fractional part of a_{Rh}*, as in figure 11c) to L_c, defined as a real space correlation length. The L_c is further related to the mean island separation $L_{av} = \frac{1}{\sqrt{N_{av}}}$ (where N_{av} is the island density, as can be determined from Scanning Tunneling Microscopy (STM), at least in the case of the clean surface alloys). The precise relationship between L_c and L_{av} is nontrivial [20]. Both theory and experiments have proposed a calibration such as

$$L_{av}=\lambda L_c,$$

where $\lambda \approx 1.6$ [20]. Let a_{Rh} be the real space unit vector in the Rh surface unit cell, and let a_{La}=2*(Radius of La atom). Applying this model, we obtain with r=0.762, and R*=ra^*_{Rh}, that

$(1/r)a_{Rh} \approx 2$*(Radius of La atom), which is what we expected to be approximately the edge to edge separation between neighbouring islands in the anti-phase domain description (see Ref. [1] for a real space schematic diagram). Furthermore, the real space correlation length [20] is $L_c = 2(1/r)a_{Rh} = 2.66a_{Rh} \approx 2a_{La}$, and finally using λ=1.6 we obtain L_{av}= 1.6*2*1.32a_{Rh} = 4.22a_{Rh} = 11.82 Å. It is observed that the result supply an average C,C or O,O separation of approximately that of a (4x4) superstructure (i.e. 4 times a_{Rh}) . It is tempting to believe that each domain has only one pair of Carbon and Oxygen atoms on it. This can also be argued from the fact that, at higher temperatures in the monolayer case, a c(4x4) pattern was observed. Such a pattern would not fit on the smaller sub-monolayer domains. Therefore, we argue that the ring pattern may appear as a statistical distribution of C,O with an average C,C or O,O distance similar to the average island separation.

Figure 11d shows the surface after heating to 873 K. The LEED pattern shows here distinct spots within the region of the stripes in figure 10a. The spot splitting is of the order of a (10x10) super structure pattern. Superposed on this pattern one also finds the ring pattern. It is difficult to draw exact conclusions out of this structure. However, one find it likely that also this ring structure represents some statistical order relating the mean C,C separation of approximately 4.2a_{Rh} (11.8 Å), but coexisting with a long range order structure. It is noted that the (10x10) spots appear within the streaks. This is an indication that the atomic C,O bonds follows the disordered domains. It is also possible that the atomic C+O coverage have increased the order of the La-Rh(100) sub-monolayer surface alloy.

The main differences between the thick (monolayer) and the thin (sub-monolayer) alloy can be summarised as follows; At low La-coverage, the domains are small and a large number of Rh(100) surface atoms are exposed. The latter probably gives rise to peak A1, not present in the monolayer TPD trace. The average C,C or O,O distance is about 4.2a_{Rh} in the sub-monolayer alloy, in comparison to the c(4x4) structure implying distances of the order of $4\sqrt{2}a_{Rh} \approx 5.65a_{Rh}$. One expects thus in the current case the increased adsorbate interactions to lower the TPD peak D, which we in fact found to be lowered by approximately 100 K.

The C1s core level spectra from CO/(1x1)+ La-Rh(100) alloy is shown in figure 12.

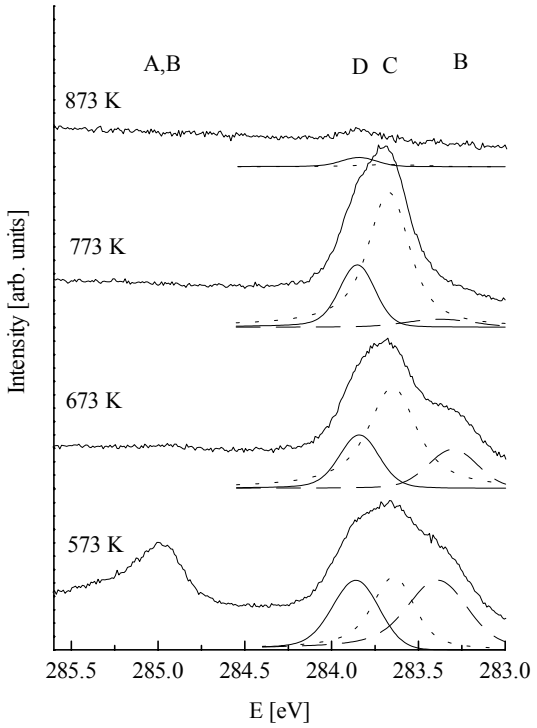

Figure 12: The figure shows C1s recorded from CO/La-Rh(100) corresponding to figure 10 and 11, heated to 573, 673, 773, 873 and 923 K, from the bottom to the top respectively. The photon energy was 360 eV. The peaks are labelled A, B, C and D with relation to the TPD spectra in figure 10.

The main difference compared to the C1s spectra in figure 3 is that CO is already dissociated or desorbed at 673 K (c.f. 773 K in figure 3). It is plausible that that the reduced coverage (leading to the new peak A1) cause a more efficient dissociation at lower temperatures. The peak denoted B in figure 12 is located at 283.4 eV at 673 K. This is approximately where it was located in figure 3 at 773 K. A new peak appears that is located at 283.7 eV, while peak D is the same as in figure 3. We denote the new peak; C, with relation to peak C in the TPD spectrum in figure 10. The intensity of peak C increases as peak B vanishes towards 773 K. The remaining peak at 773 K is thus composed of atomic carbon in two sites, which we thus denote C and D, with relation to the TPD spectra in figure 10. Atomic Carbon in these sites desorb at lower temperatures compared to the monolayer case, which is interpreted as above from larger adsorbate interactions.

5. SUMMARY AND CONCLUSION

A strong modification of the surface electronic properties and the bonding of CO to the La-Rh(100) surface alloy, has been demonstrated for both sub-monolayer and monolayer coverages of La/Rh(100). The TPD spectrum for CO/La-Rh(100) shows a mixture of desorption temperatures between those of CO/Rh(100) and CO on as-deposited La/Rh(100).In particular, it has been found that CO partly dissociates at low temperatures on the La-Rh(100) surface alloy, due to the presence of La in the near surface region. The photo emission spectra of C1s, O1s, La 5p, Rh 3d and valence band region, has been correlated to the peaks in the TPD spectra, and to the LEED patterns. We have observed different atomic carbon and atomic oxygen binding sites, which were correlated to the TPD peaks. We have attempted to identify the various sites, but since the detailed structure of the system remains undetermined, the discussion must be regarded as somewhat speculative.

Adsorbate interactions were thought to be responsible for a 100 K lowered desorption temperature in case of the sub-monolayer alloy. At higher temperatures a c(4x4) LEED pattern was the preferred structure for dissociated CO on the c(2x2) monolayer alloy. The sub-monolayer alloy showed here a ring pattern, superposed on a (10x10) superstructure and streaks.

A semi-quantitative analysis of the temperature dependent partial CO and C+O coverages have been demonstrated based on LEED, core level photoemission spectroscopy and TPD.

REFERENCES

[1] M. Kildemo, T. Ramsvik and S. Raaen, Surface Science 490 (2001) 1.

[2] L.Z. Mezey and J. Giber, Jpn. J. Appl. Phys. 21 (1982) 169.

[3] see, e.g, R.J. Madix, in *The Chemical Physics of Solid Surfaces and Heterogeneous Catalysis, Vol 4: Fundamental Studies of Heterogeneous Catalysis*, edited by D.A. King and D.P. Woodruff (Elsevier, Amsterdam - Oxford - New York, 1982), pp.1-23

[4] see, e.g., J.W.A. Sachtler and G.A. Somorjai, J. Catalysis 81 (1983) 77.

[5] R.B. Schwarz and W.L. Johnson, Phys. Rev. Lett. 52 (1983) 415.

[6] S. Raaen, C. Berg, and N.A. Braaten, Surf. Sci. 269/270 (1992) 953, and references cited therein.

[7] D.M. Wieliczka and C.G. Olson, J. Vac. Sci. Technol. A **8** (1990) 891.

[8] C.J. Baddeley, A.W. Stephenson, C. Hardacre, M. Tikhov, and R.M. Lambert, Phys. Rev. B. 56 (1997) 12589.

[9] A. Ramstad and S. Raaen, Phys. Rev. B. 59 (1999) 15935.

[10] E. Bertel, N. Memmel, G. Rangelov, and U. Bischler, Chemical Physics **177** (1993) 337.

[11] M. A. Van Hove, W. H. Weinberg, C. M. Chan, *Low Energy Electron Diffraction*, (Springer, 1986) 84.

[12] D. G. Castner, B. A. Sexton and G. A. Somorjai, Surf. Sci. **71** (1978) 519.

[13] F. Strisland, A. Ramstad, T. Ramsvik and A. Borg, Surf. Sci. (1997) L1020.

[14] Nilsson, B. Eriksson, N. Mårtensson, J. N. Andersen and J. Onsgaard, Phys. Rev. B 38 (1988) 10357.

[15] N. Mårtensson and A. Nilsson, J. of El. Spec. and Rel. Phen. 75 (1995) 209.

[16] M. Zacchigna, C. Astaldi, K. C. Prince, M. Sastry, C. Comicioli, R. Rosei, C. Quaresima, C. Ottaviani, A. Antonini, M. Matteucci and P. Perfetti, Surf. Sci. 347 (1996) 53.

[17] see e.g. D. A. King Surf. Sci. 47 (1975) 384.

[18] A. Baraldi, G. Comelli, S. Lizzit, D. Cocco, G. Paolucci, R. Rosei,Surf. Sci. 267 (1996) L67.

[19] J. N. Andersen, E. Lundgren, R. Nyholm and M. Qvarford, Surf. Sci. 289 (1993) 307.

[20] L. Bardotti, C. R. Stoldt, C. J. Jenks, M. C. Bartelt, J. W. Evans, and P. A. Thiel, Phys. Rev. B 57 (1998) 12544.

[21] G. L. Nyberg, M. T. Kief and W. F. Egelhoff, Jr., Phys. Rev. B (1993) 14509.

Paper VII

Homoepitaxial growth of Co on Co(11$\bar{2}$0) studied by STM

T. Worren, T. Ramsvik and A. Borg

Applied Surface Science 142 (1999) 48 - 51

ELSEVIER

Applied Surface Science 142 (1999) 48–51

applied surface science

Homoepitaxial growth of Co on Co(11$\bar{2}$0) studied by STM

Turid Worren *, Trond Ramsvik, Anne Borg

Department of Physics, Sem Saelands vei 7, Norwegian University of Science and Technology, N-7034 Trondheim, Norway

Abstract

We present the first experimental results from homoepitaxial growth of Co on Co(11$\bar{2}$0) studied by scanning tunnelling microscopy (STM). The unreconstructed Co(11$\bar{2}$0) surface consists of zigzag rows of atoms running along the [0001] direction of the Co crystal. From the STM images, we observe that the Co islands are elongated along the [0001] direction, indicating that the growth is anisotropic. A plot of the auto-correlation function confirms the anisotropy. To investigate the growth further, the substrate temperature and deposition rate were varied at a constant coverage of $\sim(5\pm1)$%. The size distribution of the Co islands deposited is very sensitive to the substrate temperature, and larger and fewer islands are observed for higher temperatures. © 1999 Elsevier Science B.V. All rights reserved.

PACS: 61.16; 68.35.Bs; 68.35.Fx

Keywords: Homoepitaxial growth; Metal-on-metal growth; Cobalt; Single crystal surfaces; Surface diffusion; Scanning tunnelling microscopy

1. Introduction

Metal-on-metal growth processes have attracted a lot of interest over the years, both theoretically and experimentally. Recently, highly anisotropic growth has been reported for, e.g., Au/Au(100) [1] and Pt/Pt(100) [2,3]. These studies were performed on hexagonally reconstructed Au(100) and Pt(100), respectively. The highly anisotropic diffusion on these surfaces was attributed to the row-like structure of the Au(100) and Pt(100) surface reconstructions.

In this paper, the first experimental results from homoepitaxial growth of Co on Co(11$\bar{2}$0) studied by scanning tunnelling microscopy (STM) are presented. The unreconstructed Co(11$\bar{2}$0) surface was chosen due to its inherent anisotropic surface structure. The surface consists of zigzag rows of atoms running along the [0001] direction of the Co crystal. In addition, CO adsorption has been found to induce highly anisotropic Co diffusion on this surface [4].

2. Experimental

The experiments were carried out using a room temperature (RT) Omicron UHV STM. The Co(11$\bar{2}$0) single crystal was cleaned by cycles of argon sputter-

* Corresponding author. Tel.: +47-7359-3419; Fax: +47-7359-3420; E-mail: worren@phys.ntnu.no

0169-4332/99/$ - see front matter © 1999 Elsevier Science B.V. All rights reserved.
PII: S0169-4332(98)00636-9

ing at ~550 K and subsequent annealing at ~650 K in UHV. Co was evaporated from a resistively heated tungsten (W) basket. Various evaporation rates were used, and they were estimated from the STM images to be in the range from ~0.03 to ~0.1 ML/min. During deposition, the substrate was kept at a temperature ranging from 296 K to 413 K.

3. Results and discussion

Upon deposition of small amounts of Co on Co(11$\bar{2}$0) at RT, Co islands elongated along the [0001] direction are observed. Fig. 1 displays the island structure formed after evaporating ~0.17 ML Co. The Co islands are nucleated both inside terraces and at step edges. Preferentially, nucleation occurs at step edges intersecting the [0001] direction, as is illustrated in the upper right corner of Fig. 1. The shape of the islands indicate either anisotropy in island growth, or in adatom diffusion, or a combination of the two. The inset in the lower left corner shows the detailed structure of an island. The predominant growth along the zigzag rows of the substrate is here clearly seen. The two images have equal deposition times.

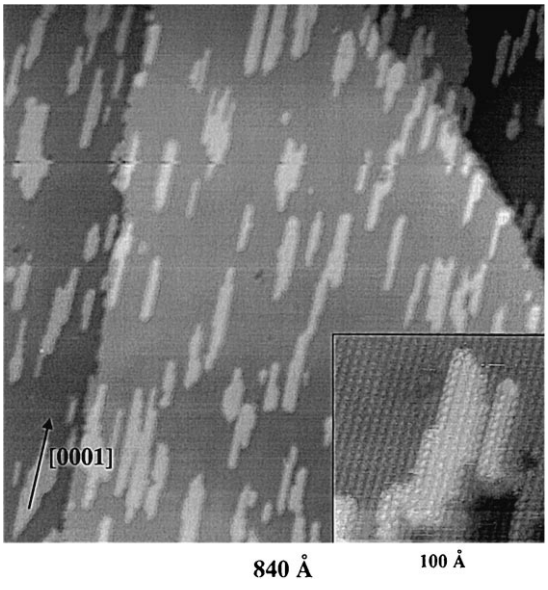

Fig. 1. Adsorption of ~0.17 ML Co on Co(11$\bar{2}$0). The image covers 840×840 Å^2. The greyscale range from black to white is 5.1 Å. Growth of islands preferentially along the [0001] direction is observed. The inset shows the detailed structure of a Co island.

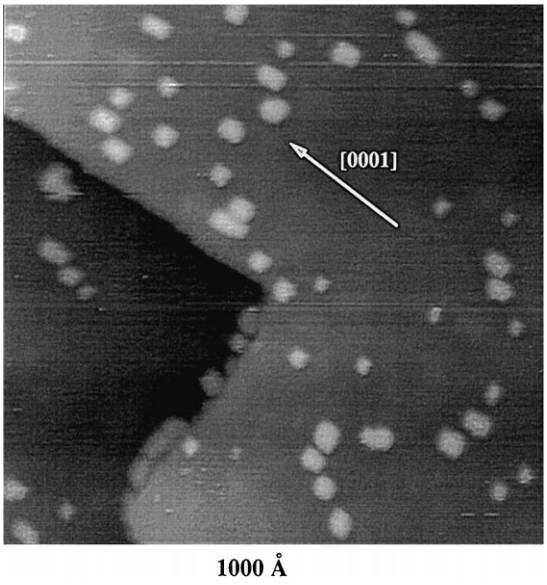

Fig. 2. Deposition of ~0.06 ML Co on Co(11$\bar{2}$0). The image area is 1000×1000 Å^2, and the greyscale covers 5.6 Å from black to white. No nucleation of islands at the step edge parallel to [0001] is observed.

Further deposition of Co causes the islands to grow in size and to coalesce with neighbouring islands. At coverage ~0.4 ML and ~0.6 ML, the coalescence is easily observed. When ~60% of the Co(11$\bar{2}$0) surface is covered, second layer islands are observed to nucleate on top of the first layer islands.

In Fig. 2, an area with step edges both intersecting and running parallel to [0001] is displayed. Along the [0001]-oriented edge, no islands are nucleated, while the step edge intersecting [0001] is decorated with deposited Co. This finding suggests higher diffusion velocity of added Co parallel than perpendicular to the zigzag chains along [0001].

A difference in diffusion velocities can be visualised through a plot of the inter-island vectors for a large number of islands. This plot results in a 2D auto-correlation function as shown in Fig. 3a. One of the eight STM images used to generate the auto-correlation function can be seen in Fig. 3b. Around the common origin of the auto-correlation plot, there is

an area elongated in the [0001] direction with no inter-island vectors. The shape of the area demonstrates that the typical spacing between islands is much larger along than perpendicular to [0001]. This indicates larger mobility of added Co atoms parallel to than perpendicular to [0001]. For a system with anisotropic growth and not anisotropic diffusion, the auto-correlation plot would be isotropic.

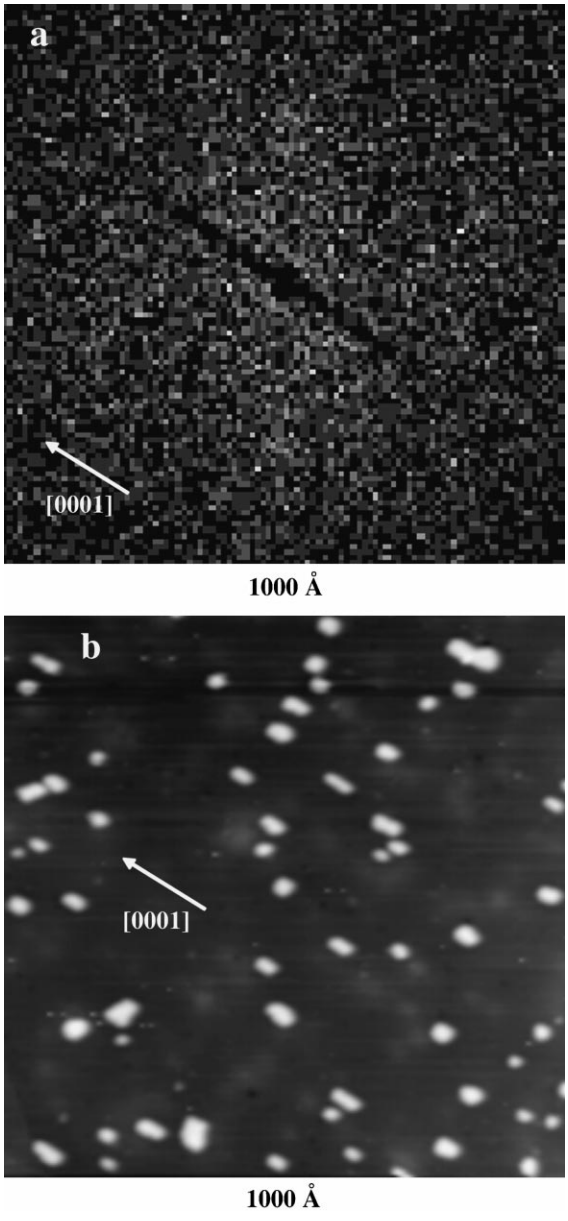

Fig. 3. (a) Two-dimensional auto-correlation function demonstrating the diffusion anisotropy. A total of 342 islands are included. (b) One of the eight images used to generate the auto-correlation function. Co, ~0.05 ML, was deposited. The image area is 1000×1000 Å^2, and the greyscale covers 3.2 Å from black to white.

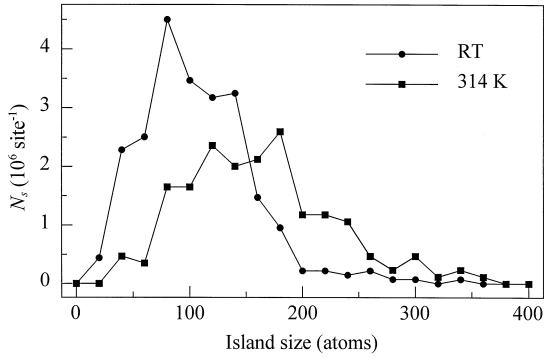

Fig. 4. Island size distribution for two different temperatures, RT and 314 K. Co, ~0.05 ML, was deposited at a rate of $\sim 1.3\cdot10^{-3}$ atoms/(site·s).

To investigate the growth further, the substrate temperature and deposition rate were varied at a constant coverage of $\sim(5\pm1)$%. Fig. 4 shows the size distribution N_s of islands formed on large terraces at two different temperatures. N_s, the density of islands containing s atoms, is calculated as described in Ref. [3]. At higher temperatures, and also lower deposition rates, the islands are fewer and larger. The size distribution appears to be more temperature-sensitive for the Co/Co(11$\bar{2}$0) system as compared to Pt/Pt(100) [3]. Qualitatively, similar changes in the N_s are observed for a temperature difference of ~18° for Co and ~38° for Pt. This may suggest that the diffusion barrier for Co on Co(11$\bar{2}$0) is smaller than 0.43 eV, which is the value reported for Pt on Pt(100) [3].

4. Summary

The homoepitaxial growth of Co on Co(11$\bar{2}$0) has been investigated by STM. The diffusion of Co adatoms is found to be highly anisotropic with larger mobility of added Co atoms parallel than perpendicular to [0001]. The size distribution of the Co islands deposited is very sensitive to the substrate tempera-

ture, and larger and fewer islands are observed for higher temperatures.

Acknowledgements

The financial support from the Norwegian Research Council and the VISTA program is acknowledged.

References

[1] S. Günther, E. Kopatzki, M.C. Bartelt, J.W. Evans, R.J. Behm, Phys. Rev. Lett. 73 (1994) 553.
[2] T.R. Linderoth, J.J. Mortensen, K.W. Jacobsen, E. Lægsgaard, I. Stensgaard, F. Besenbacher, Phys. Rev. Lett. 77 (1996) 87.
[3] J.J. Mortensen, T.R. Linderoth, K.W. Jacobsen, E. Lægsgaard, I. Stensgaard, F. Besenbacher, Surf. Sci. 400 (1998) 290.
[4] H.J. Venvik, A. Borg, C. Berg, Surf. Sci. 397 (1998) 322.